COVALENT DRUG BINDING:

A MECHANISTIC EXPLORATION TO ENHANCE SAFETY AND EFFICACY

CHAN CHUN YIP

(B.Sc. Pharm (Hons.), NUS)

A THESIS SUBMITTED

FOR THE DEGREE OF DOCTOR OF PHILOSOPHY

DEPARTMENT OF PHARMACY

NATIONAL UNIVERSITY OF SINGAPORE

2015

Declaration

I hereby declare that this thesis is my original work and it has been written by me in its entirety. I have duly acknowledged all the sources of information which have been used in the thesis.

This thesis has also not been submitted for any degree in any university previously.

Chan Chun Yip

18 November 2015

Acknowledgments

This thesis represents the collective contributions of numerous individuals to whom I would like to express my deepest gratitude. First and foremost, my heartfelt thanks to Prof Eric Chan, my doctoral advisor who has been a wonderful mentor since I was an Honors Year student. Thank you for taking a chance on someone rough around the edges, and investing time and effort in shaping and moulding me to be a better person both professionally and personally. You are a person who truly leads by example and clearly walks the talk. I am grateful that you are always challenging and inspiring me, and in the process, you have taught me that I have, in myself, the capacity to achieve greater heights. Thank you for trusting me, giving me the freedom and encouraging me to explore new ideas and research interests, and for providing all the necessary support to ensure the success of these endeavours. You are always ready to lend a listening ear despite your busy schedule, and I deeply appreciate all your advice and counsel. I continue to learn from you in so many ways, and I thank God for blessing me with you as my mentor and role model.

I am deeply appreciative of my collaborators at the Singapore Eye Research Institute: Dr Zhou Lei and Ms Koh Siew Kwan, who believed in the potential of this project, and has tirelessly and generously provided invaluable support and technical expertise, without which our investigation on drug-induced protein glutathionylation would not have commenced and now come to fruition. I am very grateful for your strong commitment to this work and belief in its potential that helped sustain it through difficult times. My sincere gratitude to Dr Ong Pei Shi for partnering us in investigating the pharmacodynamic interaction between lapatinib and endoxifen. Thank you for personally teaching me the cell culture

and molecular biology techniques needed for this study, and for tirelessly co-supervising 2 Honors Year students with us. I have learnt a great deal from your guidance in and out of the lab. To my collaborators at GlaxoSmithKline R&D Singapore: Dr Edward Browne, Dr Kishore Pasikanti and Ms Su Zhiting, my deepest gratitude for their unwavering support with investigating the pharmacokinetic interaction between lapatinib and endoxifen using the MDCKII-MDR1 model. A big thank you to Prof Christina Chai for hosting me in your lab to perform organic synthesis, for kindly treating me as part of your research group and for all the advice, support and encouragement. I am thankful to Dr Ngai Mun Hong, Yan Ting, Yanbo and Kuan Chieh for help with the synthetic work, and more memorably the camaraderie in and out of the Chai lab. My warmest gratitude also to Dr Vinita Uttamsingh and Dr Sophia Nguyen from Concert Pharmaceuticals for providing deuterated lapatinib analogues for our evaluation.

My sincere thanks to past and present members of the Metabolic Profiling Research Group: Lee Sun for her guidance and friendship from my days as an Honours student; Alex, Davis, Devester, Kwok Foong, Preben, Peirong and Wanjing for their invaluable contributions as undergraduate students to the different parts of this work, making it greater than the sum of its individual parts; Hui Ting, Lee Cheng, Lian Yee, Yanjun, Gopal, Yee Min and Dorinda for providing me with their kind assistance for parts of my project; Liyan, Aneesh, Aparna, Yun Shan, Thiru, Kai Lun, Ronald, Gopal and Theebarina for making MPRG a wonderful and fun group, as well as Hai Ning for being a great friend and generously sharing resources; you are all part of precious memories and have left an indelible mark in my journey. A special thanks to Lian Yee for all the encouragement you have provided to me; your treasured friendship, cherished

care and unflagging support through thick and thin made it possible to complete this journey, and I would not exchange it for anything in this world.

I would like to convey my gratefulness to the Department of Pharmacy, NUS, for my education and I would like to thank in particular Dr Chew Eng Hui and Dr Ho Han Kiat for their sharp comments and suggestions which kept this project on the right track; Ms Ng Sek Eng, Ms Tan Bee Jen and Mr Sukaman for their excellent technical support and administrative efficiency. I would also like to acknowledge the financial support from NUS Pharmacy, GlaxoSmithKline, the President's Graduate Fellowship and funding from the FYP research grants for making this project a reality. I would also like to remember the late Prof Sidney Nelson, who carried out pionerring investigations on acetaminophen toxicity and inspired us to investigate acetaminophen-induced protein glutathionylation.

To my dad and mum: no words can adequately express my thanks and gratitude for all your love, care, concern and patience; supporting me through difficult times, and celebrating my achievements and successes; for your unwavering belief and unceasing encouragement; and being ever ready with a listening ear and a comforting shoulder. As difficult as it sometimes was for me during these eight years that I was away from home, it must have been harder for you; I am grateful for your trust and support which enabled me to pursue my dreams. Thank you for making countless trips between home and Singapore to visit me and keep me well-stocked with necessities, and never once griping or complaining. To the rest of my family and loved ones: I could not have completed this journey without you. Each of you gave of yourself in some way that made this possible. I thank God every day that I have you in my life.

And finally, to my Lord and Saviour Jesus Christ: thank you for leading me through all these years, and for placing me at the right time and right place, with the right people, doing the right thing. Looking back, I can see Your hand in action guiding me and providing me with all that I need. Thank you for giving me a new perspective of Your creation as a scientist. Having glimpsed the marvelous intricacies of Your work in this thesis, I am utterly convinced that "… in Him all things were created: things in heaven and on earth, visible and invisible, whether thrones or powers or rulers or authorities; all things have been created through Him and for Him. He is before all things, and in Him all things hold together." (Col 1:16-17, NIV). Glory be to Him.

Table of Contents

Summary

Covalent drug binding to proteins results in deleterious effects. Adverse drug reactions (ADRs) occur when overt covalent binding alters protein structure and function directly, or indirectly, by covertly inducing aberrant protein post-translational modifications such as protein glutathionylation. Collectively, these drug-induced protein modifications disrupt protein function and cellular homeostasis. However, the identity of many targets and the biological consequences of their modifications remain unknown. Using acetaminophen (APAP) as a model toxicant, we uncovered a suite of proteins glutathionylated by APAP, and correlated them to signatures of APAP hepatotoxicity using proteo-metabonomic mapping. Based on the mapping, we further elucidated the mechanisms of action of prophylactics and antidotes against APAP hepatotoxicity. Overt covalent binding can lead to inactivation of CYP450 enzymes and cause drug-drug interactions (DDIs). We explored drug deuteration to reduce reactive metabolite formation and patient genotyping to stratify susceptibility to DDIs caused by lapatinib. We negated the apparent liability of covalent binding by investigating the interaction between lapatinib and endoxifen, revealing potent pharmacodynamic and pharmacokinetic synergism that overcomes tamoxifen resistance and enhances breast cancer pharmacotherapy. This work offers a fresh perspective on covalent drug binding by first elucidating its mechanisms and consequences, which informs innovative strategies to improve both safety and efficacy of drugs.

Publications and Conference Abstracts

The following manuscripts were written based on this thesis:

- **JCY Chan**, L Zhou and ECY Chan. The Isotope-Coded Affinity Tag Method for Quantitative Protein Profile Comparison and Relative Quantitation of Cysteine Redox Modification. Current Protocols in Protein Science In Press.

- HK Ho, **JCY Chan**, KD Hardy and ECY Chan. Mechanism-based inactivation of CYP450 enzymes: a case study of lapatinib. Drug Metabolism Reviews 47 (February 2015) 21-28.

The following conference abstracts were presented based on this thesis:

- **JCY Chan**, PXL Teng, WJ Ng, PR Lim, ZT Su, KP Kumar, E Browne, PS Ong, ECY Chan. Combinatorial Lapatinib and Endoxifen Exhibits Pharmacodynamic and Pharmacokinetic Synergism in Tamoxifen-Resistant Breast Cancer. 20th North American Regional ISSX Meeting, October 18-22, Orlando, Florida, USA. *Third Prize Predoctoral Poster Award.*

- JCY Chan, ACK Soh, SK Koh, L Zhou, ECY Chan. Protein Glutathionylation: A New Dimension of Covalent Binding in Acetaminophen Toxicity. 20th North American Regional ISSX Meeting, October 18-22, Orlando, Florida, USA.

- **JCY Chan**, P Lim, PS Ong, ECY Chan. Leveraging Pharmacodynamic and Pharmacokinetic Synergism in the Treatment of Breast Cancer. 10th

AAPS-NUS PharmSci@Asia 2015, April 9, Singapore. *Best Poster Presentation Award.*

- **JCY Chan,** DYM Choo, ECY Chan. Impact of CYP3A5 genetic polymorphism on mechanism-based inactivation by lapatinib. 19th North American Regional ISSX Meeting and 29th JSSX Annual Meeting 2014, October 19-23, San Francisco, California, USA. *Invited Podium Presentation for "Drug-drug Interactions: Novel Mechanisms and Advances in Prediction" session*.

- **JCY Chan**, ACK Soh, SK Koh, L Zhou, ECY Chan. Protein glutathionylation: the hidden hand in acetaminophen toxicity. 19th North American Regional ISSX Meeting and 29th JSSX Annual Meeting 2014, October 19-23, San Francisco, California, USA. *Second Prize Predoctoral Poster Award cum Podium Presentation*.

- **JCY Chan**, P Lim, PS Ong, ECY Chan. A metabolism-driven combinatorial approach to overcome ER/HER2 crosstalk in breast cancer. 19th North American Regional ISSX Meeting and 29th JSSX Annual Meeting 2014, October 19-23, San Francisco, California, USA.

- **JCY Chan**, BL Nunn, DR Goodlett, SK Koh, L Zhou, ECY Chan. GluICAT: A novel liquid chromatography-mass spectrometry-based method for profiling protein glutathionylation. 10th International ISSX Meeting 2013, September 29-October 3, Toronto, Canada. Drug Metabolism Reviews 2014, 26-27 (45), Suppl 1. *Predoctoral Poster Award Finalist.*

List of Tables

List of Figures

List of Supplementary Tables

List of Supplementary Figures

List of Abbreviations

4-OHT	4-hydroxytamoxifen
ACE	Angiotensin-converting enzyme
ACN	Acetonitrile
Acetyl-CoA	Acetyl-coenzyme A
ADP	Adenosine diphosphate
ADR	Adverse drug reaction
AIF	Apoptosis-inducing factor
Akt	Protein kinase B
AMAP	3'-hydroxyacetanilide
ANOVA	Analysis of variance
ANT	Adenine nucleotide translocase
APAP	Acetaminophen
ASK1	Apoptosis signal-regulating kinase 1
AST	Aspartate aminotransferase
ALT	Alanine aminotransferase
ATP	Adenosine triphosphate
BBB	Blood-brain barrier
BCA	Bicinchoninic acid
BSA	Bovine serum albumin
CβS	Cystathionine β-synthase
C_{max}	Peak plasma concentration
CI	Combination index
CNS	Central nervous system
COX	Cyclooxygenase
Cu,Zn-SOD	Cytosolic superoxide dismutase 1
CYP450	Cytochrome P450
DAB	Denaturing alkylation buffer
DDI	Drug-drug interaction
DEDC	Diethyldithiocarbamate
DIE	Deuterium isotope effect
DMEM	Dulbecco's modified Eagle's medium
DMSO	Dimethylsulfoxide
DNA	Deoxyribonucleic acid
DRI_{50}	Dose reduction index at 50% cytotoxicity
DTT	Dithiothreitol
EDTA	Ethylenediaminetetraacetic acid
EGFR	Epidermal growth factor receptor
ERα	Estrogen receptor α
FASP	Filter-aided sample preparation
FBS	Fetal bovine serum
FDA	Fluorescein diacetate
FDR	False discovery rate
GAPDH	Glyceraldehyde-3-phosphate dehydrogenase
GCL	Glutamate cysteine ligase
Grx	Glutaredoxin
GPx	Glutathione peroxidase
GR	Glutathione reductase
GS	Glutamine synthetase
GSH	Glutathione

GSNO	Nitrosoglutathione
GSSG	Oxidized glutathione
GSTπ	Glutathione-*S*-transferase π
HAT	Histone acetyl transferases
HCl	Hydrochloric acid
HED	2-hydroxyethyl disulfide
HER2	Human epidermal growth factor receptor 2
HLA	Human leukocyte antigen
HDAC	Histone deacetylases
HLM	Human liver microsomes
HPLC	High-performance liquid chromatography
IC_{50}	Half-maximal inhibitory concentration
ICAT	Isotope-coded affinity tag
IS	Internal standard
JNK	c-jun-N-terminal kinase
k_{obs}	Rate constant of inactivation
k_{inact}	Maximal rate constant of inactivation
K_I	Inhibitor concentration at half the maximal rate constant of inactivation
k_{inact}/K_I	Potency of inactivation
LC/MS	Liquid chromatography/mass spectrometry
LC/MS/MS	Liquid chromatography/tandem mass spectrometry
MAPK	Mitogen-activated protein kinase
MAT	Methionine adenosyltransferase
MBI	Mechanism-based inactivation
MCU	Mitochondrial Ca2+ uniporter
MHC	Major histocompatibility complex
MI complex	Metabolic-intermediate complex
MnSOD	Mitochondrial superoxide dismutase 2
MPTP	Mitochondrial permeability transition pore
MRM	Multiple reaction monitoring
MS	Mass spectrometry
MWCO	Molecular weight cut-off
NAC	N-acetylcysteine
NAD	Nicotinamide adenine dinucleotide
NADPH	Nicotinamide adenine dinucleotide phosphate
NAPQI	N-acetyl-*p*-benzoquinone imine
ND lapatinib	N-dealkylated lapatinib
NDMT	N-desmethyltamoxifen
OD lapatinib	O-dealkylated lapatinib
P_{app}	Apparent permeability
PARP	Poly(ADP-ribose) polymerase
PBPK	Physiologically-based pharmacokinetic
PBS	Phosphate-buffered saline
PDI	Protein disulfide isomerase
pERα	Phosphorylated estrogen receptor α
P-gp	P-glycoprotein
pHER2	Phosphorylated human epidermal growth factor receptor 2
PMCA	Plasma membrane Ca2+ ATPase
PR	Progesterone receptor
PTM	Post-translational modification
rCYP3A4	Recombinant CYP3A4

rCYP3A5	Recombinant CYP3A5
RNS	Reactive nitrogen species
ROS	Reactive oxygen species
SAH	S-adenosylhomocysteine
SAMe	S-adenosylmethionine
SCX	Strong cation exchange
SD	Standard deviation
SDS	Sodium dodecyl sulfate
SDS-PAGE	Sodium dodecyl sulfate-polyacrylamide gel electrophoresis
sER	Smooth endoplasmic reticulum
SERCA	Smooth endoplasmic reticular Ca2+ ATPase
Srx	Sulfiredoxin
SULT	Sulfotransferase
TCA	Trichloroacetic acid
TCEP	Tris(2-carboyxethyl)phosphine
TPIS	Triosephosphate isomerase
UGT	UDP-glucuronosyltransferase
US FDA	United States Food and Drug Administration
VDAC	Voltage-dependent anion channel
WHO	World Health Organization

Chapter 1 Introduction

1.1 The Burden of Adverse Drug Reactions

Despite decades of drug development efforts and clinical experience, adverse drug reactions (ADRs) remain a critical issue in pharmacotherapy. The World Health Organization (WHO) defines ADRs as 'a response to a drug that is noxious, unintended and occurs at doses normally used in man for the prophylaxis, diagnosis or therapy of disease or for modification of the physiological function' (*1*). ADRs contribute to increased clinical morbidity and mortality (*2*), up to half of which are preventable (*3*). ADRs account for up to 30% of hospital admissions in North America, accompanied by prolonged hospital stays and elevated risks of iatrogenic complications such as hospital acquired infections (*4*). This is further exacerbated in vulnerable pediatric and geriatric populations, where up to 30% of ADRs in children are life-threatening or fatal (*5*).

The economic burden of ADRs on healthcare systems is significant, as ADRs are estimated to cost USD 30.1 billion annually due to increased hospitalization, prolongation of hospital stays and additional clinical investigations (*4*). Further indirect costs are also incurred by patients and their caregivers due to reduced worker productivity (*4*). From an industry perspective, 30% of compound attrition during the development process is attributed to toxicity (*6*), which increases research and development expenditure and further magnifies the costs of medicines.

Unsurprisingly, considerable effort has been devoted to understanding the mechanistic basis of drug toxicities in order to design safer medications. For example, pharmaceutical companies develop comprehensive preclinical toxicity

screening programs, ranging from cell-based models to animal studies, using a variety of molecular biology tools such as gene knockouts and knockdowns, systems biology platforms and *in silico* algorithms to detect potential toxicities of new chemical entities (*6*). However, the reliability and predictivity of these approaches remain unsatisfactory, as attrition rates due to toxicity remain high (*7*). This situation is clearly illustrated in a review by Lasser *et al.* which found that of a total of 548 drugs approved between 1975-1999, 45 drugs (8.2%) acquired one or more black box warnings, and 16 (2.9%) were withdrawn from the market owing to ADRs that were not predicted from animal testing and/or clinical trials (*8*).

1.2 Classification of ADRs

A number of approaches have been developed to classify ADRs, each with varying considerations of clinical presentation, pharmacology, mechanisms of toxicity and patient factors. The following classification is adapted from the framework proposed by Smith and Obach (*9*) which places greater emphasis on pharmacology and mechanistic features, and facilitates subsequent discussion in section 1.5. ADRs can be broadly categorized into type A, type B and type C reactions. Type A (augmented) reactions are associated with an exaggerated therapeutic response related to the primary pharmacology of the drug (e.g. hypotension with antihypertensives), occurring either at the target site (e.g. hypoglycaemia with sulphonylureas) or at a distant region (e.g. headache with nitroglycerin) (*10*). Type A reactions are usually common, dose dependent, predictable, associated with a low mortality risk and managed through dose adjustment or discontinuation of treatment (*10*).

Conversely, type B (bizarre or idiosyncratic) reactions are uncommon (between 1 in 10 000 to 1 in 100 000) (*11*), unpredictable with a high risk of mortality (*10*) and not associated with the pharmacological action. Type B reactions are also described as idiosyncratic drug reactions (IDRs) and the two terminologies will be used interchangeably. Because the frequency of type B reactions is relatively low, they are often not detected until the drug has gained broad exposure in the patient population. Additional features of type B reactions also include repeat administration for onset, delayed onset, rapid onset upon rechallenge, lack of an apparent dose dependence, adaptation and tolerance, cross-sensitivity with other drugs, and pharmacogenetic association (*9*). Collectively, these features suggest an underlying immunological pathogenesis. For example, the delay in onset may be attributed to activation of the adaptive immune system, which requires a longer duration to initiate an immune response. In contrast, once the initial response is established, immunological memory primes the immune system for a much faster response, accounting for the rapid onset of toxicity upon repeat exposure to the implicated drug. Examples of type B reactions include carbamazepine-induced Stevens-Johnson syndrome and flucloxacillin-induced hepatotoxicity.

Similar to type B reactions, type C (chemical) reactions is unrelated to the pharmacology of the drug. However, distinct from type B reactions, it is characterized by a rapid onset, typically occurring after a single high dose, and predictable. A crucial feature of type C reactions is the toxicity being a consequence of covalent complex formed between the drug or its reactive metabolite with cellular macromolecules, and the fraction of the complexes formed is proportional to the extent of toxicity (*9*). In other words, the toxicity spectrum generally reflects an apparent dose-response relationship, which accounts for its predictability. The classical example of a type C reaction is

hepatotoxicity elicited by acetaminophen (APAP) overdose. Although distinctive features of type B and C reactions have been presented, some drugs exhibit overlaps between the two classes and the distinction is not always clear in practice.

1.3 Xenobiotic Metabolism and Reactive Metabolite Formation

Xenobiotics are broadly defined as chemical compounds which are foreign to a living organism (*12*), and include substances such as drugs, pesticides and dyes. Xenobiotics are typically metabolized via phase I (functionalization) reactions, which include oxidative, reductive and hydrolytic pathways, where a functional group such as OH, NH_2 or COOH is added or exposed, and aqueous solubility of the resulting metabolite is increased modestly (*11*). Phase II (conjugation) reactions involve attaching bulky groups such as glucuronides, sulfates and other moieties to an existing or newly introduced phase I functionality, resulting in a marked increase in hydrophilicity relative to the unconjugated counterpart (*11*). An exception is with methylation and acetylation which cause a moderate increase in hydrophobicity. Xenobiotics can undergo phase I followed by phase II reactions, or directly proceed to phase II conjugations. The increase in aqueous solubility facilitates the excretion of metabolites via the urine or bile.

The liver is the main organ of biotransformation, where phase I reactions are primarily mediated by cytochrome P450 (CYP450) enzymes, a superfamily of heme-containing enzymes that catalyze the oxidative metabolism of structurally diverse endogeneous and exogeneous compounds, including drug molecules. CYP450 enzymes are categorized into several subfamilies, members of which include CYP1A2, CYP2C9, CYP2C19, CYP2D6 and CYP3A4/5, which participate in the metabolism of more than 80% of drugs (*13*). Of these enzymes, the CYP3A4/5 family comprising primarily CYP3A4 and CYP3A5 is involved in

the biotransformation of more than 50% of currently marketed drugs (*13*). Several non-CYP450 enzymes such as monoamine oxidases, peroxidases, aldehyde oxidase, and alcohol dehydrogenases are also capable of phase I biotransformations (*11*). Separately, phase II reactions are catalysed by their respective transferases such as UDP-glucuronosyltransferases (UGT), sulfotransferases (SULT) and others. Apart from the liver, extra-hepatic sites of metabolism such as the gut, lung, kidney, skin and heart also contribute to overall biotransformation.

Drug metabolism is generally considered a detoxification mechanism to terminate the action of drugs, preventing their accumulation to toxic levels. In the case of prodrugs, metabolism exposes the pharmacophore to permit target engagement and elicit pharmacological activity. However, for certain drugs the same biotransformation processes can generate electrophilic, reactive metabolites, a phenomenon termed 'bioactivation'. This process can involve phase I and/or II reactions, either through a single enzymatic reaction or via sequential biotransformations to yield the reactive intermediate.

Due to the electrophilic nature of these reactive metabolites, they react readily with nucleophilic cellular macromolecules such as proteins and DNA. The resulting covalent complex is termed as an adduct. This work focuses the consequences of adduct formation with proteins.

1.4 Covalent Drug Binding and Protein Adduct Formation

Covalent binding of xenobiotics to proteins was first observed by Elizabeth and James Miller nearly 70 years ago, who found that rat liver proteins were coloured yellow by a carcinogenic dye, methylaminoazobenzene (*14*). The concept that covalent binding was responsible for the toxicity of drugs and other xenobiotics

was developed from the seminal work of Mitchell, Gillette and colleagues (*15*) in the 1970s on APAP toxicity, which established that APAP was metabolized in the liver by CYP2E1 to form an electrophilic reactive metabolite, N-acetyl-*p*-benzoquinone imine (NAPQI) that in turn formed adducts with liver proteins. The extent of covalent binding by NAPQI correlated with the degree of hepatotoxicity induced by APAP. Both covalent binding and toxicity could be attenuated by reaction with hepatic glutathione (GSH), a nucleophilic scavenger later found to be critical in the detoxification of reactive xenobiotics, thus substantiating the causal relationship of covalent binding with APAP hepatotoxicity (*16*).

From these studies, the covalent binding hypothesis was developed, positing that electrophilic functionalities arising from xenobiotic metabolism result in increased reactivity, thus promoting random and indiscriminate binding to cellular macromolecules such as proteins and DNA. Such off-target and promiscuous binding may interfere with or modify normal biological protein function, ultimately culminating in drug-induced toxicity.

1.5 Toxicological Significance of Covalent Binding

1.5.1 Overt Consequences of Covalent Binding

In this thesis, the term "overt" consequences of covalent binding is used to refer to the formation of a drug-protein adduct and the resulting effect of the adduction on the function of the victim protein. This is in contrast to the "covert" consequences referred to in section 1.5.2.

1.5.1.1 Mechanism-based Inactivation

As opposed to detoxification, biotransformation of drugs or xenobiotics by CYP450 enzymes may result in bioactivation and the generation of reactive metabolites that bind covalently and irreversibly to the enzyme prior to their release from the active site. This phenomenon is known as 'mechanism-based

inactivation' (MBI), a unique form of enzyme inhibition where the reactive metabolite inactivates the enzyme responsible for its generation. Hence, MBI is also described as 'suicide inactivation'. The reactive metabolite can form an adduct with either the CYP450 apoprotein or the porphyrin ring of the heme prosthetic group, each resulting in unique toxicological consequences (*13*).

From a functional perspective, MBI of CYP450 enzymes cause permanent inactivation of the enzyme which persists until fresh enzymes are synthesized (*13*). The magnitude of inactivation is proportional to the fraction of reactive metabolites that successfully form the protein adduct, thus is dose-dependent and is a type C reaction. Given the prominent role of CYP450 enzymes in drug metabolism, their inactivation can give rise to serious DDIs which arise when 'victim' drugs accumulate in the patient, leading to supratherapeutic effects, or subtherapeutic effects if the victim drug is a prodrug. Accordingly, the clinical sequelae can range from unexpected toxicity to inefficacious therapy, requiring dose adjustment or complete avoidance of the particular drug combination. For example, mibefradil, a calcium channel blocker approved for the treatment of hypertension in 1997, was withdrawn within a year of approval due to life-threatening DDIs with CYP3A4 substrates, including nifedipine, simvastatin, tacrolimus, cyclosporine and digoxin (*17*). In one instance, after consuming a single dose of the antihypertensive nifedipine 24 h after the last dose of mibefradil, the patient suffered from refractory hypotension and bradycardia, and died within 24 h of ingestion (*18*).

From a structural standpoint, if the reactive metabolite binds to the apoprotein, MBI can lead to the haptenization of CYP450 enzymes. A hapten is defined as a low molecular weight chemical that binds irreversibly to a protein through the formation of a covalent bond (*19*). Although a foreign substance, drugs do not

normally activate the immune system due to their small size; however when covalently bound to proteins, these haptens appear foreign to the immune system and trigger an immunological response, either against only the haptenized protein or both haptenized and native unhaptenized proteins. For the former, toxicity persists for as long as the drug is administered and until the hapten is cleared; while for the latter, it can result in autoimmune toxicity that continues even after therapy discontinuation. A classical example of this outcome is tienilic acid, which is a mechanism-based inactivator of CYP2C9. Tienilic acid was developed for the treatment of arterial hypertension and launched in 1979, but was withdrawn after a few months due to unexpected hepatotoxicity. Subsequent investigations revealed that the thiophene ring of tienilic acid was bioactivated by CYP2C9 to an electrophilic S-oxide, that in turn alkylated the OH group of serine 365 in the active site of CYP2C9 (*20*). Auto-antibodies directed against the CYP2C9-expressing liver and kidney (anti-LKM_2 antibodies) were found in 60% of patients experiencing tienilic acid-induced hepatitis (*21*), which were reactive against both native and adducted CYP2C9 (*22*), suggesting that the haptenization of CYP2C9 by tienilic acid triggered immune-mediated hepatitis. Other examples of MBI leading to the generation of auto-antibodies include dihydralazine-induced hepatitis (CYP1A2) and halothane-induced hepatitis (CYP2E1) (*22*).

A different outcome is observed when the reactive metabolite binds to the porphyrin ring. This occurs as a result of alkylation of one of the four pyrrole nitrogens of the porphyrin ring, triggering a dissociation of the heme group from the CYP450 enzyme where the iron is released, while the protoporphyrin ring accumulates (*23*). In genetically predisposed individuals, this can cause acute porphyria, which presents as a neuropsychiatric syndrome characterized by autonomic involvement in the form of tachycardia and hypertension, as well as

motor disturbances that can progress to respiratory paralysis and fluctuating psychiatric manifestations ranging from depression to violent agitation or frank psychosis (*24*). For over a hundred years certain drugs have been known to precipitate attacks of acute porphyria and are contraindicated in susceptible individuals. Drugs which have been identified mechanistically to trigger this condition via MBI include nifedipine, griseofulvin and carbamazepine (*22, 24*). Both CYP450 apoprotein haptenization and porphyrin alkylation can be considered type B reactions.

Although MBI has been described extensively in literature with reference to CYP450 enzymes, it is not restricted solely to the CYP450 family. Theoretically, any enzyme that metabolically generates a reactive metabolite that in turn adducts the active site is susceptible to MBI. These include non-CYP450 enzymes such as nitric oxide synthase (*25*) and angiotensin-converting enzyme (ACE) (*26*). Interestingly, MBI is not necessarily always a detrimental event. For example, MBI of ACE has been exploited as a therapeutic strategy to develop potent and long-lasting anti-hypertensives (*26*).

1.5.1.2 Type B idiosyncratic drug reactions

In the last decade, significant advances were made in resolving the underlying mechanisms of type B IDRs. Certain IDRs have been found to be precipitated by the formation of a hapten with drugs. In this regard, it is similar to haptens formed as a result of MBI; however the protein targets are not restricted to metabolic proteins such as CYP450 enzymes, and bioactivation of the drug to a reactive metabolite may not be a pre-requisite. In other words, the toxicities caused by MBI are a subset of IDRs, but for ease of discussion, they have been reviewed earlier in section 1.5.1.1.

Flucloxacillin-induced hepatotoxicity exhibits all the features of type B reactions, including a strong pharmacogenetic association with the *HLA-B*57:01* allele, where individuals carrying this allele exhibit a significantly greater risk for flucloxacillin-induced hepatotoxicity (odds ratio of 80.6) (*27*). The human leukocyte antigen (HLA) locus of genes codes for the major histocompatibility complex (MHC) cell surface proteins, which present self and non-self (foreign) antigens to circulating T cells, the latter of which triggers the adaptive immune system to mount an immune response. Haptens act as foreign antigens which are endocytosed by antigen-presenting cells such as dendritic cells. They then undergo antigen processing to form peptide fragments which are then loaded unto the peptide-binding cleft of an MHC complex and presented on the cell surface. The immunogenic hapten-derived peptide can be recognized by circulating T cells bearing complementary T cell receptors, which then initiates the adaptive immune cascade of events (*28*). Flucloxacillin possesses a β-lactam ring which is inherently reactive and has been shown to bind to nucleophilic lysine residues of serum albumin without requiring prior bioactivation. However, despite the ubiquitous presence of flucloxacillin-albumin adducts in flucloxacillin-treated patients, only patients bearing the *HLA-B*57:01* allele exhibit flucloxacillin-induced hepatotoxicity, presumably because the MHC class I molecule coded by this allele possesses a binding cleft with the appropriate topology to accommodate the immunogenic flucloxacillin-bound peptide (*29*). While the HLA allele defines the successful presentation of the immunogenic peptide, the effector T cells which recognize the MHC-peptide complex defines the liver-specific toxicity of flucloxacillin. All T cell clones responsive to flucloxacillin express the chemokine receptors CCR2 and CCR9, which direct the migration and accumulation of immune cells in the liver (*29*).

Apart from flucloxacillin, other drugs such as sulfamethoxazole and nevirapine exhibit IDRs with strong evidence that covalent binding is the key trigger (*19*); however the exact mechanisms are still under investigation. Unlike flucloxacillin, bioactivation of sulfamethoxazole and nevirapine to reactive metabolites precedes the toxicological event. Interestingly, the skin-specific toxicities for both drugs is attributed to local bioactivation by metabolic enzymes within the skin (sulfamethoxazole – phase I flavin-containing monooxygenase 3; nevirapine – phase II sulfotransferase) (*19*), as opposed to a systemic pathway via a particular effector T cell population as observed with flucloxacillin.

1.5.1.3 Type C dose-dependent toxicity

Pioneering work on what are now recognized as type C toxicants including APAP, bromobenzene, phenacetin, and 4-ipomeanol helped define the covalent binding hypothesis and establish the foundations of mechanistic toxicology. Common to all type C toxicants is bioactivation to a reactive metabolite, followed by covalent binding, crucially, in a dose-dependent manner. This feature permits demarcation of a reproducible dose threshold for toxicity, and can be reliably extrapolated based on body weight for dosing special patient populations such as pediatrics. Importantly, the dose-toxicity relationship forms the basis of managing overdoses through the use of nomograms. For example, healthy adults with normal liver function can tolerate a daily dose not exceeding 4 g of APAP, while pediatric dosing is recommended at 10-15 mg/kg/dose (*30*). For APAP overdose, the Rumack-Matthew nomogram guides treatment using N-acetylcysteine with considerations of APAP plasma concentration and time post-ingestion.

Available evidence suggests that metabolism-dependent covalent binding is the inciting event in type C reactions. 4-ipomeanol is a natural cytotoxin isolated from sweet potatoes infected with the mold *Fusarium solani*, responsible for

pulmonary toxicities in animals including cattle and rodents. Subsequent investigations revealed that the furan ring of 4-ipomeanol is bioactivated by CYP450 enzymes (e.g. CYP4B1 in rodent lungs) to electrophilic epoxides and α,β-unsaturated di-aldehyde reactive metabolites capable of covalent binding (*31*). Pre-treatment of rats with CYP450 inhibitors such as pyrazole markedly reduced *in vivo* covalent binding and lethal toxicity of 4-ipomeanol (*32*). Conversely, pre-treatment of rats with diethylmaleate, which depletes endogeneous GSH, a nucleophilic scavenger, markedly increased 4-ipomeanol covalent binding and toxicity (*32*). Separately, modulations of CYP450 activity by inducers and inhibitors, as well as GSH levels in rodent studies of APAP toxicity (*33, 34*) have reproduced similar trends as those of 4-ipomeanol. Furthermore, peak levels of APAP covalent binding consistently preceded hepatic necrosis by 1-2 h (*15*), indicating a temporal, cause-and-effect relationship. Collectively, these evidences underscore the key role of covalent binding as a critical driver in initiating type C toxicity.

1.5.2 Covert Effects of Covalent Binding

The formation of protein adducts with drugs or their reactive metabolites described in the previous section can be regarded as a form of *exogeneous* post-translational modification (PTM) of proteins. Since protein function is determined by its 3-dimensional structure, it is immediately obvious that overt protein modification through covalent binding can modulate the functional properties of proteins. Less well-recognized, however, is that covalent binding by drugs can exert a covert, secondary change in protein structure by inducing *endogeneous* PTMs such as acetylation and glutathionylation.

Endogeneous PTMs play crucial roles in regulating many complex biological networks, maintaining homeostasis and responding to perturbations such as

cellular stress. For example, epigenetic control of gene expression is regulated via reversible acetylation of histones by histone acetyl transferases (HATs) and histone deacetylases (HDACs), where histone acetylation results in chromatin decondensation, allowing access to transcription factors and co-activators (*35*). Cellular metabolism levels can dynamically modulate protein acetylation based on the relative cellular concentrations of nicotinamide adenine dinucleotide (NAD^+) and acetyl-coenzyme A (acetyl-CoA). In a fasting state, increasing levels of NAD^+ activate sirtuins possessing HDAC-like activities. Sirtuins mediate protein deacetylation by cleaving NAD^+ to nicotinamide and ADP–ribose, and transfering the acetyl group from acetyl-CoA to ADP–ribose (*35*). Conversely, when nutrient abundance increases, acetyl-CoA levels rise, leading to an increase in acetyltransferase activities and protein acetylation (*35*). Thus protein acetylation is thought to behave as a metabolic sensor and transduces signals depending on the cellular metabolic status. Congruent with this theory, many mitochondrial proteins can be acetylated which culminates in altered activity (*36*), suggesting that acetylation can modulate mitochondrial metabolism.

When constitutive protein PTM patterns are altered, perturbations in cellular homeostasis occur that may in turn lead to pathological outcomes. For example, abnormal acetylation has been documented in cancer (*37*), as it dysregulates gene expression and cellular metabolism as observed in malignancy. This analogy can be extended to covert protein modifications induced by drugs, and it becomes obvious that drugs that trigger aberrant PTMs and may yield unintended beneficial or adverse effects.

Aspirin (acetylsalicylate) is widely used for its antipyretic, analgesic, anti-inflammatory and anti-thrombotic effects. Aspirin binds covalently to, transacetylates and inhibits the cyclooxygenases (COX)-1 and -2. Inhibition of

COX-2 produces the analgesic and anti-inflammatory effects, while inhibition of COX-1 results in ulceration and stomach bleeds, well-known adverse effects of aspirin (*38*). The covalent inhibition of platelet COX-1 blocks the conversion of arachidonic acid to thromboxane A_2 which has pro-thrombotic activity (*39*). Beyond acetylation of COX enzymes, aspirin can induce aberrant acetylation of over 500 proteins involved in tumour suppression (e.g. EIF2, eIF4/p70S6K and mTOR), bioenergetics (e.g. glycolysis, gluconeogenesis) and other pathways (*40*). However, the functional consequence of this neo-acetylation pattern is still unclear, and needs to be established to elucidate the biological implications of aspirin-induced acetylation.

Another endogeneous PTM induced by covalent binding is protein glutathionylation, which is perpetrated by APAP. APAP-induced protein glutathionylation will be discussed in greater detail in Chapter 2. The ability of drug covalent binding to modulate basal physiological PTM patterns is a critical but understudied area that represents an additional dimension of the covalent binding hypothesis.

1.5.3 Limitations of the Covalent Binding Hypothesis

Despite the numerous examples provided in this chapter on ADRs elicited by drug covalent binding, there are limits to the applicability of the covalent binding hypothesis. A crucial argument is that not all instances of covalent binding translate to appreciable toxicity; and *vice versa* not all toxicities (with reference to type B and type C reactions) arise as a result of covalent binding.

For instance, while the association between covalent binding and APAP toxicity is clear, the regioisomer of APAP, 3'-hydroxyacetanilide (AMAP) causes equivalent levels of covalent binding as APAP, yet is non-hepatotoxic in mice (*41*). Further investigations revealed that APAP and AMAP bind differentially to liver proteins, where AMAP displays greater selectivity for proteins in the endoplasmic reticulum (*42*), while APAP preferentially forms adducts with mitochondrial proteins (*43*). These observations led to the refinement of the covalent binding hypothesis to include the paradigm that only a subset of protein adducts are critical to mediate toxicity, also known as the critical target hypothesis. In other words, the total binding to cellular proteins may be less relevant than selective modifications of specific critical targets (*44*). However, the identities of these critical targets have proven elusive, due to methodological and analytical limitations. For example, although over 30 liver proteins including enzymes have been found to be adducted to APAP, the activity of most modified enzymes were only modestly affected (*44*), and are not thought to be critical drivers of hepatotoxicity.

The poor predictivity of covalent binding for toxicity, particularly IDRs is the subject of much scholarship, and has been extensively reviewed in literature (*11, 16, 44-47*). As alluded to earlier, one key reason lies in the inability to comprehensively profile and identify the protein targets of covalent binding, due

to current methodological and analytical limitations. It is impossible to determine the consequences of covalent binding without inferring potentially perturbed pathways from adducted proteins. Even for well-investigated drugs like APAP, about 30 adducted proteins have been identified, which are likely only a fraction of the total adducted species. This incomplete picture hampers toxicological interpretations.

Secondly, the drug-protein adduct can induce secondary PTMs such as acetylation and glutathionylation. Current knowledge on the ability of drugs to induce such PTMs is limited. Furthermore, it can be difficult to distinguish between drug-induced, aberrant PTMs and basal, homeostatic PTMs.

Thirdly, the biological effects of a PTM, whether exogenously or endogenously derived are often unknown, and can range from unchanged, amplified or attenuated protein function. This adds additional complexity to the interpretation of the effects of covalent binding. Although biochemical assays can be performed to elucidate the biology of a PTM, they often are performed in a simplified, reconstituted cell-free system which lacks the dynamic *in vivo* interactions of a biological network and may not reveal the complete biological function of the PTM. Greater efforts are required to address these gaps in order to advance our understanding of covalent binding in toxicity.

1.6 Pharmacological Significance of Covalent Binding

Because of the possibility that covalent binding may elicit toxicity, traditionally, overt covalent binding as a mechanism of action is considered unfavorable in drug development due to the potential for off-target reactivity and toxicological sequelae. Nevertheless, covalent drugs (i.e. drugs that bind covalently to the target protein to elicit pharmacological effects) feature prominently in terms of revenue

and prescription rates (*48*). For example, 26 covalent drugs collectively account for USD 33 billion in worldwide annual sales, while in 2008, clopidogrel and esomeprazole accounted for 60 million prescriptions in America (*48*). Covalent drugs are utilized for a wide range of indications, including cardiovascular (aspirin, clopidogrel), infectious disease (β-lactam antibiotics), gastrointestinal (esomeprazole), central nervous system (rasagiline), oncology (5-fluorouracil) and many others. In almost all cases, their covalent nature was not by rational design, but discovered through serendipity as the mechanism of action surfaced during the late optimization stage, or even post-marketing (*49*).

Despite concerns of toxicity, there has been a resurgence of interest in covalent drugs in recent years due to the recognition of several unique advantages. Mechanistically, the binding of a covalent inhibitor begins by non-covalent interactions with the target protein, positioning the electrophile in close proximity to the target nucleophilic residue. The resulting complex undergoes covalent bond formation, giving rise to the desired irreversible inhibition (*48*). Covalent drugs permit the possibility of achieving increased potency and isoform selectivity by targeting a poorly conserved amino acid residue. Uniquely, a sustained duration of action can be achieved as inhibition persists until further target protein synthesis, essentially uncoupling pharmacodynamic effects from pharmacokinetics of drug exposure, allowing less frequent dosing and lower doses, possibly minimizing dose-dependent off-target covalent binding. Additionally, covalent binding overcomes situations of high concentration levels of endogenous substrate (e.g. ATP) competing with reversible inhibitors (e.g. kinase inhibitors). Studies also demonstrate that irreversible inhibitors may be more effective against drug resistance, as covalent EGFR inhibitors remained active against mutant EGFR forms, while reversible inhibitors displayed no

activity (*50*). It is hypothesized that mutant forms of EGFR reduce the non-covalent affinity between the inhibitor and its target, resulting in diminished or abolished activity for reversible inhibitors. However, given sufficient exposure to the covalent inhibitor, even mutants that react slower due to the poorer affinity eventually become fully inhibited, hence the covalent inhibitor retains activity.

With these considerations, medicinal chemistry strategies are focused on balancing reactivity with selectivity. Functionalities that have moderate electrophilicity, such as acrylamides have become the moiety of choice, which target nucleophiles such as thiols of cysteine residues, particularly those that are poorly conserved or rare among members of a protein family to achieve selectivity (*48, 49*). These efforts led to the development of a number of candidates currently in clinical development or have been approved by the U.S. Food and Drug Administration (US FDA), such as allitinib, neratinib, ibrutinib, afatinib, abiraterone, telapravir and others (*49*). Despite these advances from an efficacy viewpoint, concerns regarding off-target covalent binding and the toxicity aspects remain. While tempered electrophiles such as acrylamides may in general react slower with cysteines, around 10% of solvent-exposed cysteines are hyper-reactive, and off-target binding with this subset of cysteines is unpredictable even with careful tuning of binding characteristics (*51*). Additionally, the role of bioactivation of these electrophilic functionalities require due consideration, as these processes can modulate the reactivity of the electrophiles and thus the propensity for off-target covalent binding. For example, apart from directly reacting with the endogenous nucleophile GSH to form a conjugate, the acrylamide moiety of allitinib is also epoxidated by CYP450 enzymes followed by dihydrodiol formation by epoxide hydrolase, or GSH conjugation, the latter of which is suggestive of the formation of a reactive

metabolite (*52*). With the increasing interest in covalent drugs juxtaposed against the background of covalent binding and toxicity, it is clear that additional efforts are required to meet the challenge of interrogating the complete covalent binding repertoire of covalent drugs, including on- and off-target binding.

1.7 Research Objectives and Significance

1.7.1 Research Question and Objectives

Although covalent drug binding and protein adduct formation have long been implicated in ADRs, there remains a significant disconnect between the initial adduction event and subsequent toxicological outcomes due to a number of reasons which have been discussed in section 1.5.3, that in turn impedes efforts to develop approaches which can reduce or prevent ADRs. This knowledge gap is made more apparent when taking into account that covalent binding as a pharmacological strategy is becoming increasingly prominent in drug development. The overarching aims of this thesis are therefore to (1) explore covalent drug binding from a mechanistic perspective and (2) leverage insights gained from these findings to enhance safety and efficacy of pharmacological therapy. The specific objectives of this thesis are as follows:

1. Elucidate the consequences of covert protein modification in the form of drug-induced protein glutathionylation using APAP as a model toxicant.

2. Determine the influence of structural modification via selective deuteration and CYP3A5 genotype on CYP3A inactivation and reactive metabolite formation using lapatinib as a model toxicant.

3. Develop an effective combinatorial drug treatment to overcome tamoxifen resistance in breast cancer by circumventing the irreversible inactivation of CYP3A by lapatinib.

1.7.2 Thesis Outline

As presented in the preceding sections, both the causes and consequences of covalent drug binding are multi-faceted. In order to address the objectives stated previously, APAP and lapatinib are used as probe toxicants to investigate different aspects of covalent binding which are further elaborated below.

In Chapter 2, we performed a mechanistic investigation of covert drug-induced protein glutathionylation in human HepaRG hepatocytes using APAP as a toxicant. We present literature evidence supporting aberrant glutathionylation by APAP as a process secondary to covalent binding, and proceed to elucidate the influence of glutathionylation on the toxicological manifestations of APAP toxicity. Our findings also provide mechanistic insights which illuminate the mode of action for known prophylactics and antidotes which protect against or reverse APAP hepatotoxicity. We further demonstrate that aberrant APAP-induced glutathionylation is a time-, dose- and bioactivation-dependent process, and suggest that covert protein glutathionylation is a previously unknown mechanism of ADRs. Chapter 3 details two strategies to mitigate the deleterious effects of covalent binding using lapatinib as a model toxicant. Previously, our research group has determined the mechanisms by which lapatinib undergoes bioactivation to result in CYP3A inactivation. Building upon these investigations, we explore selective drug deuteration as an approach to reduce the bioactivation of lapatinib to reactive metabolites and the associated inactivation of CYP3A. We also elucidate the potential of using CYP3A5 genotype to prospectively stratify individuals who might be at increased risk of CYP3A inactivation and reactive metabolite formation by lapatinib. In **Error! Reference source not found.**, we attempt to turn the apparent liability resulting from lapatinib-induced CYP3A inactivation into a pharmacological opportunity, by developing a combinatorial

drug treatment using lapatinib and endoxifen to overcome tamoxifen-resistance in breast cancer.

1.7.3 Significance of Project

Understanding the mechanisms of drug-induced toxicity is crucial in developing efficacious and safe pharmaceuticals. Even though much work has been done on the effects of covalent binding in toxicity, several mechanistic aspects such as covert protein modification secondary to covalent binding remain unaddressed. With a clear understanding of such covert protein modifications, judicious interventions at biological pathways affected by these modifications serve as opportunities for therapeutic interventions. This work also illustrates how mechanistic information regarding the overt effects of covalent binding can be translated into viable strategies to mitigate the deleterious effects of protein adduction. Finally, this project encourages a different perspective on covalent binding by demonstrating that it is not necessarily a detrimental event, and the knowledge can be applied to optimize pharmacotherapy. Collectively, this thesis offers a fresh outlook on covalent drug binding and innovative strategies to improve both efficacy and safety of drugs.

Chapter 2 Drug-induced Protein Glutathionylation

2.1 Chapter Summary

Background: Protein glutathionylation of cysteine thiols is an important regulatory post-translational modification governing cellular homeostasis. APAP can covertly induce aberrant protein glutathionylation, as a secondary outcome of covalent binding between its reactive metabolite and proteins. Perturbation of basal glutathionylation could explain the hepatotoxicity of APAP. However, due to a lack of suitable analytical approaches, this phenomenon has not yet been investigated.

Objective: In this chapter, we aimed to develop an LC/MS-based proteomics method to comprehensively profile cellular protein glutathionylation. Subsequently, we applied this methodology to characterize and understand the biological consequences of aberrant glutathionylation induced by APAP.

Methodology: The GluICAT technique was modified from the OxICAT approach by incorporating the filter-aided sample preparation (FASP) protocol, which provides an efficient solution to overcome the technical difficulties in profiling protein glutathionylation. GluICAT was then used to examine APAP-induced glutathionylation in HepaRG cells in a time-, dose- and bioactivation dependent manner. 3'-Hydroxyacetanilide (AMAP), a reportedly non-toxic regioisomer of APAP, was used as a comparator.

Results and discussion: Using GluICAT, APAP was found to cause aberrant glutathionylation of critical proteins involved in energy metabolism, protein turnover, defense against cellular stress, calcium dynamics and mitochondrial permeability transition pore (MPTP) opening. Proteo-metabonomic mapping revealed a remarkable coherence between the functional impairments induced by

glutathionylation and metabolic derangements caused by APAP, particularly in energy metabolism and GSH synthesis. Glutathionylation also provided an explanation for altered calcium dynamics and could be involved in MPTP opening. Importantly, aberrant glutathionylation accounted for many of the key hallmarks of APAP toxicity. Longitudinal analysis suggested that protein glutathionylation of key proteins occurred in the early stages (3-6 h) of APAP toxicity, characterized by impairment of mitochondrial respiration, loss of ATP synthesis, GSH depletion and abnormal calcium dynamics. Furthermore, temporal glutathionylation patterns suggested that a key group of glutathionylated proteins was responsible for toxicity, which appeared to be distinct from other proteins glutathionylated, possibly as a consequence of toxicity. The former was likely a result of overt covalent binding, while the latter correlated with temporal increases in oxidative stress. APAP-induced glutathionylation was also dose- and bioactivation-dependent, further underscoring the relationship between covert glutathionylation and overt covalent binding. Finally, AMAP and APAP unexpectedly exhibited broad overlaps in glutathionylated proteins, agreeing with recent findings that both agents were toxic in human liver.

Conclusion: Aberrant protein glutathionylation by APAP is likely to be driven by overt covalent binding, and is responsible mechanistically for the early events in APAP toxicity. This study highlights a previously unrecognized mechanism of drug-induced liver injury which is secondary to covalent binding. Our findings will encourage examination of drug-induced protein glutathionylation in compounds where covalent binding is implicated in toxicity, particularly those sharing the quinone-imine toxicophore with APAP.

2.2 Chapter Introduction

2.2.1 Protein Post-translational Modifications

Despite consisting of a conserved set of 20 common amino acids that serve as fundamental building blocks, the human proteome is one of the most diverse set of biological molecules. While the human genome is estimated to consist of about 25 000 genes (*53*), the proteome is far larger in size, estimated at over 1 million proteins (*54*). This diversity is driven in part by alternative splicing in mRNA, creating sequence variants of proteins that translate into an assortment of functional activity. Modifications on the side chains of amino acid residues by the covalent attachment of chemical moieties, termed post-translational modifications (PTMs) further extend the range of protein functions as these structural changes modulate numerous cellular functions, including metabolism, signal transduction, protein turnover and cell division (*55*). Over 200 different PTMs have been identified, ranging from glycosylation, ubiquitination, methylation, acetylation, amidation, glutathionylation and the most widely studied, phosphorylation (*56*). Nearly all amino acid side chains can undergo some form of PTM, making the range of possible modified proteins nearly limitless.

2.2.2 Mechanisms of Cysteine Glutathionylation

Although cysteine is one of the least abundant amino acids in eukaryotic proteins (estimated at 1.9%) (*57*), it is frequently observed to concentrate in functionally important sites in proteins, playing regulatory, catalytic, cofactor binding and other roles (*58*). The functional significance of cysteine is further substantiated by a higher frequency of genetic diseases occurring due to cysteine mutations than is expected from its natural abundance (*59*). The prominence of cysteine is due in part to its exceptional PTM versatility. Its thiol side chain can undergo a variety of chemical modifications, including disulfide formation, farnesylation,

geranylgeranylation, glutathionylation, isoprenylation, nitrosylation, oxidation, palmitoylation and sulfhydration (*60*), with correspondingly varied biological effects. Cysteine glutathionylation, occasionally referred to as glutathiolation has gained interest in recent years as part of a group of *redox-sensitive* thiol modifications that also include oxidation and nitrosylation.

Unlike PTMs such as phosphorylation, which are generally enzymatically-driven, oxidation, nitrosylation and glutathionylation can be spontaneous events, making these modifications sensitive to changes in oxidative stress. Chemically, the thiol group possesses an average pK_a of around 8.6 which means that most cysteines remain protonated in the reducing cytoplasmic milleu, but the pK_a can vary between 3.5 to 10, depending on the microenvironment surrounding the cysteine thiol (*61*). For example, the pK_a can be lowered by positively charged or protonated amino acids which stabilize the thiol in the deprotonated, thiolate form, and increases its reactivity and nucleophilicity (*61*). Apart from the intrinsic reactivity of a particular thiol group, solvent accessibility also determines if the cysteine residue interacts with other chemical moieties capable of thiol modification. Cysteine residues buried within the hydrophobic core of a protein are less likely to be modified compared with surface, solvent exposed residues (*61*). Finally, the pH of the macroenvironment also influences the likelihood of deprotonation, particularly if the pH is higher than the pK_a. The pH of cellular compartments and organelles can vary from as low as 4.7 (lysosome), to 7.2 (nucleus and cytosol) and 8 (mitochondria) (*62*). Thus the reactivity of a particular thiol is dependent on a dynamic equilibrium between the intrinsic and extrinsic factors.

Cysteines undergo glutathionylation through a variety of mechanisms, as illustrated in Figure 2-1. This includes (1) oxidation to a sulfenic acid followed by reaction with GSH, (2) thiol-disulfide exchange with oxidized glutathione (GSSG), (3) nitrosylation of the cysteine residue followed by reaction with reduced GSH, (4) reaction of the reduced cysteine thiol with nitrosoglutathione (GSNO), or (5) reaction between two thiyl radicals (*63*) (Figure 2-1). These reactions can be mediated either chemically through reactive oxygen/nitrogen species (ROS/RNS), or enzymatically, as documented with glutathione-*S*-transferase π (GSTπ) and glutaredoxin 1 (Grx1) (*64*). Conversely, cellular deglutathionylation is exclusively an enzymatic process which is mediated by Grx1, glutaredoxin 2 (Grx2), sulfiredoxin (Srx) and protein disulfide isomerase (PDI) (*63*). An important point to note is that while oxidative stress can induce a variety of thiol modifications, thiol oxidation and nitrosylation can ultimately lead to protein glutathionylation. Therefore, glutathionylation could be considered to represent the continuum of redox-sensitive thiol modifications.

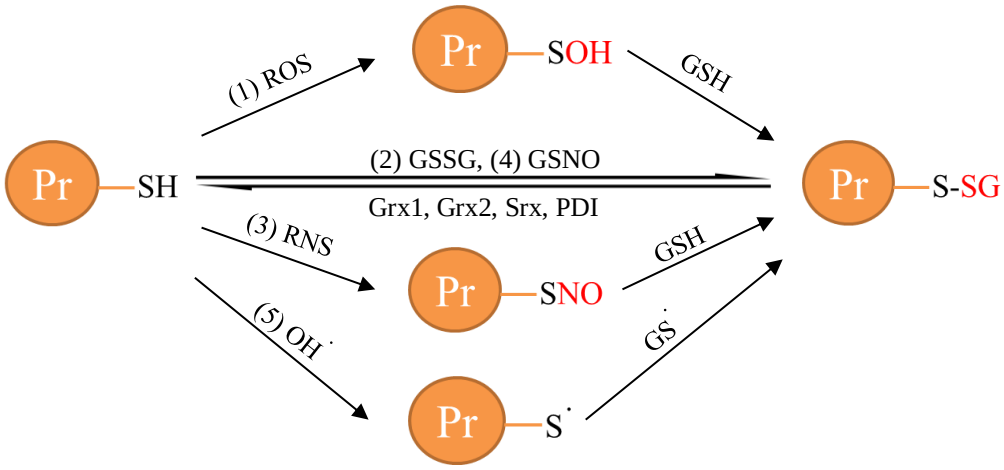

Figure 2-1 Mechanisms of cysteine glutathionylation via reaction with ROS, RNS, GSSG, GSNO or $OH^{\cdot}$. Pr-SH: free protein thiol; Pr-SOH: protein sulfenic acid; Pr-SNO: nitrosylated protein thiol; Pr-S-SG: glutathionylated protein; ROS: reactive oxygen species; RNS: reactive nitrogen species; GSNO: nitrosoglutathione; $OH^{\cdot}$: hydroxyl radical; Pr-$S^{\cdot}$: protein thiyl radical; $GS^{\cdot}$: glutathiyl radical.

2.2.3 Biological Consequences of Cysteine Glutathionylation

Glutathionylation results in a change in size and charge of the cysteine residue, where the addition of the tripeptide causes an increase in molecular weight by 305 Da and a net increase in negative charge contributed by the glycine residue of GSH (*65*). This structural and electronic change can alter the functional properties of the protein, particularly if the modified cysteine residue is located in a functionally important region. In the case of enzymes, this most often results in an inhibition of enzymatic activity when the modified cysteine is present in the active site, and is often observed in enzymes involved in energy metabolism (*63*). However, this is not always the case, as an increase in catalytic activity (e.g. phosphatase activity of carbonic anhydrase III) (*66*), alteration in DNA binding of transcription factors (*67, 68*), and modulation of protein stability (*69, 70*) have been documented.

Given that glutathionylation can modulate protein function, it is plausible that beyond individual proteins, glutathionylation can regulate more complex pathways and networks. Protein glutathionylation has often been described as analogous to phosphorylation, due to the many parallels between these two PTMs. Glutathionylation meets several criteria to be ascribed a regulatory role. Firstly, like phosphorylation, glutathionylation is reversible; secondary, it can be regulated enzymatically, as is phosphorylation via kinases; and finally, there is a certain degree of specificity, as only cysteines in a particular microenvironment and milleu are sufficiently reactive to undergo glutathionylation (*63*). However, there are unique characteristics of glutathionylation that differ from that of phosphorylation. For example, glutathionylation can occur non-enzymatically in response to a change in the cellular redox status, while phosphorylation is dependent on kinase activity. Also, while clear amino acid consensus sequences

that facilitate phosphorylation have been described, no such motifs have been found that predicts glutathionylation sites.

The redox-sensitive nature of glutathionylation renders it suitable as a regulatory mechanism to protect the cell against oxidative stress. For example, oxidative stress-induced glutathionylation of glyceraldehyde-3-phosphate dehydrogenase (GAPDH) and triosephosphate isomerase (TPIS) involved in glycolysis reroutes metabolic substrates such as glucose-6-phosphate into the pentose phosphate pathway, which is a key pathway responsible for generating nicotinamide adenine dinucleotide phosphate (NADPH), an electron donor for the antioxidant enzymes glutathione reductase and thioredoxin reductase, and is essential to maintain the reducing environment of the cytosol and counteract oxidative stress. Upon alleviation of oxidative stress, glutaredoxin reverses GAPDH and TPIS glutathionylation, restoring their catalytic activity (*71*). Apart from regulating metabolic fluxes, glutathionylation has also been described to modulate signal transduction pathways (kinases and Ras proteins), cell survival and apoptosis (caspases and death receptors), calcium homeostasis, protein degradation via ubiquitination, cellular migration (cytoskeletal proteins), energy metabolism (glycolysis, fatty acid β-oxidation, citric acid cycle and oxidative phosphorylation) and other pathways, which have been extensively reviewed (*64, 65*, *72*, *73*).

In some cases, glutathionylation may not have a discernible impact on protein function. It has been speculated that glutathionylation serves as a mechanism to protect cysteine thiols from permanent damage in oxidative stress. By forming mixed disulfides with redox-sensitive cysteine thiols, they are no longer available for further reactions such as irreversible oxidation to sulfonic acids (

Figure 2-2), which are resistant to cellular repair mechanisms and leads to proteasomal degradation (*73*). This allows the preservation of cysteine and protein integrity until the oxidative stress is overcome and deglutathionylation mechanisms restore the thiol to its basal state (*73*).

Figure 2-2 Cysteine thiol oxidation states. Free thiols can be oxidized to higher oxidation states such as sulfenic, sulfinic and sulfonic acids by ROS or RNS. Lower oxidation states such as sulfenic and sulfinic acids are reversible, while sulfonic acids are considered irreversible (*74*).

Unsurprisingly, dysregulation of cysteine glutathionylation has been reported in various disease conditions, particularly those which develop against a background of oxidative stress. These include diabetes, cardiovascular disease (e.g. myocardial infarction, cardiac hypertrophy and atherosclerosis), pulmonary disease (e.g. chronic obstructive pulmonary disease), malignancies, and neurodegenerative disease (e.g. Alzheimer's disease, Parkinson's disease, Huntington's disease and amyotrophic lateral sclerosis) (*64*). Importantly, aberrant oxidation, nitrosylation and glutathionylation of mitochondrial proteins feature prominently in these disease conditions. However, in such situations, it can be challenging to separate instances of cysteine glutathionylation that are drivers or mediators of pathogenesis from those that are a consequence of oxidative stress. Nevertheless, the role of cysteine glutathionylation as a functional PTM is undisputed, as glutathionylation has been observed under basal conditions to constitutively regulate the function of haemoglobin, γ-crystallin in human lens and actin (*73*).

2.2.4 Covalent Binding in APAP Hepatotoxicity

As described briefly in Chapter 1, early work on elucidating the mechanisms of APAP hepatotoxicity centered on covalent binding of the electrophilic reactive metabolite, NAPQI, to critical cellular proteins. The essential role of covalent binding as the initial trigger of the toxic insult is underscored by the attenuation and amplification of hepatotoxicity when covalent binding was diminished and magnified by the use of CYP450 inhibitors and inducers respectively, and peak levels of covalent binding consistently preceded hepatic necrosis by 1-2 h in rodent models (*15*). Clinical data further supports the association between covalent binding and toxicity, where patients experiencing the most severe toxicity exhibited the highest levels of APAP adducts in plasma, and adduct levels in serum correlate with hepatic transaminase levels in these patients (*75*).

Protein adduction by APAP is believed to trigger mitochondrial dysfunction, although the mechanism is currently unclear. This dysfunction is characterized by inhibition of mitochondrial respiration and enhanced mitochondrial oxidative stress (*76*). The major source of oxidative stress is derived from increased generation of superoxide from the electron transport chain, which can react with nitric oxide to form peroxynitrite, a potent oxidant and nitrating species. The increased mitochondrial oxidative stress, presumably due to APAP covalent binding, is thought to result in dissociation of the thioredoxin-apoptosis signal-regulating kinase 1 (ASK1) complex, leading to the activation of ASK1, which phosphorylates and activates c-jun-N-terminal kinase (JNK) (*77*). It has been suggested that oxidative stress or APAP adduction to GSTπ causes the release of sequestered JNK from GSTπ, permitting its phosphorylation (*77*). The activation of JNK leads to its translocation to the mitochondria, where it further amplifies mitochondrial ROS and peroxynitrite formation through a yet unknown

mechanism. The inhibition of JNK activation was reported to cause a profound suppression of peroxynitrite formation and mitochondrial ROS formation, and was a highly effective intervention against APAP toxicity (*76*), underscoring the importance of activated JNK to the mechanism of toxicity.

The exacerbated mitochondrial oxidative stress is thought to lead to mitochondrial DNA damage, loss of mitochondrial enzymatic activities and trigger the opening of the mitochondrial permeability transition pore (MPTP) (*78*). The latter causes the collapse of mitochondrial membrane potential needed to sustain ATP synthesis, as well as rupture of the outer mitochondrial membrane, triggering release of endonuclease G and apoptosis-inducing factor (AIF) which translocate to the nucleus and cause DNA fragmentation, culminating in necrotic cell death (*77*).

Despite the causal relationship between covalent binding and toxicity, it is clear that there remains a significant disconnect between the initial adduction event and the subsequent toxic sequelae. Over 30 hepatic proteins were found to form adducts with APAP, and diminished activities have been reported for some of these proteins, including glutamine synthetase, glutamate dehydrogenase, carbamyl phosphate synthetase, aldehyde dehydrogenase, N-10 formyltetrahydrofolate dehydrogenase and glutamate dehydrogenase (*75*, *79*). However the activities of these enzymes were only moderately inhibited (approximately 25%), insufficient to account for the toxicity observed with APAP. Adduction of glutathione peroxidase (GPx) produced the greatest decrease in its activity (60%) (*80*), however GPx-/- knockout mice did not exhibit an increase in liver injury after APAP treatment (*81*). Similarly, when examining the list of APAP protein adducts, no critical targets can be clearly ascribed to the toxicity manifestations and hallmarks of APAP-induced hepatotoxicity. The

inverse scenario, where hepatotoxic doses of APAP affect hepatic enzymatic activities without detectable adduct formation also supports the observation that covalent binding alone is an insufficient explanation for APAP toxicity (*82*). For example, calcium-dependent ATPases, plasma membrane Na^+-K^+-ATPase and protein phosphatase activities are decreased after exposure to toxic doses of APAP with no evidence of APAP binding to these enzymes (*82*).

2.2.5 APAP-induced Protein Glutathionylation

As described in Chapter 1, the effects of covalent binding are not confined to the overt effects of protein adduction, but can also manifest as covert, secondary changes to protein structure by inducing aberrant, endogenous PTMs. In the case of APAP, literature evidence suggests that in addition to overt protein adduct formation, APAP can induce protein glutathionylation as a form of indirect protein modification. In the late 1980s, a series of reports by Nelson and colleagues indicated that APAP treatment depleted free protein thiols *in vitro* in isolated rat hepatocytes (*83, 84*) and *in vivo* in mouse liver (*80*). Importantly, the loss in free protein thiols was much greater than the loss expected from detectable covalent binding of protein thiols alone (*80*). Treatment of liver homogenates from these mice with the chemical reductant dithiothreitol (DTT) restored free thiol levels, and it was concluded at the time that the loss of free protein thiols was due to thiol oxidation (*80*). Given that mitochondrial oxidative stress is a key event in the progression of APAP toxicity, thiol modifications are not unexpected. Interestingly, despite causing equivalent levels of covalent binding, the non-toxic regioisomer, AMAP did not result in a similar decrease in liver protein thiols in mice (*80*). Further work by Nelson and colleagues provided evidence of the formation of an *ipso* conjugate of NAPQI with GSH that interestingly, could react with another free thiol (e.g. of a protein cysteine), resulting in the

glutathionylation of that cysteine and release of APAP. The reverse could also happen, where an *ipso* protein adduct reacts with GSH resulting in protein glutathionylation and release of APAP (Figure 2-3). In other words, an *ipso* adduct derived from NAPQI conjugating either with a protein cysteine or GSH, can cross react with other free thiols of proteins and GSH, ultimately resulting in protein glutathionylation. Using papain as a model protein containing an active site cysteine, an *ipso* adduct of NAPQI with papain was formed that could be displaced by GSH to release free APAP from the protein adduct. Crucially, as a result of this reaction a mixed disulfide was formed between the thiol group of papain and GSH, resulting in its glutathionylation (*85*). This critical piece of evidence proved for the first time that covalent binding by APAP is not irreversible, but can in fact induce a secondary, covert protein modification in the form of glutathionylation via the formation of an *ipso* conjugate. More importantly, this work illustrates that contrary to current understanding, protein glutathionylation is not solely the result of oxidative stress (section 2.2.2), but can arise from the direct action of reactive metabolite formation and adduction to GSH or cellular proteins. Additionally, protein glutathionylation can occur early during the time-course of toxicity as long as an *ipso*-GSH adduct has been formed. Finally, this provides an explanation for the formation of glutathionylated proteins at sites (e.g. mitochondria) distant from the smooth endoplasmic reticulum where the CYP450 enzymes are localized. While NAPQI is inherently unstable and reacts rapidly with surrounding nucleophiles, it is possible that the *ipso*-GSH adduct is sufficiently stable to be transported to the mitochondria where it can glutathionylate proteins. Because the *ipso*-GSH adduct can also decompose to yield NAPQI within the physiological pH range, it serves as a latent carrier of NAPQI that causes covalent binding in other organelles. This is in contrast to the

accepted convention that marked protein adduction occurs only after severe GSH depletion. The mechanisms of APAP-induced protein glutathionylation via both adduction and oxidative stress are illustrated in Figure 2-3.

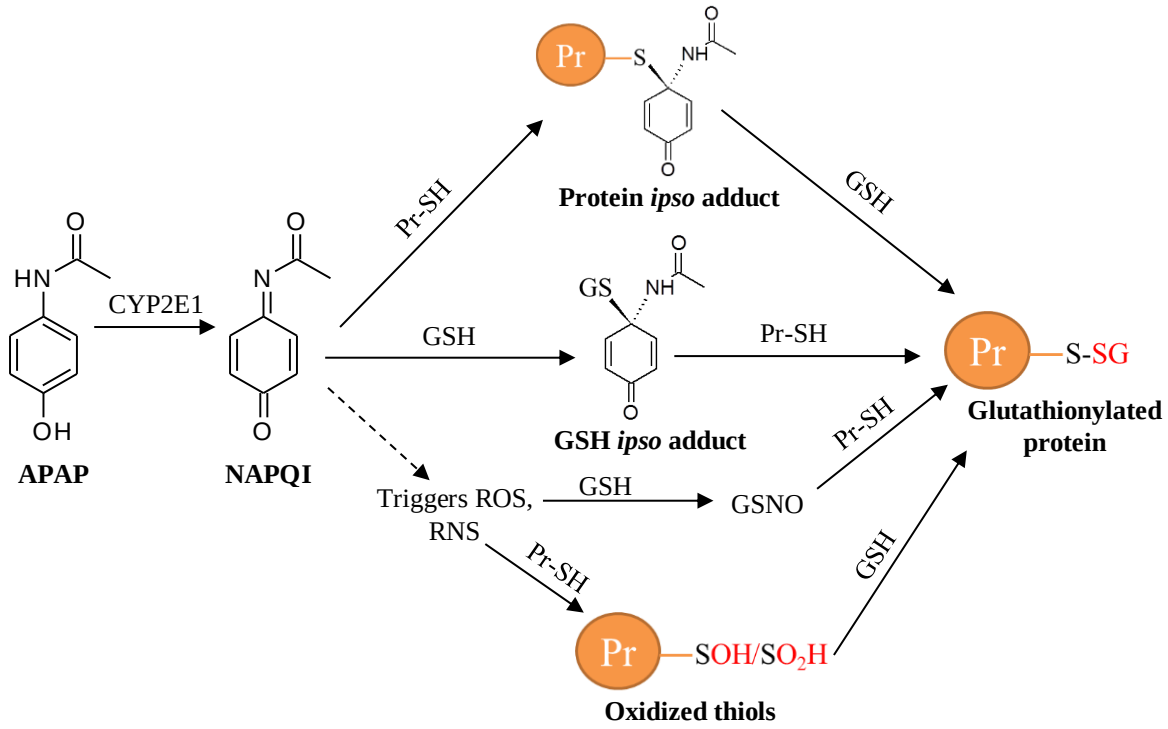

Figure 2-3 Mechanisms of APAP-induced protein glutathionylation secondary to NAPQI formation. Pr-SH: free protein thiol; ROS: reactive oxygen species; RNS: reactive nitrogen species; GSNO: nitrosoglutathione; Pr-S-SG: glutathionylated protein.

Yang *et al.* provided further evidence that APAP exposure led to protein glutathionylation in mice. Using immunohistochemical staining with anti-APAP and anti-GSH antibodies, it was demonstrated that regions of APAP adduct formation and protein glutathionylation overlapped (*86*), indicating a spatial correlation between protein adduction and glutathionylation. This substantiates the mechanism of APAP-induced protein glutathionylation proposed by Nelson and colleagues (*85*). The magnitude of glutathionylation was also time-dependent, and exhibited a zonal distribution by spreading outwards from the centrilobular region over time (*86*).

Despite strong evidence that APAP can induce aberrant protein glutathionylation, there are no comprehensive investigations on the suite of glutathionylated proteins and the pathways affected by APAP. This represents an important gap in our current mechanistic understanding of APAP toxicity.

2.2.6 Approaches to Detect Protein Glutathionylation

A variety of techniques have been developed to profile protein glutathionylation, and can be broadly divided into gel-based and non-gel-based protein separation approaches. The earliest gel-based methods utilize radiolabelled GSH incorporated with ^{3}H or ^{35}S, *in situ* metabolic labeling with ^{35}S-cysteine, anti-GSH antibodies or biotinylated GSH as handles to detect glutathionylated proteins, which are then separated using SDS-PAGE and detected by autoradiography, fluorescence, chemiluminescence or liquid chromatography/mass spectrometry (LC/MS) via excision of gel spots of interest (*87*). These approaches are constrained by several inherent limitations of gel-based separation which include (1) inter-gel variability, (2) demand for complicated software-based image analysis and normalization, (3) poor separation of hydrophobic proteins, (4) under-representation of membrane-bound proteins, (5) limited dynamic range, and (6) loss of low-abundance proteins (*88*). Thus such gel-based approaches are unsuitable for an unbiased, proteome-wide detection of glutathionylated proteins. These limitations can be overcome through the use of in-solution, LC/MS based techniques, which uses LC to separate proteins or digested peptides followed by detection using MS with high reproducibility, large dynamic range and sensitivity, and unbiased detection of hydrophobic or hydrophilic proteins. In this chapter, we aimed to first develop an LC/MS-based proteomic method capable of performing proteome-wide detection and identification of glutathionylated proteins. We then applied this novel

methodology to comprehensively profile and correlate the global change in protein glutathionylation to the toxicological manifestations of APAP hepatotoxicity.

2.3 Materials and Methods

2.3.1 Materials

Acetaminophen (APAP), 3′-hydroxyacetanilide (AMAP), 2-hydroxyethyl disulfide (HED), glyceraldehyde-3-phosphate, glyceraldehyde-3-phosphate dehydrogenase (GAPDH), sodium diethyldithiocarbamate trihydrate (DEDC), sodium arsenate, β-nicotinamide adenine dinucleotide (NAD+), reduced L-glutathione (GSH), dithiothreitol (DTT), sodium dodecyl sulfate (SDS), tris(2-carboyxethyl)phosphine (TCEP) hydrochloride, trichloroacetic acid (TCA) and hydrogen peroxide were purchased from Sigma-Aldrich (St Louis, MO, USA). NADPH tetrasodium salt was purchased from Santa Cruz Biotechnology (Santa Cruz, CA, USA). Glutaredoxin-1 C14S mutant (Grx1) was purchased from Cayman Chemicals (Ann Arbor, MA, USA). Tris base was purchased from J. T. Baker (Phillipsburg, NJ, USA). Glutathione reductase (GR) was obtained from Roche Diagnostics (Basel, Switzerland). Sequencing Grade Modified Trypsin was purchased from Promega (Madison, WI, USA). Pierce BCA protein assay kit was obtained from Thermo Scientific (Waltham, MA, USA). Phosphate-buffered saline was obtained from Vivantis (Selangor, Malaysia). Cleavable ICAT (isotope-coded affinity tag) reagents were purchased from ABSciex (Framingham, MA, USA). Filter-aided sample preparation (FASP) kits were obtained from Expedeon (Cambridgeshire, UK). Water was purified using a Milli-Q water purification system (Millipore, Bedford, MA, USA). All other solvents and reagents used were of analytical grades.

2.3.2 Development of the GluICAT Methodology to Profile Protein Glutathionylation

2.3.2.1 Indirect Monitoring of GAPDH Glutathionylation and Deglutathionylation

1 mg/mL GAPDH was incubated with 1.5 mM H_2O_2 and 5 mM GSH in 270 µL 100 mM Tris-HCl pH 7.6 buffer for 1 h at room temperature (25°C) to artificially induce glutathionylation of its thiol group (*89*). GAPDH activity was measured spectrophotometrically as previously described (*90*). Briefly, the assay mixture contained 0.2 mg/mL GAPDH, 0.1 mM EDTA, 1 mM NAD^+, 1 mM sodium arsenate and 1 mM glyceraldehyde-3-phosphate in 100 µL of 100 mM Tris-HCl pH 7.6. The activity of GAPDH was measured by following the conversion of NAD^+ to NADH at 340 nm for 15 min at room temperature (25°C). Glutathionylated GAPDH (GAPDH-SG) was then deglutathionylated using a mixture of 0.4 mM NADPH, 5 mM GSH, 0.9 U/mL GR, 0.1 U Grx1 and 0.1 mM EDTA at 37°C for 15 min and GAPDH activity was again assayed as described. Untreated native GAPDH activity was also measured as a baseline. Reduction of GAPDH-SG was performed using DTT as a positive control. All experiments were conducted in triplicates.

2.3.2.2 Direct Monitoring of GADPH Deglutathionylation

2.9 mg/mL GAPDH was glutathionylated by incubation with 6 mM H_2O_2 and 30 mM GSH in 550 µL 100 mM Tris-HCl pH 7.6 for 30 min. GAPDH-SG deglutathionylation was assayed spectrophotometrically as previously described (*91*). Briefly, the assay mixture contained 4.16 mg/mL GAPDH-SG, 10 mM NAPDH, 10 mM GSH, 4 U/mL GR, 0.5 U/mL Grx1, and 0.1 mM EDTA in 250 µL 100 mM Tris-HCl pH 7.6. The deglutathionylation process was monitored by following NAPDH consumption for 30 min at room temperature (25°C). Negative

control measurements were conducted in the absence of Grx1. A mixed disulfide formed between HED and GSH was used as a positive control for the deglutathionylation reaction as previously described (*92*). All experiments were conducted in triplicates.

2.3.2.3 GluICAT Processing of Glutathionylated GAPDH

GAPDH-SG was generated as described above and subjected to a modified OxICAT method (*93*), termed GluICAT. Briefly, 200 µL of ice-cold 100% (w/v) TCA was added to 100 µg of GAPDH-SG to quench thiol reactivity and precipitate GAPDH-SG. The precipitate was centrifuged at 14 000 *g* for 30 min at 4°C to obtain a pellet. Denaturing alkylation buffer (DAB) containing 6 M urea, 200 mM Tris-HCI, pH 8.5, 10 mM EDTA, and 4% (w/v) SDS was freshly prepared before use. The protein pellet was rinsed once with 500 µL ice-cold 10% (w/v) TCA, followed by a second rinse with 200 µL ice-cold 5% (w/v) TCA. The pellet was then redissolved in 80 µL DAB, followed by alkylation with light ICAT reagent for 2 h. GAPDH-SG was precipitated using 500 µL of -20°C cold acetone and maintained at -20°C overnight. The acetone precipitate was centrifuged at 14 000 *g* for 30 min at 4°C, and the protein pellet was rinsed twice with 500 µL -20°C cold acetone to remove excess light ICAT. The protein pellet was redissolved in DAB and prepared for the deglutathionylation step using FASP. The protein solution was loaded onto a spin column and SDS was removed by washing 3 times with 6 M urea, followed by 3 washes with 50 mM ammonium bicarbonate to condition the membrane for the subsequent deglutathionylation step. To effect deglutathionylation, the following mixture was added: 10 mM GSH, 10 mM NADPH, 4 U/mL GR and 0.5 U/mL Grx1 in 100 µL 50 mM ammonium bicarbonate and incubated for 1 h at 37°C on the spin column. Excess GSH was removed by washing 4 times with 50 mM ammonium bicarbonate.

Newly reduced cysteines were labelled with heavy ICAT reagent for 2 h, followed by removal of excess heavy ICAT by washing 3 times with 50 mM ammonium bicarbonate. Proteins were then digested with trypsin (1:30 trypsin/protein ratio) for 12-16 h at 37°C. Peptides were eluted with 50 mM ammonium bicarbonate and 0.5 M sodium chloride. Peptides were purified using avidin affinity chromatography according to manufacturer recommendations. Finally the biotin tag was cleaved and samples were desalted using UltraMicro Spin Columns (Nest Group, Southborough, MA, USA) before LC/MS/MS analysis. In a separate arm, Grx1 was omitted from the deglutathionylation mixture as a control. Experiments in each arm (with and without Grx1) were performed in triplicates.

2.3.2.4 LC/MS/MS Detection of GluICAT-treated Glutathionylated GAPDH.

LC/MS/MS was performed using an Ultimate 3000 nanoLC system (Dionex, Thermo Fisher Scientific, MA, USA) coupled to an ABSciex 5600 triple TOF (ABSciex, Framingham, MA, USA). A 50 cm × 75 µm i.d. Acclaim PepMap RSLC C_{18} column was employed (Dionex, Thermo Fisher Scientific, MA, USA). This column was connected to a spray tip (New Objectives, Woburn, MA), which was directly coupled to the nano-spray interface of the ABSciex 5600 tripleTOF mass spectrometer. Samples were loaded onto a trap column (Acclaim PepMap 100 C_{18}, 2cm × 75µm i.d., Dionex, Thermo Fisher Scientific, MA, USA) at a flow rate of 5 µL/min. After a 3 min wash with loading buffer (2/98 v/v of ACN/water with 0.1% formic acid), the system was switched into line with the C_{18} analytical capillary column. A step linear gradient of mobile phase B (2/98 v/v of water/ACN with 0.1% formic acid) from 5% to 25% over 10 min, 25%-60% for 9 min, and lastly, 60%-95% over 1 min at flow rate of 300 nL/min was utilized for this analysis. Third generation Nanospray Source was installed and other

instrumentation settings were as follows: Ionspray Voltage Floating (ISVF) = 2200 V, curtain gas (CUR) = 30, ion source gas 1 (GS1) = 12, interface heater temperature (IHT) = 125°C, declustering potential (DP) = 100 V, nebuliser current (NC) = 3 for nitrogen gas. Data was acquired using TOF MS + Hi Sensitivity product ion with Analyst TF 1.6 software (ABSciex, Framingham, MA, USA). TOF-MS scan (experiment 1) parameters were set as follows: 0.25 s TOF MS accumulation time in the mass range of 350 to 1250 Da was followed by MS/MS scan based on the following parameters: mass range was set at 100 to 1500 Da; switching criteria were set to ions greater than *m/z* = 350 and smaller than *m/z* = 1250 with charge state of 2 to 5 and an abundance threshold of greater than 120 cps. Former target ions were excluded for 4 s and also excluded after 1 repeat. The maximum number of candidate ions to monitor per cycle was 20 spectra with an accumulation time of 100 ms. All injections were performed in triplicates. The data was processed using ProteinPilot software 4.5 (ABSciex, Framingham, MA, USA) with database search using Uniprot Knowledgebase (UniProtKB).

2.3.3 GluICAT Profiling of APAP-induced Protein Glutathionylation in HepaRG Cells

2.3.3.1 Cell Culture

HepaRG cells at passage 13 were obtained from Biopredic International (Rennes, France). The cells were seeded in T-75 flasks at 2 x 10^6 undifferentiated cells/flask and grown to confluence in 710 growth medium (Biopredic, Rennes, France). The cells were cultured under a humidified atmosphere of 5% CO_2 at 37°C for 14 days before passaging. Medium was renewed every 3 days. Passages 13 and 14 were neither differentiated nor used as per the vendor's instructions. Differentiation was induced on day 14 by replacing 710 growth medium with 720

differentiation medium (Biopredic, Rennes, France) for a further two weeks. The cells were maintained up to 4 weeks after differentiation and were used at passage 15-18 for drug treatment and biochemical analyses.

2.3.3.2 Biochemical Analyses

All biochemical analyses were performed in a 96-well plate format. Undifferentiated HepaRG cells were seeded in 96-well plates at a density of 9000 cells/well and then differentiated as described above. After differentiation, 720 differentiation medium which contains 1.7% DMSO was replaced with HepaRG Tox Working Medium (Life Technologies, Carlsbad, CA, USA) which contains 0.5% DMSO and maintained for an additional week. Cells were treated with 30 mM APAP for 3, 6, 12 and 24 h for all assays. Cell viability was assessed by the CellTiter-Glo Luminescent Cell Viability Assay (Promega, Madison, WI, USA). Mitochondrial ROS generation was measured using MitoSOX Red Mitochondrial Superoxide Indicator (Life Technologies, Carlsbad, CA, USA). Mitochondrial superoxide was measured at λ_{ex} = 396 nm and non-specific oxidation at λ_{ex} = 510 nm, while λ_{em} = 580 nm was used for both (*94*). Cellular percentage GSH relative to untreated control as an indicator of cell health and oxidative stress was quantified using the luminescence-based system of GSH/GSSG-Glo Assay (Promega, Madison, WI, USA). All biochemical assays were performed according to manufacturer's instructions.

2.3.3.3 Drug Treatment of HepaRG Cells

Undifferentiated HepaRG cells were seeded in 6-well plates at a density of 2 × 10^5 cells/well, differentiated, and then maintained in HepaRG Tox Working Medium for 1 week in a total volume of 2 mL per well as mentioned above. To investigate the time-dependency of APAP glutathionylation, cells were treated with 30 mM APAP for 3, 6, 12 and 24 h. To determine dose-dependence of

APAP glutathionylation, cells were treated with 0.5 mM or 30 mM APAP for 3 h. To assess the influence of CYP2E1 bioactivation on APAP glutathionylation, cells were pretreated with DEDC, a CYP2E1 inhibitor for 30 min. The culture media was then replaced with DEDC-free media containing 0.5 mM APAP for 3 h. Cells were also treated with 30 mM AMAP for 6 h to determine the glutathionylation profile with the reported non-toxic regioisomer. For vehicle-treated controls, cells were treated with 1.9% ethanol for 6 h. Every vehicle or drug treatment was performed in triplicates across 3 cell passages.

2.3.3.4 Harvesting of Drug-treated Cell Lysate

Drug-containing culture media was removed from each well at the appropriate time-points and cells were rinsed twice with ice-cold phosphate-buffered saline. 500 µL of ice-cold 10% (w/v) TCA was added to each well and kept on ice for 10 min. Cells were then scraped and the suspension was transferred into a 1.5 mL microtube. Each well was rinsed with 500 µL of ice-cold 10% (w/v) TCA and added to the same microtube. All tubes were kept on ice for 30 min and vortexed every 10 min. Samples were stored at -80°C until further processing.

2.3.3.5 GluICAT Processing of Drug-treated Cell Lysate

Cell lysates were centrifuged at 14 000 *g* for 30 min at 4°C. Denaturing alkylation buffer (DAB) containing 6 M urea, 200 mM Tris-HCI, pH 8.5, 10 mM EDTA, and 4% (w/v) SDS was freshly prepared before use. The protein pellet was rinsed once with 500 µL ice-cold 10% (w/v) TCA, followed by a second rinse with 200 µL ice-cold 5% (w/v) TCA. The pellet was then redissolved in 80 µL DAB and quantified using the BCA assay according to manufacturer's instructions. An aliquot containing 100 µg of protein was removed and additional DAB added to a final volume of 80 µL. Subsequent sample processing steps were as described in

section 2.3.2.3. LC/MS/MS data acquisition of ICAT-tagged peptides was performed as described in section 2.3.2.4.

2.3.3.6 Data Analysis

Data from the biochemical analyses were expressed as mean ± standard deviation (SD). Comparisons between multiple groups were performed with one-way analysis of variance (ANOVA) followed by a post-hoc Bonferroni test, where $p < 0.05$ was considered significant.

For GluICAT data, all peptides identified from the database were filtered according to the following criteria: at least 95% confidence, and possessing a heavy-to-light (H:L) ratio of at least 0.01. Peptides that did not meet the criteria were removed from further analysis. Triplicate sets of peptide data from the vehicle-treated control arm were consolidated into a single mastersheet using Microsoft Excel 2010 (Microsoft Corporation, Redmond, WA, USA) and the average H:L value across the triplicates was obtained. The average control H:L values were then manually curated as follows: For each identified peptide with a complete set of 3 H:L values, the H:L values were inspected and where necessary the two closest values were retained. This was essential to minimize skew in average control H:L values due to outliers. In most cases, two of the three control H:L values were close numerically and the outlier was easily identified and discarded. In cases where a peptide was represented by less than 3 H:L values because it was not detected or identified with at least 95% confidence in one or more replicates, no further manual curation was performed. The consolidated list of control peptides (each now represented by a single average H:L value) was then used for comparison with drug-treated peptides as follows: Peptides were cross-matched between the consolidated control list and each drug-treated replicate, and the quotient of [H:L treated / H:L control] for each peptide in each

drug-treated replicate was obtained. A particular peptide was considered to be glutathionylated only if the [H:L treated / H:L control] ratio exceeded 1.5-fold in at least 2 of 3 drug-treated replicates. Only peptides satisfying this stringent criterion were subjected to further pathway analysis.

2.3.3.7 Pathway Analysis and Proteo-metabonomic Mapping

Glutathionylated proteins were submitted for pathway analysis and searched by UniProt accession number using the Reactome Pathway Knowledgebase pathway analysis tool (version 53) (*95*). A false discovery rate (FDR) less than 5% was applied to returned pathways. Manual inspection of the glutathionylated proteins to identify candidates relevant to the known manifestations of APAP toxicity was also performed. Enrichment analysis was also performed using the PANTHER and GO Ontology database to determine the molecular function and subcellular localization of glutathionylated proteins respectively. Proteo-metabonomic mapping was applied to pathways meeting the FDR criteria to ascertain the relevance of these pathways to APAP toxicology. A comprehensive literature search to retrieve references related to metabonomics studies of APAP toxicity was performed using the Web of Science portal (Thomson Reuters, Philadelphia, PA, USA) with a combination of the keywords ‘acetaminophen’, ‘paracetamol’ ‘metabolomics’, ‘metabonomics’, ‘metabolic’, ‘phenotyping’, ‘profiling’, ‘biomarkers’, ‘toxicity’, ‘hepatotoxicity’ or ‘dysfunction’. A list of metabolite biomarkers was compiled from reports of APAP-induced metabolic perturbations and used to manually annotate glutathionylated protein pathways obtained from the Reactome search. Mapped proteomic-metabonomic pathways were then examined for their biological relevance and relationship to the known manifestations of APAP toxicity.

2.3.3.8 Heat Map Representation of Glutathionylation Patterns

For the temporal study, H:L fold-change values of peptides that were glutathionylated in at least 1 time-point were compiled using Microsoft Excel 2010. The average H:L fold-change across triplicate experiments was calculated for each time-point, thus each peptide is described longitudinally during the period of 3-24 h post-APAP exposure by 4 H:L fold-change values. The dynamic range of H:L fold-change values between different peptides can vary up to 3 orders of magnitude (as some peptides are more extensively glutathionylated than others), which exceeds the dynamic range that can be represented using a colour gradient heat map. The average H:L fold-change value across the 4 time-points for each peptide was further computed for normalization purposes. In order to reduce the dynamic range, the H:L fold-change value of *each* time-point was normalized against the corresponding *average* H:L fold-change value (across the 4 time-points) for that particular peptide. To compare among high dose (30 mM) APAP, low dose (0.5 mM APAP) and DEDC followed by 0.5 mM APAP, H:L fold-change values for each peptide in the different treatment arms were normalized against that of 30 mM APAP. Normalized H:L fold-change values were then used to construct heat maps illustrating longitudinal, dose-dependent and bioactivation-dependent glutathionylation patterns.

2.4 Results

2.4.1 Development of GluICAT Methodology to Profile Protein Glutathionylation

2.4.1.1 Indirect Monitoring of GAPDH Glutathionylation and Deglutathionylation

The cycle of GAPDH glutathionylation and deglutathionylation is illustrated in Figure 2-4. Native GAPDH was exposed to H_2O_2 and GSH to induce glutathionylation of the redox-sensitive cysteine (Cys^{149}) within its active site, while subsequent treatment of glutathionylated GAPDH (GAPDH-SG) with Grx1 reversed this process. Figure 2-5 illustrates the corresponding GAPDH activity at each treatment stage. GAPDH activity as measured by NADH formation was highest prior to glutathionylation. The activity declined significantly after treatment with H_2O_2 and GSH, correlating with the glutathionylation of the redox-sensitive cysteine residue within its active site. The activity was partially restored after treatment with Grx1 that reversed the glutathionylation of its active site. This provided indirect evidence that GAPDH-SG was generated, and subsequently successfully deglutathionylated by Grx1. DTT-mediated reduction of GAPDH-SG was used as a positive control, as shown in Figure S1.

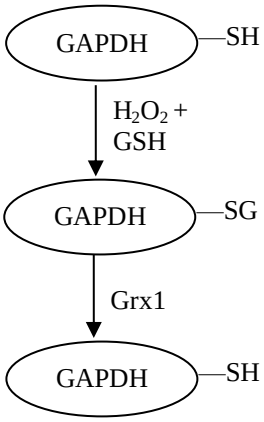

Figure 2-4 Cycle of glutathionylation and deglutathionylation of GAPDH.

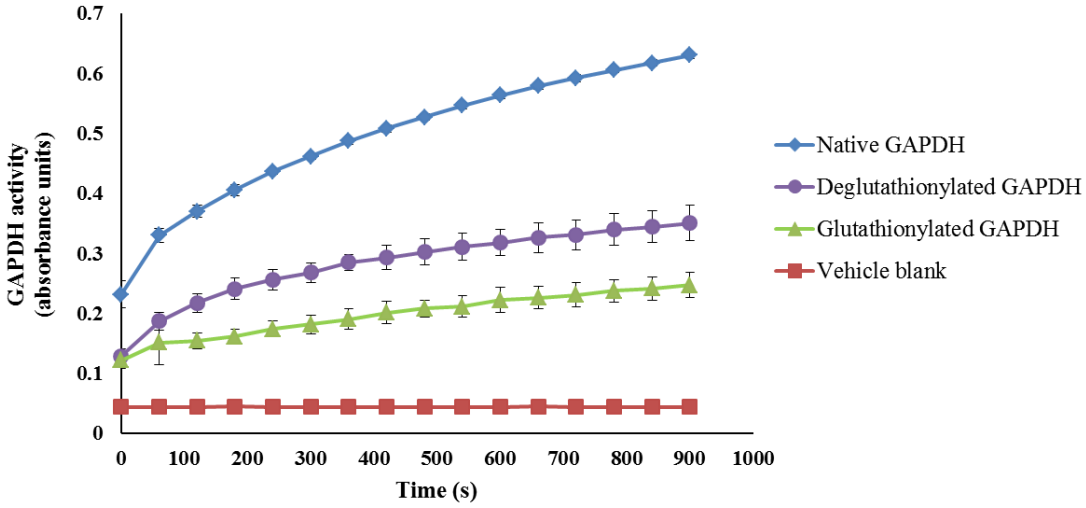

Figure 2-5 Indirect monitoring of GAPDH glutathionylation and deglutathionylation based on GAPDH activity (mean of 3 replicates).

2.4.1.2 Direct Monitoring of GAPDH-SG Deglutathionylation

During the process of deglutathionylation, GSH is oxidized to GSSG by Grx1, while GSSG is in turn reduced by GR using NADPH as a reducing equivalent (Figure 2-6). GAPDH-SG deglutathionylation could be directly measured by coupling the deglutathionylation activity of Grx1 to GR and tracking the consumption of NADPH by GR. Figure 2-7 shows the direct monitoring of GAPDH deglutathionylation by Grx1. The decline in absorbance at 340 nm relative to native GAPDH indicates that GAPDH-SG which serves as a substrate for Grx1 was successfully glutathionylated. Figure S2 shows the same positive control reaction using the mixed disulfide formed between HED and GSH as a substrate (HED-SG). Both the indirect and direct evidences of GAPDH-SG formation and deglutathionylation validated GAPDH-SG as a model glutathionylated protein for the subsequent GluICAT method development.

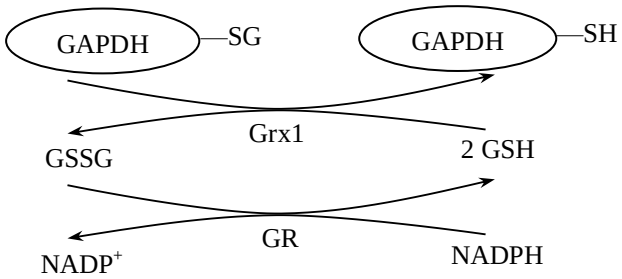

Figure 2-6 Deglutathionylation of GAPDH-SG mediated by Grx1 coupled to GSSG reduction by GR.

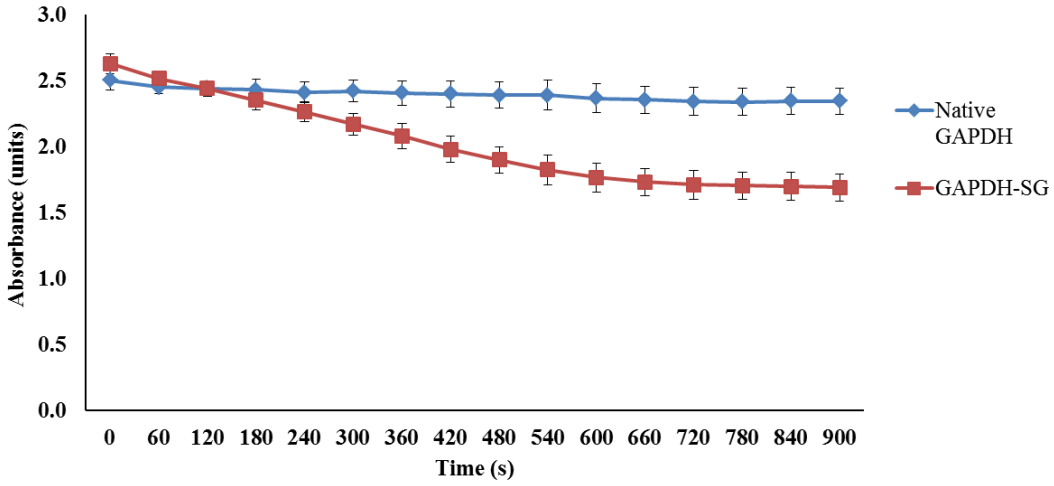

Figure 2-7 Direct monitoring of GAPDH-SG deglutathionylation based on NADPH consumption (mean of 3 replicates).

2.4.1.3 GluICAT profiling of glutathionylated GAPDH

In GluICAT, which was adapted from the OxICAT methodology introduced by Leichert *et al*. (*93*), reduced thiol groups are tagged with light ICAT, while glutathionylated thiol groups are selectively reduced by Grx1 and tagged with heavy ICAT (Figure 2-8). The ICAT molecule contains a thiol-reactive iodoacetamide moiety which binds irreversibly to reduced thiols. Light and heavy ICAT are so named because light ICAT contains a 9-carbon linker labelled with light ^{12}C isotope, while the linker in heavy ICAT is labelled with heavy ^{13}C isotope. For a singly-charged peptide, both light and heavy ICAT tagged peptides co-elute after LC separation but are separated by a mass difference of 9 Da during

MS detection. Figure 2-9 illustrates MS spectra for a doubly-charged peptide, where light and heavy ICAT tagged peptides are separated by 4.5 Da. This characteristic signature of co-elution appearing as twin peaks in the MS spectra is used to detect and quantitate the H:L ratio. The extent of glutathionylation of a particular peptide in a single sample is determined based on the heavy to light ICAT ratio, or H:L ratio, where a high H:L ratio indicates a greater degree of glutathionylation (*93*).

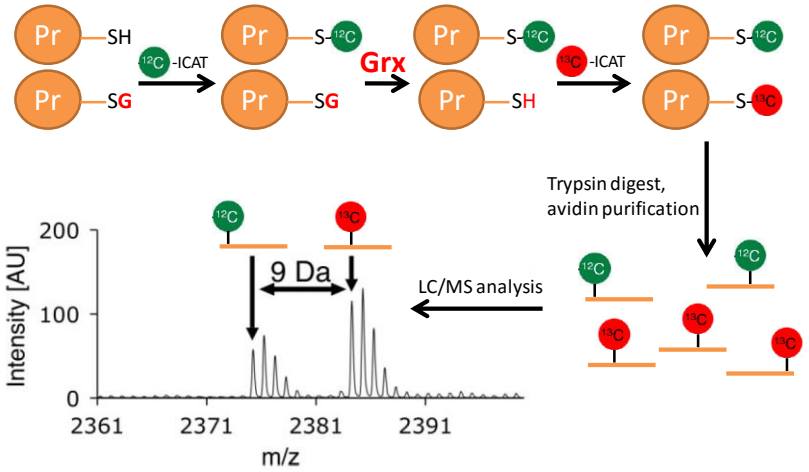

Figure 2-8 Schematic illustrating the GluICAT method. Reduced thiols are tagged with light ICAT, while glutathionylated thiols are reduced by Grx1 and tagged with heavy ICAT, and subsequently detected by LC/MS.

Figure 2-10 shows the overall heavy to light ratio (H:L) of the ICAT tagged GAPDH proteins post-GluICAT analysis. GAPDH (untreated), GAPDH-SG (with Grx1) and GAPDH-SG (without Grx1) yielded H:L ratios of 0.51, 8.79 and 3.61, respectively. GAPDH has a H:L ratio less than 1, indicating that most of the thiol groups of GAPDH were in the reduced form, and thus tagged with light ICAT. Relative to untreated GAPDH, GAPDH-SG (with Grx1) yielded a higher H:L ratio, suggesting that it was glutathionylated. In the OxICAT method, Leichert *et al.* used a threshold of H:L ratio greater than 1.5-fold relative to untreated controls to identify peptides that have been oxidized (*93*). Applying the same criteria for GluICAT, GAPDH-SG (with Grx1) yielded a H:L ratio 23-fold higher than

GAPDH (untreated), confirming that it was glutathionylated. In the absence of Grx1, no deglutathionylation of GAPDH-SG occurred and the glutathionylated thiol residues remained inaccessible to heavy ICAT, and the H:L ratio of GAPDH-SG (without Grx1) was significantly lower than that of GAPDH-SG (with Grx1). At first glance, it appeared peculiar that GAPDH-SG (without Grx1) yielded a higher H:L ratio than that of GAPDH (untreated). This was however not unexpected as compared to GAPDH (untreated), GAPDH-SG (without Grx1) possessed fewer reduced thiols to be tagged with light ICAT, thus the smaller denominator amplified the H:L ratio relative to GAPDH (untreated).

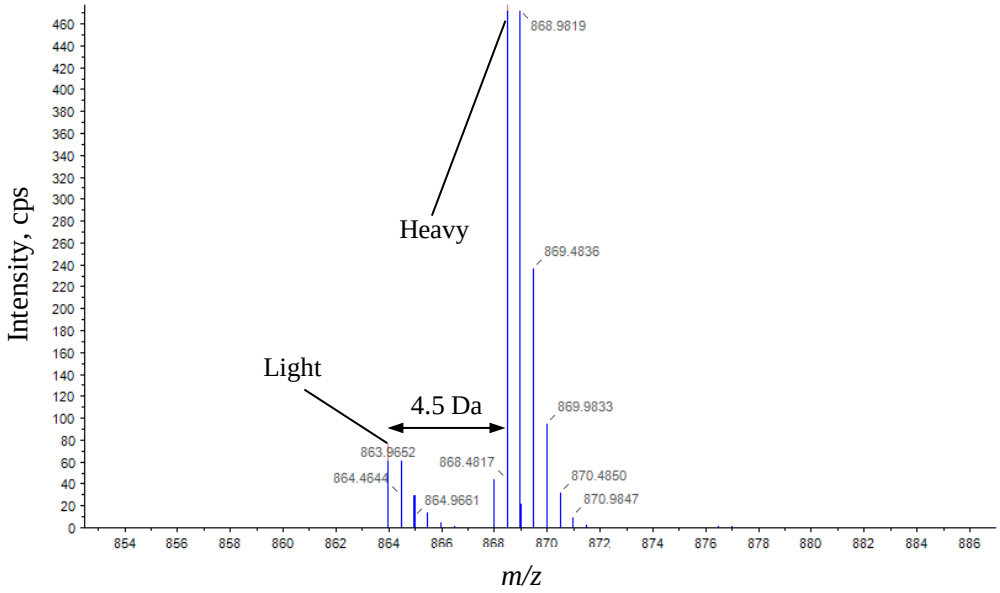

Figure 2-9 Representative MS spectrum for the tryptic GAPDH peptide VPTPNVSVVDLTCR obtained from GAPDH-SG. Shown here is the light and heavy ICAT tagged version of the tryptic peptide, separated by a mass difference of 4.5 Da as this peptide is doubly charged (+2). The H:L ratio is 7.81.

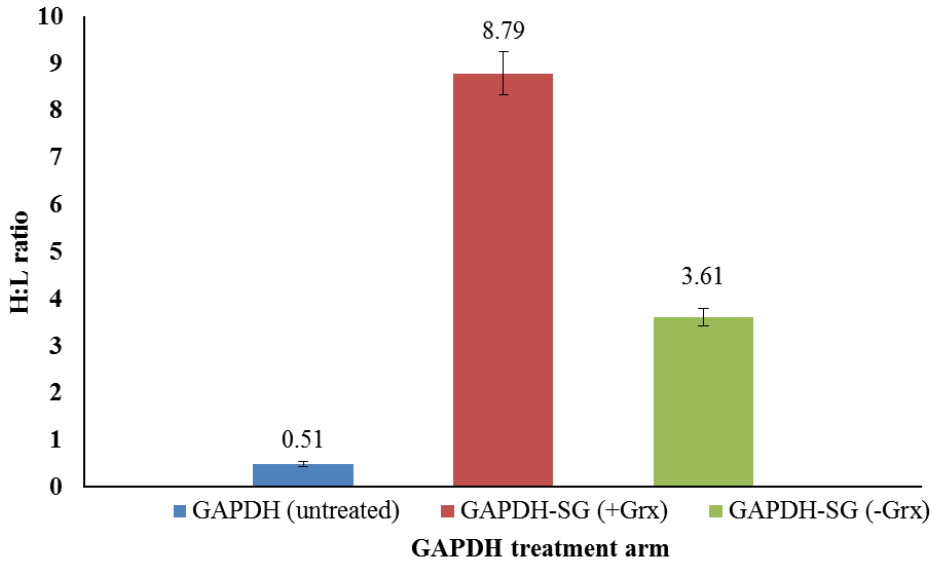

Figure 2-10 H:L ratios for GAPDH (untreated) and GAPDH-SG (with (+) or without (-) Grx1) from the tryptic GAPDH peptide VPTPNVSVVDLTCR (mean of 3 replicates).

2.4.2 Time-course of APAP Toxicity in HepaRG Cells

Measurements of biochemical perturbations known to be caused by APAP were performed in conjunction with the time-points monitored for APAP-induced glutathionylation (Figure 2-11). Cell viability and GSH levels declined in a time-dependent manner, significantly from 3 h onwards. Oxidative stress as measured by superoxide and non-specific oxidant formation increased in a time-dependent manner, significantly from 12 h onwards.

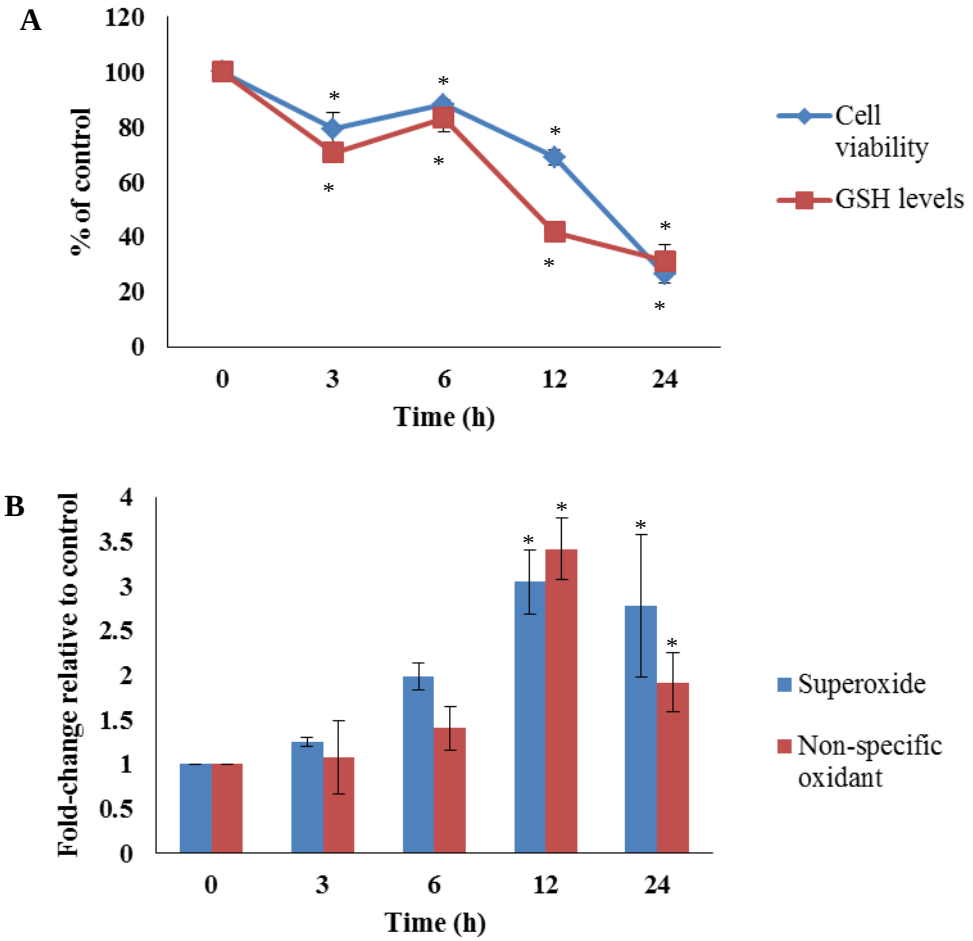

Figure 2-11 Time-course of (A) cell viability and GSH levels and (B) superoxide and non-specific oxidant formation in HepaRG cells exposed to 30 mM APAP over 24 h. An asterisk indicates $p < 0.05$ compared to the control.

2.4.3 GluICAT Profiling of APAP-induced Protein Glutathionylation in HepaRG Cells

2.4.3.1 Pathway Analysis of APAP-induced Glutathionylation

Peptides must exhibit a H:L ratio greater than 1.5-fold compared to the control in at least 2 of 3 replicates to be considered candidate glutathionylated peptides. Instead of merely taking the average H:L fold-change across three replicates, the fold-change in each individual replicate was considered. This additional criterion (where peptides must exceed the 1.5-fold threshold in at least 2 replicates) was important to minimize the effects of skew of the mean due to an abnormally high or low H:L fold-change in any one replicate. Without this criterion, we observed

instances where the average H:L fold-change was skewed above the 1.5-fold threshold due to a single outlier, while the other replicates had low H:L values below the 1.5-fold threshold, and this might lead to peptides falsely identified as glutathionylated. For peptides that satisfied the criteria, average H:L fold-change values were manually inspected for each peptide and outliers removed where necessary.

A total of 898 peptides corresponding to 588 proteins were found to be glutathionylated in any one of the 4 time-points monitored (3, 6, 12 or 24 h of APAP exposure). A complete list of glutathionylated proteins is provided in Table S1. Figure 2-12 illustrates the distribution of protein function for the glutathionylated proteins. 49% of these proteins exhibit catalytic activity, while 29% are mitochondrial proteins and 13% reside in the endoplasmic reticulum. Pathway analysis of glutathionylated proteins using Reactome revealed three groups of biological processes that were aberrantly glutathionylated by APAP: (1) energy metabolism, (2) protein turnover, and (3) defense against cellular stress. *Energy metabolism* broadly encompassed proteins involved in glycolysis, import of fatty acids across the mitochondrial membrane, mitochondrial fatty acid β-oxidation, pyruvate metabolism, citric acid cycle, respiratory electron transport and ATP synthesis, gluconeogenesis, pentose phosphate pathway and fatty acyl-CoA biosynthesis. *Protein turnover* involved proteins participating in amino acid metabolism, protein initiation, elongation and termination, protein folding and protein degradation. *Defense against cellular stress* included proteins responsible for detoxification of reactive oxygen species, phase I and II metabolism, GSH and sulfur amino acid metabolism, and cellular response to heat stress. Further manual analysis of the glutathionylated proteins revealed proteins relevant to calcium dynamics and formation of the MPTP. Proteins and peptides found to be

glutathionylated by APAP temporally in these three groups are summarized in Table 2-1, Table 2-2, Table 2-3 and Table 2-4. Collectively, these three groups comprise 239 peptides and 179 proteins, approximately 27% and 30% of total glutathionylated peptides and proteins respectively.

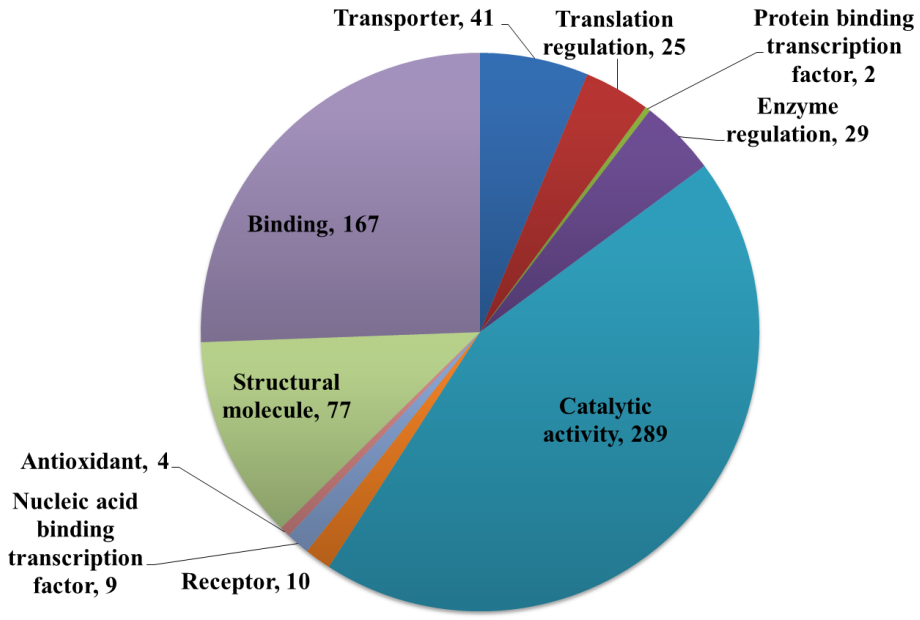

Figure 2-12 Distribution of protein functions for proteins glutathionylated by APAP at any time-point. Numerals indicate number of proteins in each category. Some proteins may be listed in more than one category.

Table 2-1 Glutathionylation profile of proteins involved in energy metabolism as a function of time. Values in red represent the average H:L fold-change of peptides normalized to the control that exceed a 1.5-fold threshold across at least 2 replicates.

Pathway	Accession	Description	Gene Symbol	Peptide	H:L fold-change across time (h)			
					3	6	12	24
Glycolysis	P30153	Serine/threonine-protein phosphatase 2A 65 kDa regulatory subunit A alpha isoform	2AAA	EFCENLSADCR	1.35	-	1.14	2.49
				LNIISNLDCVNEVIGIR	1.08	1.71	1.24	0.86
	Q14738	Serine/threonine-protein phosphatase 2A 56 kDa regulatory subunit delta isoform	2A5D	CVSSPHFQVAER	1.70	-	1.12	-
	P04075	Fructose-bisphosphate aldolase A	ALDOA	ALANSLACQGK	1.96	0.79	0.94	1.08
	P60174	Triosephosphate isomerase	TPIS	IAVAAQNCYK	1.76	1.62	0.98	0.84
	P00558	Phosphoglycerate kinase 1	PGK1	ACANPAAGSVILLENLR	1.26	0.89	1.01	36.18
	P06733	Alpha-enolase	ENOA	QIGSVTESLQACK	9.70	7.15	5.49	0.07
	P14618	Pyruvate kinase PKM	KPYM	AAMADTFLEHMCR	0.90	1.60	1.17	0.50
				GIFPVLCK	0.99	1.74	1.07	0.59
				NTGIICTIGPASR	1.65	0.85	0.96	1.08
Import of palmitoyl-CoA into the mitochondrial matrix	O43772	Mitochondrial carnitine/acylcarnitine carrier protein	MCAT	CLLQIQASSGESK	8.76	0.93	1.13	0.99
	P50416	Carnitine O-palmitoyltransferase 1, liver isoform	CPT1A	FCLTYEASMTR	6.17	-	0.04	0.04
Mitochondrial fatty acid β-oxidation	P28330	Long-chain specific acyl-CoA dehydrogenase, mitochondrial	ACADL	AFVDNCLQLHEAK	1.35	1.89	1.41	-
	P49748	Very long-chain specific acyl-CoA dehydrogenase, mitochondrial	ACADV	CLTEPSSGSDAASIR	3.15	3.44	2.47	1.27
				GLQVPSELGGVGLCNTQYAR	2.33	1.21	1.43	1.18
	P55084	Trifunctional enzyme subunit beta, mitochondrial	ECHB	FNNWGGSLSLGHPFGATGCR	3.07	-	2.97	-
	P30084	Enoyl-CoA hydratase, mitochondrial	ECHM	ALNALCDGLIDELNQALK	1.63	0.93	1.06	0.71
	Q16698	2,4-Dienoyl-CoA reductase, mitochondrial	DECR	VHAIQCDVRDPDMVQNTVSELIK	2.12	2.14	2.11	1.16

Pathway	Accession	Description	Gene Symbol	Peptide	H:L fold-change across time (h)			
					3	6	12	24
	P05165	Propionyl-CoA carboxylase alpha chain, mitochondrial	PCCA	MADEAVCVGPAPTSK	2.72	1.39	1.60	0.98
	P05166	Propionyl-CoA carboxylase beta chain, mitochondrial	PCCB	AFENDVDALCNLR	5.56	5.62	-	-
				CADFGMAADK	1.74	0.99	0.87	1.42
	Q96PE7	Methylmalonyl-CoA epimerase, mitochondrial	MCEE	DCGGVLVELEQA	85.5	-	1.00	-
Pyruvate metabolism	P09622	Dihydrolipoyl dehydrogenase, mitochondrial	DLDH	ILGPGAGEMVNEAALALEYGAS CEDIAR	3.26	2.92	2.64	-
	P08559	Pyruvate dehydrogenase E1 component subunit alpha, somatic form, mitochondrial	ODPA	VDGMDILCVR	2.74	1.24	1.60	1.05
	P10515	Dihydrolipoyllysine-residue acetyltransferase component of pyruvate dehydrogenase complex, mitochondrial	ODP2	ASALACLK	2.73	2.58	1.13	0.51
Citric acid cycle	O75390	Citrate synthase, mitochondrial	CISY	LPCVAAK	5.94	1.28	1.46	1.79
	Q99798	Aconitate hydratase, mitochondrial	ACON	CTTDHISAAGPWLK	1.63	1.45	1.38	0.85
	P51553	Isocitrate dehydrogenase [NAD] subunit gamma, mitochondrial	IDH3G	HACVPVDFEEVHVSSNADEEDIR	1.11	1.59	0.94	1.03
				LGDGLFLQCCR	1.94	-	-	-
	P48735	Isocitrate dehydrogenase [NADP], mitochondrial	IDHP	DLAGCIHGLSNVK	1.34	1.87	1.46	1.24
	P50213	Isocitrate dehydrogenase [NAD] subunit alpha, mitochondrial	IDH3A	CSDFTEEICR	1.93	0.03	0.99	2.04
	Q02218	2-Oxoglutarate dehydrogenase, mitochondrial	ODO1	DVVVDLVCYR	1.90	3.06	1.18	1.27
				CSTPGNFFHVLR	3.62	-	-	-
	P09622	Dihydrolipoyl dehydrogenase, mitochondrial	DLDH	ILGPGAGEMVNEAALALEYGAS CEDIAR	3.26	2.92	2.64	-
	P53597	Succinyl-CoA ligase [ADP/GDP-forming] subunit alpha, mitochondrial	SUCA	IICQGFTGK	1.30	1.00	1.19	2.47
				LIGPNCPGVINPGECK	1.63	-	1.09	0.29
	P31040	Succinate dehydrogenase [ubiquinone] flavoprotein subunit, mitochondrial	SDHA	GLSEAGFNTACVTK	1.86	-	1.73	1.15
				GVIALCIEDGSIHR	1.23	1.78	1.00	0.37

Pathway	Accession	Description	Gene Symbol	Peptide	H:L fold-change across time (h)			
					3	6	12	24
	P21912	Succinate dehydrogenase [ubiquinone] iron-sulfur subunit, mitochondrial	SDHB	CGPMVLDALIK	2.24	3.92	1.85	0.82
	Q99643	Succinate dehydrogenase cytochrome b560 subunit, mitochondrial	C560	SLCLGPALIHTAK	1.21	2.46	1.68	1.06
	P40926	Malate dehydrogenase, mitochondrial	MDHM	GCDVVVIPAGVPR	2.49	1.33	1.14	1.30
Respiratory electron transport, ATP synthesis	P28331	NADH-ubiquinone oxidoreductase 75 kDa subunit, mitochondrial	NDUS1	DCFIIYQGHHGDVGAPIADVILPGAAYTEK	1.85	1.14	-	1.26
	O95299	NADH dehydrogenase [ubiquinone] 1 alpha subcomplex subunit 10, mitochondrial	NDUAA	CEVLQYSAR	2.32	-	1.29	-
	P49821	NADH dehydrogenase [ubiquinone] flavoprotein 1, mitochondrial	NDUV1	GAGAYICGEETALIESIEGK	1.99	1.94	8.73	-
	P31040	Succinate dehydrogenase [ubiquinone] flavoprotein subunit, mitochondrial	SDHA	GLSEAGFNTACVTK	1.86	-	1.73	1.15
				GVIALCIEDGSIHR	1.23	1.78	1.00	0.37
	P21912	Succinate dehydrogenase [ubiquinone] iron-sulfur subunit, mitochondrial	SDHB	CGPMVLDALIK	2.24	3.92	1.85	0.82
	Q99643	Succinate dehydrogenase cytochrome b560 subunit, mitochondrial	C560	SLCLGPALIHTAK	1.21	2.46	1.68	1.06
	P31930	Cytochrome b-c1 complex subunit 1, mitochondrial	QCR1	NALVSHLDGTTPVCEDIGR	1.38	1.00	1.22	2.12
				SICYAETGLLGAHFVCDR	5.21	-	1.44	0.93
	P22695	Cytochrome b-c1 complex subunit 2, mitochondrial	QCR2	ENMAYTVECLR	2.53	2.34	2.00	2.55
				NALANPLYCPDYR	2.98	1.25	1.20	5.83
	P08574	Cytochrome c1, heme protein, mitochondrial	CY1	HLVGVCYTEDEAK	1.16	1.88	0.78	0.43
	P24539	ATP synthase F(0) complex subunit B1, mitochondrial	AT5F1	CIADLK	1.88	1.47	1.39	-
	P13804	Electron transfer flavoprotein subunit alpha, mitochondrial	ETFA	LGGEVSCLVAGTK	0.94	1.03	1.45	2.98
				TIYAGNALCTVK	3.90	1.20	2.59	1.32
	P38117	Electron transfer flavoprotein subunit beta	ETFB	HSMNPFCEIAVEEAVR	1.26	1.34	1.39	2.09
	Q16134	Electron transfer flavoprotein-ubiquinone oxidoreductase, mitochondrial	ETFD	QNVAVNELCGR	1.25	8.49	1.23	-

Pathway	Accession	Description	Gene Symbol	Peptide	H:L fold-change across time (h)			
					3	6	12	24
	P42704	Leucine-rich PPR motif-containing protein, mitochondrial	LPPRC	FCPAGVYEFVPVEQGDGFR	105	131	117	137
				LEDVALQILLACPVSK	1.05	1.89	1.63	1.38
				LIASYCNVGDIEGASK	1.61	1.10	1.33	1.18
Gluconeogenesis	P00505	Aspartate aminotransferase, mitochondrial	AATM	TCGFDFTGAVEDISK	2.88	1.02	0.95	0.48
				VGAFTMVCK	2.20	1.17	0.66	0.70
				ACANPAAGSVILLENLR	1.26	0.89	1.01	36.18
	Q16822	Phosphoenolpyruvate carboxykinase [GTP], mitochondrial	PCKGM	YVAAAFPSACGK	0.99	1.17	1.83	3.21
	P40925	Malate dehydrogenase, cytoplasmic	MDHC	MGVLDGVLMELQDCALPLLK	7.25	-	6.29	-
				GCDVVVIPAGVPR	2.49	1.33	1.14	1.30
	P04075	Fructose-bisphosphate aldolase A	ALDOA	ALANSLACQGK	1.96	0.79	0.94	1.08
	P06733	Alpha-enolase	ENOA	QIGSVTESLQACK	9.70	7.15	5.49	0.07
	P00558	Phosphoglycerate kinase 1	PGK1	ACANPAAGSVILLENLR	1.26	0.89	1.01	36.18
	P11498	Pyruvate carboxylase, mitochondrial	PYC	GLYAAFDCTATMK	4.96	3.14	3.48	4.84
	P53007	Tricarboxylate transport protein, mitochondrial	TXTP	GIGDCVR	1.48	1.59	1.14	0.80
	P40926	Malate dehydrogenase, mitochondrial	MDHM	GCDVVVIPAGVPR	2.49	1.33	1.14	1.30
	P60174	Triosephosphate isomerase	TPIS	IAVAAQNCYK	1.76	1.62	0.98	0.84
Pentose phosphate pathway	P11413	Glucose-6-phosphate 1-dehydrogenase	G6PD	DNIACVILTFK	3.47	1.96	1.27	0.84
				DVMQNHLLQMLCL	2.88	1.26	1.01	1.45
				LILDVFCGSQMHF	2.33	1.09	1.34	0.92
	P52209	6-Phosphogluconate dehydrogenase, decarboxylating	6PGD	MVHNGIEYGDMQLICEAYHLMK	6.29	-	9.79	-
				SAVENCQDSWR	1.77	2.05	1.50	0.97
	P29401	Transketolase	TKT	CSTFAAFFTR	2.24	0.98	1.06	1311
				AIIVDGHSVEELCK	1.92	3.77	1.18	0.68
	P37837	Transaldolase	TALDO	ALAGCDFLTISPK	1.76	2.10	1.10	0.66
Fatty acyl-CoA biosynthesis	P49327	Fatty acid synthase	FAS	AALQEELQLCK	1.09	1.82	1.14	2.34
				AAPLDSIHSLAAYYIDCIR	3.06	4.64	2.65	2.78
				ACLDTAVENMPSLK	15.8	5.37	0.98	1.21
				AINCATSGVVGLVNCLR	4.68	0.09	0.48	0.09

Pathway	Accession	Description	Gene Symbol	Peptide	H:L fold-change across time (h)			
					3	6	12	24
				CTVFHGAQVEDAFR	1.72	1.54	1.16	0.96
				LSIPTYGLQCTR	2.79	1.30	0.95	1.41
				MASCLEVLDLFLNQPH	1.53	3.60	1.15	1.18
				SFYGSTLFLCR	1.06	1.52	0.98	1.31
				TGGAYGEDLGADYNLSQVCDGK	2.85	2.07	2.40	0.04
	P33121	Long-chain-fatty-acid--CoA ligase 1	ACSL1	AAEGEGEVCVK	1.17	1.35	1.14	1.94
				CGVEVTSMK	1.73	1.02	1.22	1.95
				GFEGSFEELCR	2.12	2.16	1.39	1.31
				GIQVSNNGPCLGSR	2.61	1.39	1.33	3.57
				LIAIVVPDVETLCSWAQK	2.42	3.07	1.59	1.24
	O95573	Long-chain-fatty-acid--CoA ligase 3	ACSL3	NTPLCDSFVFR	3.30	1.36	1.21	1.48
	O60488	Long-chain-fatty-acid--CoA ligase 4	ACSL4	TALLDISCVK	1.12	1.63	1.39	1.39
	Q9ULC5	Long-chain-fatty-acid--CoA ligase 5	ACSL5	GLAVSDNGPCLGYR	1.14	1.09	1.65	2.39
				IVQAVVYSCGAR	1.40	1.43	1.37	2.38
	P53396	ATP-citrate synthase	ACLY	AVQGMLDFDYVCSR	1.02	1.13	1.26	1.86
				FICTTSAIQNR	2.11	1.45	1.57	-
	P53007	Tricarboxylate transport protein, mitochondrial	TXTP	GIGDCVR	1.48	1.59	1.14	0.80
	Q53GQ0	Very-long-chain 3-oxoacyl-CoA reductase	DHB12	MININILSVCK	1.52	2.32	1.80	0.46

N.B. '-' denotes not detected in at least 2 of 3 replicates

Table 2-2 Glutathionylation profile of proteins involved in protein turnover as a function of time. Values in red represent the average H:L ratio of peptides normalized to the control that exceed a 1.5-fold threshold across at least 2 replicates.

Pathway	Accession	Description	Gene Symbol	Peptide	H:L fold-change across time (h)			
					3	6	12	24
Amino acid metabolism	Q9UDR5	Alpha-aminoadipic semialdehyde synthase, mitochondrial	AASS	AGGILQEDISEACLILGVK	1.05	1.65	1.13	0.72
				QLLCDLVGISPSSEHDVLK	1.08	4.00	0.86	1.34
	P35520	Cystathionine beta-synthase	CBS	CIIVMPEK	1.69	-	-	-
	Q14353	Guanidinoacetate N-methyltransferase	GAMT	TEVMALVPPADCR	1.29	-	1.21	2.72
	P30038	Delta-1-pyrroline-5-carboxylate dehydrogenase, mitochondrial	AL4A1	CDDSVGYFVEPCIVESK	3.29	-	1.83	2.55
	P31327	Carbamoyl-phosphate synthase [ammonia], mitochondrial	CPSM	SAYALGGLGSGICPNR	1.68	0.98	1.17	-
	P23526	Adenosylhomocysteinase	SAHH	QAQYLGMSCDGPFKPDHYR	5.12	-	-	-
	O15382	Branched-chain-amino-acid aminotransferase, mitochondrial	BCAT2	EVFGSGTACQVCPVHR	8.21	-	-	-
				LCLPSFDK	13.63	1.06	1.27	1.14
				LELLECIR	12.00	4.60	2.40	0.90
	Q9UBQ7	Glyoxylate reductase/hydroxypyruvate reductase	GRHPR	GVAGAHGLLCLLSDHVDK	1.28	2.27	1.39	1.13
				NCVILPH	1.58	1.08	1.33	1.14
	P09622	Dihydrolipoyl dehydrogenase, mitochondrial	DLDH	ILGPGAGEMVNEAALALEYGAS CEDIAR	3.26	2.92	2.64	-
	P19623	Spermidine synthase	SPEE	QFCQSLFPVVAY	1.81	-	-	-
	P00505	Aspartate aminotransferase, mitochondrial	AATM	TCGFDFTGAVEDISK	2.88	1.02	0.95	0.48
				VGAFTMVCK	2.20	1.17	0.66	0.70
	P21953	2-oxoisovalerate dehydrogenase subunit beta, mitochondrial	ODBB	GLLLSCIEDK	1.92	2.23	1.25	-
	P34896	Serine hydroxymethyltransferase, cytosolic	GLYC	YYGGAEVVDEIELLCQR	2.09	1.39	1.71	1.40
	Q02218	2-oxoglutarate dehydrogenase, mitochondrial	ODO1	DVVVDLVCYR	1.90	3.06	1.18	1.27

Pathway	Accession	Description	Gene Symbol	Peptide	H:L fold-change across time (h)			
					3	6	12	24
				CSTPGNFFHVLR	3.62	-	-	-
	P04424	Argininosuccinate lyase	ARLY	CAGLLMTLK	3.12	-	1.47	-
				MAEDLILYCTK	4.71	3.25	1.50	2.96
	P49189	4-trimethylaminobutyraldehyde dehydrogenase	AL9A1	SPLIIFSDCDMNNAVK	1.58	1.15	1.12	1.20
	P48506	Glutamate--cysteine ligase catalytic subunit	GSH1	GYVSDIDCR	104	44.4	46.1	1.00
	P31937	3-hydroxyisobutyrate dehydrogenase, mitochondrial	3HIDH	HGYPLIIYDVFPDACK	2.02	1.05	1.06	0.90
Eukaryotic translation initiation, elongation, termination	P25398	40S ribosomal protein S12	RS12	LVEALCAEHQINLIK	1.37	2.89	1.27	1.00
				QAHLCVLASNCDEPMYVK	3.41	-	1.30	1.4
	P23396	40S ribosomal protein S3	RS3	ACYGVLR	1.90	1.17	1.26	1.09
				GCEVVVSGK	1.81	1.93	1.27	1.24
				GLCAIAQAESLR	2.22	1.19	3.21	3.25
	P61247	40S ribosomal protein S3a	RS3A	LFCVGF	2.31	4.25	1.41	-
	P62241	40S ribosomal protein S8	RS8	NCIVLIDSTPYR	1.37	2.46	1.07	0.77
	P05388	60S acidic ribosomal protein P0	RLA0	AGAIAPCEVTVPAQNTGLGPEK	2.22	0.93	1.38	2.13
				CFIVGADNVGSK	1.8	0.58	0.84	0.50
				NVASVCLQIGYPTVASVPH	3.03	1.20	1.63	0.94
	P62906	60S ribosomal protein L10a	RL10A	VLCLAVAVGH	4.01	-	1.36	-
				VLCLAVAVGHVK	3.23	-	0.59	-
	P30050	60S ribosomal protein L12	RL12	CTGGEVGATSALAPK	3.43	1.53	1.32	0.55
	P39023	60S ribosomal protein L3	RL3	TVFAEHISDECK	1.39	1.09	1.62	1.28
				VACIGAWHPAR	1.94	0.97	2.48	-
				YCQVIR	2.26	0.94	-	-
	P62910	60S ribosomal protein L32	RL32	ELEVLLMCNK	1.70	1.34	1.37	1.32

Pathway	Accession	Description	Gene Symbol	Peptide	H:L fold-change across time (h)			
					3	6	12	24
	P36578	60S ribosomal protein L4	RL4	GPCIIYNEDNGIIK	1.37	0.82	1.88	1.01
				SGQGAFGNMCR	1.73	-	1.56	1.94
	P46777	60S ribosomal protein L5	RL5	AAAYCTGLLLAR	1.64	0.82	1.11	1.48
				DIICQIAY	2.33	0.79	1.48	0.85
				IEGDMIVCAAYAHELPK	2.61	2.32	1.56	0.88
				VGLTNYAAAYCTGLLLAR	2.09	2.02	-	-
	Q01518	Adenylyl cyclase-associated protein 1	CAP1	CVNTTLQIK	2.07	0.79	1.08	0.35
				INSITVDNCK	1.49	1.8	1.07	0.41
	P12814	Alpha-actinin-1	ACTN1	CQLEINFNTLQTK	92.6	6.89	11.6	5.18
				DGLGFCALIHR	0.99	2.19	0.65	0.03
				EGLLLWCQR	0.94	1.76	0.89	1.03
	P23528	Cofilin-1	COF1	HELQANCYEEVKDR	2.15	1.20	1.00	0.92
	P68104	Elongation factor 1-alpha 1	EF1A1	DGNASGTTLLEALDCILPPTRPTDKPLR	1.49	2.33	1.21	0.77
				SGDAAIVDMVPGKPMCVESFSDYPPLGR	0.92	54.0	3.38	1.35
	P13639	Elongation factor 2	EF2	CLYASVLTAQPR	2.75	1.39	1.1	0.67
				STLTDSLVCK	1.09	0.44	0.68	1.80
				YVEPIEDVPCGNIVGLVGVDQFLVK	0.24	0.08	0.72	2.00
	P60842	Eukaryotic initiation factor 4A-I	IF4A1	VVMALGDYMGASCHACIGGTNVR	2.81	-	-	-
	P62495	Eukaryotic peptide chain release factor subunit 1	ERF1	CGTIVTEEGK	2.83	-	-	-
	P47813	Eukaryotic translation initiation factor 1A, X-chromosomal	IF1AX	LEAMCFDGVK	1.69	-	1.30	0.02

Pathway	Accession	Description	Gene Symbol	Peptide	H:L fold-change across time (h)			
					3	6	12	24
	P41091	Eukaryotic translation initiation factor 2 subunit 3	IF2G	YNIEVVCEYIVK	1.92	-	0.90	-
	P55884	Eukaryotic translation initiation factor 3 subunit B	EIF3B	NLFNVVDCK	2.79	2.16	2.09	2.25
	P60228	Eukaryotic translation initiation factor 3 subunit E	EIF3E	IHQCISIN	1.42	1.10	1.15	2.86
				LFIFETFCR	2.23	-	2.43	-
	O75822	Eukaryotic translation initiation factor 3 subunit J	EIF3J	ITNSLTVLCSEK	6.16	2.03	1.33	0.82
	Q9UBQ5	Eukaryotic translation initiation factor 3 subunit K	EIF3K	FICHVVGITYQHIDR	2.08	-	1.35	-
	P02675	Fibrinogen beta chain	FIBB	ECEEIIR	1.63	2.09	-	-
				LESDVSAQMEYCR	0.78	3.33	3.75	3.43
				TPCTVSCNIPVVSGK	2.91	5.05	3.56	1.08
	P02679	Fibrinogen gamma chain	FIBG	CHAGHLNGVYYQGGTYSK	0.80	1.60	2.09	2.13
				VAQLEAQCQEPCKDTVQIHDITGK	3.74	5.77	4.55	0.87
	P21333	Filamin-A	FLNA	VHSPSGALEECYVTEIDQDK	2.25	1.42	1.59	0.02
	P04075	Fructose-bisphosphate aldolase A	ALDOA	ALANSLACQGK	1.96	0.79	0.94	1.08
	P62937	Peptidyl-prolyl cis-trans isomerase A	PPIA	ANAGPNTNGSQFFICTAK	4.72	3.88	3.80	0.06
				TNGSQFFICTAK	1.56	0.78	0.84	1.21
	P07737	Profilin-1	PROF1	CYEMASHLR	1.99	1.60	1.06	-
				IDNLMADGTCQDAAIVGYK	3.37	-	4.21	-
	Q12846	Syntaxin-4	STX4	CNSMQSEYR	1.69	-	-	-
	O75083	WD repeat-containing protein 1	WDR1	MTVDESGQLISCSMDDTVR	12.4	2.10	0.27	1.18
Protein folding	Q9BVA1	Tubulin beta-2B chain	TBB2B	LTTPTYGDLNHLVSATMSGVTTCLR	1.66	-	-	-
	Q9BQE3	Tubulin alpha-1C chain	TBA1C	AVCMLSNTTAVAEAWAR	0.91	-	0.73	1.74

Pathway	Accession	Description	Gene Symbol	Peptide	H:L fold-change across time (h)			
					3	6	12	24
				LADQCTGLQGFLVFHSF	1.34	-	10.9	1.47
				MVDNEAIYDICR	10.9	10.6	10.7	8.46
				TTLEHSDCAFMVDNEAIYDICR	1.47	1.77	1.03	-
	P68363	Tubulin alpha-1B chain	TBA1B	AYHEQLSVAEITNACFEPANQMVK	1.36	1.25	1.97	1.14
				LADQCTGLQGF	1.58	-	1.26	0.74
				TTLEHSDCAFMVDNEAIYDICR	2.03	-	1.22	0.93
				YMACCLLYR	1.99	-	1.44	3.17
	P50991	T-complex protein 1 subunit delta	TCPD	SIHDALCVIR	1.65	2.21	1.24	0.49
	P50990	T-complex protein 1 subunit theta	TCPQ	IGLSVSEVIEGYEIACR	1.63	1.70	0.89	0.43
	P68366	Tubulin alpha-4A chain	TBA4A	AYHEQLSVAEITNACFEPANQMVK	1.36	1.13	1.69	1.14
				MVDNEAIYDICR	12.0	10.6	10.33	8.46
				SIQFVDWCPTGF	6.53	-	7.97	-
				TTLEHSDCAFMVDNEAIYDICR	1.47	1.77	1.03	-
				YMACCLLYR	1.99	-	1.44	3.17
	P48643	T-complex protein 1 subunit epsilon	TCPE	SLHDALCVIR	1.70	2.21	1.24	0.49
	P17987	T-complex protein 1 subunit alpha	TCPA	ALNCVVGSQGMPK	2.11	-	1.34	1.01
				GANDFMCDEMER	3.35	1.95	2.66	2.29
				IACLDFSLQK	3.11	3.28	1.22	1.05
				ICDDELILIK	0.98	1.51	1.24	0.93
	P60709	Actin, cytoplasmic 1	ACTB	DDDIAALVVDNGSGMCK	25.71	0.76	27.24	1.39
Protein degradation	Q92890	Ubiquitin fusion degradation protein 1 homolog	UFD1	CFSVSMLAGPNDR	99.7	-	-	-
	P61086	Ubiquitin-conjugating enzyme E2 K	UBE2K	ISSVTGAICLDILK	15.1	-	-	-
	P49792	E3 SUMO-protein ligase RanBP2	RBP2	IAELLCK	2.41	1.17	1.29	-

Pathway	Accession	Description	Gene Symbol	Peptide	H:L fold-change across time (h)			
					3	6	12	24
	Q14258	E3 ubiquitin/ISG15 ligase TRIM25	TRI25	NTVLCNVVEQFLQADLAR	2.74	-	44.7	-
	Q7Z6Z7	E3 ubiquitin-protein ligase HUWE1	HUWE1	VLGPAACR	1.66	1.21	1.26	-
	Q63HN8	E3 ubiquitin-protein ligase RNF213	RN213	STDFLPVDCPVR	1.70	-	-	-
	P62333	26S protease regulatory subunit 10B	PRS10	AVASQLDCNFLK	3.05	1.30	13.36	1.21
	Q99460	26S proteasome non-ATPase regulatory subunit 1	PSMD1	QCVENADLPEGEK	1.83	3.58	1.86	0.70
			PSMD1	MEEADALIESLCR	1.27	1.90	0.74	-
	O00232	26S proteasome non-ATPase regulatory subunit 12	PSD12	AIYDTPCIQAESEK	23.3	1.14	2.18	1.80
	Q9UNM6	26S proteasome non-ATPase regulatory subunit 13	PSD13	FLGCVDIK	1.30	1.80	1.15	0.81
	Q16401	26S proteasome non-ATPase regulatory subunit 5	PSMD5	FFGNLAVMDSPQQICER	108	-	-	-
			PSMD5	TTLCVSILER	1.76	-	-	-
	Q15008	26S proteasome non-ATPase regulatory subunit 6	PSMD6	VYQGLYCVAIR	1.79	0.61	1.03	0.02

N.B. '-' denotes not detected in at least 2 of 3 replicates

Table 2-3 Glutathionylation profile of proteins involved in defense against cellular stress as a function of time. Values in red represent the average H:L ratio of peptides normalized to the control that exceed a 1.5-fold threshold across at least 2 replicates.

Pathway	Accession	Description	Gene Symbol	Peptide	H:L fold-change across time (h)			
					3	6	12	24
Detoxification of reactive oxygen species	P04040	Catalase	CATA	LCENIAGHLK	3.04	1.05	1.19	0.34
	P30048	Thioredoxin-dependent peroxide reductase, mitochondrial	PRDX3	ANEFHDVNCEVVAVSVDSHFSH LAWINTPR	5.49	-	4.02	-
	P00441	Superoxide dismutase [Cu-Zn]	SODC	HVGDLGNVTADKDGVADVSIED SVISLSGDHCIIGR	1.22	1.63	1.81	-
	P04179	Superoxide dismutase [Mn], mitochondrial	SODM	GHLQIAACPNQDPLQGTTGLIPL LGID	83.76	-	-	-
	Q96HE7	ERO1-like protein alpha	ERO1A	YSEEANNLIEECEQAER	0.97	0.94	1.94	1.34
	Q06830	Peroxiredoxin-1	PRDX1	LNCQVIGASVDSHFCH	0.98	-	3.43	-
Phase I functionalization	P21397	Amine oxidase [flavin-containing] A	AOFA	ICELYAK	2.23	2.13	1.33	0.58
	P27338	Amine oxidase [flavin-containing] B	AOFB	CIVYYK	3.03	-	1.21	-
				LCELYAK	2.12	2.13	1.33	0.58
	P07327	Alcohol dehydrogenase 1A	ADH1A	NPESNYCLK	300	150	-	-
	P00325	Alcohol dehydrogenase 1B	ADH1B	MVAVGICR	5.66	2.55	1.81	1.14
				NPESNYCLK	335	131	115	1.00
	P00326	Alcohol dehydrogenase 1C	ADH1G	NPESNYCLK	333	-	-	-
	P05181	Cytochrome P450 2E1	CP2E1	DLTDCLLVEMEK	2.70	51.58	3.90	-
	P10632	Cytochrome P450 2C8	CP2C8	DFIDCFLIK	3.01	0.96	1.27	1.31
	P00352	Retinal dehydrogenase 1	AL1A1	AYLNDLAGCIK	2.19	1.00	1.00	1.16
				FPVFNPATEEELCQVEEGDKEDV DK	236	164	68.7	-
				LECGGGPWGNK	4.95	2.69	1.33	-
				LNDLAGCIK	2.70	1.43	1.11	0.88

Pathway	Accession	Description	Gene Symbol	Peptide	H:L fold-change across time (h)			
					3	6	12	24
				YCAGWADK	2.73	1.29	0.91	1.10
	Q9NR19	Acetyl-coenzyme A synthetase, cytoplasmic	ACSA	GATTNICYNVLDR	1.83	72.98	1.22	2.27
	Q16850	Lanosterol 14-alpha demethylase	CP51A	CIGENFAYVQIK	1.07	1.07	1.48	2.41
	Q9HBI6	Phylloquinone omega-hydroxylase CYP4F11	CP4FB	LQCFPQPPK	1.32	1.27	1.10	2.76
Phase II conjugation	P10620	Microsomal glutathione S-transferase 1	MGST1	VFANPEDCVAFGK	4.95	2.94	2.97	12.16
	P40261	Nicotinamide N-methyltransferase	NNMT	IFCLDGVK	2.45	3.18	1.35	0.89
	P48506	Glutamate--cysteine ligase catalytic subunit	GSH1	GYVSDIDCR	104	44.4	46.1	1.00
	P36269	Gamma-glutamyltransferase 5	GGT5	FLNVVQAVSQEGACVYAVSDLR	2.78	39.8	-	-
				HQAPCGPQAF	1.17	0.69	2.38	-
	P48637	Glutathione synthetase	GSHB	IEPEPFENCLLR	4.70	-	-	-
	P23526	Adenosylhomocysteinase	SAHH	QAQYLGMSCDGPFKPDHYR	5.12	-	-	-
	P51580	Thiopurine S-methyltransferase	TPMT	SWGIDCLFEK	2.74	-	-	-
	O60701	UDP-glucose 6-dehydrogenase	UGDH	DPYEACDGAH	0.88	1.10	1.59	1.00
				DVLNLVYLCEALNLPEVAR	4.65	4.50	1.45	1.07
	O60656	UDP-glucuronosyltransferase 1-9	UD19	NHIMHLEEHLLCHR	6.40	-	1.09	0.59
	Q06520	Bile salt sulfotransferase	ST2A1	ICQFLGK	1.00	0.92	1.24	2.13
GSH and sulfur amino acid metabolism	P35520	Cystathionine beta-synthase	CBS	CIIVMPEK	1.69	-	-	-
	P23526	Adenosylhomocysteinase	SAHH	QAQYLGMSCDGPFKPDHYR	5.12	4.33	-	-
	P48506	Glutamate--cysteine ligase catalytic subunit	GSH1	GYVSDIDCR	104	44.4	46.1	1.00
	P48637	Glutathione synthetase	GSHB	IEPEPFENCLLR	4.70	-	-	-
	P19623	Spermidine synthase	SPEE	QFCQSLFPVVAY	1.81	-	-	-
	P52788	Spermine synthase	SPSY	LYCPVEFSK	2.55	-	-	-
Cellular response to heat	O95816	BAG family molecular chaperone regulator 2	BAG2	FQSIVIGCALEDQK	2.37	-	0.85	0.84
	Q8N163	Cell cycle and apoptosis regulator protein 2	CCAR2	GEASEDLCEMALDPELLLLR	2.64	-	4.49	-

Pathway	Accession	Description	Gene Symbol	Peptide	H:L fold-change across time (h)			
					3	6	12	24
stress				TVDSPICDFLELQR	1.97	-	1.47	1.61
	Q15185	Prostaglandin E synthase 3	TEBP	LTFSCLGGSDNFK	1.73	1.92	2.69	3.31
	P68104	Elongation factor 1-alpha 1	EF1A1	DGNASGTTLLEALDCILPPTRPTDKPLR	1.49	2.33	1.21	0.77
				SGDAAIVDMVPGKPMCVESFSDYPPLGR	0.92	54.0	3.38	1.35
	P49792	E3 SUMO-protein ligase RanBP2	RBP2	IAELLCK	2.41	1.17	1.29	-
	Q8N1F7	Nuclear pore complex protein Nup93	NUP93	CGDLLAASQVVNR	1.61	1.26	1.15	1.41
	P34932	Heat shock 70 kDa protein 4	HSP74	FLEMCNDLLAR	0.98	2.71	1.01	-
	O95757	Heat shock 70 kDa protein 4L	HS74L	AQFEQLCASLLAR	3.14	3.04	1.23	-
	P08107	Heat shock 70 kDa protein 1A/1B	HSP71	CQEVISWLDANTLAEKDEFEHK	5.07	-	-	-
	P11142	Heat shock cognate 71 kDa protein	HSP7C	CNEIINWLDK	1.15	3.82	1.00	1.78
	P07900	Heat shock protein HSP 90-alpha	HS90A	CLELFTELAEDK	0.91	1.63	0.33	-
				FENLCK	3.66	-	-	-
	P08238	Heat shock protein HSP 90-beta	HS90B	AKFENLCK	1.58	-	-	-
				FENLCK	3.60	-	-	-
				VFIMDSCDELIPEYLNFIR	67.5	34.3	79.2	50.3
	P55072	Transitional endoplasmic reticulum ATPase	TERA	EAVCIVLSDDTCSDEK	59.4	-	40.2	-
				LADDVDLEQVANETHGHVGADLAALCSEAALQAIR	91.9	281	64.0	37.6

N.B. '-' denotes not detected in at least 2 of 3 replicates

Table 2-4 Glutathionylation profile of proteins involved in calcium dynamics and the mitochondrial permeability transition pore (MPTP) formation as a function of time. Values in red represent the average H:L ratio of peptides normalized to the control that exceed a 1.5-fold threshold across at least 2 replicates.

Pathway	Accession	Description	Gene Symbol	Peptide	H:L fold-change across time (h)			
					3	6	12	24
Calcium dynamics	P16615	Sarcoplasmic/endoplasmic reticulum calcium ATPase 2	AT2A2	ANACNSVIK	-	1.24	-	1.68
				GTAVAICR	2.32	1.30	1.18	1.35
	P20020	Plasma membrane calcium-transporting ATPase 1	AT2B1	TICLAFR	5.00	-	1.10	-
Mitochondrial permeability transition pore formation	P21796	Voltage-dependent anion-selective channel protein 1	VDAC1	YQIDPDACFSAK	1.67	0.99	1.28	0.88
	P45880	Voltage-dependent anion-selective channel protein 2	VDAC2	SCSGVEFSTSGSSNTDTGK	1.26	0.81	1.32	2.58
	Q9Y277	Voltage-dependent anion-selective channel protein 3	VDAC3	SCSGVEFSTSGHAYTDTGK	0.87	0.83	1.68	1.84
				VCNYGLTFTQK	0.97	0.96	1.68	2.50
	P12235/ P05141	ADP/ATP translocase 1/2	ADT1/ ADT2	QYKGIIDCVVR	3.42	2.64	1.18	1.15
	P62937	Peptidyl-prolyl cis-trans isomerase A	PPIA	ANAGPNTNGSQFFICTAK	4.72	3.88	3.80	0.06

N.B. '-' denotes not detected in at least 2 of 3 replicates

2.4.3.2 Proteo-metabonomic Mapping of APAP-induced Glutathionylation

A total of 19 primary research articles investigating APAP-induced metabolic perturbations were retrieved from literature and are presented in Table 2-5. These investigations utilized both animal models (mice, rat and pig) and human subjects, and various biological matrices (serum, plasma, whole blood, urine and liver). A total of 81 metabolites were reported to be perturbed by APAP and are involved in a variety of biological processes including glycolysis, pyruvate metabolism, mitochondrial fatty acid β-oxidation, citric acid cycle, glycogen turnover, GSH and sulfur amino acid metabolism, phospholipid turnover, and amino acid and bile acid homeostasis.

Table 2-5 Summarized reports of APAP-induced metabolic perturbations from literature and in-house data.

Pathway	Model system	Matrix	Analytical platform	Metabolites	Directionality	Ref
Glycolysis, pyruvate metabolism	Mouse	Plasma	NMR	Lactate	Elevated	(*96*)
		Liver		Lactate	Elevated	
	Rat	Urine	NMR	Lactate	Elevated	(*97*)
	Human	Plasma	NMR	Lactate	Elevated	(*98*)
	Human	Serum	NMR	Lactate	Elevated	(*99*)
	Mouse	Plasma	NMR	Pyruvate	Elevated	(*96*)
	Rat	Plasma	NMR	Pyruvate	Elevated	(*97*)
	Rat	Urine	NMR, LC/MS	Pyruvate	Decreased	(*100*)
	Rat	Liver	CE/TOFMS	Phosphoenolpyruvate	Elevated	(*101*)
Mitochondrial fatty acid β-oxidation	Mouse	Serum	LC/MS	Palmitoyl, oleoyl, myristoylcarnitine	Peak at 4 h followed by decline	(*102*)
				Carnitine	Peak at 8 h followed by decline	
				Acetylcarnitine	Decreased	
	Mouse	Plasma	LC/MS	Palmitoyl, oleoyl, myristoyl, palmitoleoyl carnitine	Peak at 2 h followed by decline	(*103*)
	Mouse	Serum	LC/MS	Palmitoyl, linoleoyl, oleoyl carnitine	Elevated from 3-12 h	(*104*)
	Mouse	Serum	LC/MS	Palmitoyl, oleoyl, myristoyl, palmitoleoyl carnitine	Elevated	(*105*)
	Mouse	Serum	LC/MS	Palmitoyl, oleoyl carnitine	Elevated	(*106*)
	Mouse	Serum	LC/MS	Palmitoyl carnitine	Elevated	(*107*)
	Human	Plasma	LC/MS	Palmitoyl, linoleoyl, oleoyl carnitine	No change from healthy patients	(*104*)
	Human	Serum	LC/MS	Palmitoyl, oleoyl, myristoyl, palmitoleoyl carnitine	Elevated	(*108*)
	Rat	Serum	GC/MS	*Fatty acids: O*leic acid, vaccenic acid, linoleic acid, eicosatrienoic acid, arachidonic acid, eicosapentaenoic acid, docosahexaenoic acid, myristic acid, palmitic acid, palmitoleic acid, margaric acid, stearic acid, α-linolenic acid, arachidic acid	Elevated	(*109*)
	Rat	Plasma	NMR	Unspecified lipid	Decreased	(*97*)
	Mouse	Liver	NMR	Triglycerides, monounsaturated fatty acids	Elevated	(*96*)
				Polyunsaturated fatty acids	Decreased	

Pathway	Model system	Matrix	Analytical platform	Metabolites	Directionality	Ref
		Plasma		Triglycerides	Elevated	
	Mouse	Serum	LC/MS	Triglycerides, free fatty acids	Elevated	(*103*)
	Mouse	Serum	LC/MS	Triglycerides, free fatty acids	Elevated	(*106*)
Citric acid cycle	Rat	Urine	NMR	2-oxoglutarate, citrate, succinate	Decreased	(*97*)
	Rat	Urine	NMR, LC/MS	2-oxoglutarate, citrate, succinate	Decreased	(*100*)
	Rat	Liver	CE/TOFMS	Citrate	Elevated	(*101*)
				Malate, succinate	Decreased	
	Rat	Urine	LC/MS, GC/MS	Isocitrate, aconitate, oxaloacetate	Decreased	In-house
	Human	Urine	NMR	Citrate	Decreased	(*98*)
Glycogen turnover	Mouse	Liver	UV/Vis	Glycogen	Decreased	(*110*)
		Blood		Glucose	Peak at 2 h followed by decline	
	Mouse	Liver	NMR	Glycogen, glucose	Decreased	(*96*)
		Plasma		Glucose	Elevated	
	Rat	Urine	NMR, LC/MS	Glucose	Decreased	(*100*)
	Rat	Liver		Glycogen	Decreased	
		Serum		Glucose		
Amino acid	Mouse	Liver	NMR	Alanine, isoleucine, leucine, lysine, valine, phenylalanine, tyrosine	Elevated	(*96*)
	Rat	Plasma	NMR	Isoleucine	Elevated	(*97*)
	Pig	Serum	NMR	Isoleucine, tyrosine, phenylalanine	Elevated	(*111*)
				Valine	Decreased	
	Human	Plasma	NMR	3-hydroxyisovalerate, isoleucine, acetylglycine, glutamine, isobutyrate, phenylalanine	Elevated	(*98*)
GSH and sulfur amino acid metabolism	Mouse	Liver	CE/TOFMS	Spermine, hypotaurine, S-adenosylmethionine, glycine, glutamine, spermidine, cysteine, glutamate, taurine	Decreased	(*101*)
	Rat	Urine	NMR	Taurine	Elevated	(*97*)
	Rat	Urine	NMR, LC/MS	Trigonelline	Decreased	(*100*)

Pathway	Model system	Matrix	Analytical platform	Metabolites	Directionality	Ref
				S-adenosylmethionine Taurine		
	Rat	Urine	NMR	5-oxoproline	Increased	(*112*)
	Mouse	Liver	CE/TOFMS	Methionine, S-adenosylhomocysteine, ophthalmic acid	Elevated	(*101*)
	Rat	Liver	LC/MS, GC/MS	Taurine, hypotaurine Ophthalmic acid, 5-oxoproline, γ-glutamyl-2-aminobutyrate	Decreased Increased	(*113*)
Phospholipid turnover	Mouse	Liver	NMR	All phospholipid species, arachidonic acid Choline, phosphocholine	Decreased Elevated	(*96*)
Bile acids	Rat	Plasma	LC/MS, GC/MS	*Glycine conjugated bile acids:* Glycocholate, glycochenodeoxycholate *Taurine conjugated bile acids:* Taurocholate, taurochenodeoxycholate	Elevated Decreased	(*113*)
	Human	Serum	LC/MS	Glycodeoxycholic acid	Increased	(*114*)
Others	Rat	Plasma	NMR	Trimethylamine, creatinine	Elevated	(*97*)
	Rat	Urine	NMR	Allantoin, hippurate, creatinine, trimethylamine *N*-oxide	Decreased	(*97*)
	Rat	Urine	NMR, LC/MS	Trimethylamine *N*-oxide, dimethylamine, hippurate, glycine, N,N-dimethylglycine, N-isovalerylglycine, betaine, *trans*-aconitate, pipecolinate, ferulic acid Creatine, acetate	Decreased	(*100*)
	Human	Urine	NMR	Hippurate 3-chlorotyrosine, glutarate	Decreased Elevated	(*98*)
		Plasma		Acetone, acetate, ethanol	Elevated	
	Rat	Urine	LC/MS, GC/MS	Hippurate, pantothenate, phenylacetylglycine, pipecolinate, ferulic acid sulfate Indoxysulfuric acid, pyrocatechol sulfate	Decreased Elevated	In-house

Proteo-metabonomic mapping revealed significant overlaps between the biological processes affected by glutathionylation and metabolic perturbations. Pathways that were successfully mapped were glycolysis and pyruvate metabolism (Figure 2-13), fatty acid β-oxidation (Figure 2-14), citric acid cycle (Figure 2-15), respiratory electron transport and ATP synthesis (Figure 2-16), and GSH and sulfur amino acid metabolism (Figure 2-17). Glutathionylated proteins in each map are marked in red text, and up/down arrows indicate the direction of change (increase/decrease) for relevant metabolites. Where divergent changes were reported in literature, the corresponding biological matrices used to perform the measurements are indicated in italics.

The proteo-metabonomic maps accounted for majority of the energy metabolism pathways. Given that most of the proteins in these pathways possess catalytic function, and the substrate repertoire of these proteins are generally narrow, these features increased the mapping accuracy and enhanced the confidence in the inferred protein-metabolite intersections. On the other hand, despite reports of altered amino acid levels, the proteins involved in amino acid metabolism were unexpectedly poorly mapped as the number of relevant metabolic derangements was low. Additionally, amino acids are involved in multiple pathways, and the metabolic perturbations could not be assigned to one particular glutathionylated pathway. Mapping was also not possible for protein turnover, detoxification of reactive oxygen species and cellular response to heat stress pathways as these did not intersect with small molecule metabolite fluxes measured by metabonomics or metabolism studies. Proteins involved in phase I and II metabolism have a broad range of endogeneous and exogeneous substrates and could not be confidently mapped to the small number of metabolic changes reported in literature.

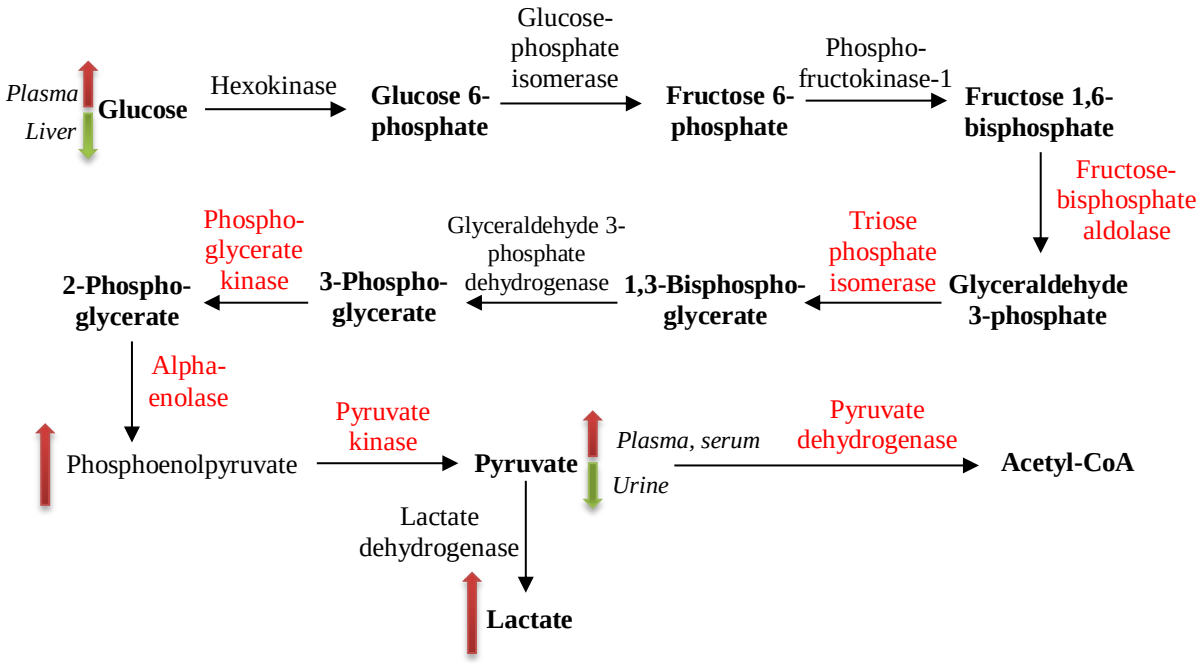

Figure 2-13 Proteo-metabonomic map of glycolysis and pyruvate metabolism.

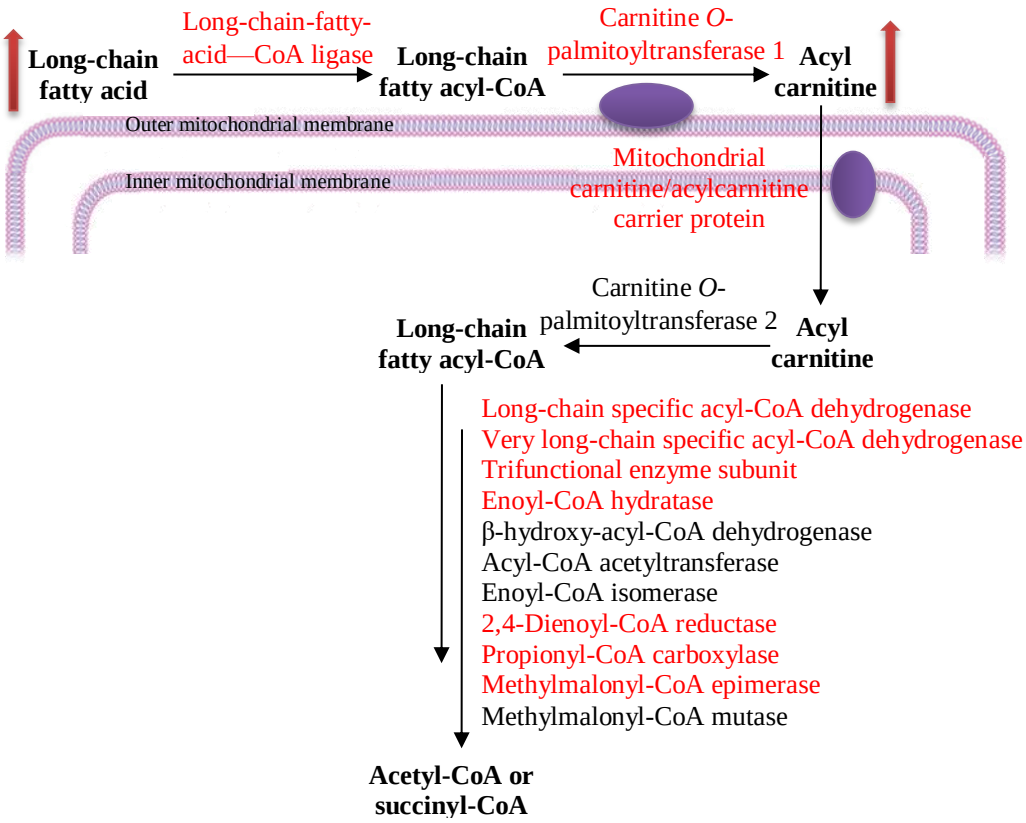

Figure 2-14 Proteo-metabonomic map of fatty acid β-oxidation.

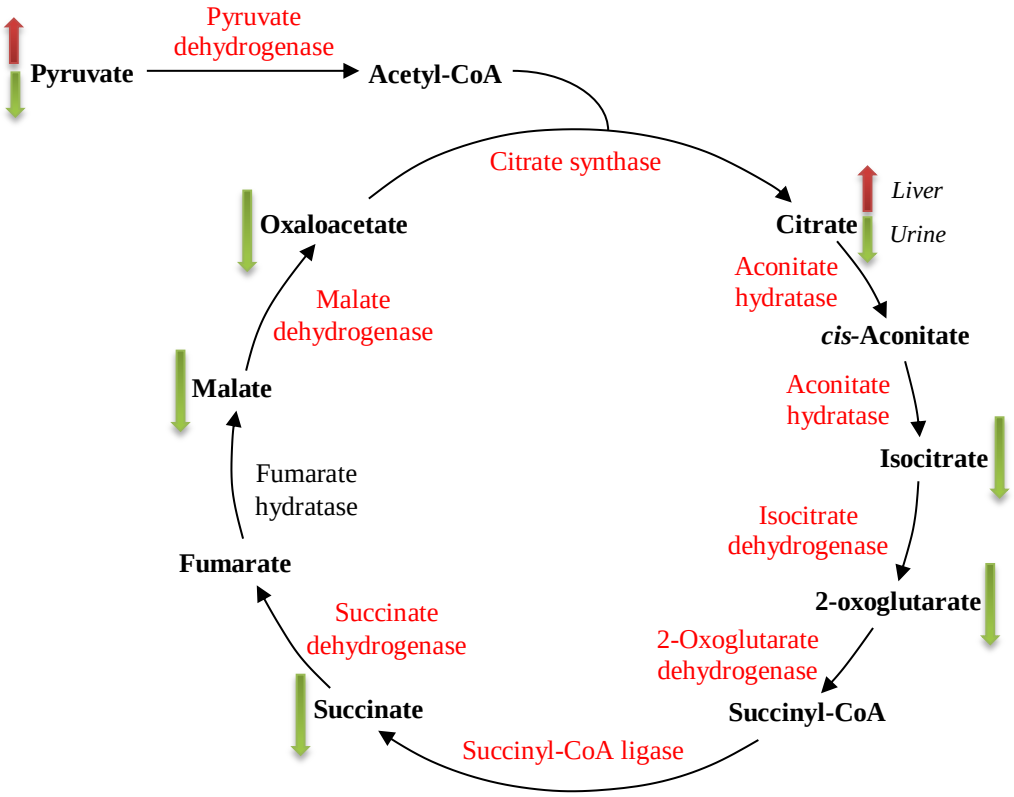

Figure 2-15 Proteo-metabonomic map of the citric acid cycle.

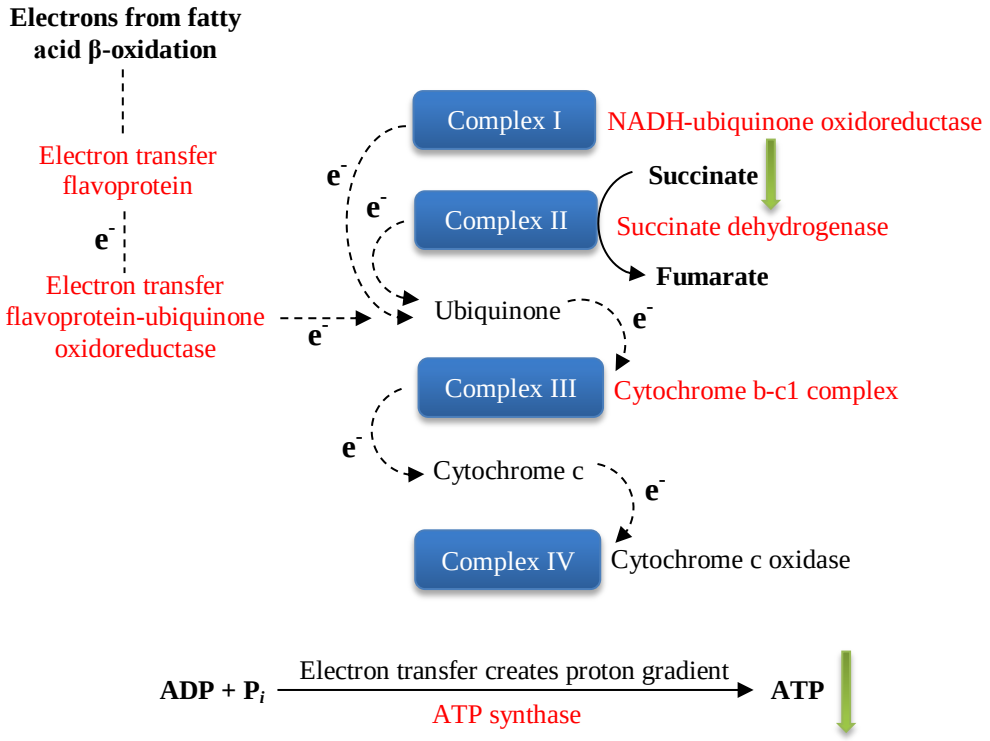

Figure 2-16 Proteo-metabonomic map of respiratory electron transport and ATP synthesis.

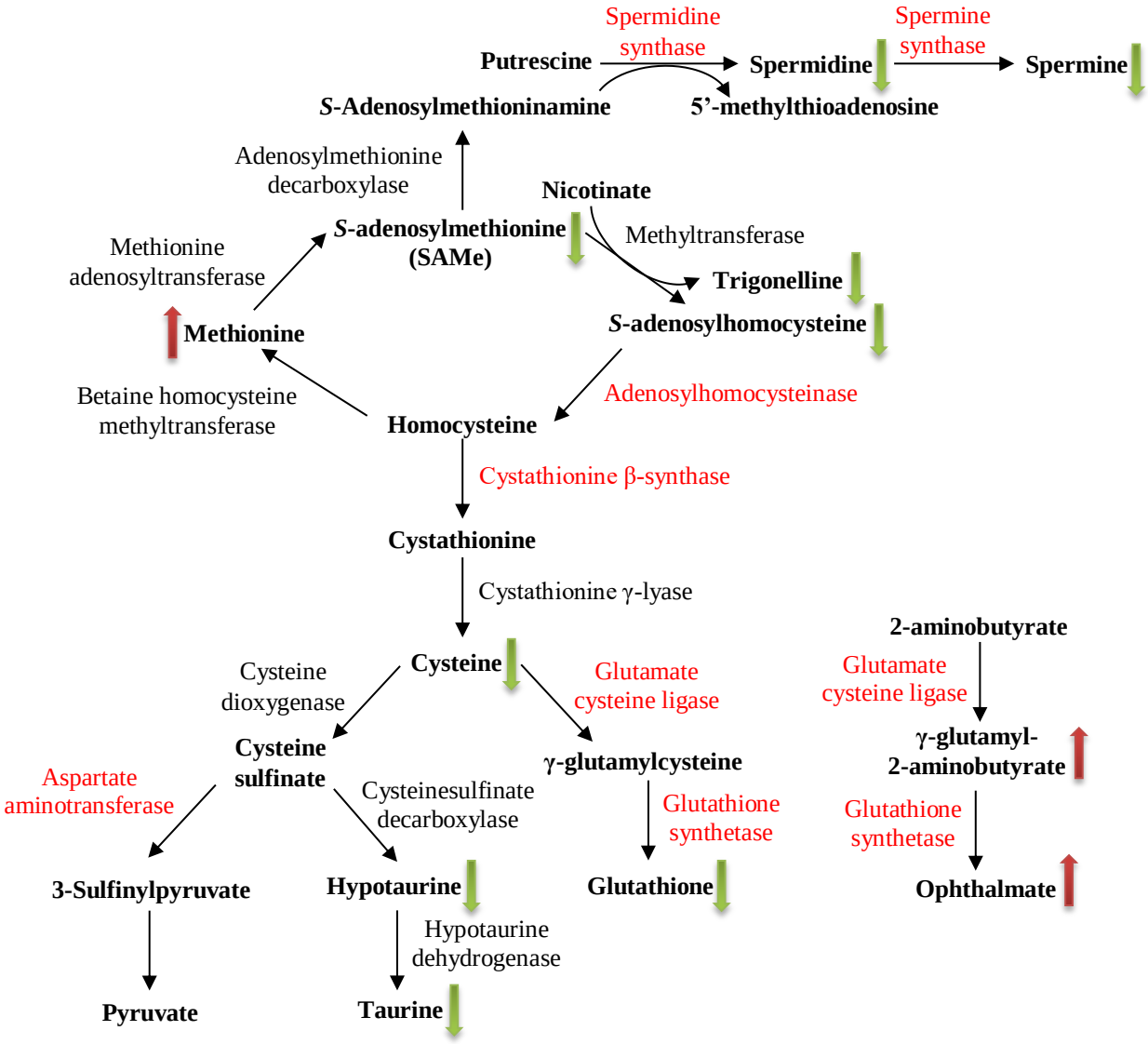

Figure 2-17 Proteo-metabonomic map of GSH and sulfur amino acid metabolism.

2.4.3.3 Longitudinal Progression of APAP-induced Protein Glutathionylation

An overview of the temporal H:L fold-change pattern is presented in the heat map in

Figure **2-18**. In general, glutathionylated peptides can be grouped into 3 distinct clusters based on their peak normalized H:L fold-change values: early (3 h), mid (6-12 h) or late (24 h). For visualization purposes, the peak normalized H:L fold-change values were used to construct the heat map; however, to facilitate analysis of these differentially glutathionylated peptides, the 1.5-fold threshold was

applied to the list of peptides in each cluster to filter them by glutathionylation status. Pathway analysis using Reactome applied to glutathionylated proteins found in the early cluster returned similar results as those reported in section 2.4.3.1, indicating that early glutathionylated peptides participate in key pathways relevant to APAP toxicity. However, when pathway analysis was applied to glutathionylated proteins in the mid and late cluster, the top returned pathways were not found to be relevant to APAP toxicity. When the returned results were further searched to locate the pathways associated with energy metabolism, protein turnover and defense against cellular stress, there was a marked increase in the FDR values for these pathways, and they did not fall within the FDR < 0.05 threshold.

When examined on the basis of glutathionylation status instead of temporal clusters, the highest number of glutathionylated peptides was observed at 3 h, followed by a 50% decrease at 6 h, and was stable thereafter until 24 h (Figure 2-19). Although the total number of glutathionylated peptides remained steady from 6-24 h, the number of glutathionylated peptides in the 3 groups of key biological processes continued to decrease over time. The temporal decrease in the number of glutathionylated peptides that are relevant to APAP toxicity appeared to be balanced by an increase in glutathionylation of other peptides. The percentages of peptides that did not fall into the three groups of key pathways were 67% at 3 h, 65% at 6 h, and increased to 78% at 12 h and 84% at 24 h.

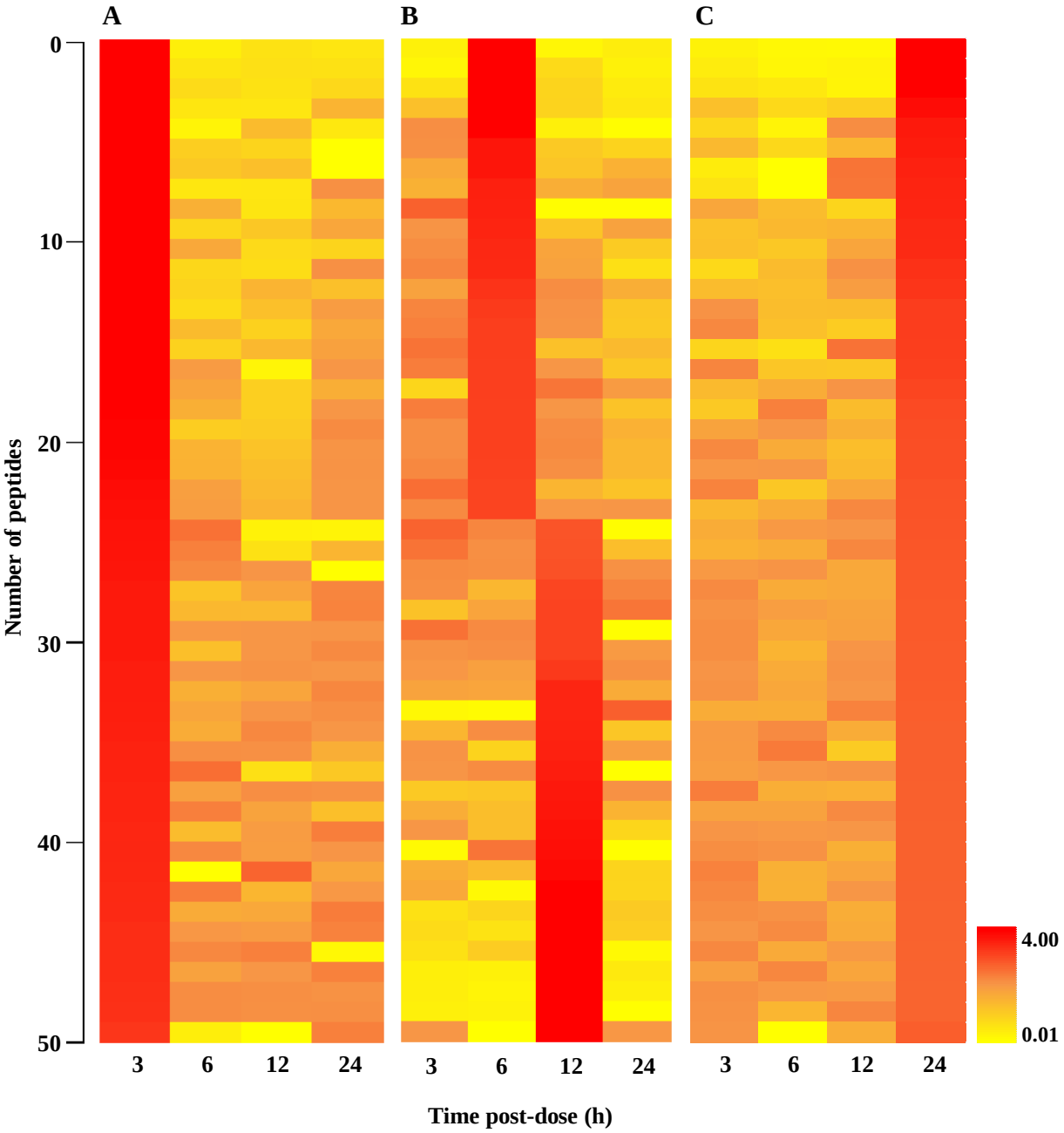

Figure 2-18 Heat map illustrating clustering of glutathionylated peptides in 3 distinct groups based on their peak normalized H:L fold-change values: (A) early (3 h), (B) mid (6-12 h) and (C) late (24 h). The top 50 peptides (by H:L fold-change value) in each cluster are presented (mean of triplicate experiments).

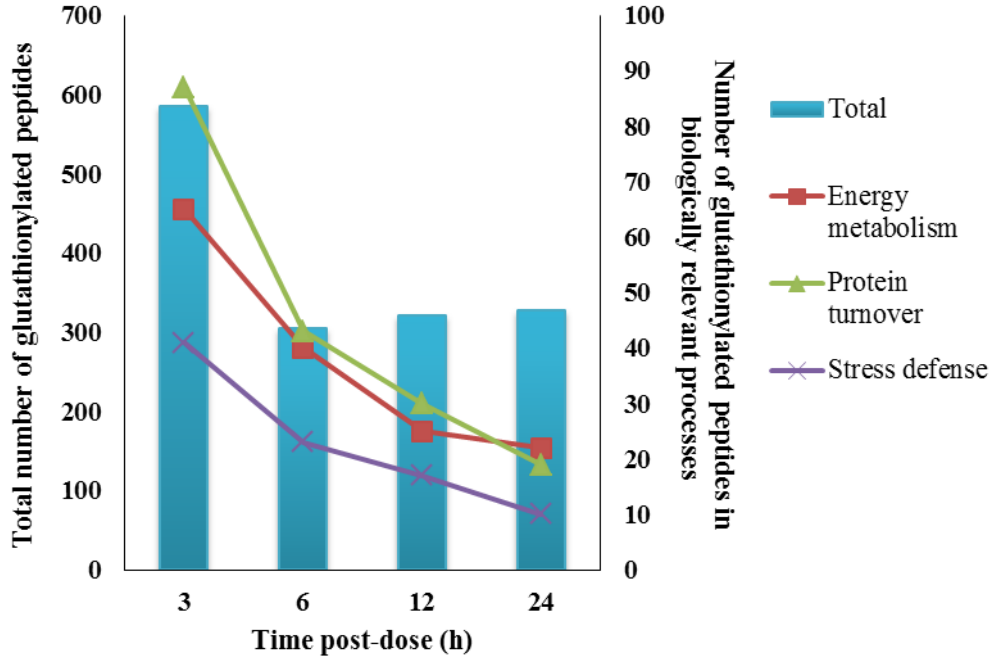

Figure 2-19 Number of glutathionylated peptides as a function of time post-dose, plotted by total number and as a subset of biologically relevant processes.

2.4.3.4 Effect of Dose and Bioactivation on APAP-induced Protein Glutathionylation

The glutathionylation patterns associated with 0.5 mM APAP and 0.5 mM APAP + DEDC treatments were compared with that established for 30 mM APAP at the 3 h time-point. Figure 2-20 represents the H:L fold-change pattern for the peptides derived by normalizing the H:L fold-change values for 0.5 mM APAP and 0.5 mM APAP + DEDC against that of 30 mM APAP. As identified in section 2.4.3.1, these peptides play critical roles in energy metabolism, protein turnover, and defense against cellular stress across the three treatment arms. For all three biological processes, 0.5 mM APAP and 0.5 mM APAP + DEDC treatments resulted in a decrease in H:L fold-change values compared with that of 30 mM APAP. Figure 2-21 illustrates the number of peptides glutathionylated (as defined by the 1.5-fold change in H:L values) by APAP across all three treatment conditions. Comparing 30 mM APAP against 0.5 mM APAP, there was a small

percentage decrease (7%) in total number of glutathionylated peptides. This percentage reduction became more prominent (26%) when the data was compared against 0.5 mM APAP + DEDC treatment. When focusing on the peptides glutathionylated within the 3 key biological processes, the differences among the 3 treatments became apparent. For all three sets of biological processes, the number of glutathionylated peptides decreased by approximately 50% in the 0.5 mM APAP and 0.5 mM APAP + DEDC treatment groups when compared against 30 mM APAP. When comparing the effect of the CYP2E1 inhibitor on APAP-induced glutathionylation (0.5 mM APAP versus 0.5 mM APAP + DEDC), there was no change in the number of glutathionylated peptides involved in energy metabolism; however, the number of glutathionylated peptides involved in protein synthesis and folding, as well as defense against cellular stress decreased by a further 30%.

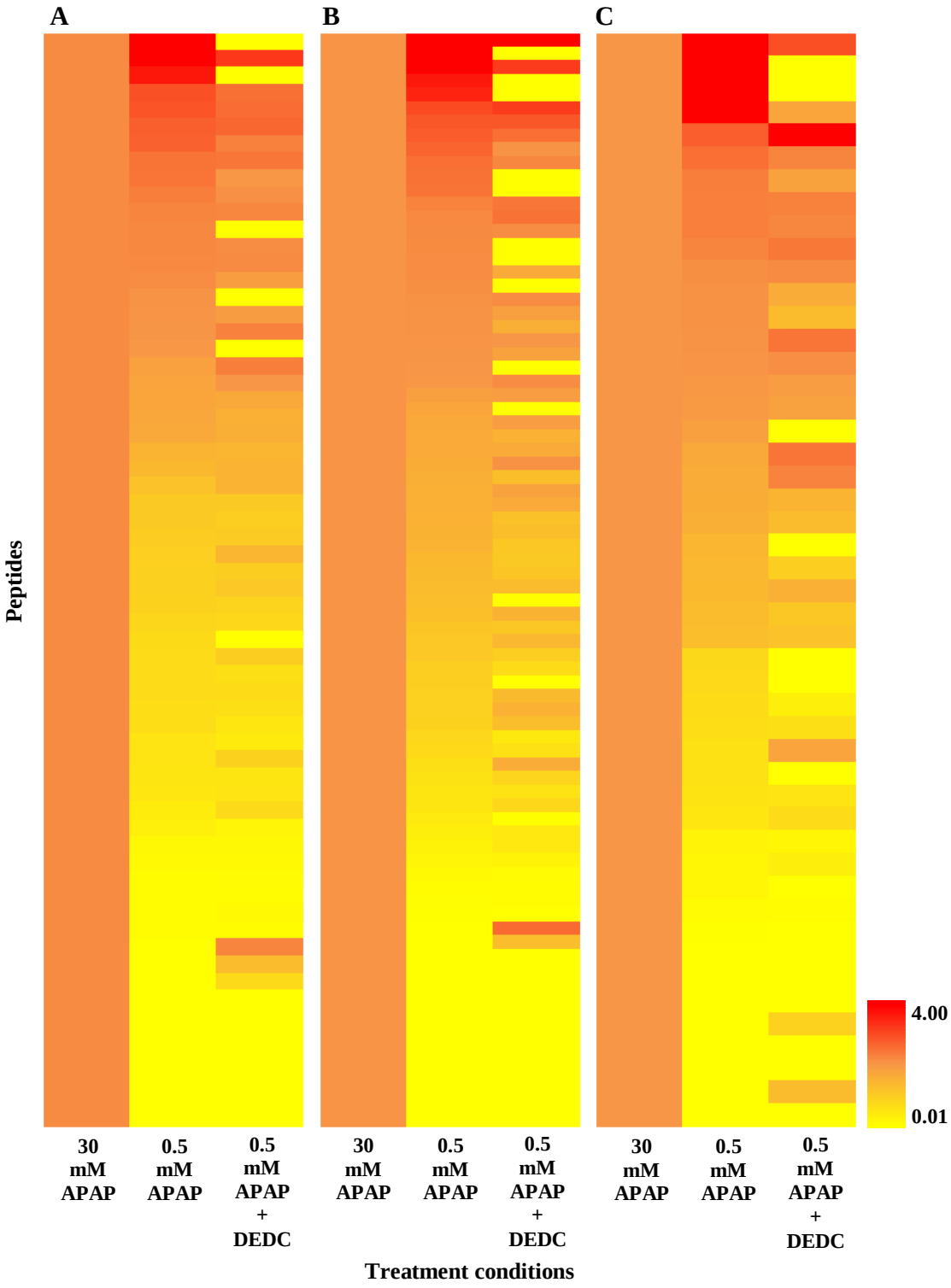

Figure 2-20 Heat map illustrating H:L fold-change pattern for the peptides involved in (A) energy metabolism, (B) protein turnover, and (C) defense against cellular stress among three different treatment conditions. H:L fold-change values were normalized against that of 30 mM APAP for comparative purposes.

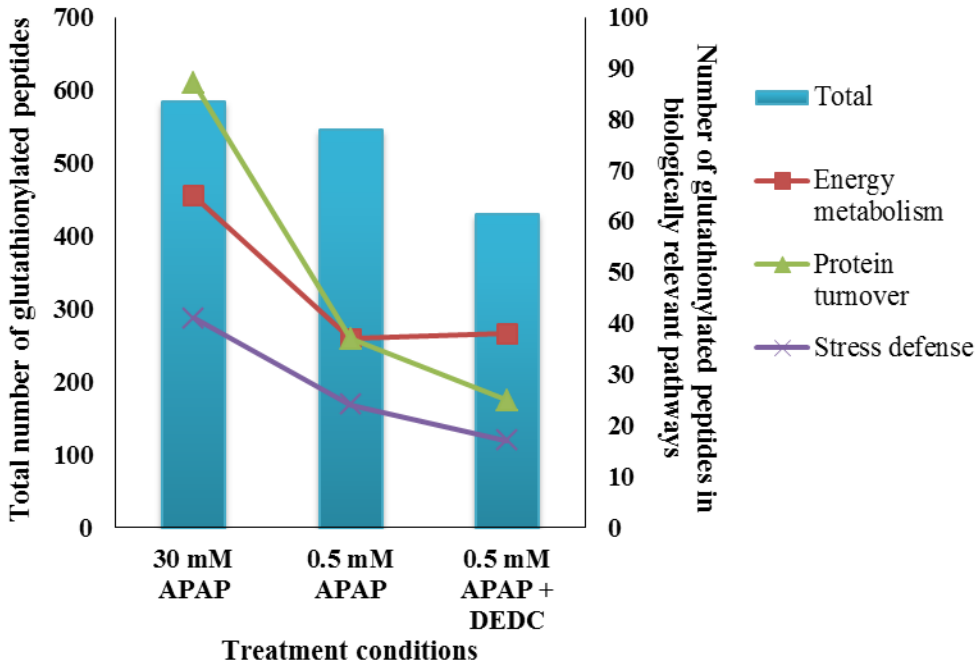

Figure 2-21 Number of glutathionylated peptides among different APAP treatment conditions, plotted by total number and as a subset of biologically relevant processes.

2.4.3.5 Comparative Analysis of AMAP- and APAP-induced Protein Glutathionylation

A total of 265 peptides corresponding to 186 proteins were found to be glutathionylated by 30 mM AMAP at 6 h of exposure. Figure 2-22 summarizes the comparative analysis of proteins glutathionylated by 30 mM AMAP and 30 mM APAP. Of these, 74% of total proteins glutathionylated by AMAP were also glutathionylated by APAP at any one of 4 time-points monitored. Overlaps between proteins glutathionylated by AMAP and APAP were also found for a majority of the proteins in energy metabolism (83%), protein turnover (48%), defense against cellular stress (73%), and calcium dynamics and MPTP formation (100%). Figure 2-23 illustrates the distribution of protein functions associated with proteins glutathionylated by AMAP. 62% of proteins glutathionylated by AMAP possessed catalytic function, while 42% of these proteins were

mitochondrial proteins, while none were found to be localized in the endoplasmic reticulum.

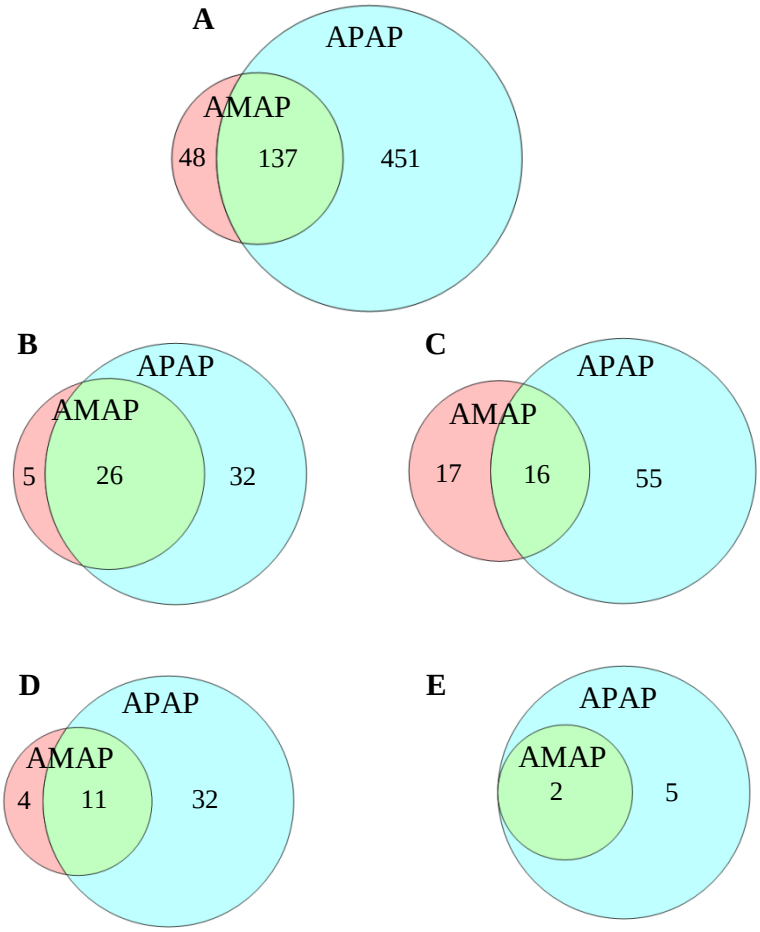

Figure 2-22 Venn diagrams illustrating the overlaps of glutathionylated proteins induced by AMAP and APAP and categorized according to (A) total number, (B) energy metabolism, (C) protein turnover, (D) defense against cellular stress and (E) calcium dynamics and mitochondrial permeability transition pore formation pathways. Numbers within Venn diagram compartments indicate the respective number of proteins. Circles coloured in red and blue represent proteins glutathionylated by AMAP and APAP respectively, and green represents overlapping proteins.

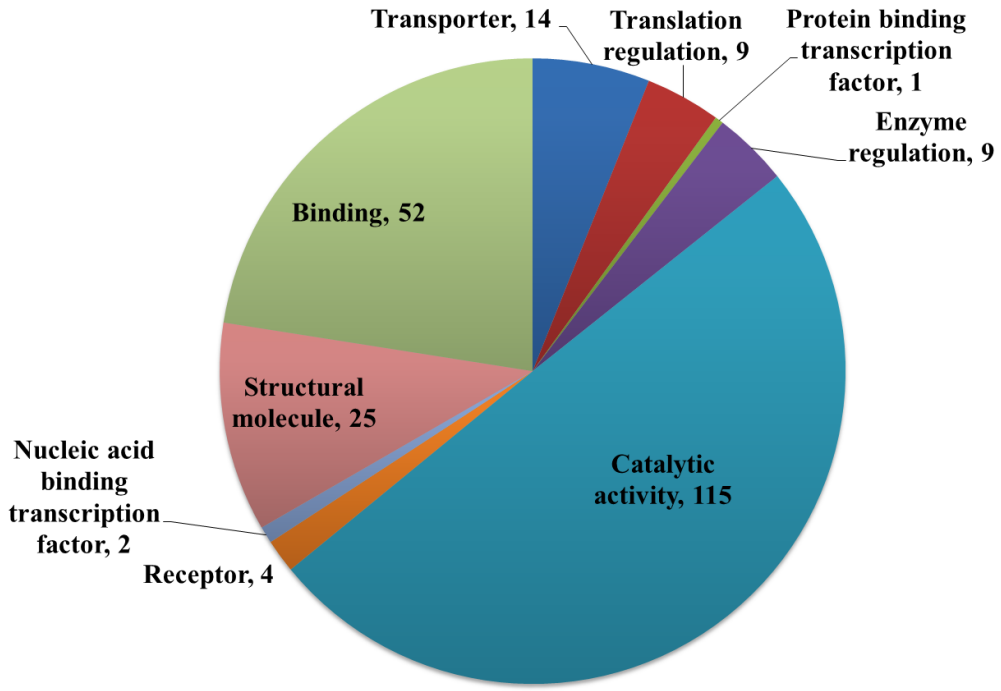

Figure 2-23 Distribution of protein functions associated with proteins glutathionylated by AMAP. Numerals indicate number of proteins in each category. Some proteins may be listed in more than one category.

2.5 Discussion

2.5.1 Development of the GluICAT Methodology to Profile Protein Glutathionylation

Given the evidence that APAP could induce aberrant protein glutathionylation, we sought to investigate the suite of proteins glutathionylated by APAP and determine the biological consequences of this perturbation. An examination of literature at the start of this study revealed that all current approaches to detect glutathionylated proteins involve gel-based methods (*87, 115*), which are constrained by a number of limitations (section 2.2.6). These limitations could be overcome through the use of an in-solution, LC/MS-based approach. As there was no published methodology that met our requirements, we sought to develop a global LC/MS-based proteomic approach to comprehensively profile the glutathionylated proteome.

We chose to build our approach upon the OxICAT method (*93*) which was developed to profile general thiol modifications in oxidatively stressed *E. coli*. The OxICAT method circumvents the limitations of gel-based 2D-gel electrophoresis by using an unbiased, in-solution LC/MS approach to interrogate the thiol modified proteome. In this method, all reduced cysteine thiols are initially labeled with light ICAT. Modified thiols are then reduced in solution with the chemical reductant tris(2-carboxyethyl)phosphine (TCEP), before being labeled with heavy ICAT and digested by trypsin before separation using LC. In other words, thiols that were originally in the reduced form are labeled with light ICAT, while those that were modified are labeled with heavy ICAT. Modified and reduced peptides co-elute chromatographically but differ by a mass difference of 9 Da on the mass spectrum, and this can be detected using MS for

quantification and tandem MS/MS for identification. The extent of thiol modifications is thus reflected in the H:L ratio, where a high ratio indicates extensive thiol modifications. However, the OxICAT method is not able to distinguish specific forms of thiol modifications e.g. nitrosylation versus glutathionylation, as the thiol reductant TCEP is non-specific. To overcome this limitation, we attempted to substitute TCEP with a mutant form of Grx1 which is highly specific in catalyzing deglutathionylation (*116*). We have termed this method the GluICAT method, and the main steps are outlined in Figure 2-8.

The first step in the development of GluICAT was to generate a model glutathionylated protein. GAPDH was chosen for this purpose as it contains a redox-sensitive cysteine residue (Cys^{149}) at its active site. Glutathionylation of this cysteine residue leads to inhibition of its activity, and allowed us to assess the generation of GAPDH-SG. Deglutathionylation of GAPDH-SG was demonstrated by the restoration of GAPDH activity. GAPDH-SG deglutathionylation was also observed directly by monitoring the decrease in NAPDH spectrophotometrically. Collectively, our findings confirmed the generation of GAPDH-SG, and the ability of Grx1 to deglutathionylate GAPDH-SG, thus GAPDH was subsequently used as a model glutathionylated protein for GluICAT.

The next step involved modifying the OxICAT method by substituting the reducing agent TCEP with Grx1 to specifically detect glutathionylated proteins. However, it was not possible to directly substitute TCEP with Grx1. TCEP is a chemical reductant that can operate under harsh conditions, while Grx1 is an enzymatic reductant, and requires gentle, non-denaturing conditions for its deglutathionylating activity. In the OxICAT reducing step, the protein pellet is dissolved in 6 M urea and 0.5% SDS, followed by the addition of TCEP and

heavy ICAT to immediately alkylate newly-reduced thiols. These conditions denature Grx1 and alkylate the catalytic cysteine residue in the active site of Grx1, rendering it inactive. As modification of the deglutathionylation procedure was warranted, we employed FASP to remove denaturing buffers and alkylating agents prior to the deglutathionylation step.

Originally developed to remove SDS from protein samples prior to trypsin digestion (*117, 118*), FASP provides a simple solution to the challenges of GluICAT protocol. Central to the FASP procedure is the use of a 30 kDa molecular weight cut-off (MWCO) spin filter to retain proteins while allowing undesired components of the suspension buffer to be removed, which is illustrated in Figure 2-24. It has been demonstrated that despite the large MWCO, proteins smaller than the MWCO are retained (*118*). This is attributed to the unfolded nature of detergent-treated proteins which prevents them from passing through the membrane. Additionally, SDS could be easily and nearly completely removed by repeated washes with urea. Urea dissociates SDS from proteins and sequesters SDS into micelles that in turn pass through the pores of the membrane filter (*117*). As a result, up to 4% w/v of the chaotropic detergent SDS could be used in the initial solubilization step, ensuring complete solubilization of hydrophobic proteins (e.g. membrane-bound proteins) without the need for sonication that may lead to protein shearing. Without FASP, SDS concentration had to be limited to 0.5%, which would limit protein solubilization and overall proteome coverage. Furthermore, following the removal of denaturing urea and SDS, proteins could be resuspended in Grx1-friendly ammonium bicarbonate for successful deglutathionylation. Apart from that, FASP allowed efficient removal of GSH from the deglutathionylation mixture once the process was complete. It has been reported that at least 5 mM of GSH is needed for Grx1 deglutathionylation

activity (*119*). However, the presence of GSH is detrimental to the subsequent heavy ICAT alkylation step as GSH will compete with newly-deglutathionylated thiols for the thiol-reactive iodoacetamide moiety of heavy ICAT. With the use of FASP, proteins are retained on the membrane while excess GSH can be removed by repeated washes with a buffer. This advantage was also exploited to remove excess heavy ICAT which might alkylate trypsin and affect the subsequent digestion step. With the prior removal of SDS, efficient trypsin digestion was further ensured. Finally, use of FASP allowed us to omit the strong cation exchange step (SCX) in the conventional ICAT protocol. Traditionally, after trypsin digestion of the ICAT tagged peptides, SCX is used for sample clean-up by removing excess ICAT reagents, trypsin, SDS and reductants such as TCEP, as trypsin will digest avidin, while SDS interferes with MS detection (*120*). However, because of the extensive number of wash steps we employ throughout the protocol and trypsin is retained on the spin column post-digestion, we are able to omit SCX from the sample processing step. While the use of FASP increased sample preparation time by up to 3 h, its advantages significantly outweigh this drawback.

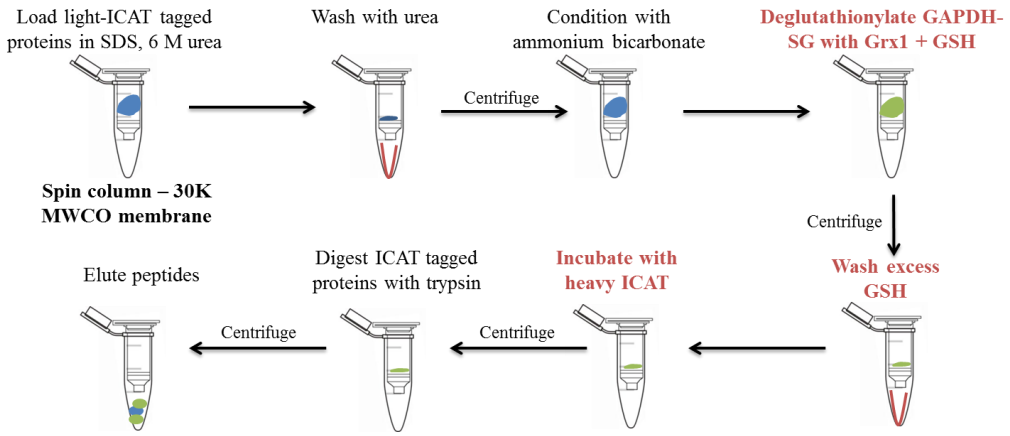

Figure 2-24 GluICAT workflow illustrating the roles of FASP.

An important consideration during sample preparation is to limit artefactual thiol modifications of redox-sensitive thiols due to oxidation by atmospheric oxygen. We adopted the OxICAT approach, where 10% TCA (w/v) was used to lower the pH of protein environment to pH 1-2 during the harvesting step (*121*). This is important because redox-sensitive thiols usually have pK_a values between 5-8, and thus are easily deprotonated to the reactive thiolate anion. By lowering the pH to several units below the pK_a, almost all thiols are protonated and less reactive. TCA also served as a cell lysis reagent and protein denaturant to inactivate endogenous glutaredoxins and thioredoxins which can mediate glutathionylation or deglutathionylation reactions. As TCA could not be present throughout the entire sample preparation, protein samples were handled and processed on ice to reduce the rate of thiol-disulfide exchange (*121*). All buffers were also degassed before use to minimize contact of thiols with dissolved oxygen. However, post-deglutathionylation, the newly deglutathionylated thiols were not acidified using TCA to avoid protein precipitation and ensure subsequent tagging with heavy ICAT. Additionally, numerous wash steps were required to ensure depletion of GSH prior to tagging with heavy ICAT. During this period, exposure of the redox

sensitive thiol to atmospheric oxygen might cause artefactual oxidation, reduce tagging by heavy ICAT and lower the H:L ratio. However this did not pose a significant problem in our method development, as indicated by the H:L ratio of GAPDH-SG (with Grx) which was 23-fold higher than that of GAPDH (untreated).

The suite of glutathionylated proteins identified using GluICAT shows remarkable correspondence with proteins that have been detected in other redox proteomics studies, which use gel-based and LC/MS-based approaches in a variety of tissue matrices including liver (*122*), heart (*123*) and macrophages (*124*). Similar findings were also reported in other organisms such as yeast (*125*) and bacteria (*93*). These suggest that qualitatively, the GluICAT method performs comparably with existing approaches. However, most of these methods focus on profiling general thiol modifications without distinguishing between glutathionylation and oxidation or nitrosylation. This is likely because of the technical difficulty in ensuring efficient deglutathionylation while keeping proteins in solution. Recently, Su *et al*. described an alternative LC/MS-based approach to identify and quantify glutathionylated proteins (*124*). In their approach, free protein thiols were first blocked with *N*-ethyl maleimide, which irreversibly alkylated all free cysteines. Subsequently, glutathionylated thiols were deglutathionylated using a spin column setup where proteins were suspended in HEPES buffer. Deglutathionylated proteins were then captured and enriched on a thiopropyl resin, followed by on-resin trypsin digestion. Digested peptides were then eluted, tagged using the isobaric, multiplex iTRAQ tags and analyzed by LC/MS. Thus the extent of glutathionylation is relative to the abundance of glutathionylated peptides eluted and quantified using LC/MS in each sample. We are heartened that the spin column was also chosen as the

approach to effect deglutathionylation by an independent research group. However, their methodology is constrained by several limitations. Firstly, during sample harvest, 1% Triton X-100, a detergent suspended in HEPES buffer containing NEM is used as the cell lysis and protein solubilization agent. This is an alternative method of quenching thiol reactivity by rapid alkylation. Using NEM has disadvantages because NEM may not be able to access and covalently alkylate all free thiols, especially those that are buried within the core of the protein. This is exacerbated by the fact that upon cell lysis, intra-organelle components such as metal ions and ROS/RNS are released and quickly oxidize proteins before NEM can covalently alkylate their free thiols (*121*). A second major limitation is that the glutathionylation signal is assumed to be proportional to the abundance of a particular peptide. However, this may not always be the case, as an increase in protein expression would also provide the same signal, and thus lead to false interpretations. In their study, cells were treated with diamide for 30 min before harvest, thus it could be argued that limited changes in protein expression would have occurred, and hence their results are unlikely to be confounded by this possibility. In the case of APAP and other toxicants, changes in protein expression have been well-documented, thus their approach might not be able to distinguish between an increase in protein expression versus a true increase in protein glutathionylation. Similarly, McGarry *et al*. recently reported the basal glutathionylation of proteins in mouse liver relying on a similar approach using resin-assisted enrichment of glutathionylated peptides followed by post-deglutathionylation labeling using isobaric iodoTMT tags (*126*). Since the mice were not challenged pharmacologically, protein expression is expected to be unchanged, hence the protein abundance signal in this instance can be considered equivalent to the glutathionylated protein signal. On the contrary, in the GluICAT

approach we label both free and glutathionylated cysteines within a sample using light and heavy ICAT respectively. Provided the extent of glutathionylation is unchanged, the H:L ratio will remain constant regardless of protein abundance. The principle of differential labeling of both free and thiol modified cysteines, and not merely appending a reporter signal only to the modified cysteine is crucial to avoid this confounding outcome. There are a number of ICAT-based redox proteomics approaches which suffer from the same pitfall, where light ICAT and heavy ICAT are used to label modified thiols exclusively in 2 different samples (*123, 127*). Although this approach permits greater throughput as both samples can be combined and analyzed simultaneously, the approach requires quantification of a separate aliquot of each sample to ascertain the protein abundance between both samples because the reporter signal (i.e. the ICAT reagent) is only appended to the modified cysteine (*125*). This unnecessarily introduces extra steps, reagent costs and analytical time.

With the advent of newer developments, we anticipate that the GluICAT methodology can be further refined and enhanced. For example, the cysteine-reactive, isobaric iodoTMT tags were recently introduced and have been used to profile nitrosylated cysteines (*128*). Prior to this, ICAT was the only cysteine-reactive tag matching our requirements that was available in the market. The iodoTMT has several advantages over ICAT which makes it attractive as an alternative tagging reagent. For example, iodoTMT is 6-plex, while ICAT is duplex. This means that 2 iodoTMT reagents can be used to differentially label reduced and glutathionylated cysteines per sample, thus 3 samples can be pooled together for analysis, reducing analytical time by a factor of 3. Additionally, quantitation of peptides labeled with iodoTMT is performed at the MS/MS level, which is more sensitive, accurate, higher signal-to-noise ratio and has a larger

dynamic range than ICAT (*129*), which is quantitated at the MS level. This would improve reproducibility and sensitivity of the GluICAT method. Incorporation of new technologies will be a focus of future investigations using the GluICAT method.

2.5.2 Analysis of APAP-induced Protein Glutathionylation

2.5.2.1 HepaRG as a Model for Investigating APAP-induced Protein Glutathionylation

Currently, along with primary human hepatocytes, HepaRG cells are the gold standard for toxicity and metabolism studies, and these cells express a functional suite of disposition-related phase I (including CYP2E1 and CYP3A4) and II biotransformation enzymes, as well as transporters at levels that closely resemble primary human hepatocytes (*130-132*). Importantly, unlike primary human hepatocytes, expression levels of these proteins are stable for weeks, permitting short- to mid-term toxicity studies. Because they are derived from a single donor, cell population characteristics and behaviour are homogeneous and reproducible across different passages (*132*). HepaRG cells were also previously established to be a suitable model for investigating APAP toxicity, as it recapitulated the mechanisms and time-course of APAP toxicity as measured by GSH depletion, APAP-protein adduct formation, mitochondrial oxidative stress and peroxynitrite formation, mitochondrial dysfunction and LDH release (*133*).

2.5.2.2 Longitudinal Biochemical Analyses of APAP Toxicity

In agreement with literature, a dose of 30 mM APAP resulted in a time-dependent decrease in HepaRG cell viability over 24 h. This was corroborated by decreases in GSH levels and increases in oxidative stress. Importantly, the extent of cell viability closely paralleled GSH depletion. McGill *et al*. previously reported similar findings using 20 mM APAP in HepaRG cells (*133*). In their study, APAP

protein adduct formation (measured using a surrogate indicator of APAP-cysteine conjugate formation isolated from cell lysate and media) increased steadily upon APAP exposure, and peaked at 6 h followed by a decline during 12-24 h. Levels of protein adducts also closely paralleled GSH consumption. Additionally, covalent binding did not require extensive GSH depletion or loss of mitochondrial membrane potential, indicating that covalent binding can occur well before evidence of mitochondrial dysfunction and cell death. While we did not measure protein adduct formation in our study, the evidence provided by McGill *et al*. suggested that if protein glutathionylation was dependent on protein adduct formation, peak glutathionylation levels should occur within 6 h. Indeed, we observed maximal glutathionylation at 3 h followed by a decrease at 6 h which remained stable thereafter (Figure 2-19). In order to mimic a situation of toxic overdose, we chose to use a concentration of 30 mM APAP in our study as that was the upper limit of solubility achieved in our hands.

2.5.2.3 Overview of APAP-induced Protein Glutathionylation

From a functional perspective, nearly half of proteins glutathionylated by APAP exhibited catalytic activity, which is in agreement with literature. A study by Su *et al*. of oxidative stress-induced protein glutathionylation in mouse macrophages determined that 47% of glutathionylated proteins in their study also exhibited enzymatic activity (*124*). Furthermore, nearly 1/3 of glutathionylated proteins in our study were localized in the mitochondria, while mitochondrial proteins typically comprise about 7% of the total liver proteome (*134*). The enrichment of mitochondrial proteins in our dataset agrees with the central role mitochondrial dysfunction plays in APAP-induced hepatotoxicity (*77*).

2.5.2.4 Proteo-metabonomic Mapping of Reactome-derived Pathways

In the subsequent section, the intersections between APAP-induced glutathionylation and the manifestations of APAP toxicity will be discussed. To draw meaningful relationships between these two areas, knowledge of the biological effects of protein glutathionylation is needed. However, the field of protein glutathionylation is still in development, and only a small number of glutathionylated proteins have been further interrogated for their functional activity. In the absence of direct measurements of the effects of protein glutathionylation, we have carefully extrapolated the consequences of glutathionylation from similar forms of redox modification such as nitrosylation. There is some evidence alluding to parallels between the more well-studied nitrosylation, and glutathionylation. For example, glyceraldehyde 3-phosphate dehydrogenase (*135*), aconitate hydratase (*136*), isocitrate dehydrogenase (*137, 138*), mitochondrial complex I (*139*), ATP synthase (*140*) and protein disulfide isomerase (*141*) have been reported to undergo both nitrosylation and glutathionylation, with both forms of thiol modifications resulting in inhibition of protein activity. Similarly, both nitrosylation and glutathionylation decreased the affinity for calmodulin binding to ryanodine receptor type 1 (*142*). Notably, there is a large overlap between nitrosylated and glutathionylated proteins, which is not unexpected given that nitrosylation can be a precursor to glutathionylation (*143, 144*). Although it may be tempting to conclude that nitrosylation and glutathionylation yield identical biological effects, this may not always be the case. For example, thioredoxin is inhibited by glutathionylation (*145*), but its nitrosylation permits its transnitrosylation of other proteins. Hence, extrapolation of data from the biological effects of nitrosylation to that of glutathionylation,

where necessary, has been performed with care, and is supported by strong supplementary evidence such as complementary metabonomics data.

Aberrant glutathionylation impairs energy metabolism. The impairment of cellular energetics as characterized by depletion of ATP levels is a hallmark of APAP toxicity (*146*). In conjunction with this observation, we found that key energy metabolism pathways were glutathionylated by APAP. The glycolytic enzymes identified to be glutathionylated in our study (Figure 2-13) were all reported to be inhibited by glutathionylation (*147, 148*), suggesting that glycolysis is impaired as a result of APAP-induced glutathionylation. Interestingly, although GAPDH has been reported by several groups to be significantly glutathionylated by oxidative stress (*147*), we did not find evidence of glutathionylation in our study, as it was only significant in one replicate of the 3 h time-point. Based on metabonomics findings of decreased hepatic glucose, elevated plasma pyruvate and increased hepatic and plasma lactate levels 6 h post-dose (500 mg/kg APAP in mice), Coen *et al.* hypothesized that glycolysis was increased as a compensatory mechanism secondary to mitochondrial impairment (*96*). Our results indicate that the glycolytic proteins were glutathionylated mostly within the first 6 h and decreased subsequently, suggesting that glycolytic impairment would occur within this period. We also observed that the three proteins forming the pyruvate dehydrogenase complex were glutathionylated by APAP, while literature evidence indicate that this results in inhibition of pyruvate dehydrogenase activity (*147*). Pyruvate carboxylase (captured under the gluconeogenesis pathway (Table 2-1)), which catalyzes carboxylation of pyruvate to oxaloacetate was also observed to be glutathionylated, although its significance is unknown. It may be premature to conclude that glycolysis was enhanced on the basis of the metabonomics findings, as glucose and pyruvate fluxes are multi-

factorial and dynamic. For example, glycolysis, the Cori cycle, citric acid cycle, alanine metabolism and gluconeogenesis can modulate the levels of pyruvate either through its production or consumption (*149*). Similarly, glucose fluxes are affected by rates of glycolysis, gluconeogenesis, glycogenolysis and glycogenesis. Likewise, the increase in lactate levels can be simply interpreted as conversion of excess pyruvate to lactate by lactate dehydrogenase, which is unaffected by glutathionylation, and thus should not be used as a measure of glycolysis. Reflecting the dynamic nature of metabolite fluxes, Coen *et al*. (*96*) and Fukuhara *et al*. (*97*) reported increased plasma pyruvate levels, while decreased levels of pyruvate in urine was reported by Sun *et al.* (*100*). The conflicting data is likely a result of the choice sampling time-points which may give contrasting snapshots of the dynamic metabolic fluxes. These divergent findings can be resolved by fluxomics investigations which trace metabolite fluxes as a function of time. Our findings strongly suggested that glycolysis is impaired during the early stages of APAP toxicity and underscored the importance of complementary multi-omics investigations to interpret dynamic systems biology data.

A majority of the proteins involved in long chain fatty acid activation, transport across the mitochondrial membrane and β-oxidation were also observed to be glutathionylated in our study, while levels of fatty acids and acylcarnitines were consistently elevated in metabonomics studies of APAP toxicity (Figure 2-14). The mitochondrial carnitine/acylcarnitine carrier protein was reported to be reversibly glutathionylated, where glutathionylation inhibits transport of acylcarnitines into the mitochondria (*150*). Separately, Go *et al*. reported that a number of proteins responsible for fatty acid activation, transport across the mitochondrial membrane and β-oxidation, including those that we observed to be glutathionylated in this present study were redox modified by cadmium, a known

hepatotoxicant that induces mitochondrial dysfunction (*122*). Crucially, a parallel metabonomics investigation revealed suppressed levels of acylcarnitines and acyl-CoA metabolites upon cadmium exposure, suggesting that redox modification of these proteins impaired fatty acid β-oxidation. However, the exact nature of the redox modification (i.e. oxidation, nitrosylation or glutathionylation) was not further elucidated. Further evidence on the effects of redox modifications on fatty acid β-oxidation were provided by Moon *et al*., where oxidation and nitrosylation of acyl-CoA dehydrogenases and 3-ketoacyl-CoA thiolase were reported in alcoholic fatty liver, and the activity of 3-ketoacyl-CoA thiolase was found to be inhibited (*151*). Although glutathionylation of proteins in this pathway has not been explored as extensively as nitrosylation, when taken together, these evidences corroborate our hypothesis that APAP induces glutathionylation of proteins involved in fatty acid β-oxidation and results in a functional impairment of their activity. This manifests from a metabolic perspective as elevated fatty acids and acylcarnitines, which are located upstream of these perturbed proteins.

A series of investigations revealed that pre-treatment of mice with clofibrate, whether acute (24 h) or chronic (10 days) prior to APAP exposure conferred protection against APAP hepatotoxicity, which was unrelated to the extent of covalent binding or GSH depletion (*152-154*). It was then discovered that PPARα activation was the underlying mechanism behind the prophylactic effect of clofibrate (*155*), a PPARα inducer. Nevertheless, the link between PPARα activation and APAP toxicity has not been clarified. Interestingly, genes involved in fatty acid β-oxidation including carnitine O-palmitoyltransferase, fatty acid ligases and acyl-CoA dehydrogenases are reported to be induced by PPARα (*156*). A separate study using the PPARα agonist Wy-14,643 also demonstrated protection from APAP toxicity, accompanied by a parallel attenuation of the

increase in palmitoylcarnitines observed in untreated mice (*107*). Collectively, our results indicate that glutathionylation is a possible mechanism that links PPARα activation, fatty acid β-oxidation and APAP toxicity. We suggest that the prophylactic effects of PPARα inducers are accomplished by the upregulation of genes involved in fatty acid β-oxidation, thereby dampening the inhibitory effect of glutathionylation (and other redox modifications) on these enzymes.

The citric cycle was also found to be extensively glutathionylated in the present study, where 7 of the 8 enzyme systems catalyzing the cycle contained at least one glutathionylated subunit (Table 2-1 and Figure 2-15). Independently, multiple metabonomics studies indicate a decrease in the levels of citric acid cycle substrates, suggesting the APAP-induced glutathionylation resulted in an inhibition of citric acid cycle proteins. Indeed, aconitate hydratase (*136*), 2-oxoglutarate dehydrogenase E2 subunit (*157*), isocitrate dehydrogenase (*158*) and succinate dehydrogenase (*159*) (also known as complex II of the electron transport chain) have been reported to undergo glutathionylation, resulting in an inhibition in these enzymes. The citric acid cycle has not been directly shown to be impaired by APAP, but indirect evidence suggests that APAP causes shortage of citric acid cycle substrates, as supplementation of GSH and N-acetylcysteine (NAC) post-APAP treatment leads to a partial recovery in ATP levels (*160*). This is attributed to the amino acid constituents of excess GSH and NAC (i.e. those not used to support GSH synthesis) being used as energy substrates in the citric acid cycle (*160*). The aberrant glutathionylation induced by APAP would thus account for the decrease in citric acid cycle substrates. Collectively, the preceding discussions indicate that the citric acid cycle is *indirectly* affected by perturbations in glycolysis and fatty acid β-oxidation, which deliver the key metabolic intermediates pyruvate, acetyl-CoA and succinyl-CoA to the cycle.

This impairment is further exacerbated by *direct* inhibition of the cycle itself via glutathionylation. Direct perturbation of the citric acid cycle by APAP thus far has not been reported, and is a novel finding of our study.

APAP has been reported to exert a significant influence on mitochondrial respiration. Both complexes I and II in isolated mouse hepatocytes were found to be inhibited by NAPQI, the latter of which was more sensitive to NAPQI (*146*). This was accompanied by a decrease in ATP levels, indicative of a functional deficit in energy metabolism. These findings were recapitulated *in vivo* in mice (*161, 162*), and complex III was also reported to be inhibited by APAP (*163*). Covalent binding of APAP to ATP synthase F_1 α subunit has been reported (*43*), while APAP was found to inhibit its activity (*164*). In parallel with these observations, complexes I-III and the ATP synthase F_0 complex subunit B1 was found to be glutathionylated by 30 mM APAP in our study. Separately, complexes I, II and ATP synthase F_1 subunit α were reported to be inhibited by glutathionylation (*159, 165, 166*). We found that the ATP synthase F_1 α subunit was glutathionylated at 3 h by 0.5 mM APAP but not with 30 mM APAP; however the reason for this discrepency is unclear. The arylation of ATP synthase F_1 α subunit (*43*) and its glutathionylation by APAP supports the hypothesis that overt covalent binding and covert glutathionylation are inter-related processes. The effects of glutathionylation on the electron transfer flavoproteins which pass electrons from fatty acid β-oxidation to ubiquinone are currently unknown, but they have been reported to undergo nitrosylation (*151, 167*) with still undetermined biological consequences. Collectively, glutathionylation of the electron transport chain and ATP synthase accounts for the drastic drop in ATP levels and mitochondrial dysfunction observed with APAP. Importantly, after APAP treatment *in vivo* (*80, 168*), hepatic ATP levels were reported to decline

rapidly (maximally within 1-1.5 h) followed by a partial recovery, which is consistent with our findings where glutathionylation and impairment of proteins involved in energy metabolism is greatest at 3 h and declines thereafter (Figure 2-19), possibly indicating restoration of ATP synthesis.

Aberrant glutathionylation triggers oxidative stress. Apart from inhibition of oxidative phosphorylation, glutathionylation of the electron transport chain, particularly of complex I is known to cause a large increase in superoxide formation (*165, 169*). Increased oxidative stress localized primarily in the mitochondria is well-documented in APAP toxicity (*168*). The primary oxidants are superoxide and peroxynitrite (*77*), which is formed by reaction between superoxide and nitric oxide, and is a highly reactive and potent oxidant and nitrating species (*170*). As described in section 2.2.4, the increased oxidative stress is believed to trigger JNK activation, which translocates to the mitochondria and further amplifies oxidative stress. The increased formation of superoxide and peroxynitrite triggers the opening of the MPTP, which leads to the collapse of mitochondrial membrane potential and loss of ATP synthesis capacity. This also triggers the rupture of the outer mitochondrial membrane and release of proteins that translocate to the nucleus and cause DNA fragmentation (*77*). Despite the significant consequences of APAP-triggered oxidative stress, the initial triggers of the oxidative stress remains unclear, and is thought to be related to covalent binding by NAPQI, although the precise mechanism and protein target mediating this event has not yet been elucidated (*171*). It was suggested that covalent inhibition of glutathione peroxidase and depletion of GSH by NAPQI contributed to the accumulation of ROS (*80*), however it is unlikely that inhibition of a single member of a family of detoxification enzymes could result in such a dramatic outcome. Instead, increased production of oxidants would explain this

observation. Of the two primary oxidants, nitric oxide, the precursor of peroxynitrite was not significantly increased during the first 6 h following APAP administration (*172*). This suggests that the increase in peroxynitrite is driven by an increase in superoxide. The source of the increased superoxide was initially proposed to arise from CYP2E1 oxidation of APAP, however it was later disproved (*77*). Furthermore, CYP2E1 is primarily expressed in the endoplasmic reticulum, while the oxidative stress is located in the mitochondria. Our results suggest that significant glutathionylation of three subunits of complex I, possibly secondary to covalent binding is a potential source of increased superoxide formation. The timeline of APAP glutathionylation of complex I, which we note to occur by 3 h, agrees with reports of an initial increase in mitochondrial oxidative stress in the first 2 h of exposure to APAP (*82*). We also observed an increase in mitochondrial oxidative stress at 3 h after exposure to APAP, although not statistically significant.

Aberrant glutathionylation may perturb GSH synthesis. GSH depletion is another key hallmark of APAP toxicity, and has been ascribed to conjugation with NAPQI to facilitate its excretion and detoxification, and also quenching of oxidant species. However, there is evidence that the decrease in GSH levels may also be due to compromised GSH synthesis. For example, Harman *et al*. found no evidence of recovery in GSH levels even when hepatocytes were washed free of APAP after a 1.5 h exposure (*173*). Furthermore, by measuring the rate of GSH turnover in APAP-treated rats, Lauterberg *et al.* provided evidence that toxic doses of APAP suppressed GSH synthesis (*174*). Interestingly, we found that a number of proteins involved in GSH synthesis and sulfur amino acid metabolism were glutathionylated by APAP (Figure 2-17). In a prior pilot study not presented here, where HepaRG cells were treated with APAP for 6 h as a single replicate,

we found that both isoforms of methionine adenosyltransferase (MAT), which catalyzes the rate limiting step of cysteine synthesis (*175*) were glutathionylated by APAP (Table S2). The consequence of MAT glutathionylation is unknown, however nitrosylation was reported by Pérez-Mato *et al*. to inhibit MAT activity in rat hepatocytes (*176*). In spite of this preliminary observation, MAT did not meet the glutathionylation criteria at any point of the longitudinal investigation (MAT glutathionylation was observed in only 1 replicate of the 3 h time-point, Table S2) or with low dose APAP, and the reason for this discrepancy is unclear. Nevertheless, MAT remains an intriguing candidate that might undergo glutathionylation, as MAT is reported to be covalently bound by APAP (*43*). In support of this, the peptide that was glutathionylated in our pilot study was identical to that reported by Pérez-Mato *et al*. as nitrosylated by GSNO (*176*). Metabonomics studies further corroborate this hypothesis, as levels of *S*-adenosylmethionine (SAMe) and *S*-adenosylhomocysteine (SAH) are decreased in APAP toxicity accompanied by an accumulation of methionine. The level of trigonelline, which is generated from the methyl acceptor nicotinate during the conversion of SAMe to SAH was also decreased. Furthermore, SAMe supplementation exerted therapeutic effects similar to NAC in ameliorating liver injury in APAP overdose (*177*). Collectively, these suggest that MAT, if glutathionylated, might be inhibited and would explain the inhibition of GSH synthesis as well as decrease in associated metabolites. This requires further investigation, possibly using alternative analytical methods to determine if MAT is glutathionylated by APAP.

In our study, cystathionine β-synthase (CβS) was found to be glutathionylated by APAP. Interestingly, glutathionylation was reported to increase its activity 2-fold above basal levels (*178*). Nevertheless, GSH synthesis remains suppressed,

possibly due to MAT inhibition, and the increased CβS activity is futile as it lacks the upstream substrates. This is supported by suppressed taurine and hypotaurine levels, products of cysteine degradation, indicating a decrease in cysteine levels. On the other hand, besides providing energy substrates to maintain the citric acid cycle, supplementation with SAMe and NAC would also support increased cysteine synthesis rates which is likely to occur in response to CβS glutathionylation. Levels of spermidine and spermine, which are metabolites upstream of SAMe were decreased, and could be attributed to depletion of SAMe. Interestingly, spermidine synthase and spermine synthase, the enzymes responsible for their synthesis were glutathionylated, and it is possible that glutathionylation resulted in their inhibition. Finally, glutamate cysteine ligase (GCL) and glutamate synthetase (GS), the two key enzymes responsible for GSH synthesis were also found to be glutathionylated by APAP. While it is tempting to infer that glutathionylation might compromise their activity thereby contributing to the suppression of GSH synthesis, metabonomics findings suggest otherwise. In the absence of cysteine as a substrate, 2-aminobutyrate is conjugated to glutamic acid by GCL, and finally to glycine by GS to generate ophthalmate (*101*). This is evidenced by increased levels of γ-glutamyl-2-aminobutyrate and ophthalmate, which indicate that GCL and GS retain their catalytic activity. This observation illustrates how proteo-metabonomic mapping may be used to guide interpretations of the effects of PTMs such as glutathionylation, particularly in instances where the biological consequences of the PTM for a particular protein are unknown.

Aberrant glutathionylation may compromise protein turnover. While there is good correlation between proteomics and metabonomics data for the pathways discussed above, in the case of protein turnover and defense against cellular stress

there are limited reports from which deep analysis can be performed. Perturbations of protein turnover after APAP exposure have been reported both *in vitro* and *in vivo*. Interestingly, APAP can inhibit protein synthesis in isolated hepatocytes as early as 5 min (*179*) which remains suppressed at 1 h after exposure (*180*). Similarly, protein synthesis in mice is suppressed at 3 h, but recovers to 90% of control levels at 24 h (*181*). Inhibition of protein degradation (*179*) has also been noted for APAP. In general, in situations of elevated oxidative stress, both bacteria and eukaryotic cells exhibit suppressed protein synthesis activity, which has been ascribed in part to inactivation of enzymes involved in energy metabolism and amino acid synthesis (*182*), similar to what we have described for APAP-induced protein glutathionylation. Research in this area appears to be more focused on prokaryotes, however there are similar elements of the protein synthesis machinery between prokaryotes and eukaryotes. A number of ribosomal proteins (e.g. L5, L14, L7/L12, L27, L31, S2, S4, S17 and S2), elongation factors (e.g. ET-Tu, EF-G) and aminoacyl-tRNA synthetases have been found to undergo cysteine oxidation in bacteria, but the consequences are unclear (*182*). Oxidation of Cys^{182} in *E. coli* threonyl-tRNA synthetase, which is responsible for the editing of translated proteins results in protein mistranslation and misfolding (*183*). However, the lack of studies in eukaryotic proteins hampers interpretation and extrapolation of the effects of thiol modifications from prokaryotic studies. The evidence for glutathionylation in protein degradation is better defined. Both the E2 ubiquitin-conjugating enzyme and the 26S proteasome also undergo glutathionylation (*65, 184*), resulting in inhibition of ubiquitination and proteasomal degradation, which corroborates our findings and reports of inhibition of protein degradation by APAP. It is unlikely that perturbation of

protein turnover is the cause of APAP toxicity, but could be a contributing factor to exacerbate the original insult.

Aberrant glutathionylation may affect antioxidant defense. For antioxidant defense enzymes, APAP is known to inhibit the activities of mitochondrial superoxide dismutase 2 (MnSOD) (*185*), catalase, glutathione peroxidase and glutathione transferase (*186*). The critical role of MnSOD in APAP toxicity was demonstrated in mice heterozygous for MnSOD deficiency, which had increased liver injury and peroxynitrite formation (*77*). On the other hand, overexpression and knockout of cytosolic superoxide dismutase 1 (Cu,Zn-SOD) both unexpectedly promoted survival in mice after APAP exposure (*187*). Glutathionylation of Cu,Zn-SOD is reported to inhibit its activity *in vitro* (*188*); however in the light of evidence of APAP resistance in Cu,Zn-SOD knockout mice, the relevance of this PTM by APAP is unclear. Separately, glutathionylation of MnSOD in rats has been observed with unknown consequences (*189*). Glutathionylation of microsomal glutathione-S-transferase 1 is associated with a gain in activity and is thought to enhance the detoxification of electrophiles (*190*). Glutathionylation of peroxiredoxin 1 has been shown to inhibit its chaperone activity (*191*). Finally, glutathionylation of heat shock protein 70 was demonstrated to increase its chaperone activity and reduce protein aggregation (*192*). On the other hand, glutathionylation of the chaperone heat shock protein 90 was found to increase its degradation. Overall, the contribution of APAP-induced glutathionylation of proteins involved in defense against cellular stress is still unclear, but may impair cellular recovery mechanisms.

2.5.2.5 Additional Glutathionylated Proteins Related to APAP-induced Hepatotoxicity

Proteo-metabonomic mapping provides strong evidence that aberrant glutathionylation is a precipitating or augmentative mechanism underlying impairments in energy metabolism and mitochondrial respiration, the initial increase in mitochondrial oxidative stress and suppressed GSH synthesis that exacerbates GSH depletion. Nevertheless, there are other aspects of APAP toxicity that are not revealed by proteo-metabonomic mapping, as these do not directly involve metabolite perturbations. This warrants careful inspection of the glutathionylated proteins to extract additional correlations between glutathionylation and APAP toxicity.

Aberrant glutathionylation disrupts calcium dynamics. Maintenance of calcium homeostasis in the cell is of vital importance as calcium is an important secondary messenger that is involved in regulating numerous cellular processes, including muscle contractility, neuronal learning and memory, secretion of hormones, cell proliferation, transcription factor activation, mitochondrial citric acid cycle and ATP synthesis, apoptosis and others (*193*). Excessively high cytosolic calcium activates cellular proteases, phospholipases and endonucleases, and contributes to cell death (*193*). Given the critical role of calcium, cells normally maintain an intracellular calcium level of around 100 nM (*194*). This is accomplished by continuous extrusion of calcium from the cell out to the extracellular space by the ATP-dependent plasma membrane Ca^{2+} ATPase (PMCA), which is referred to by different authors as plasma membrane calcium-transporting ATPase, Ca^{2+}-Mg^{2+} ATPase or plasmalemmal Ca^{2+}-ATPase. Additionally, the low intracellular calcium is supported by sequestration of calcium into the smooth endoplasmic reticulum (sER) and mitochondria, mediated by the smooth endoplasmic reticular

Ca^{2+} ATPase (SERCA) transporter (*195*) and mitochondrial Ca^{2+} uniporter (MCU) respectively (*196*). Numerous studies have highlighted APAP-induced calcium dysregulation, characterized by a 10-fold increase in cytosolic and mitochondrial calcium to micromolar levels (*197-199*), which occurred as early as 45 min after APAP exposure (*198*). This increase strongly paralleled the time-course of covalent binding (*200*), and was shown to precede cytotoxicity (*199*). The increase in cytosolic calcium was attributed to inhibition of PMCA and diminished extrusion of intracellular calcium, either by arylation or oxidation of redox-sensitive thiols on PMCA (*83, 198, 201*). However, no evidence of a protein adduct to PMCA has been found (*82*), while addition of DTT was shown to reverse PMCA inhibition, restore cytosolic calcium to baseline levels and prevent APAP-induced cytotoxicity, presumably by reducing the affected PMCA thiols (*202*). Nevertheless, this is only a conjecture, and the exact mechanism of PMCA inhibition by APAP remains unknown. Specific chelation of cytosolic calcium (*203*) and co-administration of calcium channel blockers such as diltiazem, nifedipine and verapamil (*204, 205*) were able to reduce APAP toxicity by varying degrees, suggesting a causal relationship between the rise in intracellular calcium levels and APAP toxicity. The mechanism by which calcium channel blockers exert their protective effects has not been fully elucidated. These agents typically bind to L-type voltage-gated calcium uptake channels to prevent calcium influx in excitable cells, thus eliciting their anti-hypertensive or anti-arrhythmic effects (*205*). The liver is known to express one subtype of the L-type voltage-gated calcium channel (*206*), which could be a target of calcium channel blockers. Despite strong evidence indicating that dysregulation of calcium homeostasis is part of the sequence of events mediating APAP toxicity, little work

has been published on this phenomenon after an intense period of investigation from the mid-1980s to mid-1990s.

We found in our study that PMCA1 and SERCA2 were glutathionylated by APAP, while MCU was not found to undergo glutathionylation. PMCA has been reported to be inhibited by glutathionylation in aortic endothelial cells (*207*), while glutathionylation of SERCA, induced by nitrosylation in cardiac myocytes, was found to activate pumping of cytosolic calcium into the sER (*208*). PMCA glutathionylation by APAP provides the missing mechanistic link to explain the inhibition of calcium efflux by APAP, and agrees with prior hypotheses that thiol oxidation of PMCA is responsible for its inhibition. The effect of APAP on SERCA uptake of cytosolic calcium is mixed, with some reports indicating that APAP did not increase sER calcium levels (*198*) within 2.5 h, while others observed an increase, albeit not statistically significant, at 4 h with 500 mg/kg APAP, and a statistically significant decrease at 4 h with 750 mg/kg APAP (*209*) in mice. We postulate that these contrasting results could possibly be attributed to APAP-induced SERCA glutathionylation, which promotes calcium sequestration into the sER (*208*). Calcium release from sER is mediated by the inositol triphosphate receptor (IP_3R), which is sensitive to intra-reticular calcium levels, and spontaneous calcium release occurs when the sER is overloaded with calcium following continuous SERCA-mediated calcium uptake (*210, 211*). Taken together, it is possible that SERCA glutathionylation initially results in augmented calcium uptake from the cytosol as a mechanism to reduce cytosolic calcium levels. However, if the rise in cytosolic calcium levels remains unchecked (e.g. due to impaired PMCA calcium extrusion), the enhanced sER calcium accumulation past a certain tipping point eventually triggers sER calcium release, exacerbating the elevated cytosolic calcium levels. While potentially explaining

the variable reports of sER calcium fluxes, this hypothesis remains speculative and requires a detailed time-course study of sER calcium dynamics and SERCA glutathionylation in parallel. It should be noted that SERCA2, the isoform found in cardiac muscle and other non-muscle cells (*212*) was reported to be glutathionylated at Cys^{674} in rat cardiomyocytes, and is responsible for the increased calcium uptake activity. In our study, we found that SERCA2 was glutathionylated at Cys^{635} at 3 h, and at Cys^{471} at 24 h. We did not detect the tryptic peptide containing Cys^{674} in our study as it was only 4 amino acids long, with a size of 495.6 Da. When doubly charged (+2), its *m/z* of 248.8 is below the lower limit of the mass range set for TOF-MS1 scan (section 2.3.2.4). Glutathionylation at the other two sites found in our study is novel and has not been reported, although unspecified thiol modifications at Cys^{471}, Cys^{669} and Cys^{998} were reported to be induced by cadmium in mouse liver (*122*), while nitrosylation of Cys^{560} and Cys^{998} were reported in untreated mouse liver (*213*) with undetermined effects. Although the effects of glutathionylation at Cys^{471} and Cys^{635} in our study are presently unknown, it indicates that SERCA is susceptible to glutathionylation at multiple sites, and at least one site is reported to exhibit a functional consequence. Further studies using alternative proteases for protein digestion such as LysC would capture Cys^{674} in a larger peptide, and permit detection of glutathionylation, if present. Separately, we did not find evidence for glutathionylation of MCU in our study. To the best of our knowledge, MCU is not redox regulated by nitrosylation or glutathionylation. This corroborates existing data that mitochondrial calcium uptake is not affected by APAP (*209*).

After nearly two decades of little progress in the area of APAP-induced calcium dysregulation, Kheradpezhouh *et al*. recently reported a novel and unexpected protein as a key player in the cellular influx of calcium post-APAP exposure. In a

series of elegant experiments, the transient receptor potential melastatin 2 (TRPM2) was demonstrated to mediate the hepatocellular uptake of calcium after *in vitro* exposure to APAP or H_2O_2 for 1 h. Calcium influx was almost completely blocked by TRPM2 inhibitors, while knockdown using siRNA and knockout of TRPM2 in rat and mouse hepatocytes respectively achieved a similar effect. These results were demonstrated using whole cell patch-clamp techniques, which provide a longitudinal trace of ion fluxes. This approach is superior to previous studies on calcium dynamics which only yielded snapshots of calcium fluxes. Collectively, these demonstrated that TRPM2 is an important ion channel mediating hepatocellular calcium influx. Ablation of TRPM2 channels in knockout mice decreased AST and ALT levels significantly by up to 7-fold, demonstrating a protective effect against APAP toxicity *in vivo*. The mechanism of APAP-induced TRPM2 calcium influx was further demonstrated to be dependent on ADP-ribose, which acts as a ligand to activate TRPM2 (*214*). This agrees with independent studies which reported that oxidative stress induced the activation of TRPM2, not directly through thiol modifications, but by causing mitochondrial dysfunction, which triggers opening of the MPTP. This causes hydrolysis of NAD^+ to ADP-ribose by NAD^+ glycohydrolase (*215*), which is normally sequestered in the mitochondrial intermembrane space and is released upon MPTP opening. Another mechanism shown to increase cytosolic ADP-ribose levels is the activation of poly(ADP-ribose) polymerase (PARP), which then results in TRPM2 activation (*216*). Interestingly, these two events have also been reported in APAP toxicity. MPTP opening is a well-known consequence of APAP toxicity and is strongly implicated in APAP-induced mitochondrial dysfunction (*77*), while PARP, which is involved in DNA repair, is activated upon DNA damage by APAP. Inhibition of MPTP opening and PARP activation

have protective effects against APAP toxicity (*77*, *217*). Additionally, more than two decades ago, NAPQI was shown to trigger NAD^+ hydrolysis, which was prevented by incubation with cyclosporin A, an inhibitor of the MPTP (*218*); however the significance of these events were not understood at the time. Collectively, these evidences strongly support the findings of Kheradpezhouh *et al*. and corroborate the important role of TRPM2 in the derangement of calcium homeostasis by APAP. Kheradpezhouh *et al*. further noted that in view of their results, it is unlikely that PMCA inhibition is responsible for the increase in intracellular calcium levels upon APAP exposure; but rather, it appears that PMCA inhibition accompanies hepatocellular injury (*214*).

We agree with the comprehensive evidence presented by Kheradpezhouh *et al*. that TRPM2 is responsible for APAP-induced calcium entry, and TRPM2 inhibition is an attractive target for therapeutic intervention in APAP overdose. However, we are hesitant to dismiss the role of PMCA inhibition in APAP-induced calcium dysfunction. As discussed previously, restoration of PMCA activity by addition of DTT soon after NAPQI exposure was shown to decrease cytosolic calcium to baseline levels and prevent cytotoxicity (*202*). Hence, similar to TRPM2, PMCA modulation can also ameliorate the deleterious effects of APAP, indicating that PMCA does contribute towards the abnormal calcium dynamics. We believe that these two seemingly incongruous proposals can be unified in a single, holistic mechanistic explanation of calcium derangement, by considering that the rise in intracellular calcium levels could be a combination of *both* increased calcium influx through TRPM2, and inhibition of calcium efflux via PMCA. This hypothesis implies that although activation of TRPM2 alone does cause increased calcium influx, constitutive homeostatic mechanisms such as PMCA-mediated calcium efflux should reverse or dampen the influx of

calcium. We cite two examples to support this theory. Inamura *et al.* (*219*) and Togashi *et al.* (*220*) reported that exposure to ADP-ribose *alone* caused an increase in calcium efflux that was *gradually reduced*, although not to baseline levels. This decline occurred as soon as 1 min after application of ADP-ribose, but was attributed to 'desensitization', of an unknown mechanism. We propose that this decline in calcium levels shortly after ADP-ribose application is, in fact the result of competent PMCA-mediated extrusion and/or mitochondria/sER sequestration of calcium, as part of normal homeostatic mechanisms. In the case of APAP or other oxidants, sustained high intracellular calcium levels are the result of a 'double-whammy' effect exemplified by amplified influx and diminished efflux due to simultaneous TRPM2 activation and PMCA inhibition. Indeed, the rise in cytosolic calcium caused by APAP as shown by Kheradpezhouh *et al*. was not dampened, but was instead sustained for 10 min. This also accounts for the sustained influx of calcium in other studies which examined the effect of oxidants on TRPM2 activation, which are likely to have also inactivated PMCA concurrently. In other words, we propose that one without the other would not account for the effect of APAP on cellular calcium dynamics, and in fact, central to the observed dysregulation is the inhibition of PMCA as a result of APAP glutathionylation, creating a perfect storm of events. Unfortunately, Kheradpezhouh *et al*. did not investigate the effects of ADP-ribose application alone on calcium dynamics in their experimental system, which would confirm or refute our proposal.

The preceding discussion illustrates the vital, albeit neglected role of calcium dynamics in APAP toxicity. In fact, calcium perturbations may also explain some yet-unanswered questions in this area, which include the initial trigger for JNK activation and also the opening of the MPTP. For example, as discussed in section

2.2.4, oxidation of glutathione-S-transferase π (GSTπ) could trigger JNK release (*77*) which is a precursor step for its activation. Alternatively, oxidation of thioredoxin can release ASK1, which can phosphorylate and activate JNK (*77*). Both GSTπ and thioredoxin have been reported to undergo glutathionylation (*147*) are promising candidates to explain the activation of JNK which is a crucial event; however we did not observe glutathionylation of either protein in this present study. Calcium has been reported to activate ASK1 and JNK (*221*), while high calcium levels in the mitochondria are well-known to trigger opening the MPTP (*222*). Interestingly, calcium has been reported to activate nitric oxide synthase, increasing nitric oxide production (*193*), which could have implications on peroxynitrite and oxidative stress generation. In light of these recent findings, further investigation of calcium dynamics is warranted.

Aberrant glutathionylation could trigger MPTP opening. While calcium can activate MPTP opening, it is possible that protein PTMs may also trigger this event. The voltage-dependent anion channel (VDAC) and adenine nucleotide translocase (ANT), also known as ADP/ATP translocase have been long thought to be the main pore-forming components, however their role has not yet been proven conclusively and remain controversial, as the MPTP can still form even when either one is absent (*222*). Interestingly, we found that VDAC1-3, as well as ANT1/2 were glutathionylated by APAP. The consequences of VDAC and ANT glutathionylation are still unknown; however there are some potential hints as to the effect of glutathionylation. For example, knockdown of cytosolic Grx1 resulted in increased oxidized VDAC (*223*) and a loss of mitochondrial membrane potential. The oxidation state of the vicinal thiols of VDAC is known to critically affect mitochondrial membrane potential and MPTP opening (*224*), and it is possible that VDAC glutathionylation may promote MPTP opening. The

effects of thiol modification of ANT remain controversial, with reports of both activation and inactivation. Queiroga *et al*. reported that carbon monoxide induced glutathionylation of ANT and also prevented the loss of mitochondrial membrane potential (*225*). Conversely, Halestrap *et al.* reported that oxidation of Cys^{160} (erroneously reported as Cys^{159}) in ANT rendered the MPTP insensitive to ADP-mediated inhibition of calcium-dependent MPTP opening, indirectly suggesting that Cys^{160} oxidation promoted calcium-dependent pore opening (*226*). Interestingly, VDAC and ANT were recently reported to also be nitrosylated. Nitrosylation induced by GSNO appeared to potentiate mitochondrial swelling, an indication of MPTP opening (*140*). However, the authors did not demonstrate a direct cause-effect relationship between VDAC/ANT nitrosylation with MPTP opening. In our study, we found that ANT was glutathionylated at 3-6 h, while VDAC was generally glutathionylated at 12-24 h. McGill *et al*. reported that a decrease in mitochondrial membrane potential, an indicator of MPTP opening occurred at 12-24 h after exposure to APAP in HepaRG cells (*133*). The time-course suggests that VDAC glutathionylation was associated with MPTP opening. Cyclophilin D has been reported to modulate pore opening, but we did not observe glutathionylation of this protein. Instead, glutathionylation of a related protein, cyclophilin A (also known as peptidyl-prolyl cis-trans isomerase A) was observed. Although the effects of glutathionylation are not known, cyclophilin A has been recently suggested to contribute to the modulatory activity of cyclophilin D on MPTP opening (*227*).

McGarry *et al*. recently reported the basal glutathionylation status of mouse liver proteins, and disclosed an ongoing study of APAP-induced glutathionylation using a resin-assisted enrichment approach to profile protein glutathionylation (*126*). It would be interesting to compare the glutathionylated proteome in our

study and that of McGarry *et al*., given that they have used an *in vivo* mouse model, while we have used an *in vitro* human model. However, a potential caveat is that their methodology would need to account for and distinguish changes in protein expression versus changes in protein glutathionylation, as currently their reported approach does not take this critical confounder into consideration.

2.5.2.6 Longitudinal Progression of APAP-induced Protein Glutathionylation

Overall, APAP-induced protein glutathionylation appeared to peak at 3 h, while McGill *et al*. profiled a temporal increase in APAP-cysteine conjugates (used as a surrogate measure of covalent binding) that peaked at 6 h and declined thereafter in HepaRG cells (*133*). This suggested that the majority of the aberrant perturbations (which include those found to be relevant to APAP toxicity) occurred during the early phase of APAP toxicity as covalent binding is developing. Heat map analysis of normalized peak H:L fold-change values indicated clustering of peptides in distinct temporal regions, suggesting that behind the broad, overall glutathionylation trend, there was a time-dependent stratification of glutathionylated peptides. Nonetheless, analysis of glutathionylated peptides in the mid and late clusters failed to reveal pathways that could be relevant to APAP toxicity. The markedly weaker associations with critical pathways of APAP toxicity during the mid to late time-points suggest that the glutathionylation pattern at these periods was diluted with proteins that do not have meaningful relationships with APAP toxicity. It is possible that while APAP induced temporal glutathionylation of different proteins, only a proportion of them are biologically relevant to the development of APAP toxicity. In other words, despite an apparent temporal clustering, there could be a large number of non-relevant, 'bystander' proteins glutathionylated as a result of collateral damage. This is likely since the number of glutathionylated peptides in the 3 key

biological processes decreased with time, yet the total number of glutathionylated peptides remained relatively unchanged. The appearance of temporal clusters is unsurprising as a parallel biochemical analysis revealed an increasing trend of oxidative stress up to 24 h (Figure 2-11), thus peptides in these clusters could be glutathionylated not as a cause, but a consequence of toxicity. Broadly speaking, the longitudinal analysis of protein glutathionylation therefore suggests that there are two groups of glutathionylated proteins: those that are glutathionylated, likely as a result of APAP bioactivation, that initiate or perpetuate the initial stages of toxicity; and those that are glutathionylated in the mid to late stages likely by oxidative stress, as an outcome of toxicity, and might not contribute to the development of toxicity. We are mindful that from a practical standpoint, since both processes can occur concurrently it is impossible to definitively assign proteins glutathionylated by overt covalent binding and those glutathionylated by oxidative stress. Nonetheless, based on the temporal pattern of covalent binding reported by McGill *et al.* in HepaRG cells (maximal at 6 h) (*133*) versus oxidative stress (maximal at 12-24 h) (Figure 2-11), APAP-induced glutathionylation of critical proteins (maximal at 3 h) more closely matches the time-course of covalent binding than oxidative stress, hence suggesting an association with the former. Investigations of the temporal patterns of total covalent binding by APAP in HepaRG cells would provide further information on a causal relationship between glutathionylation and covalent binding.

It is important to note that we are not disregarding the biological relevance of glutathionylated proteins in the mid and late clusters. It is possible that we are not able to make mechanistic connections between glutathionylation and APAP toxicity during these time-points because of incomplete information regarding the effects of proteins glutathionylated at these time periods. As a notable exception,

the opening of the MPTP and loss of mitochondrial membrane potential was reported by McGill *et al*. to occur during the 12-24 h period (*133*), and VDAC was found to be glutathionylated at the same time which allowed a potential temporal association to be established. It is expected that as more information on the biological consequences of protein glutathionylation is uncovered, the importance of glutathionylation during the mid to late stages of APAP toxicity will become clearer.

Altogether, these findings emphasize the importance of proteome-wide, deep analysis of glutathionylation. A broad-based overview using non-specific approaches like Western blotting would not be able to distinguish these two groups of glutathionylated proteins and hamper identification and analysis of the critical glutathionylated proteins. In the only other study of APAP-induced protein glutathionylation, Yang *et al.* reported that total protein glutathionylation in APAP-treated mice was unexpectedly always lower when compared to control mice at 1, 3, 6 and 24 when examined using a Western blot approach. Immunohistochemical analyses showed however that there was a spatial progression of glutathionylation in livers of APAP-treated mice from the centrilobular region outwards over time (*86*). Their findings corroborate the importance of careful interpretations of global patterns which may obscure underlying trends.

2.5.2.7 Dose- and Bioactivation-dependent Protein Glutathionylation by APAP

To determine whether APAP-induced glutathionylation is dose-dependent, we compared the glutathionylation profile of HepaRG cells treated with 30 mM APAP and 0.5 mM APAP for 3 h. The 3 h time-point was chosen for comparison as it exhibited the highest number of glutathionylated proteins with 30 mM APAP, and it was anticipated that any dose-dependent changes in the

glutathionylation profile would be most prominent at this time-point. A dose of 0.5 mM APAP was chosen to investigate the effects of mild APAP exposure on protein glutathionylation. This was due in part to dose considerations of the CYP2E1 inhibitor diethyldithiocarbamate (DEDC). DEDC, a mechanism-based inactivator of CYP2E1 (*228*) has been shown to markedly reduce lipid peroxidation, GSH depletion, malonedialdehyde formation and hepatotoxicity in mice when given 30 min before APAP administration, at an approximately 1:1 molar ratio (*229*). *In vitro*, DEDC was found to prevent cytotoxicity only if hepatocytes were pre-treated with DEDC, but did not exhibit protective effects when added after APAP exposure (*230*). However, when administered at elevated levels, DEDC itself has been shown to cause increase oxidative stress and inhibition of antioxidant defense enzymes including superoxide dismutase and catalase, decreased GSH levels, increased lipid peroxidation and hepatotoxicity *in vivo* (*231*). Furthermore, 1 mM DEDC did not affect ATP levels in rat liver slices, but caused ATP depletion and increased lipid peroxidation at doses of 5 mM and 10 mM (*232*). Based on these findings, we chose to use DEDC at concentration of 0.5 mM which is likely sub-toxic, and an equimolar dose of 0.5 mM APAP as a comparator.

Our results suggest that glutathionylation of proteins deemed biological important to the development of APAP toxicity was decreased as a result of exposure to a lower dose of APAP. Although there was only a small decrease in total number of glutathionylated peptides with 0.5 mM APAP, there was a far larger decrease for the subset of toxicologically important peptides. This seems to suggest that there was an apparent redistribution of the glutathionylation profile at low dose APAP, since the total number of glutathionylated peptides was not significantly affected. This was not further analyzed as the objective of this investigation was to

examine the effect of low dose APAP on the glutathionylation of peptides identified as important in mediating APAP toxicity namely energy metabolism, protein turnover and defense against cellular stress. This possibility is also supported by a similar observation in the longitudinal study, where the number of glutathionylated peptides in these 3 groups decreased over time while the total number of glutathionylated peptides remained steady from 6-24 h. The redistribution of protein glutathionylation as a function of time and dose would be an interesting aspect for further investigations.

The importance of APAP bioactivation in the genesis of aberrant glutathionylation is indicated by the decrease in the total number of glutathionylated peptides, as well as those deemed biologically important when comparing 0.5 mM APAP and 0.5 mM APAP + DEDC. Although the number of glutathionylated peptides involved energy metabolism was not significantly different, decreases were observed for protein turnover and defense against cellular stress. The use of DEDC to inhibit CYP2E1-dependent NAPQI formation did not abolish APAP-induced glutathionylation for several reasons. Firstly, the use of DEDC itself may introduce another source of oxidative stress, although we attempted to limit this by using a low DEDC concentration. Secondly, NAPQI formation can also be mediated by other CYP450 enzymes, including CYP3A4, although the contributions from these enzymes are reported to be low (*233, 234*). It should be noted that while some authors have reported that CYP3A4 is the primary isoform responsible for NAPQI generation (*235*), it is generally accepted that CYP2E1 is the major isoform responsible for NAPQI formation. Inhibition of CYP2E1 by DEDC thus may reduce, but not completely eliminate glutathionylation. The use of a pan-CYP inhibitor may circumvent this possibility; nevertheless we decided to utilize DEDC as there are a number of *in*

vitro and *in vivo* studies demonstrating that DEDC can protect against APAP toxicity, while no pan-CYP inhibitor has been shown to exhibit this effect. Thirdly, APAP-induced glutathionylation is likely to arise as a result of both NAPQI and ROS formation (Figure 2-11). Oxidative stress would account for background glutathionylation. As such, this result serves as a positive indication that bioactivation of NAPQI contributes to APAP-induced glutathionylation. Future follow-up studies using siRNA-based CYP2E1 and CYP3A4 knockdown systems would further clarify this phenomenon.

2.5.2.8 Comparative Analysis of AMAP- and APAP-induced Protein Glutathionylation

AMAP has often been used as a non-toxic regioisomer of APAP in comparative studies of the effects of covalent binding on toxicity. Both AMAP and APAP cause equivalent levels of covalent binding, however AMAP is non-hepatotoxic, while APAP causes liver toxicity (*236*). This apparent difference is attributed to differential covalent binding at a subcellular level, where reactive metabolites of AMAP preferentially bind to mouse liver proteins in the cytosolic and microsomal compartment, while NAPQI binds more extensively to mitochondrial and nuclear proteins (*201*). Mass spectrometric analysis of covalent adducts formed with AMAP and APAP appear to confirm this observation (*42, 43*). This is unsurprising given that the mitochondria plays a central role in APAP toxicity. Importantly, this difference was not due to preferential generation of reactive metabolites from APAP in the mitochondria (*201*). There are two phenotypic differences between APAP and AMAP that could explain mechanistically the differential toxicity observed. Firstly, despite causing equivalent levels of covalent binding in the plasma membrane, AMAP did not exhibit inhibition of PMCA activity, nor did it cause elevations in cytosolic and mitochondrial calcium

levels (*201*). Secondly, AMAP did not cause a decrease in free protein thiols, as does APAP (*80*). This suggests that a possible explanation for the non-toxic nature of AMAP is due partly to its inertness with regards to thiol modification, which also corroborates the absence of PMCA inhibition. Given the differences observed between AMAP and APAP, particularly with regards to their preferential covalent binding, we sought to use AMAP as a tool to elucidate differentially glutathionylated proteins between APAP and AMAP. Unexpectedly, there was a large overlap between proteins glutathionylated by these two agents, even for those postulated to play key roles in the genesis of APAP toxicity. Furthermore, in contrast to previous reports on proteins covalently bound by AMAP, we found that more than 1/3 of glutathionylated proteins were localized in the mitochondria, while none were found in the endoplasmic reticulum. A potential explanation for this result was provided by Hadi *et al*., who found that contrary to expectations, AMAP was toxic in rat and human liver, while remaining non-toxic in mouse liver (*237*). This is an important finding as the comparative toxicology studies between APAP and AMAP described above were performed in mice. There was a dramatic difference in ATP levels, liver morphology and viability of mouse precision cut liver slices compared with those of rat and human origin. In fact, APAP and AMAP caused the same extent of cell death in human liver. While the protein targets of APAP and AMAP in mouse, rat and human liver were not elucidated, similar protein expression profiles were found between APAP-treated mice liver, and AMAP- or APAP-treated rat and human liver, which was markedly different from that of AMAP-treated mouse liver (*237*). The reason for the species difference is still unclear, but it would be interesting to determine the glutathionylation pattern of APAP and AMAP in mouse liver.

The treatment duration of 6 h was initially chosen for AMAP as we observed substantial glutathionylation by APAP in our pilot study of the 6 h time-point. Samples for the longitudinal study of APAP and 6 h AMAP were prepared at the same time, before we observed that glutathionylation of APAP was highest at 3 h. Nevertheless, the large degree of overlap of glutathionylated proteins between APAP and AMAP corroborates the finding of similar toxicity between APAP and AMAP. As it was reported that AMAP does not modulate calcium levels and PMCA activity, we examined glutathionylation of proteins involved in calcium dynamics and found that AMAP glutathionylated SERCA but not PMCA. However, it is possible that we missed observing PMCA glutathionylation by AMAP, especially if the temporal glutathionylation profile of AMAP parallels that of APAP, as PMCA glutathionylation by APAP occurred only at the 3 h time-point.

2.6 Chapter Conclusion

Protein glutathionylation is a regulatory PTM that is redox sensitive. Perturbations of this PTM can alter cellular homeostasis and cause deleterious effects. We present a framework to illustrate the mechanisms of covert APAP-induced protein glutathionylation which is secondary to overt covalent binding. To study aberrant protein glutathionylation by APAP, the GluICAT methodology was developed which was carefully designed to circumvent many limitations of existing approaches. Global profiling of APAP-induced protein glutathionylation in HepaRG cells using GluICAT revealed a number of aberrantly glutathionylated proteins in several key biological processes that are central to APAP toxicity. Importantly, proteo-metabonomic mapping correlated functional impairment of energy metabolism networks and GSH synthesis with metabonomic perturbations caused by APAP, providing a mechanistic explanation for these aspects of APAP toxicity. Glutathionylation provides an explanation for the increase in mitochondrial oxidative stress, derangements in calcium dynamics and mitochondrial dysfunction, which are key events in the toxicity spectrum. Aberrant glutathionylation illuminates the mechanism of action for agents exhibiting prophylactic or therapeutic activity, which are suggested to counteract the debilitating effects of APAP-induced glutathionylation. A temporal analysis of glutathionylation patterns suggested that glutathionylation is likely to participate in the early stages of APAP toxicity, and proposed the existence of two groups of proteins, whereby glutathionylation of the first group precipitated and/or propagated toxicity, while glutathionylation of the second group is likely a consequence of toxicity. The former is possibly induced by covalent binding, while the latter driven by oxidative stress. Aberrant glutathionylation was also likely dose-dependent, and could be ameliorated by inhibition of APAP

bioactivation. Comparative analysis of glutathionylation patterns between AMAP and APAP unexpectedly revealed broad overlaps between proteins glutathionylated by both these agents, which is in line with recent reports that they exhibit comparable toxicity in humans. Collectively, these findings provide strong mechanistic evidence that covert, aberrant APAP-induced glutathionylation is responsible for the initial events in APAP toxicity, which occurs as a result of overt covalent binding. Our work furnishes previously unrecognized mechanisms of drug-induced liver injury to the attention of mechanistic toxicology and fuels fresh perspective into the role of covalent binding in drug-induced liver injury.

Chapter 3 Strategies to Mitigate the Deleterious Effects of Covalent Binding

3.1 Chapter Summary

Background: Covalent and coordinate binding caused by reactive metabolites can lead to irreversible inactivation of CYP450 enzymes, which can cause DDIs and ADRs. These undesirable effects are attributed to the unexpected formation of reactive metabolites. The extent of reactive metabolite formation is a function of a number of factors, including the intrinsic bioactivation potential of the molecule, dose burden administered and the metabolic capacity of the enzymes responsible for its generation. Reactive metabolite formation by lapatinib results in MI complex formation and MBI, resulting in permanent inactivation of CYP3A4/5, leading to significant DDIs with CYP3A4/5 substrates. Additionally, covalent binding by the reactive quinone-imine intermediate may be responsible for the hepatotoxicity seen with lapatinib.

Objective: In this chapter, we explore two approaches to reduce reactive metabolite formation. Firstly, we attempt to reduce the bioactivation potential of the molecule by strategic deuteration at positions critical for bioactivation. We also assessed the relationship between metabolic capacity and susceptibility to inactivation by CYP3A5 as a function of genetic disposition.

Methodology: Deuterated analogues at the benzylic and/or N-methylene position were assessed for their potential to undergo *O*-debenzylation, *N*-dealkylation and GSH adduct formation. The strength of inactivation of each analogue elicited against CYP3A4/5 was also investigated. The most promising deuterated analogue was then examined to determine if it retained pharmacological activity

similar to lapatinib. The strength of inactivation and GSH adduct formation was also assessed in a panel of CYP3A5 genotyped pooled human liver microsomes.

Results and discussion: Among the three deuterated lapatinib analogues, O-d_2 lapatinib was found to exhibit to lowest rates of *O*-debenzylation, *N*-dealkylation and GSH adduct formation, and exhibited a similar extent of cytotoxicity as lapatinib. However, it retained the same magnitude of CYP3A4/5 inactivation as lapatinib. Separately, CYP3A5*1/*1 carriers experienced the greatest decrease in CYP3A4/5 activity, were most susceptible to inactivation by lapatinib, and also generated the highest levels of quinone-imine as measured by GSH adduct formation.

Conclusion: The results of this study suggests that structural modification of lapatinib through deuteration does not ameliorate its potential for DDIs, while CYP3A5*1/*1 carriers may be most likely to experience DDIs with lapatinib.

3.2 Chapter Introduction

Lapatinib is a dual tyrosine kinase inhibitor of the epidermal growth factor receptor (EGFR) and the human epidermal growth factor receptor 2 (HER2). This orally active drug was first approved by the US FDA in 2007 for the targeted therapy of breast cancer overexpressing HER2. By reversibly competing with ATP for the intracellular ATP binding site on the receptors, lapatinib blocks auto-phosphorylation of the receptors, leading to inactivation of downstream cell proliferation and induction of apoptosis (*238, 239*). Lapatinib is typically indicated for use with capecitabine to treat HER2-positive metastatic breast cancer patients who are refractory towards therapies such as anthracyclines, taxanes and trastuzumab-containing regimens (*240*). In 2010, lapatinib was also approved for coadministration with letrozole for the treatment of patients suffering from hormone-positive and HER2-postive metastatic breast cancer (*241, 242*).

3.2.1 Generation of Reactive Metabolites from Lapatinib

Lapatinib undergoes extensive metabolism in the liver, mediated mainly by CYP3A4/5, forming reactive metabolites that are postulated to inactivate CYP3A4 (*243-245*) and CYP3A5 (*246*). This auto-catalytic inactivation proceeds via two main pathways as illustrated in Figure 3-1. *N*-dealkylation, mainly mediated by CYP3A4 (*245*), generates *N*-dealkylated lapatinib (ND lapatinib), which can be further oxidized to an alkylnitroso intermediate suggested to inactivate CYP3A4 by forming a quasi-irreversible metabolite-intermediate (MI) complex (*244*). Alkylnitroso groups are highly electrophilic, and can form strong coordinate bonds with the heme groups of CYP450 enzymes, which prevents the metabolism of other CYP450 substrates (*247*). Conversely, *O*-debenzylation is primarily mediated by CYP3A5 (*245*), where *O*-debenzylated lapatinib (OD

lapatinib) is further oxidised to a quinone-imine that covalently inactivates CYP3A5 irreversibly via mechanism-based inactivation (MBI) (*246*). In this study, the term MBI is used solely to describe the *covalent* binding of a reactive metabolite to the enzyme responsible for its formation, as opposed to being an umbrella term for irreversible time-dependent inactivation, which can include coordinate and covalent binding. In parallel, an MI complex is used in this work to describe the *coordinate* binding of a reactive metabolite to the heme group of CYP450 enzymes. Both ND lapatinib and OD lapatinib have also been detected in the plasma, urine, and faeces of human subjects (*248*), suggesting that further bioactivation to reactive lapatinib metabolites is likely *in vivo*. The auto-catalytic inhibition of CYP3A4/5 by reactive lapatinib metabolites is a clinical concern, as CYP3A4/5 play major roles in the metabolism of many drugs, potentially leading to clinically significant DDIs with other CYP3A4/5 substrates. These DDIs could consequently lead to sub- or supra-therapeutic drug levels, and consequently suboptimal therapy or drug-induced toxicity.

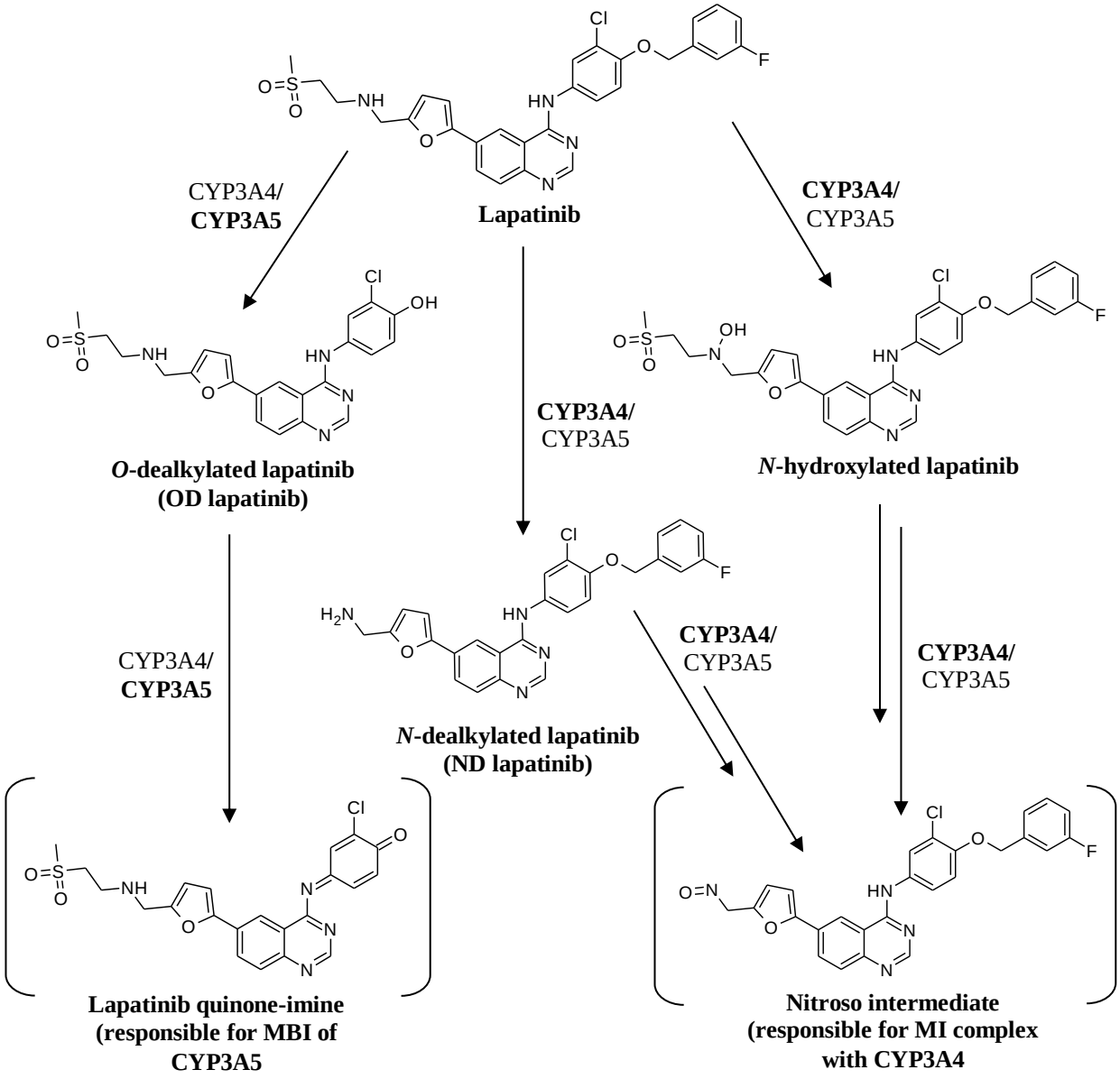

Figure 3-1 Major CYP3A4/5-dependent biotransformation pathways of lapatinib (adapted from (*245*, *246*)). Intermediates in square brackets are putative reactive metabolites believed to inactivate CYP3A4 or CYP3A5. The predominant biotransforming enzyme for each step is indicated in bold.

Interestingly, the differential inactivation of CYP3A4 and CYP3A5 through a MI complex and MBI respectively appears to be mutually exclusive, although each enzyme is capable of forming both ND lapatinib and OD lapatinib, albeit in differing amounts. For example, the inactivation of CYP3A4 which is characterized by the presence of a Soret peak is nearly completely reversible by potassium ferricyanide (*244*), and mass spectrometry analysis of the CYP3A4

apoprotein failed to identify mass shifts corresponding to the formation of a protein adduct (*244*), suggesting that the inactivation is exclusively due to the formation of an MI complex. On the other hand, the inactivation of CYP3A5 by lapatinib was shown not to be reversed by potassium ferricyanide (*245*), and together with the observed lack of a Soret peak (*244*), these findings suggest that the inactivation is likely exclusively due to MBI.

3.2.2 Adverse Drug Reactions Associated with Lapatinib

Lapatinib has been associated with frequent ADRs such as diarrhoea and skin rash which are clinically manageable (*249, 250*). However, it was reported to cause potentially fatal hepatotoxicity, leading to a black-box warning issued in 2008 (*251*). As only less than 1% of patients experienced hepatotoxicity and it occurs several days to months after initiation of treatment with lapatinib (Tykerb package insert, 2007), such toxicity appears to be a type B idiosyncratic reaction. Additionally, lapatinib-induced hepatotoxicity has been postulated to have an immunological dimension, as a series of pharmacogenomic studies revealed associations with the MHC class II *HLA-DQA1*02:01* and *HLA-DRB1*07:01* alleles, which are in strong linkage disequilibrium (odds ratio of 14) (*252-255*). Of these two alleles, modelling studies of the binding pocket amino-acid specificity suggested that *HLA-DRB1*07:01* is most likely the causal allele (*255*). The negative predictive values and positive predictive values for ALT elevations 3× the upper limit of normal were 99.1% and 11.7% respectively. In other words, essentially all individuals who experience serious lapatinib-induced liver injury carry this biomarker, but the majority of biomarker carriers do not develop serious liver injury, suggesting that there may be other concurrent cofactors or triggers that contribute to this event. While the mechanism of lapatinib-related hepatotoxicity remains unknown, the generation of a reactive intermediate from

lapatinib capable of covalent binding to CYP3A5 is suggestive of the hapten hypothesis and may be the additional cofactor that predisposes a *HLA-DRB1*07:01* allele carrier to lapatinib-induced hepatotoxicity.

3.2.3 Variables Affecting Lapatinib-induced DDIs and ADRs

While the DDIs, and possibly hepatotoxicity caused by lapatinib are precipitated by the formation of reactive metabolites leading to covalent and coordinate binding, these are not static events, but are a function of the inherent bioactivation potential of the drug, dose burden and metabolic capacities of the enzymes responsible for its bioactivation, CYP3A4 and CYP3A5. Modulation of any of these variables could change the extent of DDIs and ADRs caused by lapatinib.

3.2.3.1 Reducing Generation of Reactive Metabolites from Lapatinib

Structural modification of the pharmacophore is a well-known strategy in medicinal chemistry to alter binding properties of a drug to its pharmacological target. Similar approaches have been applied to modify the toxicophore to prevent or reduce bioactivation to form a reactive metabolite believed to be responsible for toxicity. A common example is the substitution of a labile hydrogen atom with a fluorine atom to prevent bioactivation that leads to the formation of a reactive metabolite. Care must be taken to ensure that the chemical modification does not compromise the pharmacological activity of the compound. This is illustrated in the example of amodiaquine, an antimalarial which is oxidized to form a quinone-imine. Fluorination of the 2',6'- and 4'- positions produced analogues more resistant to oxidation but still retaining activity against malarial parasites (*256*).

Despite successful examples using fluorine as a bioisostere, the physicochemical properties of fluorine are sufficiently different from hydrogen that the pharmacological activity of the fluorinated analogue may be compromised. In

recent years, drug deuteration has gained interest as a viable strategy to manipulate metabolic susceptibilities. Deuteration involves the substitution of a hydrogen (H) atom with deuterium (D), and this increases the C-D bond strength relative to the C-H bond strength, resulting in a higher energy barrier for C-D bond cleavage and hence a slower rate of reaction. This effect on reaction rate is also known as the primary deuterium isotope effect (DIE). In the context of CYP450-mediated drug metabolism, the characteristics of the DIE present a unique opportunity to modulate undesirable biotransformation pathways by selective and judicious deuteration at metabolic soft spots. For example, *O*-debenzylation of lapatinib proceeds via the mechanism as shown in Figure 3-2 where a proton is first abstracted by the heme group of the CYP enzyme, and the hydroxyl group is subsequently transferred onto the benzylic carbon. This forms an unstable hemiacetal group, which leads to a loss of the benzylic group and the formation of OD lapatinib. By substituting the benzyl proton with deuterium, the DIE slows down the rate of C-D bond cleavage. This has a carry-over effect on the subsequent steps, thus reducing the overall rate of *O*-debenzylation. A similar process governs *N*-dealkylation as well.

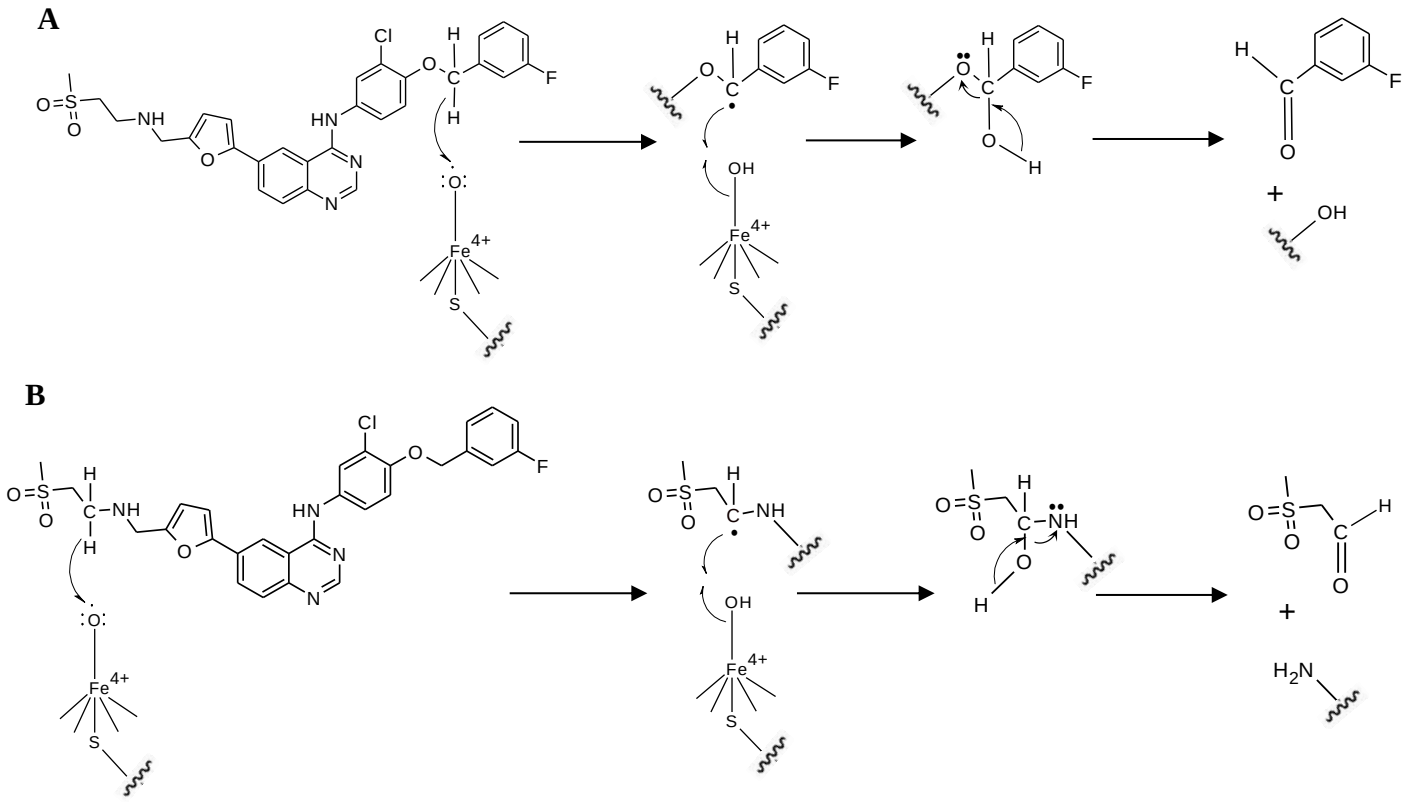

Figure 3-2 Mechanism of (A) *O*-debenzylation and (B) *N*-dealkylation of lapatinib.

Unlike fluorine substitution, the DIE generally has little influence on the physicochemical properties of deuterated compounds, as deuterium has a similar size to hydrogen and imposes minimal changes in steric effects. Although small changes such as reduced hydrophobicity (*257*, *258*), decreased acidity of carboxylic acids and phenols (*259*), and increased basicity of amines (*260*) have been reported, these physicochemical differences generally do not exert a significant influence on target engagement by the deuterated compound. Hence, deuteration has become a promising approach to improve the pharmacokinetic and/or safety profile of the drug while imposing a minimal efficacy penalty. However, it is important to note that mechanistically, a decrease in one metabolic pathway may not necessarily lead to an overall decrease in clearance, as a

compensatory increase in an alternative/competing metabolic pathway can continue to sustain metabolic clearance, a phenomenon known as metabolic switching (*261*). This may also elevate the levels of minor metabolites and elicit unanticipated consequences. Thus the effect of the DIE can be difficult to predict and requires additional *in vitro* and *in vivo* experimental elucidation.

Deuteration has been successfully applied to a number of drugs to improve their pharmacokinetic and/or safety performance. One example is C-20081 (Figure 3-3), a deuterated analogue of linezolid, which is an antibiotic indicated for serious Gram-positive infections. Deuteration of the morpholine ring led to decreased metabolism of linezolid and a 43% increase in plasma half-life, with unchanged efficacy (*262*). The reason for deuteration adjacent to the acetamide moiety is unclear, but might be a pre-emptive attempt to suppress metabolic switching as a result of attenuated morpholine ring opening. Drug deuteration can also reduce toxic metabolite production by diverting metabolism along pathways that avoid the formation of toxic metabolites, hence improving the safety profile. This can be seen in the deuteration of efavirenz (*263*). Efavirenz undergoes a four-step reaction to produce a nephrotoxic metabolite; it undergoes oxidation, sulfation at the C8 position, oxidation at the propargyl group, formation of an adduct with GSH that is finally cleaved by γ-glutamyl transpeptidase to yield the metabolite responsible for nephrotoxicity (Figure 3-4). Deuteration of efavirenz at the propargyl group diminishes the formation of reactive metabolite precursors, thus decreasing reactive metabolite concentration and hence reducing renal toxicity (Figure 3-4).

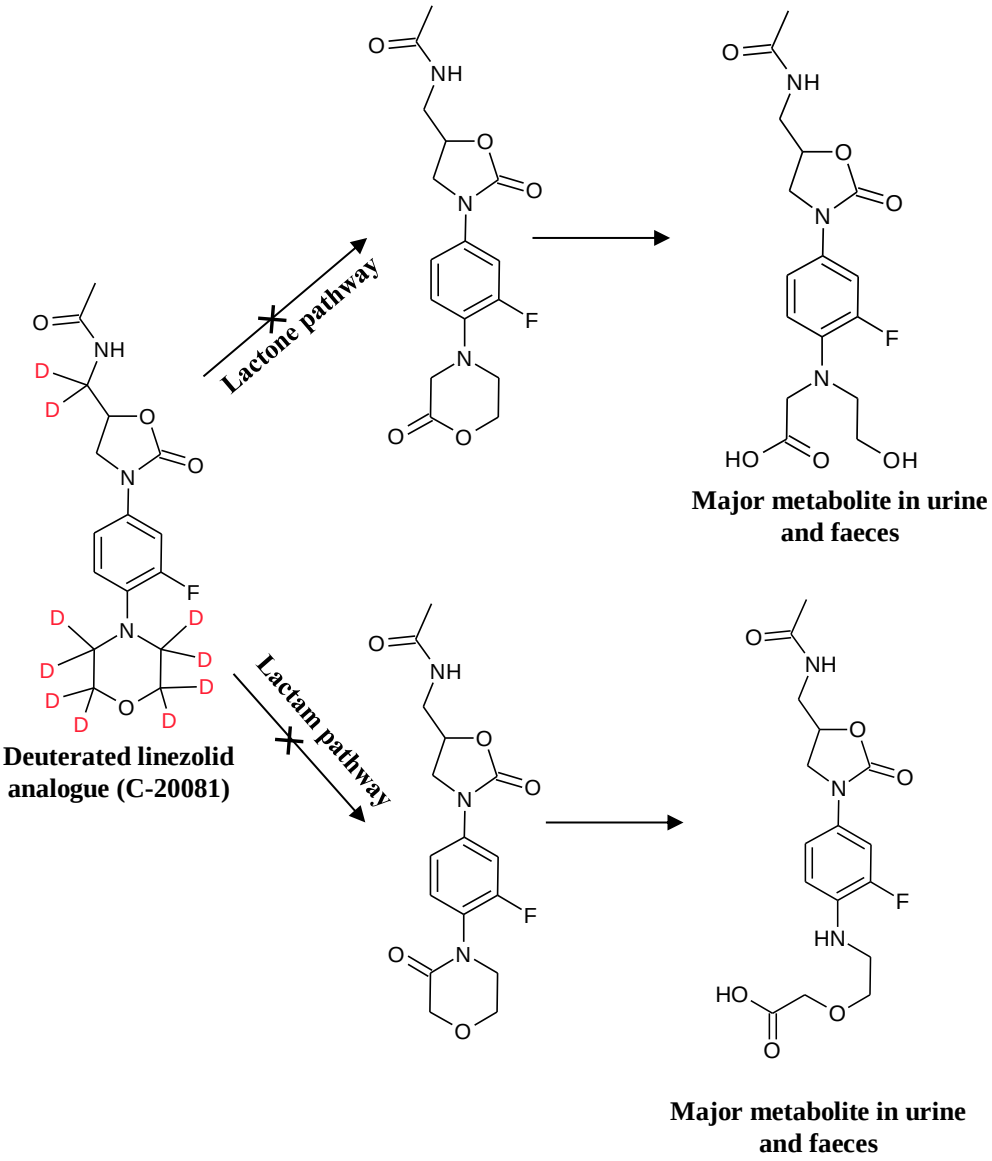

Figure 3-3 Deuteration of linezolid at the morpholine ring reduces its metabolic clearance.

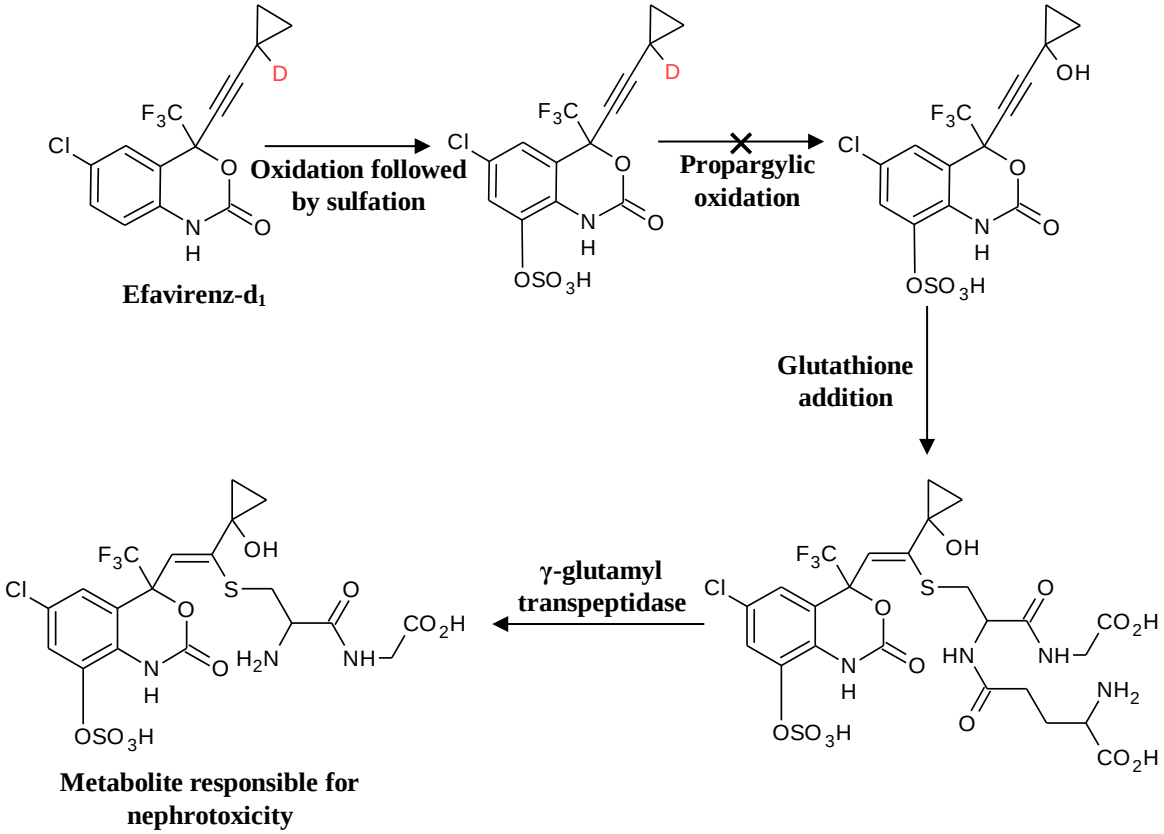

Figure 3-4 Single deuteration of efavirenz at the propargyl group reduces reactive metabolite formation.

Despite examples of successful modulation of pharmacokinetic and toxicological profiles by deuteration, the desired outcomes can be unpredictable. Due to the complexity of biological processes and various competing pathways in multistep enzyme-catalyzed reactions, the expected effects are difficult to predict from a structural perspective alone (*264, 265*). In some cases, a significant effect *in vitro* may not translate to the expected outcome *in vivo*. A deuteration study on tramadol showed that one of the deuterated tramadol analogues had a 5-fold reduction in *in vitro* metabolic clearance and was thus expected to have a longer duration of action, yet *in vivo* rat studies showed that the deuterated analogue was not superior to tramadol in terms of potency or duration of action (*266*). It is clear

that although deuteration appears to be a viable approach to modulate reactive metabolite generation and, potentially DDIs and/or ADRs from lapatinib, comprehensive experimental investigations are still required to ascertain the true effect of this structural modification.

3.2.3.2 Assessing the Capacity of Lapatinib in Generation of Reactive Metabolites

The metabolic capacity of CYP450 enzymes, and accordingly, the levels of reactive metabolites generated are determined by extrinsic and intrinsic factors. In the case of lapatinib, examples of extrinsic factors include the concomitant administration of xenobiotics that are inducers or inhibitors of CYP3A4 and CYP3A5. *In vitro* studies by Teo *et al.* and Hardy *et al.* demonstrated that CYP3A4/5 inducers such as dexamethasone and rifampin potentiated the cytotoxicity of lapatinib, which correlated with an increase in the formation of OD lapatinib, and GSH adducts of the putative quinone-imine metabolite (*267, 268*). Additionally, OD lapatinib was found to be more toxic that lapatinib itself in HepaRG cells (*268*). These findings were further substantiated in a retrospective clinical analysis which found that patients taking a combination of lapatinib and dexamethasone were 4.57 times more likely to develop lapatinib-induced hepatotoxicity than those exposed to lapatinib alone (*267*). Conversely, inhibitors such as ketoconazole were found to reduce the clearance of and increase exposure to lapatinib (*269*); however the effect of CYP3A4/5 inhibition on the extent of reactive metabolite generation and toxicity were not examined. Given the ability of CYP3A4/5 inducers to potentiate the toxicity of lapatinib, similar concerns may also be extended to possible food-drug interactions with lapatinib.

From an intrinsic perspective, metabolic capacity is determined by a number of factors including age, nutritional status, concomitant diseases (e.g. liver dysfunction) and the genetic makeup of an individual. Pharmacogenetic associations have been noted to influence either the functional characteristics or abundance of CYP450 enzymes. For example, CYP2D6 has more than 80 polymorphic forms, resulting in individuals characterised as poor- to ultra-metabolizers (*270*). For the CYP3A4/5 family, genetic polymorphism is noted to affect the level of CYP3A5 expression. Unlike CYP3A4, CYP3A5 levels are generally lower and its endogenous expression is dependent on its allele (*271*). Carriers of CYP3A5*1/*1 alleles can possess CYP3A5 levels up to 50% of total CYP3A4/5 content while CYP3A5*3/*3 carriers possess almost no functional CYP3A5, and heterozygous CYP3A5 *1/*3 carriers express intermediate CYP3A5 levels. It is important to note that this polymorphism governs the abundance, rather than the functional activity of CYP3A5 enzymes.

CYP3A5 polymorphism has been demonstrated to affect plasma concentrations of tacrolimus, an immunosuppressant with a narrow therapeutic index used in organ transplant patients. Carriers of at least one CYP3A5 *1 allele experience greater tacrolimus clearance and require higher doses to reach therapeutic concentrations (*272*). On the other hand, CYP3A4 is not known to be prominently influenced by genetic polymorphisms, although the CYP3A4*22 variant which is associated with reduced CYP3A4 mRNA levels and CYP3A4 activity, and exerts some influence on tacrolimus clearance, primarily in the non-CYP3A5 expressing *3/*3 carriers (*273*). Nevertheless, the CYP3A4*22 allele is expressed in only 8% of Caucasians and has not been detected in subjects of African or Asian descent (*273*), and thus is not thought to affect CYP3A4/5 metabolic capacity prominently. Although the role of CYP3A5 polymorphism in drug disposition is

established, its influence on xenobiotic-induced CYP450 inactivation is not conclusive.

3.2.4 Mitigating Lapatinib-induced DDIs and ADRs through Deuteration and CYP3A5 Genotyping

Given that covalent (and coordinate) binding are thought to precipitate DDIs and ADRs with lapatinib, such undesired outcomes may be attenuated by manipulating the variables that contribute to covalent binding. As described earlier, these variables include the innate bioactivation potential of the drug, dose burden and metabolic capacity of the bioactivating enzymes, the latter of which is governed by the effects of co-administered drugs and an individual's genetic disposition. While the dose burden and choice of concomitant drugs may appear to be the easiest to manipulate, decreasing the administered dose may compromise efficacy, while there may not be much flexibility in choosing alternative drugs that do not modify the metabolic capacity particularly if the therapeutic regimen is strict or limited in options. The remaining options are to reduce the bioactivation potential and to carefully consider of the genetic status of a patient. This chapter explores a two-pronged approach to achieve these objectives. Firstly, the effect of drug deuteration on the generation of reactive metabolites from lapatinib is explored using a series of deuterated lapatinib analogues. This is followed by an assessment of the effect of CYP3A5 genetic polymorphism on the magnitude of CYP3A4/5 inactivation by lapatinib and the extent of quinone-imine formation.

3.3 Materials and Methods

3.3.1 Materials

Lapatinib (free base) was purchased from LC Laboratories (Woburn, MA, USA). Deuterated lapatinib analogues (Figure 3-5 (A-C)) and their respective O-debenzylated standards (Figure 3-5 (D-F)) were provided by Concert Pharmaceuticals (Lexington, MA, USA). HPLC-grade acetonitrile (ACN) was purchased from Tedia Company Inc. (Fairfield, OH, USA). Dimethyl sulfoxide (DMSO) was obtained from ACS Chemical Inc. (Point Pleasant, NJ, USA). Pooled human liver microsomes (HLM) (Lot No. 18888 and 70196), recombinant CYP3A4 (rCYP3A4), recombinant CYP3A5 (rCYP3A5), and NADPH-regenerating system consisting of NADPH A ($NADP^+$ and glucose-6-phosphate) and NADPH B (glucose-6-phosphate dehydrogenase) were obtained from BD Gentest (Franklin Lakes, NJ, USA). Single donor HLM genotyped for CYP3A5*1/*1 (n = 4), CYP3A5*1/*3 (n = 4), and CYP3A5*3/*3 (n = 4) were purchased from commercial sources such as BD Gentest and XenoTech, LLC (Lenexa, KS, USA) (See Table S3 showing characteristics of the different CYP3A5-genotyped HLM donors). 6β-Hydroxytestosterone and 1'-hydroxymidazolam were purchased from Cerilliant Corporation (Round Rock, TX, USA). A crude preparation of 4-hydroxymidazolam was generated using rat liver microsomes that were isolated in-house (*274*). Water was obtained using a Milli-Q water purification system (Milipore, Bedford, MA, USA). Carbamazepine, glutathione (GSH), trypan blue, RPMI medium 1640 without phenol red and fluorescein diacetate (FDA), were purchased from Sigma-Aldrich (St. Louis, MO, USA). Midazolam was obtained from Tocris Bioscience (Bristol, United Kingdom). Testosterone was purchased from Tokyo Chemical Industry CO., Ltd. (Tokyo, Japan). Formic acid was obtained from BDH Chemicals

(Radnor, PA, USA). BT-474 cell line was a kind gift from Dr. Yang Yi Yan (Institute of Bioengineering and Nanotechnology, Singapore). Fetal bovine serum (FBS) was obtained from Hyclone Laboratories (Logan, Utah, USA). Trypsin was obtained from Life Technologies, Invitrogen (Waltham, MA, USA). Phosphate-buffered saline (PBS) was obtained from Vivantis (Selangor, Malaysia). 1% penicillin/streptomycin was obtained from PAN Biotech (Aidenbach, Germany). All other reagents were of analytical grade.

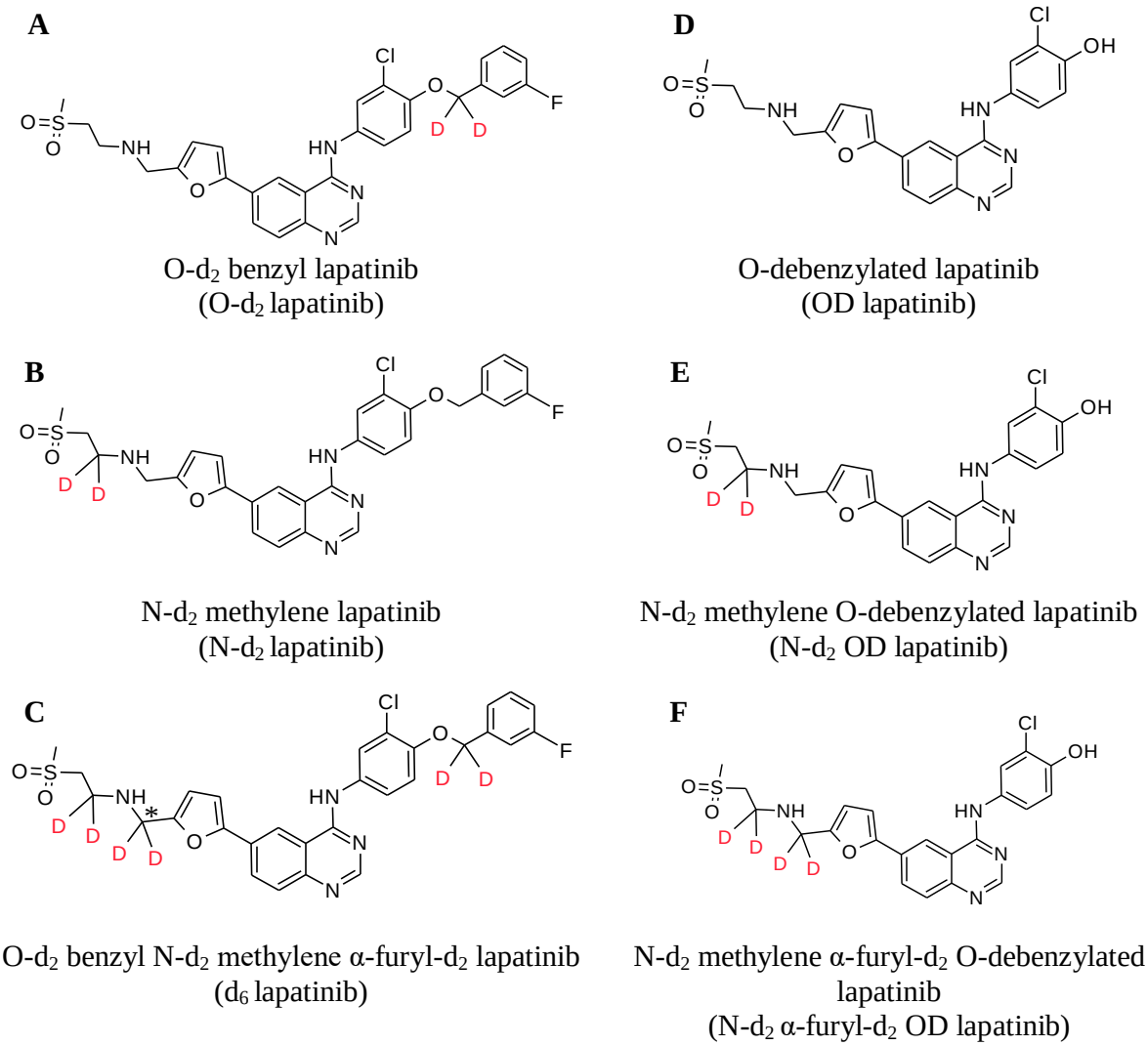

Figure 3-5 (A-C) Deuterated lapatinib analogues and (D-F) corresponding deuterated OD lapatinib standards. *Additional deuterated carbon in d_6 lapatinib.

3.3.2 Kinetic Studies of Lapatinib Metabolite and GSH Adduct Formation from Lapatinib and Deuterated Lapatinib Analogues in Pooled HLM, rCYP3A4 and rCYP3A5

Incubation experiments were performed in 96-well plates. Incubation mixtures for kinetics studies of lapatinib metabolites formation consisted of pooled HLM (0.5 mg/mL), 100 mM potassium phosphate buffer (pH 7.4), NADPH B and varying concentrations of lapatinib or its deuterated analogues (0-100 μM). The mixtures were pre-warmed at 37°C for 5 min. Each reaction was initiated by adding 5 μL of NADPH A. The final volume in each well was 100 μL, and the final organic content in each incubation mixture was less than 0.5% v/v. After incubation at 37°C for 10 min, a 50 μL aliquot was withdrawn and quenched with an equal volume of ice-cold ACN containing 0.5 μM of carbamazepine (internal standard (IS)). To assess GSH adduct formation kinetics, the reaction mixture was enriched with 50 mM GSH, and all other parameters were kept identical. Kinetic studies of lapatinib metabolite formation were repeated using 50 pmol/mL of rCYP3A4 or rCYP3A5, and all other parameters were kept identical. The samples were centrifuged at 4,000 *g* for 30 min at 4°C, and the supernatants were removed for determination of the formation of OD, ND metabolites and GSH adducts derived from lapatinib and its deuterated analogues by liquid chromatography-tandem mass spectrometry (LC/MS/MS). For quantification, appropriate lapatinib standards (0-1 μM) were also prepared in the same HLM mixture mixed with an equal volume of ice-cold ACN with IS.

3.3.3 Time- and Concentration-dependent Inactivation of CYP3A4/5 by Lapatinib and Deuterated Lapatinib Analogues in Pooled HLM

3.3.3.1 Assessment of the Suitability of Midazolam as a Probe Substrate

Incubation experiments were performed in 96-well plates. A two-step incubation scheme was used, in which the metabolism of lapatinib or its deuterated analogues were allowed to occur during the pre-incubation step. Pre-incubation mixtures consisting of 0.5 mg/mL pooled HLM, 100 mM potassium phosphate buffer (pH 7.4), NADPH B and varying concentrations of lapatinib (0-20 μM) were pre-warmed at 37°C for 5 min. Each reaction was initiated by adding 5 μL of NADPH A. The final volume in each well was 100 μL, and the final organic content in each incubation mixture was less than 0.5% v/v. After 0, 3, 8, 15, 22 and 30 min of pre-incubation, 8 μL of the pre-incubation mixture was transferred to a secondary incubation mixture containing 25 μM midazolam as probe substrate (at ~5× K_m) and NADPH-regenerating system in 100 mM potassium phosphate buffer (pH 7.4). The final volume of each secondary incubation mixture was 80 μL, which facilitated a 10-fold dilution of the pre-incubation mixture. The secondary incubation mixture was incubated for another 10 min at 37°C before a 50 μL aliquot was withdrawn and quenched with an equal volume of ice-cold ACN containing 0.5 μM carbamazepine (internal standard (IS)). The samples were centrifuged at 4,000 *g* for 30 min at 4°C, and the supernatants were removed for determination of midazolam 4-hydroxylation and 1'-hydroxylation activity by LC/MS/MS. The experiment was repeated using rCYP3A5 (20 pmol/mL) in place of HLM to assess the presence of time-dependent inhibition of CYP3A5 by lapatinib using midazolam as probe substrate.

3.3.3.2 Determination of CYP3A4/5 Inactivation Kinetics by Lapatinib and Deuterated Lapatinib Analogues in Pooled HLM using Testosterone as Probe Substrate

As midazolam was found to be unsuitable as a probe substrate to assess the inactivation of CYP3A4/5 by lapatinib, testosterone was used as the probe substrate instead. The experimental conditions were identical to those in section 3.3.3.1, except that testosterone (500 μM) was used as the probe substrate, 0.5 μM prednisolone as the IS and a different set of lapatinib or deuterated lapatinib concentrations (0-100 μM). Residual CYP3A4/5 activity was monitored by determination of testosterone 6β-hydroxylation using LC/MS/MS.

3.3.4 Cytotoxicity of Lapatinib and O-d_2 Lapatinib in BT474 Breast Cancer Cells

BT474 cells were cultured in phenol red-free RPMI medium 1640, supplemented with 10% FBS and 1% penicillin/streptomycin, maintained under a humidified atmosphere of 5% CO_2 at 37°C. Cells were grown to confluence in T-75 flasks, and were seeded into 96-well plates at a density of 10 000 cells/well. The plates were incubated at 37°C, 5% CO_2 overnight. Serial dilutions of lapatinib and O-d_2 lapatinib (0-10 μM) were added to the respective wells at 200 μL per well. The cells were treated for a total of 3 days. The percentage cell survival rate was obtained using fluorescein diacetate assay (FDA) and the half-maximal inhibitory concentration (IC_{50}) was determined from cell survival curves using the sigmoidal dose-response (variable slope) algorithm in Prism 6 (Graphpad Software Inc., San Diego, CA, USA). The experiment was carried out in triplicates using cells cultured across 3 passages. The difference between lapatinib and O-d_2 lapatinib IC_{50} values were analyzed in Prism 6 via an unpaired t-test with equal variances assumed, and $p < 0.05$ was considered statistically significant.

3.3.5 Time- and Concentration-dependent Inhibition of CYP3A4/5 by Lapatinib in CYP3A5 Genotyped HLM

Preliminary experiments were conducted to optimize the conditions for the metabolism of testosterone to 6β-hydroxytestosterone in genotyped HLM, particularly in the low CYP3A4/5 activity, non-expressing CYP3A5 *3/*3 genotype. In order for the incubation experiments to be conducted with consideration of the quantitation limit of the bioanalytical assay, a microsomal protein concentration of 0.6 mg/mL and secondary incubation duration of 15 minutes were adopted in the subsequent assays involving CYP3A5-genotyped HLM. A two-step incubation scheme was employed as described in section 3.3.3.1. The concentrations of lapatinib were optimized according to the genotyped HLM donors. The pre-incubation reaction mixture was exposed to lapatinib for 0, 3, 7, 12, 20, and 30 min before being transferred to the secondary incubation mixture. All samples were subjected to LC/MS/MS analysis for determination of testosterone 6β-hydroxylation activity.

3.3.6 Phenotyping of CYP3A4/5 Activity in CYP3A5 Genotyped HLM via Testosterone 6β-Hydroxylation

Incubation experiments were performed in 96-well plates. Incubation mixtures consisting of 0.5 mg/mL genotyped HLM, 100 mM potassium phosphate buffer (pH 7.4), NADPH B and 75 µ were pre-warmed at 37°C for 5 min. Each reaction was initiated by adding 5 µL of NADPH A and allowed to proceed at at 37°C. The final volume in each well was 100 µL, and the final organic content in each incubation mixture was less than 0.5% v/v. After 10 min, 50 µL of each incubation mixture was quenched with an equal volume of ice-cold ACN containing 0.5 µM prednisolone as an IS. The samples were centrifuged at 4,000 *g* for 30 min at 4°C, and the supernatants were removed for determination of the

formation of 6β-hydroxytestosterone using LC/MS/MS. For quantification, 6β-hydroxytestosterone (0-1 μM) was also prepared in the same HLM mixture mixed with an equal volume of ice-cold ACN supplemented with IS.

3.3.7 Quantitation of Lapatinib, Midazolam and Testosterone Metabolites, and Detection of GSH Adduct Formation by LC/MS/MS

Chromatographic optimization was performed to ensure baseline separation of OD lapatinib and ND lapatinib. OD lapatinib (provided by Concert Pharmaceuticals), and ND lapatinib (synthesized in-house) were used as chromatographic standards for the optimization process. OD lapatinib, ND lapatinib, 4-hydroxymidazolam, 1'-hydroxymidazolam, 6β-hydroxytestosterone, and GSH adduct derived from lapatinib were analyzed by an Agilent 1290 Infinity LC system (Agilent Technologies, Santa Clara, CA, USA) interfaced with an AB Sciex QTrap 5500 hybrid linear ion-trap quadrupole mass spectrometer equipped with a TurboIonSpray source (Applied Biosystems, Foster City, CA, USA). Mili-Q water and HPLC-grade ACN, both acidified with 0.1% formic acid, were used as mobile phases A and B respectively. Both mobile phases were pumped through a Waters Acquity UPLC BEH C_{18} 130Å column (1.7 μm, 50 mm × 2.1 mm i.d.; Waters, Milford, MA, USA) at a flow rate of 0.6 mL/min. Using an autosampler thermostatted at 4°C, 2 μL of each sample was injected into the UPLC column maintained at 45°C. The needle was flushed with ACN post-injection to minimize carry-over effect. Tandem mass spectrometry was operated in the positive ion electrospray ionization mode. The MS source conditions were: curtain gas, 25 psi; collision gas, medium; ionspray voltage, 5500 V; temperature, 550°C; ion source gas 1, 50 psi; and ion source gas 2, 55 psi. The UHPLC elution conditions used for analysis are summarized in Table 3-1, while compound-dependent MS parameters were optimized and are summarized in Table 3-2.

Table 3-1 UHPLC elution conditions.

Analyte	Elution Conditions
OD lapatinib **ND lapatinib** **O-d_2 ND lapatinib** **N-d_2 OD lapatinib** **N-d_2 α-furyl-d_2 OD lapatinib** **α-furyl-d_2 O-d_2 ND lapatinib** **Carbamazepine (IS)**	Linear gradient 25 to 48% B (0-1.60 min), isocratic 95% B (1.61-2.10 min), and isocratic at 25% B (2.11-2.50 min)
Lapatinib-GSH adduct **N-d_2 lapatinib-GSH adduct** **N-d_2 α-furyl-d_2 lapatinib-GSH adduct** **Carbamazepine (IS)**	Linear gradient 5 to 60% B (0-1.50 min), isocratic 95% B (1.51-2.00 min), isocratic at 5% B (2.01-2.50 min)
4-hydroxymidazolam **1'-hydroxymidazolam** **Carbamazepine (IS)**	Linear gradient 20 to 80% B (0-1.40 min), isocratic 95% B (1.41-1.99 min), and isocratic at 20% B (2.00-2.50 min)
6β-hydroxytestosterone **Prednisolone (IS)**	Linear gradient 20 to 70% B (0-1.40 min), isocratic 95% B (1.41-1.99 min), and isocratic at 20% B (2.00-2.50 min)

Table 3-2 MRM transitions and compound-dependent MS parameters for the detection of OD lapatinib, ND lapatinib, lapatinib-GSH adducts, their deuterated analogues, midazolam and testosterone metabolites, and internal standards (IS).

Analyte	MRM Transition (*m/z*)	Collision Energy (V)	Declustering Potential (V)	Entrance Potential (V)	Collision Exit Potential (V)
OD lapatinib	473 → 350	43	136	14	22
ND lapatinib	475 → 366	55	136	14	22
O-d_2 ND lapatinib	477 → 366	60	136	14	22
N-d_2 OD lapatinib	475 → 350	13	40	5	12
N-d_2 α-furyl-d_2 OD lapatinib	477 → 352	13	40	5	12
α-furyl-d_2 O-d_2 ND lapatinib	479 → 368	60	136	14	22
Lapatinib-GSH adduct	778 → 655	30	75	10	3
N-d_2 lapatinib-GSH adduct	780 → 655	30	75	10	3
N-d_2 α-furyl-d_2 lapatinib-GSH adduct	782 → 657	30	75	10	3
Carbamazepine (IS)	237 → 194	27	151	7	12
4-hydroxymidazolam	342 → 325	40	125	10	14
1'-hydroxymidazolam	342 → 203	40	125	10	14
6β-hydroxytestosterone	305 → 269	20	200	7	11
Prednisolone (IS)	380 → 91	51	106	9	14

3.3.8 Data Analysis

Integration of all chromatographic peaks was performed using Analyst Software (version 1.5.2, Applied Biosystems).

3.3.8.1 Enzyme Kinetics Analysis

Final concentrations of OD and ND lapatinib were then normalized against incubation time and amount of microsomal protein used. Enzyme kinetic parameters (V_{max} and K_m) were determined through nonlinear regression analysis using Prism 6. Data were fitted to the Michaelis-Menten model. The intrinsic clearance (CL_{int}) was then determined by taking quotient of V_{max} over K_m. As GSH adduct standards were unavailable, and the amount ND lapatinib synthesized in-house was insufficient for quantitation purposes, the V_{max} values of

ND lapatinib, lapatinib-GSH and its deuterated analogues were expressed as peak area ratios, derived from the quotient of analyte peak area over IS peak area.

3.3.8.2 Determination of CYP3A4/5 Inactivation Kinetics by Lapatinib or Deuterated Lapatinib Analogues

To determine time- and concentration-dependent inactivation, the mean of triplicate analyses was used to calculate the natural log of percentage residual CYP450 activity (normalized to vehicle at each corresponding time-point). The data were fitted to linear regression and plotted against pre-incubation time. The individual gradient of each curve (k_{obs}) was subsequently plotted against inhibitor concentration to obtain the k_{obs} graph. Two kinetic parameters can be obtained from the k_{obs} graph, the maximal rate constant of inactivation (k_{inact}) and the inhibitor concentration at half the maximal rate constant of inactivation (K_I). The curve is described by the equation $k_{\mathrm{obs}} = \frac{k_{\mathrm{inact}} \times [I]}{K_I + [I]}$. The potency of the test drug as an inactivator can be described by the ratio of both parameters, i.e. k_{inact}/K_I. The k_{inact}/K_I ratios were used to compare the potencies of inactivation between the different CYP3A5 genotypes. Statistical comparisons of k_{inact}/K_I ratios, and the extent of quinoneimine formation between genotypes were performed by using one-way analysis of variance followed by the Kruskal-Wallis test for multiple comparisons, and $p < 0.05$ was considered significant. Correlation analyses were assessed using Pearson correlation coefficients, and $p < 0.05$ was considered significant. All plots were acquired using Prism 6.

3.4 Results

3.4.1 Optimization of Chromatographic Separation for OD Lapatinib and ND Lapatinib

Using a generic chromatographic gradient, the chromatographic trace for ND lapatinib show two overlapping peaks sharing the same MRM transition within the retention period of 1.4 to 1.5 min (Figure 3-6A), necessitating optimization of the elution conditions (Table 3-1) to ensure baseline separation of the two co-eluting peaks. The in-housed synthesized ND lapatinib standard confirmed that the peak at retention time of 1.12 min belonged to ND lapatinib (Figure 3-6B).

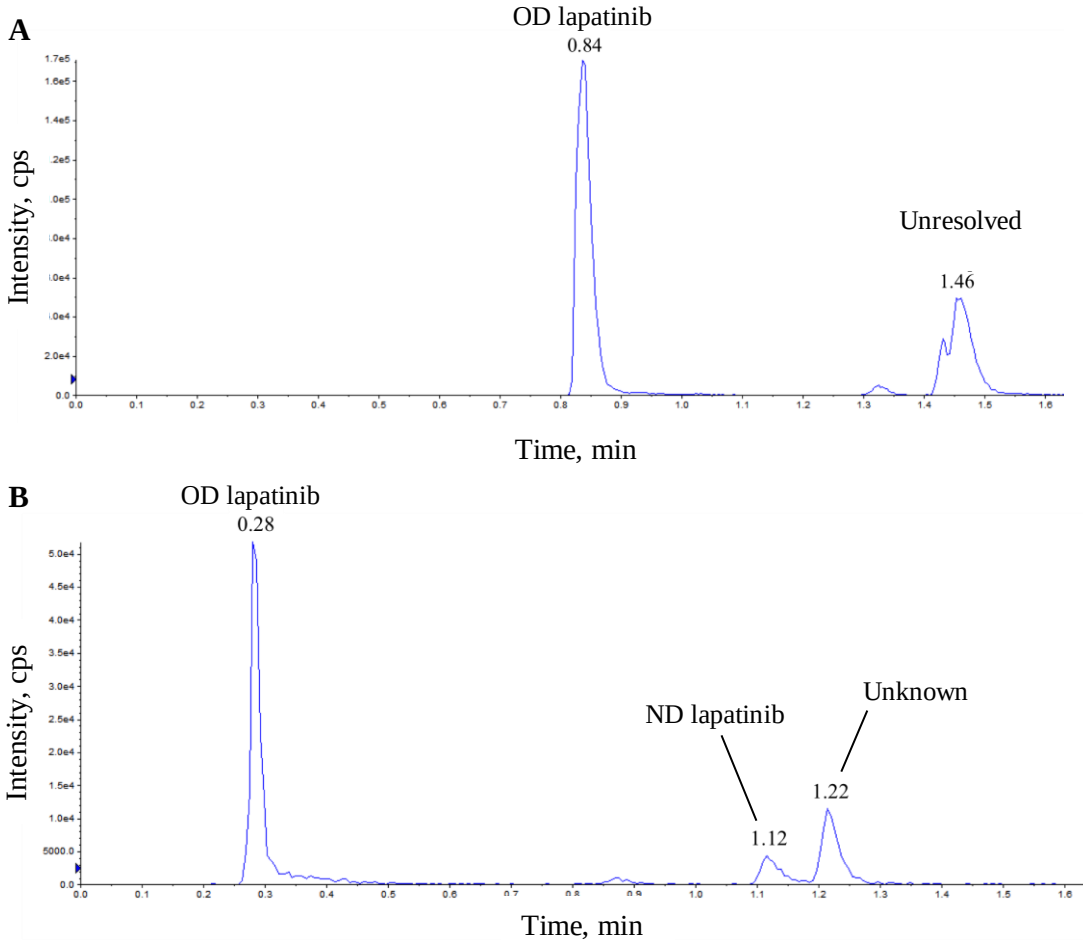

Figure 3-6 (A) Non-optimized chromatogram of ND lapatinib, showing two co-eluting peaks within the retention period of 1.4 to 1.5 min, while the peak at 0.84 min belongs to OD lapatinib and (B) optimized chromatogram of ND lapatinib with baseline-separated peaks at retention time 1.12 min (ND lapatinib) and 1.22 min (unknown compound), while OD lapatinib shifted to 0.28 min.

3.4.2 Kinetic Studies of Lapatinib Metabolite Formation from Lapatinib and Deuterated Lapatinib Analogues in Pooled HLM, rCYP3A4 and rCYP3A5

The kinetic plots for the formation of ND lapatinib and OD lapatinib from lapatinib or deuterated lapatinib analogues are shown in Figure 3-7 and Figure 3-8. The kinetic parameters CL_{int}, V_{max} and K_m for the formation of each of these metabolites in each metabolic system are summarized in Table 3-3 and Table 3-4.

As expected, lapatinib had the highest CL_{int} values across all three metabolic systems for both *N*-dealkylation and *O*-debenzylation metabolic pathways, indicating that deuteration appears to exert some influence on reducing the formation of ND lapatinib and OD lapatinib. These observations are supported by the kinetic plots which show the curves for lapatinib biotransformation to be generally higher than that of the deuterated analogues for both pathways in all three systems. Of the three deuterated lapatinib analogues, interestingly, both O-d_2 lapatinib and d_6 lapatinib consistently demonstrated the greatest reduction in CL_{int} for *N*-dealkylation in all three metabolic systems (up to 4.7- and 7.4-fold respectively), while N-d_2 lapatinib showed a moderate reduction in intrinsic clearance (up to 2.2-fold).

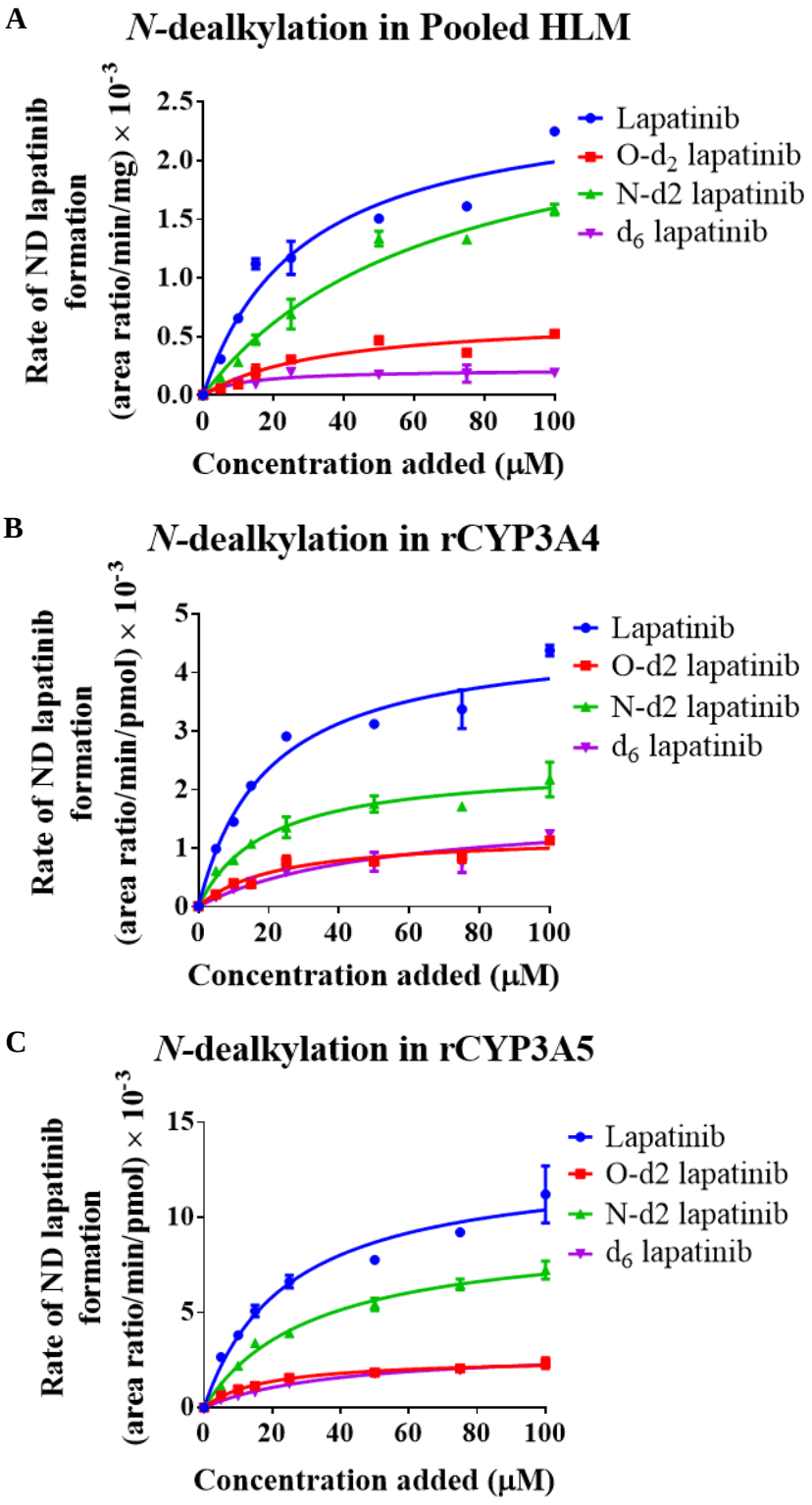

Figure 3-7 Kinetic plots for *N*-dealkylation of lapatinib and its deuterated analogues in (A) pooled HLM, (B) rCYP3A4 and (C) rCYP3A5 (mean of triplicate experiments).

A

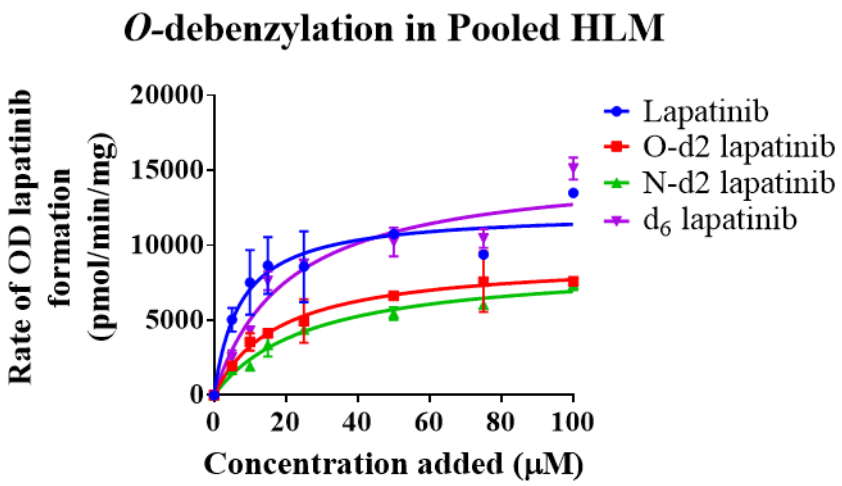

B

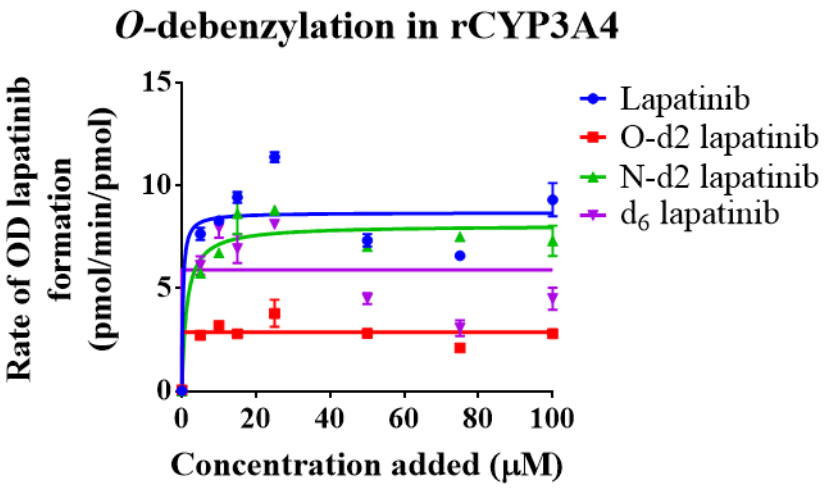

C

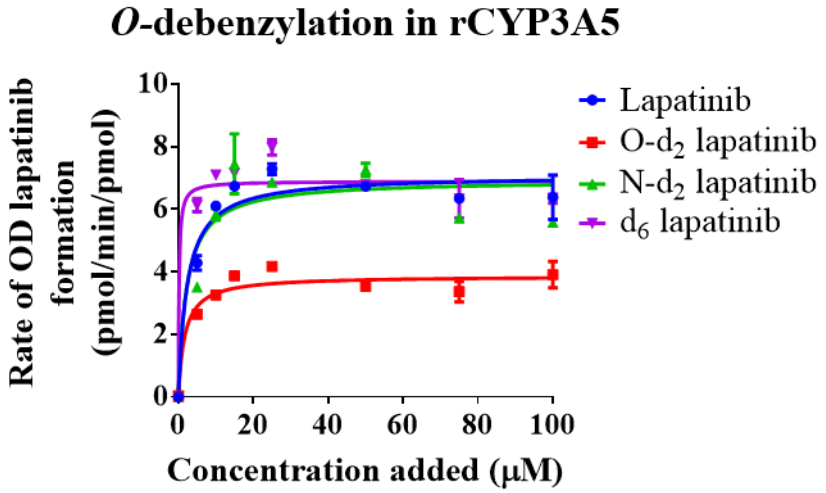

Figure 3-8 Kinetic plots for *O*-dealkylation of lapatinib and its deuterated analogues in (A) pooled HLM, (B) rCYP3A4 and (C) rCYP3A5 (mean of triplicate experiments).

Table 3-3 CL_{int} values for *N*-dealkylation of lapatinib and deuterated lapatinib analogues in pooled HLM, rCYP3A4 and rCYP3A5.

Metabolic system	Parameter	Lapatinib	O-d_2 lapatinib	N-d_2 lapatinib	d_6 lapatinib
Pooled HLM	V_{max} (area ratio/min/mg) × 10^{-3}	2.557	0.6748	2.663	0.2207
	K_m (µM)	28.50	35.62	66.71	11.77
	CL_{int} (V_{max}/K_m) × 10^{-5}	**8.97**	**1.89**	**3.99**	**1.88**
	CL_{int} fold-change	**-**	**4.7**	**2.2**	**4.8**
rCYP3A4	V_{max} (area ratio/min/pmol) × 10^{-3}	4.653	1.222	2.427	1.665
	K_m (µM)	19.49	22.27	19.19	51.50
	CL_{int} (V_{max}/K_m) × 10^{-5}	**23.9**	**5.49**	**12.6**	**3.23**
	CL_{int} fold-change	**-**	**4.4**	**1.9**	**7.4**
rCYP3A5	V_{max} (area ratio/min/pmol) × 10^{-3}	12.94	2.606	9.291	3.133
	K_m (µM)	24.43	17.57	32.26	38.83
	CL_{int} (V_{max}/K_m) × 10^{-5}	**53.0**	**14.8**	**28.8**	**8.07**
	CL_{int} fold-change	**-**	**3.6**	**1.8**	**6.6**

N.B.: CL_{int} fold-change values are obtained by comparison with lapatinib

Table 3-4 CL_{int} values for *O*-dealkylation of lapatinib and deuterated lapatinib analogues in pooled HLM, rCYP3A4 and rCYP3A5.

Metabolic system	Parameter	Lapatinib	O-d_2 lapatinib	N-d_2 lapatinib	d_6 lapatinib
Pooled HLM	V_{max} (pmol/min/mg)	12240	9095	8775	15334
	K_m (µM)	7.353	17.96	26.71	20.48
	CL_{int} (V_{max}/K_m)	**1665**	**506**	**329**	**749**
	CL_{int} fold-change	**-**	**3.3**	**5.1**	**2.2**
rCYP3A4	V_{max} (pmol/min/pmol)	8.685	2.876	8.067	5.897
	K_m (µM)	0.2927	N.D.	1.297	N.D.
	CL_{int} (V_{max}/K_m)	**29.7**	**N.D.**	**6.22**	**N.D.**
	CL_{int} fold-change	**-**	**N.D.**	**4.8**	**N.D.**
rCYP3A5	V_{max} (pmol/min/pmol)	7.077	3.864	6.928	6.891
	K_m (µM)	2.312	1.696	2.231	N.D.
	CL_{int} (V_{max}/K_m)	**3.06**	**2.28**	**3.11**	**N.D.**
	CL_{int} fold-change	**-**	**1.3**	**1.0**	**N.D.**

N.D., not determined due to ambiguous K_m values

N.B.: CL_{int} fold-change values are obtained by comparison with lapatinib

For *O*-debenzylation, the kinetic plots suggest that O-d_2 lapatinib exhibited the greatest reduction in the formation of OD lapatinib in all three systems. Although N-d_2 lapatinib appears to have the lowest CL_{int} values in pooled HLM, the kinetic plot (Figure 3-8A) suggests that both O-d_2 lapatinib and N-d_2 lapatinib have almost identical kinetic profiles, indicating that CL_{int} values are sensitive to the denominator K_m which is obtained by non-linear regression fitting. This is apparent in the CL_{int} values for rCYP34A4 and rCYP3A5, where ambiguous K_m values preclude the determination of CL_{int} values for O-d_2 lapatinib and d_6 lapatinib. Despite this apparent ambiguity, visual inspection of the kinetic plots and comparison of V_{max} values indicate that in contrast to N-d_2 lapatinib and d_6 lapatinib, the formation of OD lapatinib was the lowest for O-d_2 lapatinib in rCYP3A4 and rCYP3A5. Overall, O-d_2 lapatinib exhibited the lowest metabolic clearance for *N*-dealkylation and *O*-debenzylation in all three metabolic systems.

3.4.3 Kinetic Studies of GSH Adduct Formation from Lapatinib and Deuterated Lapatinib Analogues in Pooled HLM

The GSH adduct formed with lapatinib is indicative of the generation of the putative quinone-imine reactive metabolite responsible for CYP3A5 inactivation. GSH adducts were detected using an MRM transition of *m/z* 778 → 655 based on our previous studies (*243*, *246*), while the MRM transitions for GSH adducts formed with deuterated lapatinib analogues were derived by adding the appropriate mass number to the parent compound and the *m/z* 655 fragment, based on the remaining number of deuterium atoms in each molecule. Consistent with the kinetic measurements of *O*-debenzylation, which is the precursor step to the formation of the quinone-imine, O-d_2 lapatinib demonstrated the lowest CL_{int} values, comparable with that of d_6-lapatinib (Table 3-5). Visual inspection of the kinetic plots for GSH adduct formation support this observation (Figure 3-9). Taken together, O-d_2 lapatinib

demonstrated the greatest attenuation of *N*-dealkylation, *O*-debenzylation and GSH adduct formation among the three deuterated lapatinib analogues.

Table 3-5 CL_{int} values for GSH adduct formation from lapatinib and deuterated lapatinib analogues in pooled HLM.

Parameter	Lapatinib	O-d_2 lapatinib	N-d_2 lapatinib	d_6 lapatinib
V_{max} (area ratio/min/mg) × 10^{-3}	0.1040	0.06320	0.1328	0.06168
K_m (μM)	23.01	20.83	21.45	17.39
CL_{int} (V_{max}/K_m) × 10^{-5}	**0.452**	**0.303**	**0.619**	**0.355**
CL_{int} fold-change	**-**	**4.7**	**2.2**	**4.8**

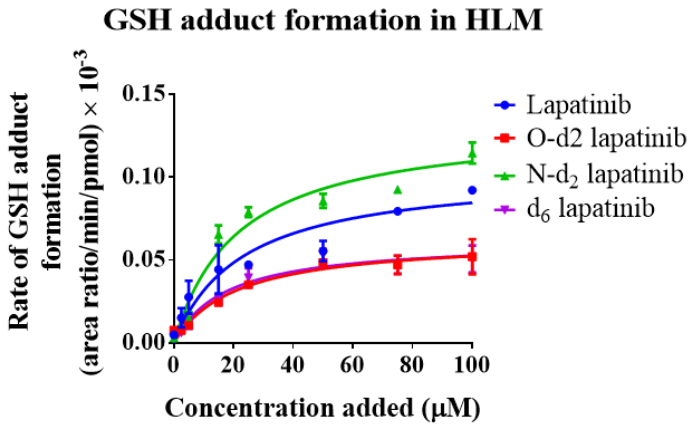

Figure 3-9 Kinetic plot for GSH adduct formation from lapatinib and its deuterated analogues in pooled HLM (mean of triplicate experiments).

3.4.4 Time- and Concentration-dependent Inactivation of CYP3A4/5 by Lapatinib and Deuterated Lapatinib Analogues in Pooled HLM

3.4.4.1 Assessment of the Suitability of Midazolam as a Probe Substrate

Testosterone and midazolam are listed by the U.S. FDA as preferred probe substrates for *in vitro* evaluation of CYP3A4/5 inhibition, where testosterone 6β-hydroxylation, midazolam 1'-hydroxylation and midazolam 4-hydroxylation can be monitored to assess CYP3A4/5 activity (*246*, *275*). Lapatinib has been reported to inactivate CYP3A4/5 in pooled HLM when assessed using testosterone 6β-hydroxylation (*243*) and midazolam 1'-hydroxylation (*276*), as well as to form an MI complex with rCYP3A4 (*244*) and cause MBI of rCYP3A5

(*246*) when assessed using testosterone 6β-hydroxylation. Midazolam 4-hydroxylation has not been used to assess CYP3A4/5 inactivation by lapatinib in pooled HLM, and both midazolam metabolic pathways have not been monitored for the same in rCYP3A5. To identify the optimal metabolic activity to be monitored as an indicator of remaining CYP3A4/5 activity, inhibition assays were performed using midazolam as a probe substrate in pooled HLM and rCYP3A5. Figure 3-10A shows that midazolam 4-hydroxylation activity decreased in a time- and concentration-dependent manner when pooled HLM was pre-incubated with lapatinib in the presence of NADPH. The inset k_{obs} plot shows that the slopes of the curves increased in a hyperbolic trend with increasing concentration of lapatinib. To further assess whether midazolam 4-hydroxylation activity can appropriately reveal the presence of MBI in CYP3A5, another inhibition assay was performed using rCYP3A5. Figure 3-10B shows that midazolam 4-hydroxylation activity was not affected in either a time- or concentration-dependent manner when rCYP3A5 was pre-incubated with lapatinib in the presence of NADPH, and the k_{obs} values failed to show a distinct hyperbolic trend in its k_{obs} plot. Collectively these suggested that midazolam is not a suitable probe substrate for monitoring the inactivation of CYP3A4/5 by lapatinib, as unlike testosterone, it does not capture the inactivation of CYP3A5.

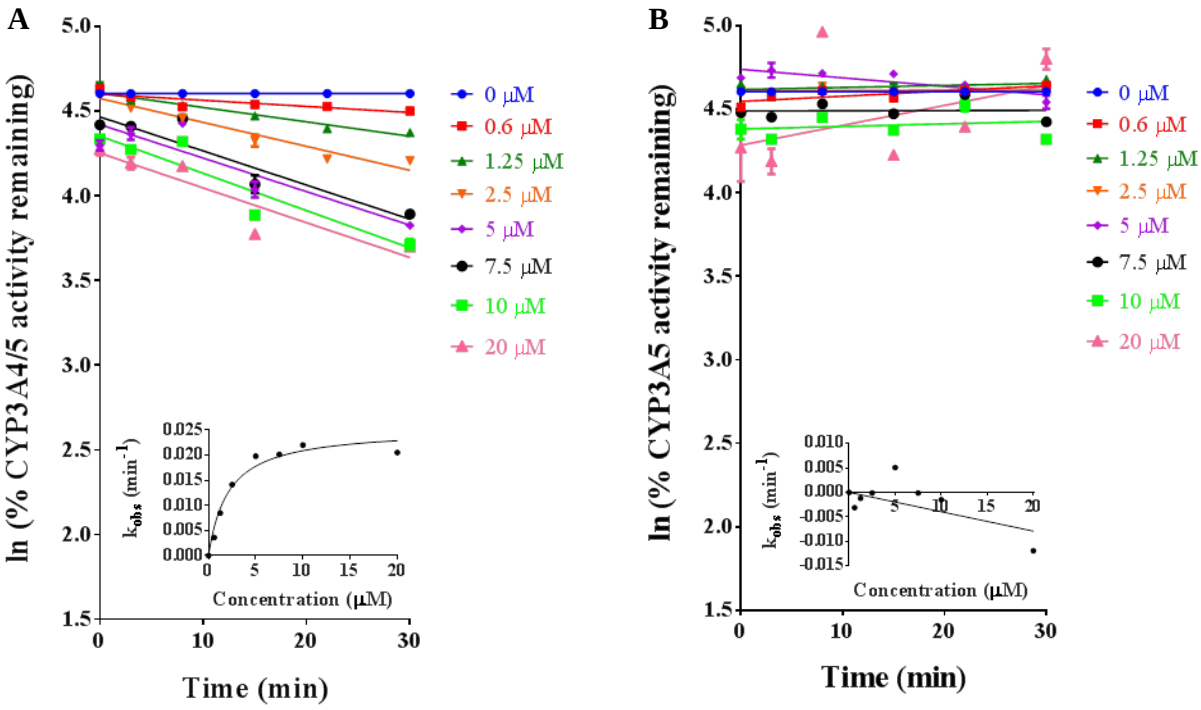

Figure 3-10 (A) Inactivation plot of CYP3A4/5 by lapatinib using pooled HLM, monitoring residual CYP3A4/5 activity by means of midazolam 4-hydroxylation. k_{inact} and K_I values were 0.02532 min^{-1} and 2.110 µM, respectively. The k_{inact}/K_I ratio was 12.0 min^{-1}mM^{-1}. (B) Inactivation plot of CYP3A5 by lapatinib using rCYP3A5, monitoring residual CYP3A5 activity by means of midazolam 4-hydroxylation. Inset k_{obs} plot lacking a distinct hyperbolic trend. k_{inact} and K_I values were not determined. For both plots, each point represents the mean of three replicates with less than 10% S.D.

3.4.4.2 Determination of CYP3A4/5 Inactivation Kinetics by Lapatinib and Deuterated Lapatinib Analogues in Pooled HLM using Testosterone as a Probe Substrate

CYP3A4/5 inactivation by lapatinib and deuterated lapatinib analogues was assessed in pooled HLM using testosterone as a probe substrate, as it has been shown to capture inactivation in both CYP3A4 and CYP3A5, while midazolam does not afford the same utility (section 3.4.4.1). Figure 3-11 shows the inactivation plots, while Figure 3-12 illustrates an overlay of k_{obs} plots for all four compounds. The corresponding inactivation parameters are presented in Table 3-6.

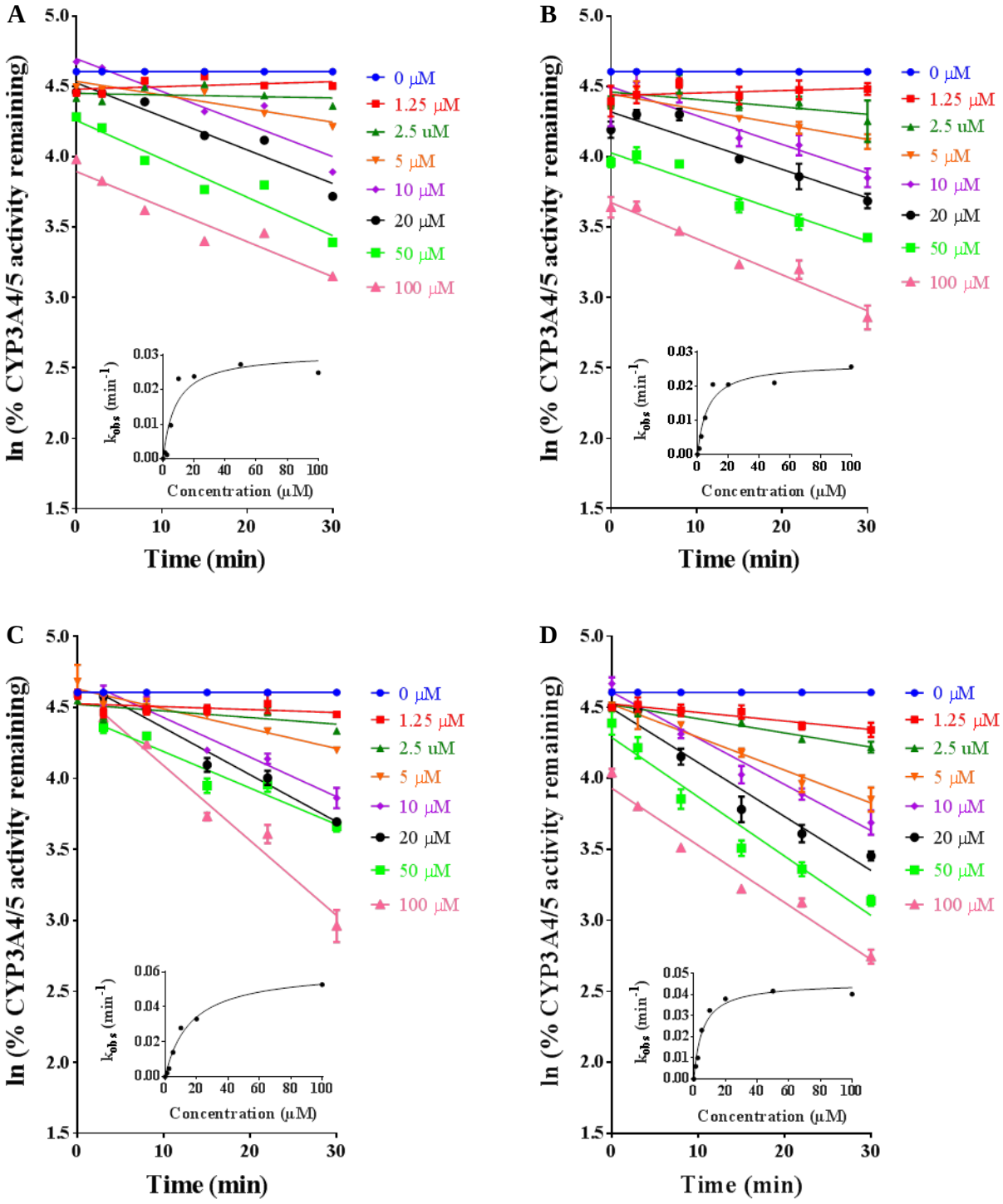

Figure 3-11 Inactivation plots of CYP3A4/5 by (A) lapatinib, (B) O-d_2 lapatinib, (C) N-d_2 lapatinib and (D) d_6 lapatinib in pooled HLM. For all plots, each point represents the mean of three replicates with less than 10% S.D.

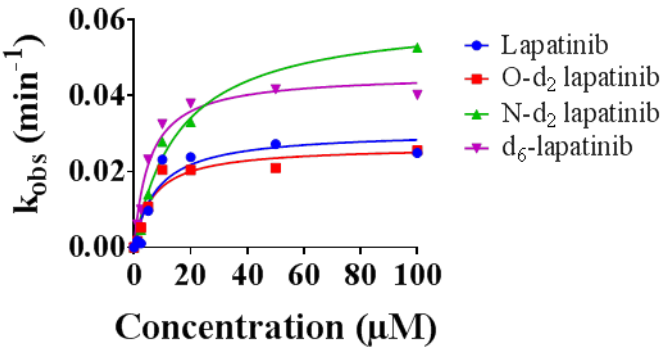

Figure 3-12 Overlay of k_{obs} plots for lapatinib and deuterated lapatinib analogues.

Table 3-6 Inactivation parameters k_{inact} and K_I derived from k_{obs} plots for lapatinib and deuterated lapatinib analogues.

Compound	k_{inact} (min^{-1})	K_I (µM)	k_{inact}/K_I (min^{-1}·mM^{-1})
Lapatinib	0.03067	8.138	3.768
O-d_2 lapatinib	0.02669	6.662	4.006
N-d_2 lapatinib	0.06141	15.99	3.841
d_6-lapatinib	0.04573	5.504	8.309

All four compounds tested showed varying degrees of inactivation of CYP3A4/5 in pooled HLM. Unexpectedly, all three deuterated compounds exhibited higher k_{inact}/K_I values than lapatinib, which indicate that they elicit a greater magnitude of irreversible time-dependent inactivation caused by MI complex formation and MBI. Although O-d_2 lapatinib demonstrated the lowest extent of OD lapatinib and ND lapatinib formation which are thought to be the precursors to lapatinib reactive metabolite generation, and also the lowest levels of GSH adduct formation which is a surrogate indicator of lapatinib quinone-imine formation, these did not translate to an improvement in inactivation characteristics, as it exhibited a comparable k_{inact}/K_I ratio to that of lapatinib, which is also supported by visual inspection of the k_{obs} plot. Collectively, these suggest that deuteration at the positions examined in this study did not have an appreciable negative impact on the magnitude of CYP3A4/5 inactivation caused by lapatinib, and d_6 lapatinib even augmented the extent of inactivation.

3.4.5 Cytotoxicity of Lapatinib and O-d_2 Lapatinib in BT474 Breast Cancer Cells

As O-d_2 lapatinib demonstrated the overall best performance among the deuterated lapatinib analogues in the preceding assays, it was selected for further evaluation to determine if it exhibits pharmacological activity similar to that of lapatinib in the HER2-overexpressing BT474 cell line. There were no significant differences between the IC_{50} values obtained for lapatinib (0.276 ± 0.059 μM) and O-d_2 lapatinib (0.391 ± 0.049 μM) ($p > 0.05$) (Figure 3-13), suggesting that O-d_2 lapatinib exhibits comparable *in vitro* efficacy as that of lapatinib.

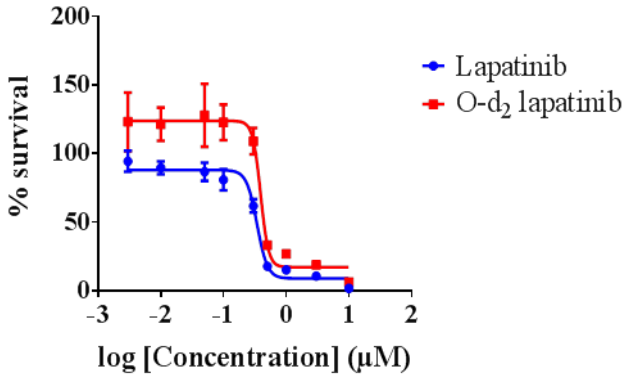

Figure 3-13 The cytotoxicity effect of lapatinib and O-d_2 lapatinib in BT474 cells. Each data point is the average of 3 independent experiments with at least 5 replicates each.

3.4.6 Time- and Concentration-dependent Inhibition of CYP3A4/5 by Lapatinib in CYP3A5-Genotyped HLM

The influence of CYP3A5 polymorphism on inactivation by lapatinib was assessed using a panel of genotyped HLM (CYP3A5*1/*1, $n = 4$; CYP3A5*1/*3, $n = 4$; CYP3A5*3/*3, $n = 4$), and the inactivation plots are shown in Figure 3-14, Figure 3-15 and Figure 3-16. Inactivation kinetic parameters (k_{inact}, K_I, and k_{inact}/K_I ratio) of lapatinib derived from the various CYP3A5-genotyped HLM donors are summarized in Table 3-7. For the CYP3A5*3/*3 donor HH507, and the inactivation parameters could not be determined. The k_{inact}/K_I ratios as a function

of the CYP3A5 genotypes are shown in Figure 3-17A. The mean k_{inact}/K_I ratios for CYP3A5*1/*1, CYP3A5*1/*3, and CYP3A5*3/*3 exhibited a decreasing trend across the genotypes, where the ratio was nearly two-fold higher for *1/*1 than *3/*3 carriers, although they were not significantly different ($p > 0.05$). When examined as a cross-section across all donors at a common lapatinib concentration (20 µM) and inactivation duration (30 min), CYP3A5*1/*1 carriers demonstrated the greatest mean loss of CYP3A4/5 activity, followed by CYP3A5*1/*3 and CYP3A5*3/*3 carriers (Figure 3-17B and C). There was considerable inter-subject variability in the kinetics and magnitude of inactivation by lapatinib.

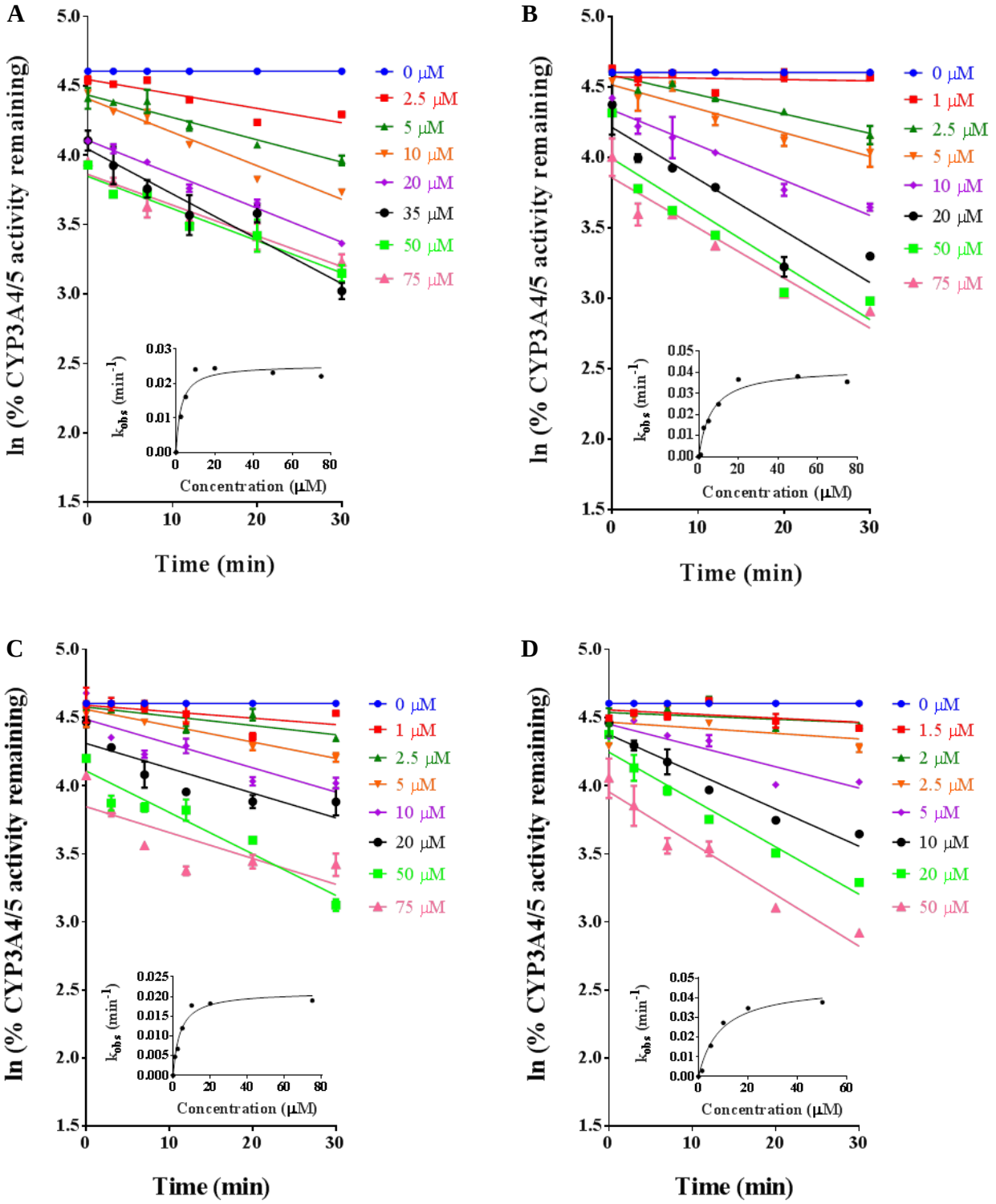

Figure 3-14 Inactivation plots of CYP3A4/5 by lapatinib on single donor HLM genotyped for CYP3A5*1/*1. Plots A, B, C and D represent donors HH785, HH860, HH867 and H0331 respectively. For all plots, each point represents the mean of three replicates with less than 10% S.D. Each respective inset shows the k_{obs} plot.

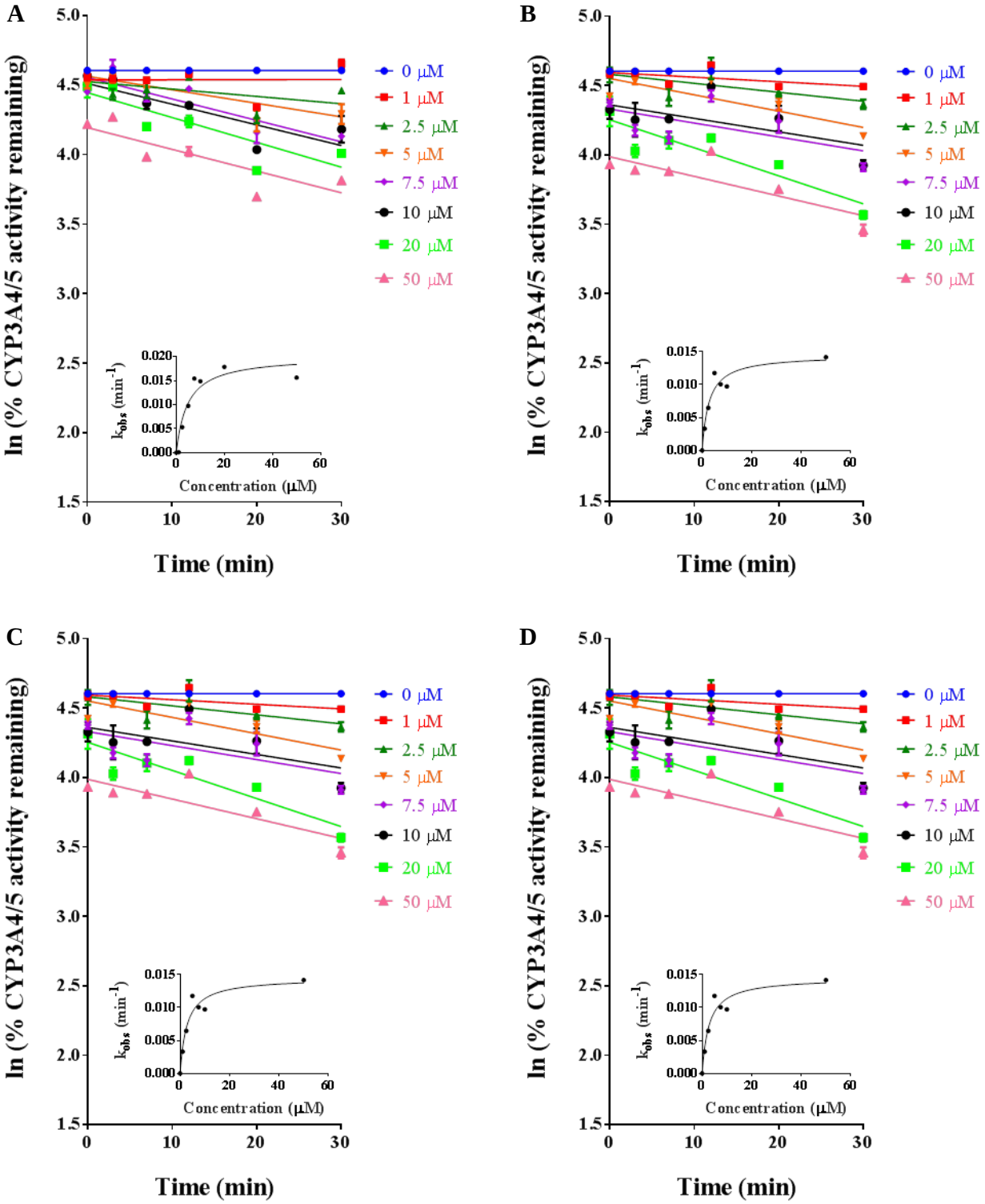

Figure 3-15 Inactivation plots of CYP3A4/5 by lapatinib on single donor HLM genotyped for CYP3A5*1/*3. Plots A, B, C and D represent donors HH757, HH868, H0239 and H0280 respectively. For all plots, each point represents the mean of three replicates with less than 10% S.D. Each respective inset shows the k_{obs} plot.

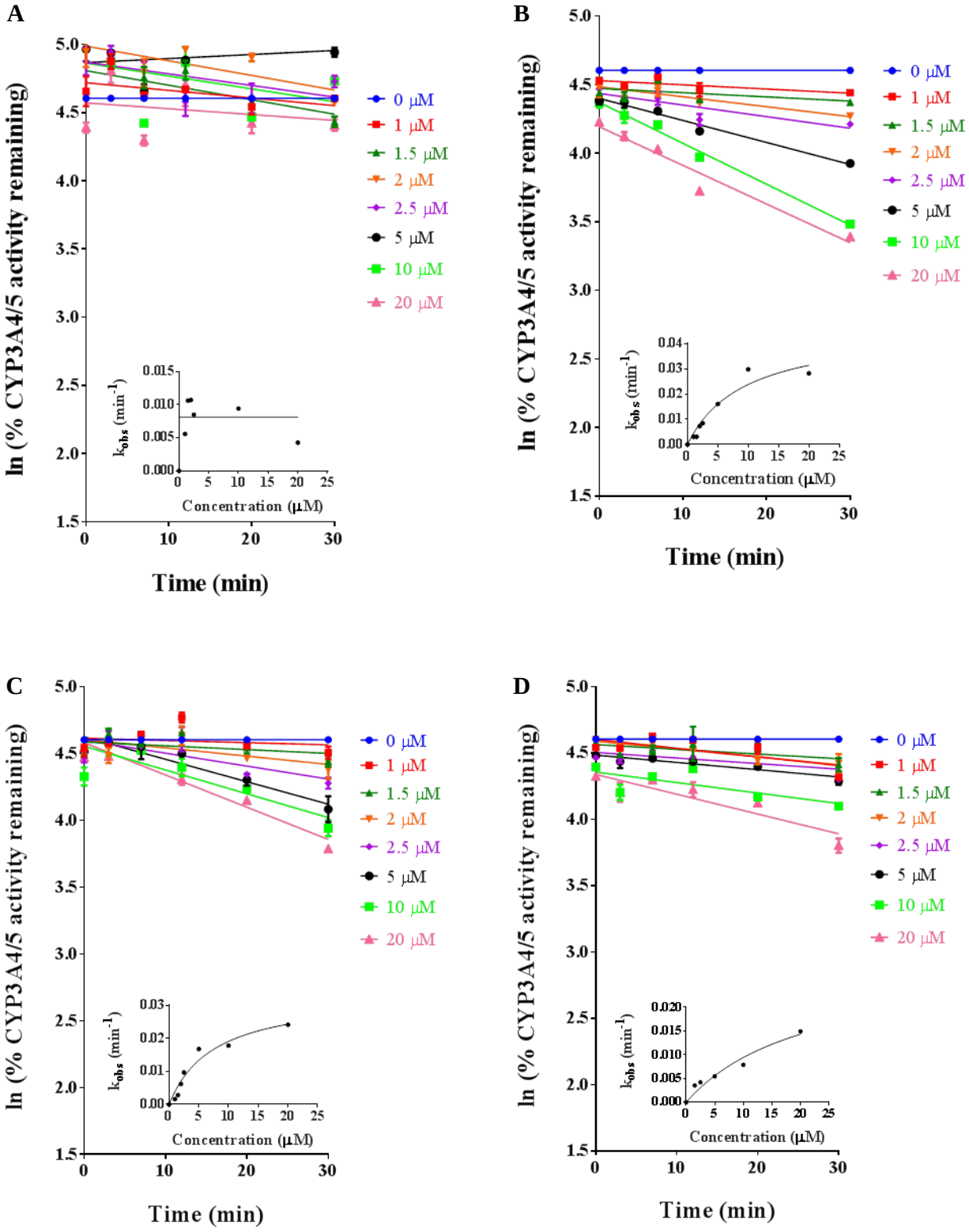

Figure 3-16 Inactivation plots of CYP3A4/5 by lapatinib on single donor HLM genotyped for CYP3A5*3/*3. Plots A, B, C and D represent donors HH507, H0307, H0204 and H0182 respectively. For all plots, each point represents the mean of three replicates with less than 10% S.D. Each respective inset shows the k_{obs} plot.

Table 3-7 Inactivation parameters k_{inact} and K_I derived from k_{obs} plots for lapatinib in various CYP3A5-genotyped HLM donors.

Donor	CYP3A5 Genotype	k_{inact} (min^{-1})	K_I (μM)	k_{inact}/K_I ($min^{-1} \cdot mM^{-1}$)
HH785	*1/*1	0.0254	2.56	9.92
HH860		0.0422	6.45	6.54
HH867		0.0212	3.71	5.71
H0331		0.0468	8.75	5.35
Mean ± S.D.		**0.0339 ± 0.0125**	**5.37 ± 2.78**	**6.88 ± 2.09**
HH757	*1/*3	0.0201	4.72	4.26
HH868		0.0145	2.77	5.23
H0239		0.0332	7.82	4.25
H0280		0.0484	5.92	8.18
Mean ± S.D.		**0.0291 ± 0.0151**	**5.31 ± 2.12**	**5.48 ± 1.86**
HH507	*3/*3	ND	ND	ND
H0307		0.0461	9.39	4.91
H0204		0.0335	7.56	4.43
H0182		0.0298	21.6	1.38
Mean ± S.D.		**0.0365 ± 0.0086**	**12.85 ± 7.63**	**3.57 ± 1.92**

N.D., not determined

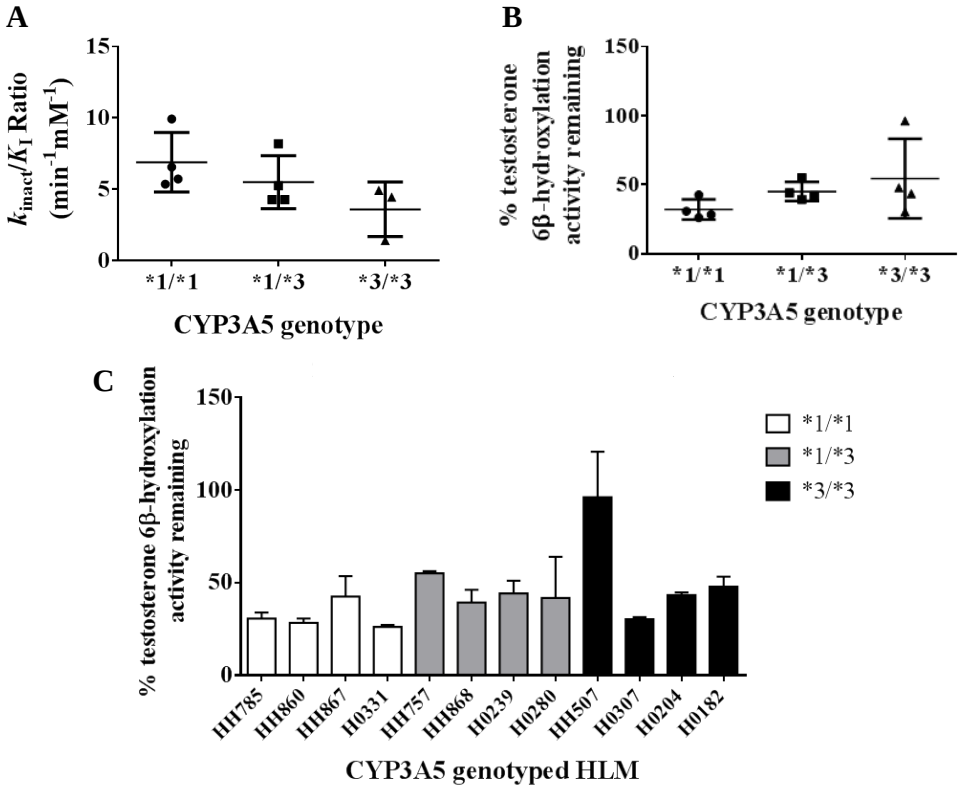

Figure 3-17 Comparison of (A) k_{inact}/K_I ratios of lapatinib and (B) CYP3A4/5 remaining activity in CYP3A5*1/*1 (●), *1/*3 (■), and *3/*3 (▲) genotypes. Each point represents a single HLM donor. (C) Bar graph illustrating CYP3A4/5 residual activity as triplicate determinations in each HLM donor. For (B) and (C), lapatinib was pre-incubated for 30 min at 20 μM.

When the k_{inact}/K_I ratios were compared with the baseline CYP3A4/5 activity of the CYP3A5 genotyped HLM as determined using testosterone 6β-hydroxylation, a significant correlation was observed (r = 0.6819; p < 0.05) (Figure 3-18A). A similar correlation was found between the percentage CYP3A4/5 activity remaining following lapatinib treatment and CYP3A4/5 baseline activity, where the higher the baseline activity, the greater the decrease in CYP3A4/5 activity following exposure to lapatinib (r = 0.6232; p < 0.05) (Figure 3-18B).

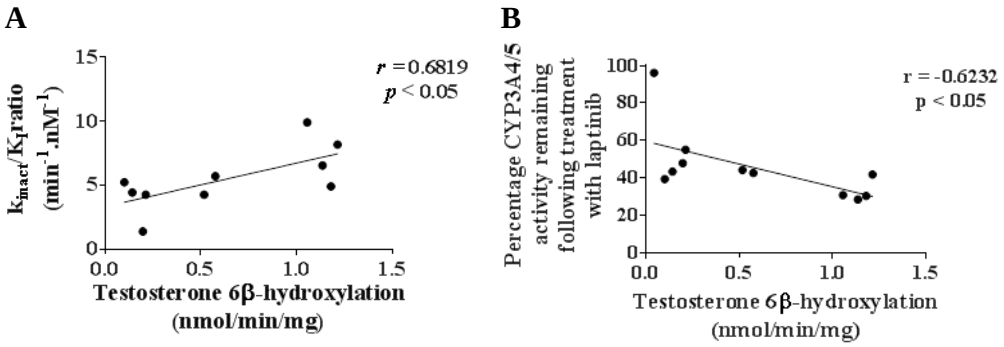

Figure 3-18 Correlation analyses describing the relationship between the extent of inactivation measured using (A) k_{inact}/K_I ratio and (B) residual CYP3A4/5 activity with baseline CYP3A4/5 activity as measured using testosterone 6β-hydroxylation in genotyped HLM. Each point represents a single HLM donor.

3.4.7 GSH Adduct Formation as a Function of CYP3A5 Genotype

The area ratios for GSH adduct formation as determined from integration of MS response in CYP3A5-genotyped HLM donors are presented in Table 3-8 and Figure 3-19A. Mean area ratios were not significantly different across the genotypes (p > 0.05), however *1/*1 carriers exhibit the greatest extent of GSH adduct formation. Again there was obvious inter-individual variability in the extent of GSH adduct formation within each genotype. Figure 3-19B shows the extent of GSH adduct formation compared with baseline CYP3A4/5 activity in each donor, with a statistically significant correlation (r = 0.9115; p < 0.0001). Finally, there was poor correlation between k_{inact}/K_I ratios and the extent of GSH adduct formation (r = 0.4439; p > 0.05) (Figure 3-19C). For the correlation graphs

using baseline CYP3A4/5 activity, donor H0331 exhibited a 2-fold higher activity than the next highest donor was excluded from the analysis as an outlier. Figure S3 illustrates the appearance of Figure 3-19B if the outlier was included.

Table 3-8 GSH adduct formation in various CYP3A5-genotyped HLM donors.

Donor	CYP3A5 Genotype	Area Ratio
HH785		2.380
HH860		4.170
HH867	*1/*1	1.750
H0331		3.590
Mean ± S.D.		**2.973 ± 1.105**
HH757		0.239
HH868		0.757
H0239	*1/*3	2.520
H0280		2.710
Mean ± S.D.		**1.557 ± 1.243**
HH507		0.053
H0307		3.540
H0204	*3/*3	0.856
H0182		0.647
Mean ± S.D.		**1.274 ± 1.548**

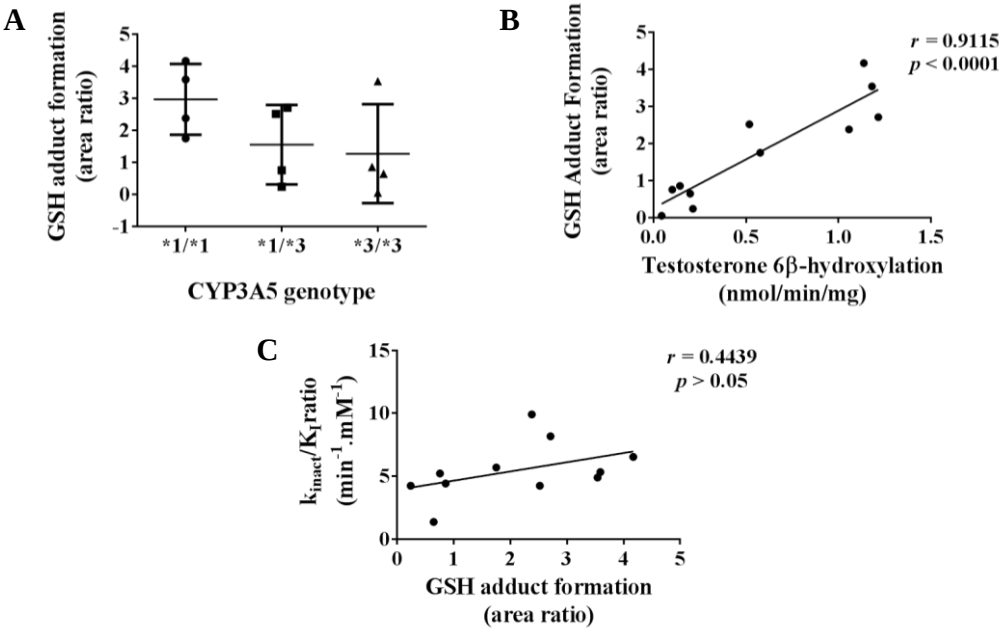

Figure 3-19 Comparison of (A) GSH adduct formation in CYP3A5*1/*1 (●), *1/*3 (■), and *3/*3 (▲) genotypes. Correlation analyses describing the relationship between (B) GSH adduct formation with baseline CYP3A4/5 activity and (C) k_{inact}/K_I ratio with GSH adduct formation. Each point represents a single HLM donor.

3.5 Discussion

3.5.1 Influence of Selective Deuteration on the Metabolic and Bioactivation Susceptibilities of Lapatinib

The development of an analytical method to detect OD lapatinib and ND lapatinib permitted kinetic profiling of the formation of both metabolites from lapatinib and its deuterated metabolites. Based on the metabolic pathways of lapatinib that lead to the formation of the reactive nitroso and quinone-imine metabolite responsible for MI complex formation with CYP3A4 and MBI of CYP3A5, judicious deuteration at positions critical to *O*-debenzylation and *N*-dealkylation were hypothesized to reduce these processes and attenuate reactive metabolite formation. Deuteration at these metabolic soft spots individually and in combination were explored in this study (Figure 3-5). d_6 lapatinib represents simultaneous deuteration of both the N-alkyl and O-benzyl positions, although it also possesses an additional deuterated carbon as indicated in Figure 3-5. An analogue with deuteration of only the N-alkyl and O-benzyl positions was unavailable to us.

O-d_2 lapatinib and N-d_2 lapatinib were hypothesized to reduce *O*-debenzylation and *N*-dealkylation respectively, while d_6 lapatinib which is deuterated at both positions was postulated to exhibit concurrent decreases in the kinetics of both pathways. The rate of *O*-debenzylation was indeed reduced by O-d_2 lapatinib, however it also unexpectedly reduced the rate of *N*-dealkylation to a greater extent than that of N-d_2 lapatinib. Interestingly, deuteration at the benzylic carbon appeared to exert a disproportionate influence on the formation of OD lapatinib and ND lapatinib. On the contrary, d_6 lapatinib, with deuterations at both positions generally did not modulate the metabolic susceptibilities of lapatinib significantly, as the apparent decrease in *N*-dealkylation is likely due to the effect

of benzylic deuteration, rather than the expected synergistic interaction of double deuterations. This finding was recapitulated in the investigation of GSH adduct levels in pooled HLM, which also established that O-d_2 lapatinib and d_6 lapatinib exhibited the greatest decrease in GSH adduct formation, suggesting that benzylic deuteration diminished the formation of the reactive quinone-imine metabolite.

Another interesting observation from the deuteration studies are the kinetics of *O*-debenzylation and *N*-dealkylation by rCYP3A4 and rCYP3A5. Using a single concentration of lapatinib (50 µM) and a single incubation time-point (30 min), Barbara *et al.* (*245*) reported that the formation of OD lapatinib was nearly 2-fold greater in CYP3A5 than CYP3A4, while Barbara *et al.* and Takakusa *et al. (244, 245)* reported that the formation of ND lapatinib was over 2-fold greater in CYP3A4 than CYP3A5. Inconsistent with their findings, our results indicate that the formation of OD lapatinib was approximately equal in rCYP3A4 and rCYP3A5 at a concentration of 50 µM lapatinib, while the formation of ND lapatinib was more than 2-fold lower in CYP3A4 than CYP3A5. As the amount of recombinant protein and incubation duration used were identical in kinetic studies involving both rCYP3A4 and rCYP3A5, the rate and amount of metabolite formation are equal, allowing a direct comparison using the kinetic plots of both recombinant systems. While the reason for these contrasting results is uncertain, it is clear that O-d_2 lapatinib is able to attenuate the metabolism of lapatinib to OD lapatinib and ND lapatinib. Importantly, because the formation of OD lapatinib and ND lapatinib were measured concurrently within the same experiment and analytical run for each enzyme system, it is interesting that deuteration at the benzylic position did not result in metabolic switching via shunting to the *N*-dealkylation pathway, but serendipitously attenuated both simultaneously.

Prior to investigating the CYP3A4/5 inactivation potential of the deuterated lapatinib analogues, we sought to establish the choice of probe substrate used to ascertain the remaining enzymatic activity after inactivation by these compounds. While testosterone has been shown to capture inactivation by lapatinib in both CYP3A4 and CYP3A5, the characterization for midazolam using both of its metabolic pathways is incomplete, particularly with CYP3A5. Barbara *et al.* (*245*) reported that lapatinib (50 μM) inhibited midazolam 4-hydroxylation but not 1'-hydroxylation in rCYP3A5 after a 30 min preincubation, while Chan *et al.* (*246*) reported an absence of inactivation in rCYP3A5 by lapatinib using midazolam 1'-hydroxylation. Thus we speculated that midazolam could capture inactivation in rCYP3A5 through the 4-hydroxylation pathway, which hitherto has not been evaluated. From a probe substrate perspective, midazolam is preferred to testosterone in this study. Using a combination of ketoconazole and the CYP3A4-selective inactivator CYP3cide, Tseng *et al.* (*277*) estimated that CYP3A5 contributed approximately 50% of midazolam 4-hydroxylation and 1'-hydroxylation, while the contribution of CYP3A5 to testosterone 6β-hydroxylation was estimated at only 16%. Our findings suggested that lapatinib did not inhibit midazolam 4-hydroxylation by CYP3A5 in a time-dependent manner, thus midazolam is unsuitable for use as a probe substrate in our study, and testosterone was retained for subsequent inactivation kinetics experiments. We also infer that the inactivation captured in pooled HLM by midazolam 4-hydroxylation likely reflects the inactivation of CYP3A4 only. The differential inactivation of testosterone and midazolam in rCYP3A5 is consistent with the findings of Chan *et al. (246)*, and suggests that the reactive metabolite of lapatinib blocks a pocket of the large CYP3A5 active site that impedes testosterone but not midazolam metabolism, affirming the need to investigate both CYP3A4 and

CYP3A5 separately, despite the fact that they share a high percentage of structural homology and exhibit broad substrate overlaps. In other words, potential DDIs with lapatinib are likely victim-drug specific and require further investigation to determine the overall strength of the interaction.

Uttamsingh *et al.* recently reported the first example where deuteration successfully reduced CYP450 inactivation. In their study, CTP-347, a deuterated analogue of the antidepressant paroxetine dramatically ameliorated the formation of the carbene reactive metabolite responsible for MI complex formation with CYP2D6. Accordingly, the time- and concentration-dependent inactivation, and Soret peak formation observed with paroxetine was abolished, and DDI with tamoxifen was also attenuated, while pharmacological activity as measured by serotonin reuptake inhibition was retained (*278*). Although deuteration of lapatinib, particularly at the benzylic carbon successfully reduced the magnitude of OD lapatinib, ND lapatinib and GSH adduct formation, these findings did not translate into a decrease in the extent of inactivation as measured by k_{inact}/K_I values. One possibility is that that although the levels of OD lapatinib, ND lapatinib and GSH adduct formation was reduced, reactive metabolites could still be generated at levels adequate to cause functionally meaningful inactivation of CYP3A4/5. A second possibility is that while benzylic deuteration might have attenuated quinone-imine formation, deuteration on the N-alkyl chain was insufficient to block nitroso and MI complex formation. Barbara *et al.* (*245*) provided evidence that nitroso formation proceeds via a secondary hydroxylamine pathway, which involves N-hydroxylation followed by dealkylation, rather than the primary hydroxylamine pathway which proceeds via dealkylation followed by N-hydroxylation. This is because the primary hydroxylamine was not detected, thus it is likely that nitroso formation proceeds via the secondary hydroxylamine

pathway (Figure 3-20). In other words, N-alkyl deuteration is ineffective in preventing nitroso formation, rendering CYP3A4 still susceptible to inactivation by lapatinib. It is not possible to generate a stable N-deuterated lapatinib analogue as the N-H proton is labile and solvent-exchangable. With respect to cytotoxicity, the reduction in GSH adduct formation by O-d_2 lapatinib could potentially attenuate lapatinib-induced hepatotoxicity, which is hypothesized to be a result of hapten formation that in turn triggers an immune-mediated response. While we did not investigate this possibility as there is currently no suitable model to recapitulate immune-mediated drug-induced liver injury, Wahlin *et al*. reported that O-d_2 lapatinib exhibited a reduction in acute cytotoxicity in HepaRG cells (*279*), suggesting that benzylic deuteration may be a promising approach to reduce lapatinib-induced hepatotoxicity.

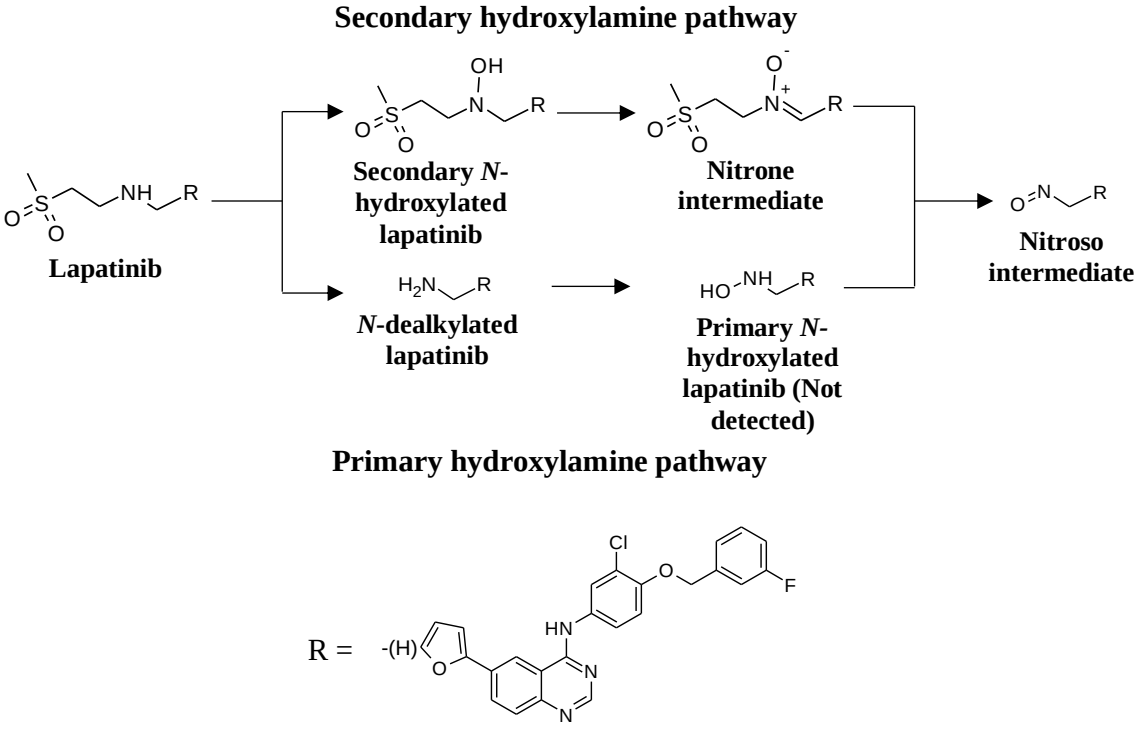

Figure 3-20 Mechanistic pathways for nitroso intermediate formation from lapatinib (adapted from (*245*)).

Most drug deuteration studies that investigate the reduction of reactive metabolite formation focus on drug safety profiles, but often neglect to assess whether efficacy remains unchanged after deuteration. In our study, despite the absence of a decrease in CYP3A4/5 inactivation, we elected to investigate if the *in vitro* efficacy of the deuterated lapatinib remains unchanged. Although uncommon, there are examples where deuteration unexpectedly induced changes in binding to a pharmacological target. In deuteration studies of sildenafil, a phosphodiesterase-5 (PDE5) inhibitor, a deuterated analogue of sildenafil reportedly exhibits a 2-fold increase in PDE5 selectivity as compared to PDE6, and greater activity *in vitro* (*280*). The HER2-overexpressing, BT474 breast cancer cell line was chosen to evaluate the pharmacodynamic effect of lapatinib and O-d_2 lapatinib as it was previously used to investigate the efficacy of HER2 antagonism by lapatinib (*281*). The absence of a significant difference between the IC_{50} values of lapatinib and O-d_2 lapatinib suggests that deuteration at the benzylic position does not modify the cytotoxic efficacy against breast cancer cells. This unchanged efficacy is also seen in other drug deuteration studies involving paroxetine (*278*), imatinib (*282*) and fludalanine (*283*).

3.5.2 Impact of CYP3A5 Genetic Polymorphism on CYP3A4/5 Inactivation by Lapatinib

Our primary objective in this study was to examine the relationship between CYP3A5 genotype and the susceptibility to inactivation by lapatinib. Although we did not observe a statistically significant difference in the mean k_{inact}/K_I ratios, the *1/*1 genotype exhibited a greater potency of inactivation compared to the *3/*3 genotype. This was supported by a greater mean decrease in CYP3A4/5 activity in *1/*1 versus *3/*3. Both measures of irreversible inactivation exhibited moderate correlations with total CYP3A4/5 activity, suggesting that the

inactivation may be broadly influenced by overall CYP3A4/5 capacity, which itself is influenced by a variety of factors including CYP3A5 genotype. GSH adduct formation, which is indicative of the quinone-imine reactive metabolite also demonstrated higher levels in the *1/*1 genotype, although this was not statistically significant. A strong correlation was observed with total CYP3A4/5 activity, suggesting that GSH adduct levels, and possibly the extent of covalent binding is strongly influenced by CYP3A4/5 capacity. Unsurprisingly, the k_{inact}/K_I ratios did not correlate well with GSH adduct levels, as the inactivation is a composite of both MI complex formation and MBI, while GSH adduct levels reflects only MBI via covalent inactivation.

CYP450 polymorphisms have been demonstrated to affect drug disposition (e.g. CYP2D6 and tamoxifen) as well as the extent of CYP450 inhibition, including reversible inhibition and irreversible inactivation. Shirasaka *et al.* reported that reversible CYP3A4/5 inhibition of ketoconazole and itraconazole as measured by IC_{50} values were most potent in CYP3A5 *3/*3 carriers, followed by *1/*1 and *1/*3 carriers (*284*). This was attributed to the lower inhibitory potency of these compounds against CYP3A5 compared with CYP3A4, thus the greater expression of CYP3A5 in carriers of at least one *1 allele serves as a reservoir of CYP3A drug metabolizing activity. Several small scale studies have also demonstrated differences in irreversible inactivation as a function of CYP450 polymorphism. Hall and colleagues reported that the inactivation parameters k_{inact}/K_I for verapamil was 30 times higher in one CYP3A5 *3/*3 donor compared to one *1/*3 donor (*285*). The much greater potency of inactivation in the *3/*3 genotype was ascribed to absence of inhibition of CYP3A5 by verapamil, thus CYP3A5-expressing genotypes are less susceptible to inactivation. However, only 1 donor each from both genotypes was studied, making it difficult to generalize

this finding. Hollenberg and colleagues found that the disulfiram metabolite, diethyldithiocarbamate exhibited a 1000-fold lower k_{inact}/K_I ratio in the inactivation of a CYP2E1*2 allele, compared with the wild-type (*228*). The effects of the *2 allele in terms of abundance or functional activity of the protein in humans is not well-described, however it has been reported to result in lower recombinant protein expression in COS-1 cells (*286*), while having comparable or greater metabolic activity than the wild-type, depending on the substrate (*286, 287*). It is important to bear in mind that the results described by Hollenberg were studied in a recombinantly generated CYP2E1*2 variant, rather than in genotyped HLM.

Although our study is not the first to explore the gene-response relationship in the context of xenobiotic-mediated inactivation of CYP450, there are several important differences in our study which merits further discussion. Firstly, the perpetrator in our study is lapatinib, which differentially inactivates *both* CYP3A4 and CYP3A5 via MI complex formation and MBI respectively. This is a crucial difference as the study of CYP3A5 polymorphism cited above investigated verapamil which preferentially inactivates CYP3A4 over CYP3A5. This is a possible reason to account for the contrasting trends regarding the potency of inactivation across CYP3A5 genotypes. In our study, we found that CYP3A5 *1/*1 carriers exhibited the greatest potency of inactivation as measured by k_{inact}/K_I ratios and decrease in CYP3A4/5 activity. In contrast, the study using verapamil documented that *1/*1 carriers were the least susceptible to inhibition and inactivation. We postulate that since CYP3A5*1 carriers generally have a higher CYP3A capacity, they possess a higher baseline CYP3A activity as measured by testosterone 6β-hydroxylation. Conversely, CYP3A5*3/*3 carriers have an intrinsically lower baseline CYP3A activity level. Upon inactivation of

both CYP3A4 and CYP3A5 by lapatinib, the *magnitude of decrease* in CYP3A activity is quantitatively greater for CYP3A5*1 carriers compared to CYP3A5*3/*3 carriers, hence the gradient of the inactivation curves, or k_{obs} is steeper in CYP3A5*1 carriers. At saturation, CYP3A5*1 carriers would have higher k_{inact} values, thus resulting in higher k_{inact}/K_I ratios. The greater decrease in CYP3A4/5 activity in *1/*1 donors is illustrated in Figure 3-17B. This effect would not manifest for a CYP3A4-selective inactivator such as verapamil.

A second important difference in our study is that this is the first to use a panel of CYP3A5 genotyped HLMs to investigate xenobiotic-mediated CYP450 inactivation. Our study clearly demonstrates that there is considerable inter-individual variability with regards to the potency of inactivation within each genotype. The study by Hall *et al*. (*285*) used only a single donor each from 2 CYP3A5 genotypes, and may not be representative of the population characteristics. For example, if we consider only donors HH785 (*1/*1) and H0182 (*3/*3), we would have concluded that *1/*1 carriers experience a 7-fold greater potency of inactivation compared with *3/*3 carriers. Conversely, we would have concluded that there is no difference in susceptibility to inactivation if we compared only donors H0331 (*1/*1) and H0307 (*3/*3). It is important to exercise caution when interpreting studies of gene-response relationships, as genetic disposition is not the sole determinant of CYP450 activity. Environmental factors such as diet or alcohol intake can give rise to exacerbated or diminished CYP3A activity independent of genotype, and thus contribute to intra-genotype variability. This emphasizes the importance of having a sufficient pool of donors per genotype when conducting such studies, or by using matched donors where possible. The small sample size of this study (4 donors per genotype) could be a possible reason for the absence of statistical significance. Nevertheless, this

investigation serves as a pilot study to elucidate the possible trend for lapatinib inactivation as a function of CYP3A5 genotype. Physiologically-based pharmacokinetic (PBPK) modeling can be used to quantify the extent of potential DDIs with lapatinib for each CYP3A5 genotype to better understand the clinical relevance of the gene-response relationship identified in this study.

3.6 Chapter Conclusion

The adverse drug reactions (e.g. hepatotoxicity) and DDIs perpetrated by lapatinib are thought to be the result of reactive metabolite formation. Judicious deuteration of lapatinib reduced *O*-debenzylation and *N*-dealkylation of lapatinib, as well as decreased quinone-imine levels as measured by GSH adduct formation. However, these findings did not translate to an attenuation of the magnitude of irreversible inactivation of CYP3A4/5, possibly because suppression of reactive metabolite formation was insufficient. Separately, CYP3A5*1/*1 carriers were found to exhibit the greatest susceptibility to CYP3A4/5 inactivation, accompanied by the largest decrease in CYP3A4/5 activity and highest GSH adduct levels. Importantly, this is the first study to characterize the effect of CYP3A5 polymorphism on CYP450 inactivation with a panel of genotyped donors, using an inactivator that simultaneously inactivates CYP3A4 and CYP3A5. These findings suggest that a gene-response relationship exists for CYP450 inactivation, and has implications on both DDI and ADRs arising from this phenomenon.

Chapter 4 Circumventing Covalent Binding via Combinatorial Lapatinib and Endoxifen Therapy

4.1 Chapter Summary

Background: *De novo* and acquired tamoxifen resistance is a major challenge in the treatment of breast cancer. One underlying cause is the development of estrogen receptor α/human epidermal growth factor receptor 2 (ERα/HER2) crosstalk, where HER2 provides an alternative pathway for generation of proliferative signals despite antagonism of ERα by tamoxifen and its active metabolites. To overcome the crosstalk and restore sensitivity to tamoxifen therapy, simultaneous inhibition of ERα and HER2 using tamoxifen and lapatinib respectively has been explored pre-clinically and clinically. However, the efficacy of this combination may be confounded by lapatinib, which is a potent covalent and coordinate inactivator of CYP3A4/5, a major enzyme responsible for bioactivation of tamoxifen to the active metabolite endoxifen.

Objective: In this chapter, we attempt to circumvent the deleterious inhibition of tamoxifen bioactivation by directly administering endoxifen with lapatinib, and explore the pharmacodynamic and pharmacokinetic interactions between lapatinib and endoxifen.

Methodology: Metabolism studies were performed to determine the extent of covalent and coordinate inhibition of tamoxifen bioactivation by lapatinib. Pharmacodynamic interactions between lapatinib and endoxifen were assessed using the combination index design in a panel of *de novo* and acquired tamoxifen-resistant cell lines. Pharmacokinetic interactions via modulation of P-glycoprotein (P-gp) efflux were explored using the MDCKII-MDR1 cell line.

Results and discussion: Lapatinib was found to inhibit tamoxifen bioactivation by up to 2.2-fold, suggesting that co-administration of lapatinib with tamoxifen may nullify expected synergistic effects *in vivo*. Strong pharmacodynamic synergism was uncovered between lapatinib and endoxifen in cell models of both *de novo* and acquired resistance to tamoxifen. Molecular biology studies confirmed that simultaneous administration of lapatinib and endoxifen disrupted the crosstalk between ERα and HER2. Additionally, lapatinib and endoxifen were both found to be substrates and inhibitors of P-gp, and exhibited mutual inhibition of drug efflux when used in combination. Importantly, these pharmacodynamic and pharmacokinetic synergistic effects occurred at drug concentration levels achievable using available dose regimens.

Conclusion: The apparent liability of lapatinib in tamoxifen bioactivation was negated by direct administration of lapatinib with endoxifen. This combination exhibits potent pharmacodynamic and pharmacokinetic synergism in tamoxifen-resistant breast cancer. This study illuminates a novel and potentially efficacious drug combination to circumvent tamoxifen resistance in breast cancer.

4.2 Chapter Introduction

Unforeseen covalent binding by a drug is often a liability due to its unpredictable, and often detrimental consequences which surface during clinical use. In the case of lapatinib, as discussed in Chapter 3, covalent binding perpetrated by its reactive quinone-imine metabolite is responsible for the MBI observed with CYP3A5, while the quasi-irreversible binding of the nitroso reactive metabolite to the heme group results in the formation of a MI complex and inactivation of CYP3A4, collectively causing permanent inhibition of CYP3A4/5 activity and potential DDIs with CYP3A4/5 substrates. Nevertheless, the presence of covalent (and coordinate) binding is not always detrimental. As illustrated in this chapter, what might be perceived as a liability can instead be turned into an opportunity.

4.2.1 Tamoxifen in the Treatment of Breast Cancer

Over 70% of breast cancer is estrogen receptor-α positive (ERα+) (*288*). For nearly three decades, tamoxifen has been the cornerstone treatment for the prevention and treatment of early and advanced ERα+ breast cancer (*289-291*) in both pre- and post-menopausal women. The widespread usage of tamoxifen is believed to have contributed significantly to the decrease in breast cancer mortality (*292*).

As a prodrug, tamoxifen is metabolized extensively by CYP450 enzymes to several key metabolites as illustrated in Figure 4-1 (*293*). Tamoxifen is metabolized to the primary metabolites 4-hydroxytamoxifen (4-OHT) and N-desmethyltamoxifen (NDMT) by CYP2D6 and CYP3A4/5 respectively, and undergo further metabolism to form the common secondary metabolite, endoxifen, which is in turn metabolized to norendoxifen (*294*).

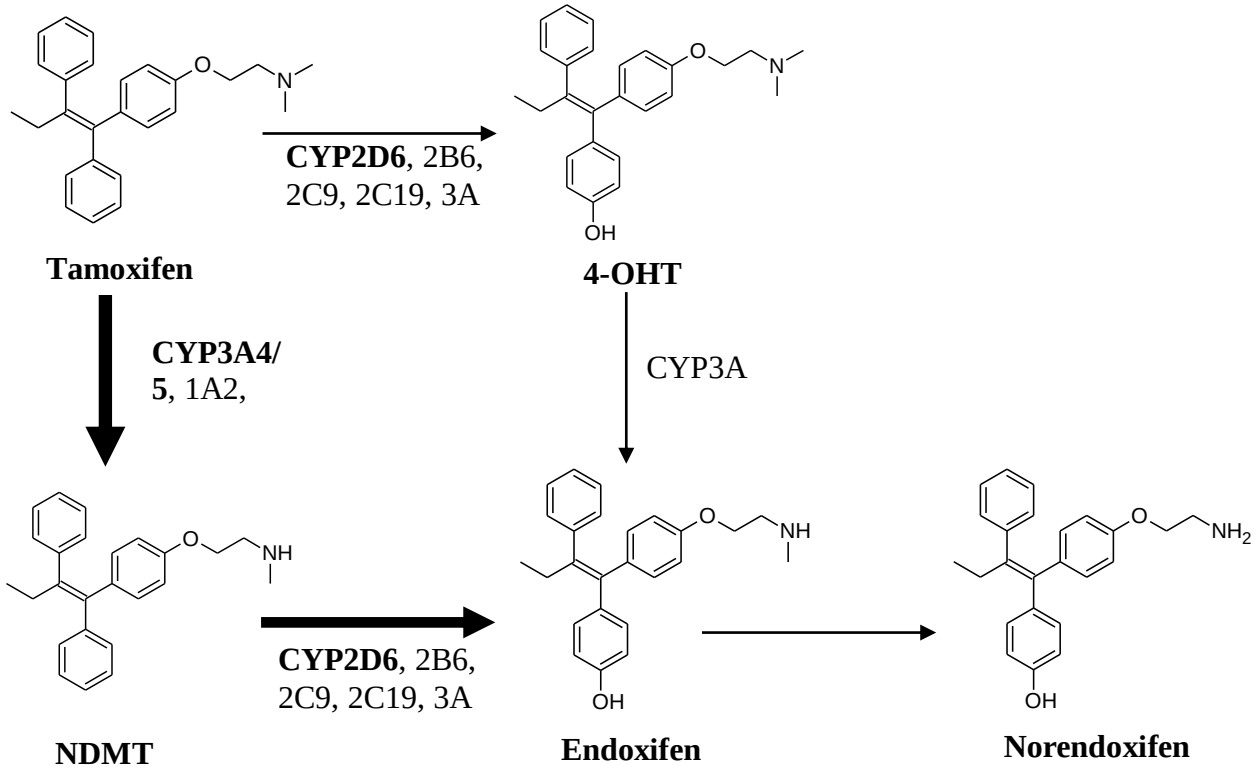

Figure 4-1 Metabolic pathway of tamoxifen and its metabolites. Thick arrows indicate predominant pathways, predominant enzymes in each pathway are indicated in bold.

Among these metabolites, 4-OHT, endoxifen, and norendoxifen are reported to be pharmacologically active (*294*, *295*). Tamoxifen metabolites exert their pharmacological effect via two mechanisms, namely, ERα antagonism or aromatase inhibition. As ERα antagonists, they compete reversibly with estrogen for binding to the nuclear receptor ERα, preventing its translocation to the nucleus, binding to the estrogen response element and transcription of genes that promote cell proliferation, survival and invasion (*296*). Additionally, endoxifen and norendoxifen are reported to be inhibitors of aromatase, which converts androgens (e.g. testosterone) to estrogens (e.g. estradiol). Collectively, ER inhibition, and aromatase inhibition which occurs upstream of ER inhibition prevents estrogen-responsive gene transcription and reduces proliferation of breast cancer cells. While 4-OHT and endoxifen demonstrate high affinity

towards ER (*297*) and are 30- to 100-fold more potent than tamoxifen *in vitro* (*293*), plasma levels of endoxifen are 6- to 7-fold higher than that of 4-OHT (*295*). As a result, endoxifen is considered the main pharmacologically active metabolite of tamoxifen (*295*). Endoxifen is additionally reported to target ERα for its degradation, a unique mechanism of action not reported for other tamoxifen metabolites (*298*).

4.2.2 Challenges in Tamoxifen Therapy

4.2.2.1 Inter-individual Variability

The dependence on CYP450-mediated bioactivation of tamoxifen exposes tamoxifen therapy to the influence of CYP450 genetic polymorphisms, giving rise to considerable inter-individual variability in tamoxifen response, which is a major clinical challenge. CYP2D6 has more than 80 polymorphic forms, resulting in individuals characterised as poor- to ultra-metabolizers (*270*). Separately, CYP3A5, a member of the CYP3A4/5 family also demonstrates genetic polymorphism (section 3.2.3.2). Efforts to establish the clinical significance of prospective genotyping for CYP2D6 and CYP3A4/5 status in tamoxifen therapy have proven to be inconclusive, as conflicting results are reported with regards to the relationship of these genotypes to plasma metabolite levels and survival rates (*299*).

4.2.2.2 Development of Tamoxifen Resistance

Tamoxifen therapy is also complicated by the heterogeneous nature of breast cancer, which is classified into different subtypes depending on the molecular phenotype (*300*). The luminal A subtype is characterised by being ERα+, human epidermal growth factor receptor 2 negative (HER2-), and progesterone receptor positive (PR+) or negative (PR-) (*300*), while the luminal B subtype is characterised by being ERα+, HER2+, and PR+ or PR-. Of the various breast

cancer subtypes, the luminal A and luminal B subtypes constitute almost 70% of all breast cancer cases in both Caucasian and Asian populations (*288*).

While patients expressing the luminal A subtype typically respond well to tamoxifen therapy (*301*), as a consequence of the long duration of treatment, up to 30% acquire tamoxifen resistance, resulting in cancer relapse over a 15-year period (*302*), leading to tumour progression and death. Additionally, the luminal B subtype exhibits *de novo* resistance to tamoxifen where it is inherently less responsive to ER antagonism and has poorer tumour grade and poorer survival rates (*303-305*).

In vitro studies using tamoxifen-resistant MCF-7 cells, generated via continual exposure to 4-OHT, demonstrated that one possible mechanism for tamoxifen resistance is the crosstalk between ERα and HER2 (*304-306*). Leary *et al.* suggested that the up-regulation of HER2 suppresses ERα function, circumvents the inhibitory signals of 4-OHT on ERα and results in continued cell proliferation (*304*). Separately, Shou *et al.* provided evidence suggesting that 4-OHT and estrogen act as agonists to the up-regulated HER2 in MCF-7 cells transfected with HER2 (*305*). This activates downstream kinases such as mitogen-activated protein kinase (MAPK) and protein kinase B (Akt), which in turn potentiates ERα function by phosphorylating and activating ERα independently of estrogen binding, a process known as ligand-independent activation (*307, 308*). These kinases were also found to suppress ERα expression at both mRNA and protein levels (*309, 310*). Collectively, these processes diminish the responsiveness of the ER to endocrine antagonism. While there are numerous mechanisms supported by *in vitro* evidence suggested to contribute to tamoxifen resistance, it is noteworthy that HER2 overexpression is the only mechanism of anti-estrogen resistance with supportive clinical data (*292*).

4.2.3 Overcoming Tamoxifen Resistance due to ERα/HER2 Crosstalk

To overcome ERα/HER2 crosstalk and restore sensitivity to tamoxifen, one promising strategy is to inhibit both pathways concurrently. This approach has shown evidence of efficacy in *in vitro* and preclinical animal studies. For example, Shou *et al.* demonstrated that co-administration of 4-OHT and gefinitib, an inhibitor of the epidermal growth factor receptor (EGFR) family including HER2, abrogated the ERα/HER2 crosstalk *in vitro* and *in vivo* (*305*). As compared to either drug alone, co-administering tamoxifen and gefinitib inhibited the growth of HER2-transfected MCF-7 tumour xenografts to a much greater extent. Separately, Leary *et al.* showed that lapatinib, an EGFR and HER2 inhibitor, restored endocrine sensitivity by increasing ERα transcriptional activity in long-term tamoxifen-treated MCF-7 cells, which exhibited endocrine resistance characterised by suppressed ERα transcription (*304*). Co-administration of 4-OHT with lapatinib completely attenuated the increased ERα activity. These results were substantiated with work by Chu *et al.* demonstrating that concurrent treatment of tamoxifen-resistant MCF-7 tumour xenografts with lapatinib and 4-OHT significantly inhibited tumour growth when compared to 4-OHT treatment alone (*306*).

Building upon the strength of these preclinical results, phase I (LAPATAM) and phase II (NCT00118157) clinical trials are currently being conducted on the co-administration of lapatinib and tamoxifen. It is important to recognize that while reversal of tamoxifen resistance was demonstrated *in vitro* using 4-OHT (*304, 306*), tamoxifen instead of 4-OHT is being investigated in clinical trials. As lapatinib is a potent inactivator of CYP3A4/5, it can potentially inhibit the formation of active tamoxifen metabolites, given that CYP3A4/5 is an integral contributor to tamoxifen bioactivation (Figure 1) (*244*, *246*). As a result, co-

administration of tamoxifen and lapatinib has important consequences as it may result in pharmacokinetic antagonism, essentially abrogating the predicted pharmacodynamic synergism.

4.2.4 Lapatinib and Endoxifen: a Superior Combination?

Given that combinatorial tamoxifen and lapatinib may exhibit pharmacokinetic antagonism, a possible solution would be to co-administer lapatinib with an active metabolite of tamoxifen to circumvent the covalent and coordinate inhibition of CYP3A4/5-dependent tamoxifen bioactivation and overcome ERα/HER2 crosstalk. Lapatinib and endoxifen appear to be promising candidates for combinatorial therapy for reasons that are detailed below. Based on literature findings, these two agents may have interactions at both the pharmacodynamic and pharmacokinetic level, both of which could augment the clinical efficacy of the proposed combination through complementary mechanisms.

Pharmacodynamic interaction. It may be argued that since lapatinib does not affect CYP2D6, this is unnecessary as tamoxifen can still undergo bioactivation by CYP2D6 to form 4-hydroxytamoxifen, and thus continue to exert antiproliferative effects. Therein however lies another clinical challenge, as relying on tamoxifen bioactivation to 4-OHT is subject to the considerable effects of CYP2D6 polymorphism. Of the known active tamoxifen metabolites, endoxifen is a promising candidate as it is the primary active metabolite downstream of CYP2D6 and CYP3A4/5 metabolism and bypasses the issues with inter-individual variability due to CYP450 polymorphism. Additionally, endoxifen possesses unique pharmacological activities such as aromatase inhibition, which is not observed for 4-OHT, and it also induces ERα degradation (*298*), which is not exhibited by norendoxifen. Given that lapatinib has already

been shown to exhibit synergism with 4-OHT, it is surprising that combinatorial lapatinib and endoxifen has not yet been explored for synergistic activity.

Pharmacokinetic interaction. Another promising aspect of this combination lies in potential pharmacokinetic synergism, as at plasma concentrations, lapatinib is both a substrate and inhibitor of the P-glycoprotein (P-gp) efflux pump (*311*), while endoxifen is reported to be a P-gp substrate (*312, 313*). P-gp is an adenosine triphosphate (ATP)-dependent efflux transporter that enables cancer cells to actively pump drugs, which are P-gp substrates, out of the cell. Physiologically, P-gp efflux transporters are found to be highly expressed in various part of the human body such as epithelial cells of the gut, endothelial cells of blood-brain barrier (BBB) and adrenal cortical cells, where their physiological role is to protect these organs from xenobiotic exposure (*314*). Given their role in xenobiotic transport, P-gp expression can modulate the pharmacokinetics of drugs. For example, the levels of P-gp transporters found in intestine, unaltered or induced by rifampicin, is inversely correlated to the intestinal absorption and bioavailability of digoxin (*315*). Beyond pharmacokinetics, P-gp upregulation can alter therapeutic outcomes by preventing intracellular drug concentrations from reaching levels needed for efficacy. In oncology, increased P-gp expression has been documented both in tumours arising from tissues that have high basal P-gp expression (e.g. colon carcinoma), and from tissues that normally expresses P-gp at low levels (e.g. ovarian cancer) after exposure to chemotherapeutic agents (*316*). In breast cancer, there is evidence to suggest that P-gp expression in tumour cells may be associated with diminished intra-tumoral drug accumulation, drug resistance, poor drug response, aggressive metastatic breast tumour and poor prognosis and (*317-321*). Tumours which overexpress P-gp can become resistant to multiple chemotherapeutic agents which are also P-gp substrates, and in some

cases, co-administration of a P-gp inhibitor such as verapamil or cyclosporin A has improved clinical efficacy (*322*) by increasing absorption and cellular uptake of the victim drug. Indeed, lapatinib has been shown *in vitro* to enhance intracellular accumulation of topotecan and doxorubicin, which are P-gp substrates, and increase systemic exposure of topotecan in a phase I trial (*323, 324*), suggesting that a similar interaction occurring via P-gp may exist for lapatinib and endoxifen. Beyond interactions at the target tissue, P-gp is also known to limit intestinal absorption due to expression in enterocytes, promote excretion into bile and urine as a result of its expression in the canalicular membrane of hepatocytes and in the luminal membrane of renal proximal tubule cells, and is part of the panel of efflux transporters that reduce CNS penetration due to expression at the luminal membrane of the endothelial cells lining the brain capillaries in the blood-brain barrier (*325*). P-gp interactions at these physiological sites could augment oral absorption, reduce biliary and urinary excretion thus sustaining plasma concentrations, and also enhance CNS penetration. The latter is particularly intriguing since the brain is a common secondary site of breast tumour metastasis (*326*).

Taken together, the combined effects of endoxifen and lapatinib on ERα and HER2 suggest potential pharmacodynamic synergism, while the intrinsic characteristics of lapatinib and endoxifen, as a P-gp substrate and inhibitor respectively hints at potential pharmacokinetic synergism. This chapter focuses on the co-administration of lapatinib and endoxifen to circumvent the potential deleterious effects of covalent and coordinate inhibition of tamoxifen bioactivation. Firstly, the extent of inhibition of tamoxifen bioactivation by lapatinib is determined using pooled human liver microsomes (HLM). The combination of lapatinib and endoxifen is subsequently investigated from both

pharmacodynamic and pharmacokinetic aspects. The former is performed in a panel of breast cancer cells, while the latter is determined in the P-gp overexpressing MDCKII-MDR1 cells. By studying the interaction between these two agents from both perspectives, we aim to demonstrate that covalent binding is not necessarily a liability, but can instead be leveraged into an opportunity to enhance therapeutic efficacy in breast cancer.

4.3 Materials and Methods

4.3.1 Materials

Tamoxifen citrate was purchased from Cayman Chemical (Ann Arbor, MI, USA). NDMT, endoxifen, norendoxifen and amprenavir were from Toronto Research Chemicals (Toronto, ON, Canada). Lapatinib was from LC Laboratories (Woburn, MA, USA). Pooled HLM were obtained from BD Gentest (Franklin Lakes, NJ, USA). HPLC-grade methanol and acetonitrile (ACN) were purchased from Tedia Company Inc. (Fairfield, OH, USA). NADPH-regenerating system consisting of NADPH A ($NADP^+$ and glucose-6-phosphate) and NADPH B (glucose-6-phosphate dehydrogenase) was acquired from BD Gentest (Woburn, MA, USA). RIPA lysis buffer, Pierce BCA protein assay kit, Halt protease inhibitor cocktail, and SuperSignal West Pico Chemiluminescent Substrate were obtained from Thermo Scientific (Waltham, MA, USA), while PhosSTOP phosphatase inhibitor cocktail tablet was purchased from Roche Life Science (Indianapolis, IN, USA). Primary antibodies against HER2, pHER2 (Tyr1248), pHER2 (Tyr1221/1222), ERα, pERα (S104/106), pERα (S118), pERα (S167) and secondary horseradish peroxidase–conjugated goat anti-mouse and anti-rabbit IgG antibodies were from Cell Signaling Technology (Danvers, MA, USA). 4-OHT, RPMI medium 1640 without phenol red, fluorescein diacetate (FDA), geneticin, dextromethorphan hydrobromide and anti-β-actin antibody were obtained from Sigma-Aldrich (St. Louis, MO, USA). Fetal bovine serum (FBS) and L-glutamine were obtained from Hyclone (Logan, UT, USA), while 1% penicillin/streptomycin was purchased from PAN Biotech (Aidenbach, Germany). Charcoal-stripped FBS was obtained from Biowest (Nuaillé, France). Dulbecco's modified eagle's medium (DMEM) with phenol red, DMEM without phenol red, Dulbecco’s phosphate buffer solution (DPBS), and HEPES buffer were from

Gibco Life Technologies (Waltham, MA, USA). Lucifer yellow CH dilithium salt was from MP Biomedicals (Santa Ana, CA, USA). Elacridar (GF120918A) were from GlaxoSmithKline (GSK) Laboratories (Middlesex, United Kingdom). Potassium phosphate monobasic (ACS grade) was purchased from Mallinckrodt Baker (Phillipsburg, NJ, USA). Water was obtained using a Milli-Q water purification system (Millipore, Bedford, MA, USA). All other chemicals and reagents used were of analytical grade.

4.3.2 Effect of Lapatinib on Tamoxifen Bioactivation

4.3.2.1 Effect of Lapatinib on Intrinsic Clearances of Tamoxifen and 4-OHT in Pooled HLM

The intrinsic clearances (CL_{int}) of tamoxifen to NDMT, and 4-OHT to endoxifen, both mediated by CYP3A4/5 were investigated in the presence and absence of lapatinib using pooled HLM. A primary incubation mixture containing 10 μM lapatinib, NADPH B, 0.5 mg/mL pooled HLM and 100 mM phosphate buffer (pH 7.4) was pre-incubated for 5 min at 37°C with shaking; subsequently, the reaction was initiated with NADPH A. After a 30 min incubation period, 10 μL of the primary incubation mixture was transferred to a secondary incubation mixture in a 96-well polypropylene plate containing NADPH A, NADPH B, tamoxifen (0−100 μM) and 100 mM phosphate buffer (pH 7.4) to achieve a 10-fold dilution of HLM to a final concentration of 0.05 mg/mL. The reaction was terminated 10 min later with 100 μL of ice-cold ACN containing 0.5 μM donepezil as an internal standard (IS). The plate was centrifuged at 2900 *g* for 30 min at 4°C to remove precipitated protein. 100 μL of the supernatant was carefully withdrawn and dispensed into another 96-well polypropylene plate for analysis with LC/MS/MS. To establish baseline CL_{int} of tamoxifen via the formation of NDMT in the absence of lapatinib, 100 mM phosphate buffer (pH 7.4) was used to replace lapatinib in the

preparation of primary incubation mixtures without lapatinib. The above procedures were repeated using 4-OHT (0-200 μM) as a probe substrate. The final organic concentration in each incubation mixture did not exceed 2% (v/v). All reactions were performed in triplicates. Samples were stored at -80°C and protected from light until analysis with liquid chromatography-tandem mass spectrometry (LC/MS/MS).

4.3.2.2 Quantification of Tamoxifen Metabolites by LC/MS/MS

Experiments were performed using an Agilent 1290 Infinity LC system interfaced with an AB Sciex Qtrap 5500 hybrid linear ion-trap quadrupole mass spectrometer equipped with a TurboIonSpray source (Applied Biosystems, Foster City, CA). Milli-Q water and HPLC-grade ACN, both acidified with 0.1% formic acid, were used as mobile phases A and B respectively. Both mobile phases were pumped through a Waters Acquity UPLC BEH C_{18} column (1.7 μm, 50 mm × 2.1 mm i.d.; Waters, Milford, MA, USA) at a flow rate of 0.6 mL/min. Elution conditions were as follows: linear gradient 38 to 39% B (0−1.00 min), linear gradient 39 to 95% (1.01−1.04 min), isocratic 95% B (1.05−1.55 min), linear gradient 95 to 38% (1.56−1.59 min) and isocratic at 38% B (1.60−2.50 min). Using an autosampler thermostatted at 6°C, 3 μL of each sample was injected onto the UPLC column maintained at 45°C. The needle was flushed with methanol post-injection to minimize carry-over effect. Tandem mass spectrometry was operated in the positive ion electrospray ionization (ESI +ve) mode. MS source conditions were: ionspray voltage, 4000 V; temperature, 450°C; curtain gas 25 psi; ion source gas 1, 45 psi; and ion source gas 2, 50 psi. Compound-dependent MS parameters were optimized using pure standards and are summarized in Table 4-1. Multiple reaction monitoring (MRM) experiment was performed for quantification of analytes. The retention times of NDMT,

endoxifen and donepezil were 1.5, 1.1 and 0.4 min respectively. Calibration samples containing NDMT and endoxifen (0, 0.005, 0.01, 0.05, 0.1, 0.5 and 1 μM), 100 mM phosphate buffer (pH 7.4) and ACN containing 0.5 μM donepezil were freshly prepared and underwent the same sample preparation for each analysis. The calibration data for NDMT and endoxifen were fitted to a linear model, with the reciprocal of the squared concentration ($1/x^2$) used as the weighting factor.

Table 4-1 MRM transitions and compound-dependent MS parameters for the detection of tamoxifen metabolites and donepezil (IS).

Analyte	MRM Transition (*m/z*)	Collision Energy (V)	Declustering Potential (V)	Entrance Potential (V)	Collision Exit Potential (V)
NDMT	358 → 58	51	101	9	12
Endoxifen	374 → 58	57	111	8	8
Donepezil (IS)	380 → 91	51	106	9	14

4.3.2.3 Data Analysis

Integration of chromatographic peaks was performed using Analyst Software (version 1.5.2, Applied Biosystems). Final concentration levels of tamoxifen metabolites calculated based on relative responses were normalized to incubation time and amount of HLM (pmol/min/mg). The data was subsequently processed with Prism 6 (GraphPad Software Inc., San Diego, CA, USA) by nonlinear regression analysis using either the Michaelis-Menten or allosteric sigmoidal model, where a comparison of fits test was performed using Prism 6 to obtain the best-fit model for determining the enzyme kinetics parameters V_{max} and K_m. CL_{int} values were calculated as the V_{max}/K_m ratio.

4.3.3 Investigation of Pharmacodynamic Interaction between Lapatinib and Tamoxifen or its Active Metabolites

This *in vitro* investigation was divided into 2 phases. In a pilot study, potential synergism between lapatinib and tamoxifen or its active metabolites (4-OHT, endoxifen and norendoxifen) were determined in the *de novo* tamoxifen-resistant phenotype. The best combination was then advanced to the second phase, where potential synergism was explored in a luminal A subtype exhibiting acquired tamoxifen resistance.

4.3.3.1 Cell Culture

De novo *tamoxifen resistance.* The MCF-7 cell line which was previously obtained from the British Columbia Cancer Centre, Vancouver, Canada was a kind gift from Dr. Chiu Ngar Chee, Gigi (National University of Singapore, Singapore), while the BT474 cell line was a kind gift from Dr. Yang Yi Yan (Institute of Bioengineering and Nanotechnology, Singapore). Both cell lines were cultured in phenol red-free RPMI medium 1640, supplemented with 10% heat-inactivated FBS and 1% penicillin/streptomycin.

Acquired tamoxifen resistance. Isogenic tamoxifen-sensitive MCF-7 and tamoxifen-resistant TAM-R cell lines were kind gifts from Dr. Julia M. W. Gee (Cardiff University, United Kingdom). MCF-7 cells were cultured in phenol red-free RPMI 1640 medium supplemented with 5% heat-inactivated FBS and 1% penicillin/streptomycin. TAM-R cells derived from the tamoxifen-sensitive parental MCF-7 cell line were cultured in phenol red-free RPMI 1640 medium, supplemented with 5% heat-inactivated charcoal-stripped FBS, 1% penicillin/streptomycin and 0.1 μM 4-OH-T to maintain tamoxifen resistance. MCF-7 cells stably transfected with HER2 (MCF-7/HER2) cell line was a kind gift from Dr. Dawn Waterhouse (British Columbia Cancer Centre, Vancouver,

Canada) and was cultured in phenol red-free RPMI medium 1640, supplemented with 10% FBS and 100 µg/mL geneticin.

All cell cultures were incubated in a humidified environment kept at 5% CO_2 and 37°C. All cell lines used were authenticated in November 2014 using short tandem repeat DNA profiling of 9 loci with 100% identity match against the DSMZ database (Genetica DNA Laboratories, Burlington, NC, USA).

4.3.3.2 In Vitro Monotherapy Cytotoxicity Assay

De novo *tamoxifen resistance.* MCF-7 and BT474 cells were seeded into 96-well plates at a density of 7 000 and 10 000 cells/well respectively. Serial dilutions of tamoxifen (0.3 – 100 µM), 4-OHT (0.3 – 100 µM), endoxifen (0.3 – 100 µM), norendoxifen (0.3 – 100 µM) and lapatinib (0.001 - 100 µM) using culture media were added to the respective wells at 200 µL per well. For vehicle controls, up to 1% ethanol was used for tamoxifen, up to 1% methanol was used for 4-OHT, endoxifen, and norendoxifen, and up to 0.5% DMSO was used for lapatinib. Cell viability was greater than 90% at these concentration levels of solvents.

Acquired tamoxifen resistance. MCF-7, TAM-R and MCF-7/HER2 cells were seeded into 96-well plates at a density of 7 000 cells/well. TAM-R cells were cultured in 4-OHT-free media for 7 days before any drug exposure. MCF-7/HER2 cells were seeded in geneticin-free media during drug treatment. Serial dilutions of tamoxifen (0.3-50 µM), endoxifen (0.3 – 30 µM), and lapatinib (0.1 - 50 µM) using culture media were added to the respective wells at 200 µL per well. For vehicle controls, up to 0.5% ethanol was used for tamoxifen and endoxifen, and up to 0.5% DMSO was used for lapatinib. These concentrations were not found to affect cell viability.

Cells were treated for a total of 5 days and the media containing drugs was refreshed after 3 days. Cell survival was measured using fluorescein diacetate (FDA) assay (*327*). The percentage cell survival was subsequently calculated and the half-maximal inhibitory concentration (IC_{50}) was determined from cell survival curves using Prism 6. Each experiment was carried out in triplicates, and the average IC_{50} for each drug was obtained. Comparisons of IC_{50} values within each cell line for tamoxifen and its metabolites, as well as for lapatinib across both cell lines were performed using one-way analysis of variance (ANOVA) followed by Tukey's post-hoc test using Prism 6, and $p < 0.05$ was considered statistically significant.

4.3.3.3 In Vitro Combination Therapy Cytotoxicity Assay

De novo *tamoxifen resistance.* In MCF-7 cells, combination therapy was performed using equipotent doses (based on monotherapy IC_{50} values) of lapatinib and tamoxifen (1:1.48 ratio), lapatinib and 4-OHT (1:1.1), lapatinib and endoxifen (1:0.954), and lapatinib and norendoxifen (1:1.22). In BT474 cells, combination therapy was performed using equipotent doses of lapatinib and tamoxifen (1:244), lapatinib and 4-OHT (1:193), lapatinib and endoxifen (1:170), and lapatinib and norendoxifen (1:252). Concentration levels of solvents did not exceed 0.7% methanol and 0.5% DMSO in vehicle controls.

Acquired tamoxifen resistance. In isogenic MCF-7 cells, combination therapy was performed using equipotent doses of lapatinib and tamoxifen (1:1.37), and lapatinib and endoxifen (1:0.79). In TAM-R cells, combination therapy was performed using equipotent doses of lapatinib and tamoxifen (1:2.24), and lapatinib and endoxifen (1:1.57). In MCF-7/HER2 cells, combination therapy was performed using equipotent doses of lapatinib and tamoxifen (1:11.6), and

lapatinib and endoxifen (1:8.21). Concentration levels of solvents did not exceed 0.5% ethanol and 0.5% DMSO in vehicle controls.

The cells were treated for a total of 5 days and the media containing drugs was refreshed on day 3. Cell survival was measured using the FDA assay and the cytotoxic effect of combinatorial treatment was evaluated using the multiple drug effect analysis by Chou and Talalay (*328, 329*). Briefly, the combination index (CI) equation for mutually nonexclusive drugs, $CI = \frac{(D)_1}{(D_x)_1} + \frac{(D)_2}{(D_x)_2} + \frac{(D)_1(D)_2}{(D_x)_1(D_x)_2}$ was used, where $(D_x)_1$ or $(D_x)_2$ is the dose of drug 1 or 2 "alone" that demonstrates a particular effect (e.g. *x*% cytotoxicity or cell kill, which is also known as fractional effect or fraction affected, f_a), while $(D)_1$ and $(D)_2$ represents the dose of both drugs "in combination" that demonstrates the same effect. $(D_x)_1$ or $(D_x)_2$ was obtained from the median-effect equation, $(D_x) = (D_m)[\frac{f_a}{1-f_a}]^{\frac{1}{m}}$, where D_m represents IC_{50} and m is the sigmoidity of the curve. By solving for different values of f_a, different CI values were obtained, where CI < 1, = 1 and > 1 indicates synergism, additive effect and antagonism respectively. In other words, if the numerator (dose of drug used in combination) is lower than the denominator (dose of drug used singly) required to achieve the same effect, CI will be less than 1 and would reflect synergism. The dose reduction index at 50% cytotoxicity (DRI_{50}) was used to determine the fold-reduction in doses in combination therapy compared with IC_{50} of monotherapy according to the method by Chou and Talalay (*329*).

4.3.3.4 Western Blot

Western blot analysis of protein expression and phosphorylation was performed for the isogenic MCF-7 and TAM-R pair representing acquired tamoxifen resistance. MCF-7 and TAM-R cells were seeded into 6-well plates at a density of

300 000 cells/well and incubated overnight. Each well was treated with 2 mL of culture media containing individual drugs or in combination at half their IC_{50} for 72 h, where MCF-7 cells were exposed to 2.6 μM tamoxifen, 1.5 μM endoxifen or 1.9 μM lapatinib, while TAM-R cells were treated with 3.8 μM tamoxifen, 2.7 μM endoxifen or 1.5 μM lapatinib. Untreated controls were cultured in media containing the highest concentration of ethanol and DMSO used in the drug-treated samples. Cell monolayers were washed twice with ice-cold phosphate buffered saline (PBS) and collected by scraping in RIPA lysis buffer containing Halt protease inhibitor cocktail and PhosSTOP phosphatase inhibitor cocktail. Cell lysates centrifuged at 14 000 *g* at 4°C for 20 min. The supernatant was withdrawn and its protein concentration quantified using Pierce BCA protein assay kit. Cell lysates (30 μg) were resolved by 10% sodium dodecyl sulphate polyacrylamide gels (SDS-PAGE) and transblotted to nitrocellulose membranes. Protein transfer and equal loading of proteins were visualized by Ponceau S staining. Membranes were blocked at room temperature (25°C) for 30 min in Tris-buffered saline with 0.1% v/v Tween 20 (TBST) containing 5% w/v bovine serum albumin (BSA), followed by incubation at 4°C overnight with primary antibody (1:1000) diluted in 5% w/v BSA in TBST. The membranes are washed thrice in TBST, and incubated in appropriate secondary antibody (1:2000) for an hour at room temperature (25°C) and developed using enhanced chemiluminescence. Primary antibodies against HER2, pHER2 (Tyr1248), pHER2 (Tyr1221/1222), ERα, pERα (S104/106), pERα (S118), pERα (S167), β-actin and secondary horseradish peroxidase–conjugated goat anti-mouse and anti-rabbit IgG antibodies were used according to manufacturer's instructions. β-actin bands were visually compared to ensure equal sample loading. Densitometric

analysis was conducted and band intensity was normalized to control for each cell line using ImageJ software version 1.48.

4.3.4 Determination of Pharmacokinetic Interaction between Lapatinib and Endoxifen

4.3.4.1 Cell Culture

Madin-Darby canine kidney sub-clone II cells transfected with multi-drug resistance protein 1 (MDCKII-MDR1) were obtained from BioCat (Heidelberg, Germany). Cells were cultured in DMEM with phenol red supplemented with 10% heat-inactivated FBS and 0.5% penicillin/streptomycin and seeded at 166 667 cells/well within the insert of the 24-well Falcon HTS Multiwell insert system (Waltham, MA, USA). Media was refreshed at every 2 or 3 days and also 1 h before the start of assay. Cultures were maintained under a humidified atmosphere of 5% CO_2 at 37°C for 1 week to allow formation of a polarized monolayer, whereby the cell surface membrane not attached to any surface, termed the apical (A) side expresses P-gp transporters, while the basolateral (B) side which is attached to the insert does not. Figure 4-2 illustrates the concept of the A and B side of the MDCKII-MDR1 monolayer.

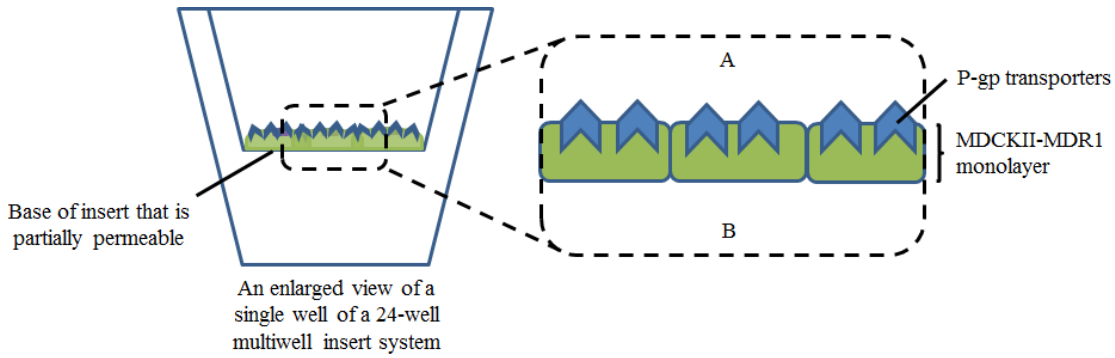

Figure 4-2 Illustration of A and B side of MDCKII-MDR1 monolayer.

4.3.4.2 Transport Assay

The transport assay involves measurement of the apparent permeability of a substrate from the A to B direction (P_{app} (A→B)), and the B to A direction (P_{app} (B→A)). These two parameters are then used to determine the efflux ratio (section 4.3.4.4). Two solutions were defined in this assay: a donor solution comprising a transport vehicle, lucifer yellow, and substrate with or without inhibitor; and a receiver solution consisting of transport vehicle only. To measure P_{app} (A→B), the A chamber was incubated with donor solution while the B chamber was incubated with receiver solution; similarly, to measure P_{app} (B→A), the B chamber was incubated with donor solution while the A chamber was incubated with receiver solution as illustrated in Figure 4-3.

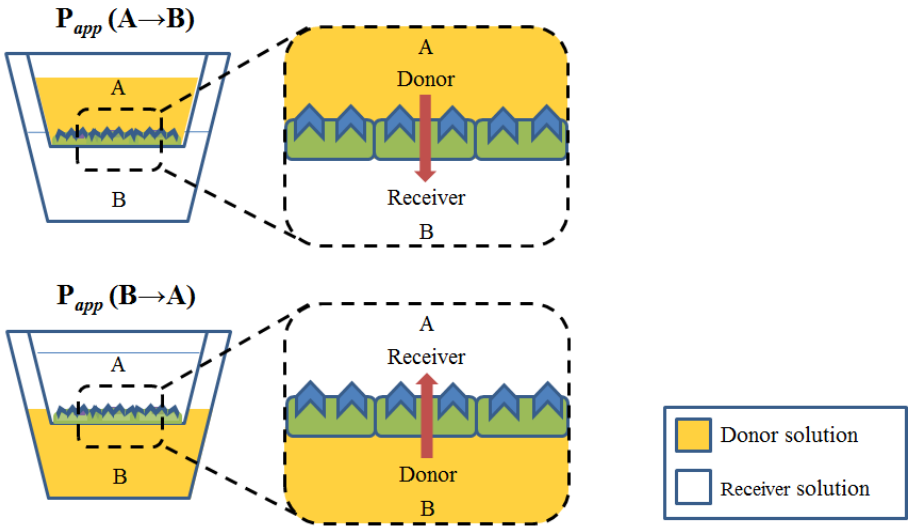

Figure 4-3 Illustration of measurement of P_{app} (A→B) and P_{app} (B→A).

Three types of transport assays were performed to evaluate the interaction of lapatinib and endoxifen with P-gp as described below.

Substrate assay. The donor solution comprised DMEM without phenol red containing 10% FBS and 0.5% penicillin/streptomycin as transport vehicle, supplemented with either lapatinib (0 – 30 μM) or endoxifen (0 – 30 μM) as substrate.

Inhibitor assay. The donor solution comprised HEPES buffer (pH 7.4) as transport vehicle, supplemented with 10 μM amprenavir as the probe substrate and either lapatinib (0 – 50 μM) or endoxifen (0 – 50 μM) as the inhibitor.

Combinatorial treatment. The donor solution comprised of DMEM without phenol red containing 10% FBS and 0.5% penicillin/streptomycin as transport vehicle, supplemented with 1 μM substrate and inhibitor (0 – 50 μM), where lapatinib/endoxifen or endoxifen/lapatinb were used as substrate/inhibitor pairs.

Treated cells were incubated and shaken on a PHMP Grant-bio (Cambridgeshire, United Kingdom) microplate shaker at 37°C at 250 rpm. All incubations were maintained for 1.5 h except when endoxifen was used as a substrate, where incubations were maintained for 3 h. At the end of the incubation, 150 μL of solution from each chamber was aliquoted into a 96 deep well block for drug analysis. 300 μL of internal standard (IS) solution was added to each well to precipitate the proteins present. IS solution was prepared from 100 μg/mL dextromethorphan stock solution diluted to 50 ng/mL in acetonitrile (ACN). The plates were then centrifuged at 2147 *g* at 10°C to pellet precipitated protein and other particles. The supernatant was injected for analysis using LC/MS/MS. All donor solutions were supplemented with 100 μM lucifer yellow to assess monolayer integrity. For each plate, a set of controls consisting of 10 μM amprenavir as probe substrate with and without 2 μM elacridar, a FDA-recommended P-gp inhibitor was employed to ascertain maintenance of P-gp efflux during the course of the experiment. Concentration levels of organic solvents did not exceed 0.8%.

4.3.4.3 Quantification of Substrates using LC/MS/MS

Samples were quantified using the instrumentation described in section 4.3.2.2. Mobile phase A was 10 mM ammonium acetate acidified with 0.1% formic acid and mobile phase B was HPLC-grade ACN delivered at flow rate of 1 mL/min. Analytes were separated using a Discovery Cyano HPLC Column Supelco 59355-U (180 Å, 5 μm, 5 cm × 4.6 mm i.d) (Sigma-Aldrich, St.Louis, MO, USA) maintained at 40°C. Elution conditions were as follows: linear gradient 30 to 90% B (0-1.2 min), held at 90% B (1.2-1.6 min) and 90 to 30% B (1.6-1.61 min). Using an autosampler thermostatted at 4 °C, 1 μL of each sample was injected into the column. Tandem mass spectrometry was operated in the positive ion electrospray ionization (ESI +ve) mode. MS source conditions were: curtain gas 20 psi; ionspray voltage, 5500 V; temperature, 400°C; ion source gas 1, 40 psi; and ion source gas 2, 40 psi. Compound-dependent MS parameters were optimised using pure standards and are summarized in Table 4-2. Multiple reactions monitoring (MRM) transition was applied for quantification. The retention times for amprenavir, endoxifen, lapatinib and dextromethorphan were 1.44, 1.50, 1.60 and 1.13 min respectively. Integration of chromatographic peaks was performed using ABSciex Analyst Software version 1.6.

Table 4-2 MRM transition and compound-dependent MS parameters for P-gp substrates and dextromethorphan (IS).

Analyte	MRM Transition (*m/z*)	Collision Energy (V)	Declustering Potential (V)	Entrance Potential (V)	Collision Exit Potential (V)
Amprenavir	506.2 → 245.2	25	76	10	18
Endoxifen	373.9 → 58.1	49	101	10	8
Lapatinib	581.1 → 365.1	53	66	10	14
Dextromethorphan (IS)	272.1 → 171.1	53	86	10	12

4.3.4.4 Determination of Efflux Ratio and Monolayer Integrity

Apprarent permeability. Apparent permeability (P_{app}) of a drug from one chamber to the other chamber is described by the following equation:

$$\text{Apparent permeability } (P_{app}) \text{ of substrate (nm/s)} = \frac{dQ/dt}{C_0 \times SA}$$

where

Q is the amount of substrate (nmol)
C_0 is the concentration at $t = 0$ s (nM)
SA is the surface area (cm^2)
t is the incubation time (s)

Efflux ratio. Efflux ratio is defined as the ratio of P_{app} (B→A) to P_{app} (A→B), as described by the following equation:

$$\text{Efflux ratio} = \frac{P_{app}\ (B \rightarrow A)}{P_{app}\ (A \rightarrow B)}$$

where

P_{app} (B→A) is the apparent permeability from B to A (nm/s)
P_{app} (A→B) is the apparent permeability from A to B (nm/s)

The efflux ratio data was subsequently processed by non-linear regression analysis using Prism 6.

Monolayer integrity. Monolayer integrity was assessed using lucifer yellow, a fluorescence dye that is impermeable through the cell membrane. By measuring the movement of lucifer yellow across the monolayer, the "leakiness" of the monolayer can be determined. An intact monolayer is a pre-requisite for a validated MDCKII-MDR1 efflux ratio assay. 100 µL of solution from each chamber was transferred into a 96-well flat bottom black plate. Lucifer yellow fluorescence of each chamber was measured at an excitation wavelength of 485 nm and emission wavelength of 530 nm. Permeability of lucifer yellow was determined using the following equation as described by Polli et al (*311*):

Permeability of lucifer = $-\left(\frac{V_D V_R}{(V_D + V_R)At}\right) ln \left[1 - \frac{(V_D + V_R)C_R(t)}{V_D C_D(t) + V_R C_R(t)}\right] \times 10^7$
yellow (nm/s)
where

V_D is the volume in donor chamber (mL)
V_R is the volume in receiver chamber (mL)
A is the surface area (cm^2)
t is the incubation time (s)
$C_D(t)$ is the measured concentration in the donor well at time t (nM)
$C_R(t)$ is the measured concentration in the receiver well at time t (nM)

Acceptance criteria for an intact monolayer was defined as permeability of lucifer yellow less than 80 nm/s.

4.4 Results

4.4.1 Effect of Lapatinib on Tamoxifen Bioactivation

In establishing CL_{int} values of tamoxifen to NDMT, and 4-OHT to endoxifen, we aimed to assess the effects of mechanism-based inactivation of CYP3A4/5 by lapatinib on the bioactivation of tamoxifen by CYP3A4/5. Metabolism of tamoxifen to NDMT was best fitted using the Michaelis-Menten model, while metabolism of 4-OHT to endoxifen was best fitted using the allosteric sigmoidal model Figure 4-4. V_{max}, K_m and CL_{int} values of each pathway in the absence and presence of lapatinib are given in Table 4-3. A 2.2- and 1.5-fold decrease in CL_{int} values were observed in the presence of lapatinib for the metabolism of tamoxifen to NDMT and 4-OHT to endoxifen respectively, indicating that lapatinib inhibited the CYP3A4/5-mediated bioactivation of tamoxifen.

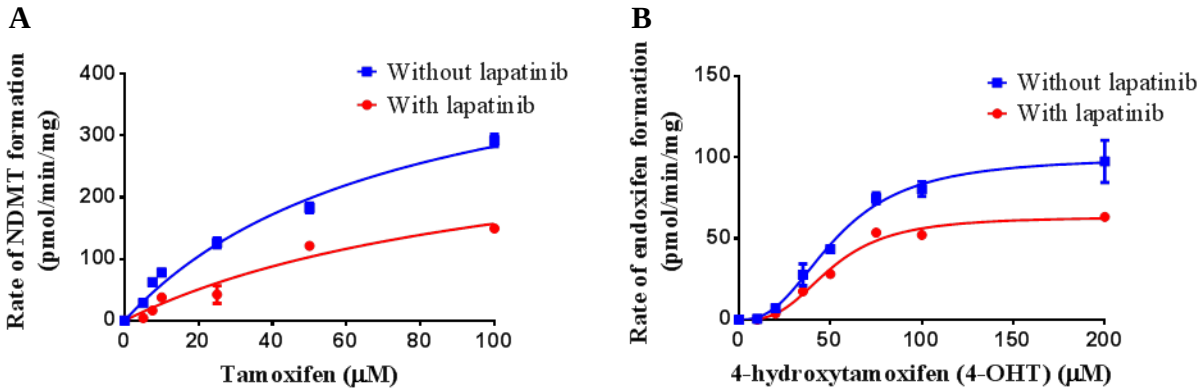

Figure 4-4 Metabolism kinetics of (A) tamoxifen to NDMT and (B) 4-OHT to endoxifen in the absence and presence of lapatinib in pooled HLM.

Table 4-3 Kinetic parameters for the metabolism of tamoxifen and 4-OHT to NDMT and endoxifen respectively in pooled HLM in the absence and presence of lapatinib.

Metabolic pathway	Treatment	V_{max} (pmol/mg/min)	Km (µM)	CL_{int} (µL/min/mg)	Fold-change
Tamoxifen to NDMT	Without lapatinib	492.3	74.26	6.63	2.2
	With lapatinib	331.7	110.9	2.99	
4-OHT to endoxifen	Without lapatinib	100.1	52.98	1.89	1.5
	With lapatinib	63.39	50.42	1.25	

4.4.2 Pharmacodynamic Interaction between Lapatinib and Tamoxifen or its Active Metabolites in the De Novo *Tamoxifen-Resistant Luminal B Subtype*

4.4.2.1 Monotherapy in MCF-7 and BT474 Cells

Figure S4 and Figure S5 shows the cytotoxicity results of 5-day treatment of MCF-7 (ERα+/HER2-) and BT474 (ERα+/HER2+) cells with tamoxifen, its metabolites or lapatinib. The MCF-7 cell line was used as a comparator against the HER2-expressing BT474 cell line. Cell proliferation was inhibited in a dose-dependent manner by all compounds in each cell line. As summarized in Table 4-4 tamoxifen was less potent than its active metabolites in MCF-7 cells, but was

comparable in BT474. Among the active metabolites, 4-OHT and endoxifen yielded comparable IC_{50} values against both cell lines, while norendoxifen was less potent in BT474. Lapatinib demonstrated nanomolar IC_{50} values in BT474 cells, while in MCF-7 it was far less potent and had an IC_{50} value comparable to those of tamoxifen active metabolites.

Table 4-4 IC_{50} values of tamoxifen, 4-OHT, endoxifen, norendoxifen, and lapatinib monotherapy in MCF-7 and BT474 cells.

Treatment	IC_{50} ± SD (μM)	
	MCF-7	BT474
Tamoxifen	9.59 ± 1.52[a]	6.58 ± 0.33[b]
4-OHT	7.24 ± 0.13	5.18 ± 0.52
Endoxifen	6.17 ± 0.86	4.56 ± 0.43
Norendoxifen	7.89 ± 1.16	6.79 ± 0.12[c]
Lapatinib	6.49 ± 0.61[d]	0.0270 ± 0.01

[a]IC_{50} value of tamoxifen against MCF-7 is significantly higher than 4-OHT, endoxifen or norendoxifen ($p < 0.05$).
[b]IC_{50} value of tamoxifen against BT474 is significantly higher than endoxifen ($p < 0.05$).
[c]IC_{50} value of norendoxifen against BT474 is significantly higher than 4-OHT or endoxifen ($p < 0.05$).
[d]IC_{50} value of lapatinib is significantly higher against MCF-7 than BT474 ($p < 0.0001$).

4.4.2.2 Combination Therapy in MCF-7 and BT474 Cells

Against MCF-7 cells, an antagonistic effect (CI > 1) was observed at low levels of cytotoxicity, or cell kill for all the drug combinations except for the combination of lapatinib and norendoxifen, which showed synergism (CI < 1) at all levels of cell kill (Figure 4-5A). Synergism was observed at $f_a \geq 0.2$ for the combination of lapatinib and endoxifen, and at $f_a \geq 0.3$ for the combinations of both lapatinib and tamoxifen, and lapatinib and 4-OHT. Against BT474 cells (Figure 4-5B), synergism was observed at all levels of cell kill for the combination of lapatinib and endoxifen, $f_a \geq 0.2$ for the lapatinib and norendoxifen combination, and $f_a \geq 0.7$ for the combinations of both lapatinib and tamoxifen, and lapatinib and 4-OHT.

Concentration levels of each drug required for 50% cytotoxicity based on dose reduction index (DRI_{50}) in each cell line is summarized in Table 4-5. The DRI_{50} represents the order of magnitude, or fold, of dose reduction required for 50% cell death in a combination therapy setting compared to that in monotherapy, which is conventionally described as IC_{50}. In other words, the DRI_{50} is used to estimate the concentration of a drug in a combination pair that achieves that same extent of cell kill (50%) as in monotherapy, and provides a means to interpret the fractional effect, f_a in concentration terms. It is noteworthy that for the luminal B BT474 cell line, the concentration levels of endoxifen required was much lower than those of tamoxifen or its active metabolites, while the concentration levels of lapatinib required was consistently lower when it was co-administered in combination with endoxifen than with tamoxifen or 4-OHT. Thus the combination of lapatinib and endoxifen was the most promising in killing BT474 cells. Although endoxifen did not demonstrate a large dose reduction against MCF-7 cells, synergism was still observed between lapatinib and endoxifen.

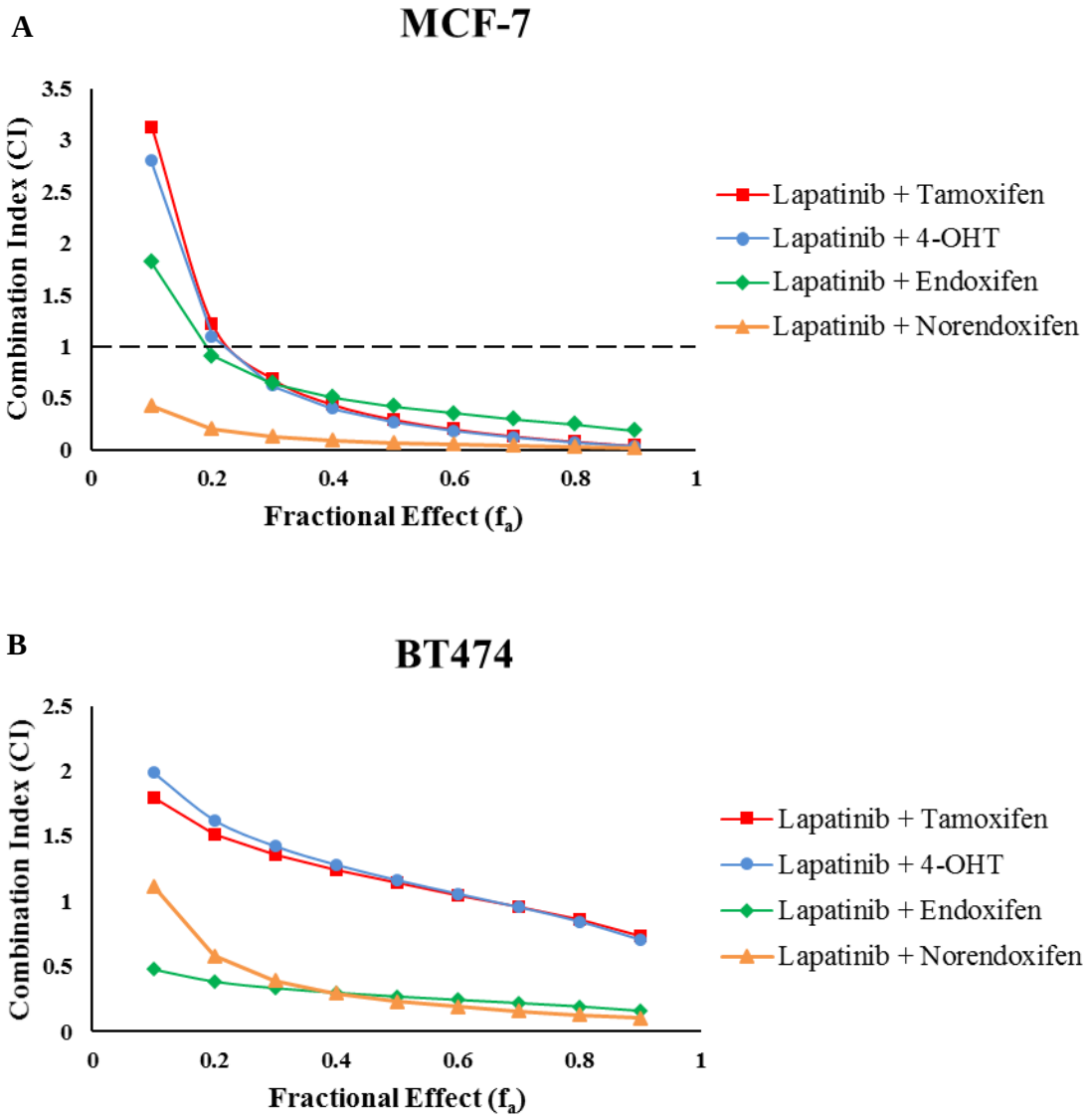

Figure 4-5 Combination index (CI) against fractional effect (f_a) plots of the combination of lapatinib and tamoxifen, lapatinib and 4-OHT, lapatinib and endoxifen, and lapatinib and norendoxifen in (A) MCF-7 and (B) BT474. CI < 1, CI = 1, and CI > 1 indicates synergism, additive effect, and antagonism, respectively.

Table 4-5 Concentration levels of tamoxifen, 4-OHT, endoxifen, norendoxifen, and lapatinib at DRI_{50} in combination therapy calculated based on fold-reduction of IC_{50} in monotherapy in MCF-7 and BT474 cells.

Cell line	Combination	DRI_{50}	Concentration of lapatinib at DRI_{50} (nM)	Concentration of tamoxifen or metabolite at DRI_{50} (nM)
MCF-7	Lapatinib + tamoxifen	Lapatinib: 7.66; tamoxifen: 7.05	847	1360
	Lapatinib + 4-OHT	Lapatinib: 9.04; 4-OHT: 7.28	718	995
	Lapatinib + endoxifen	Lapatinib: 32.8; endoxifen: 2.65	198	2328
	Lapatinib + norendoxifen	Lapatinib: 30.0; norendoxifen: 34.3	216	189
BT474	Lapatinib + tamoxifen	Lapatinib: 3.74; tamoxifen: 1.45	7.22	4537
	Lapatinib + 4-OHT	Lapatinib: 3.19; 4-OHT: 1.55	8.46	3342
	Lapatinib + endoxifen	Lapatinib: 5.93; endoxifen: 11.6	4.55	393
	Lapatinib + norendoxifen	Lapatinib: 8.72; norendoxifen: 9.49	3.10	715

4.4.3 Pharmacodynamic Interaction between Lapatinib and Tamoxifen or Endoxifen in the Luminal A Subtype with Acquired Tamoxifen Resistance

The MCF-7 cells described in this section are the parental cells from which tamoxifen-resistant TAM-R cells were derived by continuous culture in 4-OHT, and were obtained from a different source compared to those utilized in section 4.4.2. Separately, the combination of lapatinib and endoxifen showed the strongest synergism in BT474 cells based on DRI_{50} values (section 4.4.2.2). Hence only lapatinib, tamoxifen and endoxifen were studied in this section, with tamoxifen acting as a comparator.

4.4.3.1 Monotherapy in MCF-7, TAM-R and MCF-7/HER2 Cells

TAM-R cells exhibit acquired tamoxifen-resistance attributed to increased HER2 expression (*330*). MCF-7/HER2 cells were derived from MCF-7 cells stably transfected with HER2. Similar to TAM-R cells, MCF-7/HER2 cells represent acquisition of tamoxifen resistance and have been used previously to understand the role of HER2 in tamoxifen resistance (*331*). Figure S6, Figure S7 and Figure S8 shows the cytotoxicity results of 5-day treatment of MCF-7, TAM-R, and MCF-7/HER2 cells with tamoxifen, endoxifen and lapatinib. Cell proliferation was inhibited in a dose-dependent manner by all compounds in each cell line. As summarized in Table 4-6, the mean IC_{50} values of endoxifen were lower than tamoxifen in all three cell lines, but only reached statistical significance in MCF-7 cells ($p < 0.01$). Comparing between cell lines, the mean IC_{50} of both tamoxifen and endoxifen were higher in TAM-R and MCF-7/HER2 cells as compared to MCF-7 cells, which is in line with the acquisition of tamoxifen resistance in TAM-R cells; however statistical significance was observed only with endoxifen

($p > 0.05$). Mean IC_{50} of lapatinib in MCF-7 cells were comparable to TAM-R cells, and was significantly lower in MCF-7/HER2 cells ($p < 0.01$).

Table 4-6 IC_{50} values of tamoxifen, endoxifen and lapatinib monotherapy in MCF-7, TAM-R and MCF-7/HER2 cells.

Treatment	IC_{50} ± SD (μM)		
	MCF-7	**TAM-R**	**MCF-7/HER2**
Tamoxifen	5.11 ± 0.34	7.58 ± 1.80	6.55 ± 1.21
Endoxifen	2.95 ± 0.58	5.32 ± 0.83	4.59 ± 0.22
Lapatinib	3.73 ± 0.79	3.38 ± 0.93	0.558 ± 0.12

4.4.3.2 Combination Therapy in MCF-7, TAM-R and MCF-7/HER2 Cells

Against MCF-7 cells (Figure 4-6A), both combinations show synergism at all levels of cell kill, where the combination of lapatinib with endoxifen showed greater synergism than that of lapatinib with tamoxifen. Against TAM-R cells (Figure 4-6B), both combinations demonstrated similar synergistic effects above $f_a \geq 0.3$. Against MCF-7/HER2 cells (Figure 4-6C), synergism was observed at $f_a \geq 0.2$ for the combination of lapatinib and endoxifen, and $f_a \geq 0.3$ for the combination of lapatinib and tamoxifen.

Concentration levels of each drug required for 50% cytotoxicity based on dose reduction index (DRI_{50}) in each cell line are summarized in Table 4-7. When administered in combination with lapatinib, the concentration of endoxifen required was consistently lower in all three cell lines. On the other hand, the concentration of lapatinib required was highest in TAM-R, followed by MCF-7 and MCF-7/HER2, and in each instance was comparable in both combinations.

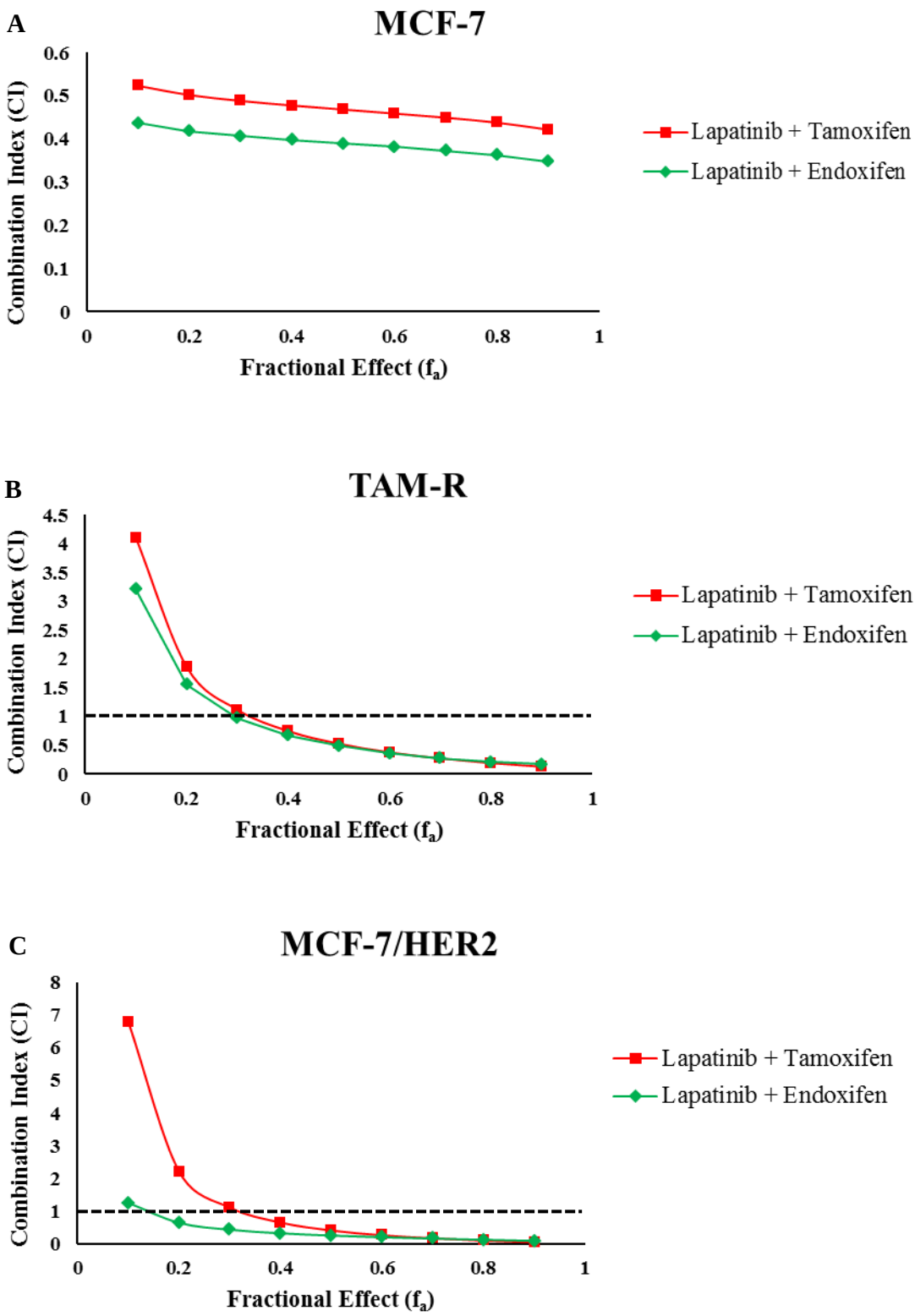

Figure 4-6 Combination index (CI) against fractional effect (fa) plots of the combination of lapatinib and tamoxifen, and lapatinib and endoxifen in (A) MCF-7 (B) TAM-R and (C) MCF-7/HER2. CI < 1, CI = 1, and CI > 1 indicates synergism, additive effect, and antagonism, respectively.

Table 4-7 Concentration levels of tamoxifen, endoxifen, and lapatinib at DRI_{50} in combination therapy calculated based on fold-reduction of IC_{50} in monotherapy in MCF-7, TAM-R and MCF-7/HER2 cells.

Cell line	Combination	DRI_{50}	Concentration of lapatinib at DRI_{50} (nM)	Concentration of tamoxifen or endoxifen at DRI_{50} (nM)
MCF-7	Lapatinib + tamoxifen	Lapatinib: 7.02; tamoxifen: 3.50	531	1460
	Lapatinib + endoxifen	Lapatinib: 7.24; endoxifen: 4.53	515	651
TAM-R	Lapatinib + tamoxifen	Lapatinib: 2.54; tamoxifen: 10.5	1331	722
	Lapatinib + endoxifen	Lapatinib: 2.48; endoxifen: 15.9	1363	335
MCF-7/HER2	Lapatinib + tamoxifen	Lapatinib: 4.2; tamoxifen: 7.25	133	903
	Lapatinib + endoxifen	Lapatinib: 12.1; endoxifen: 6.36	46.1	722

4.4.3.3 Western Blot Analysis of Combination Therapy in MCF-7 and TAM-R Cells

The basal expression and phosphorylation of ERα and HER2 in MCF-7 and TAM-R cells are shown in Figure 4-7 and Figure 4-8. Both cell lines express ERα, with MCF-7 cells expressing slightly higher levels than TAM-R cells. A greater extent of phosphorylation of ERα at the Ser-118 site was observed in untreated MCF-7 cells. On the contrary, ERα was phosphorylated to a greater extent at the Ser-167 site in TAM-R cells. Consistent with the HER2-negative phenotype of MCF-7 cells, HER2 expression and phosphorylation in MCF-7 cells were observed to be intrinsically low. HER2 expression and phosphorylation were elevated in the tamoxifen-resistant untreated TAM-R cells, which is in line with the association between acquired tamoxifen resistance and the development of ERα/HER2 crosstalk.

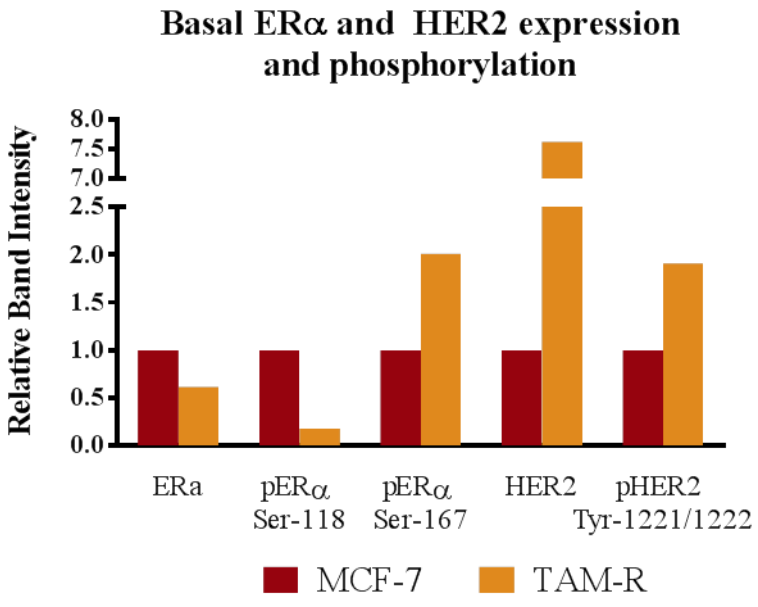

Figure 4-7 Expression and phosphorylation levels of ERα and HER2 in untreated controls of MCF-7 and TAM-R cells. For comparative purposes, the densitometric analysis was normalized against values obtained in MCF-7 cell line. The data was obtained from a single experiment.

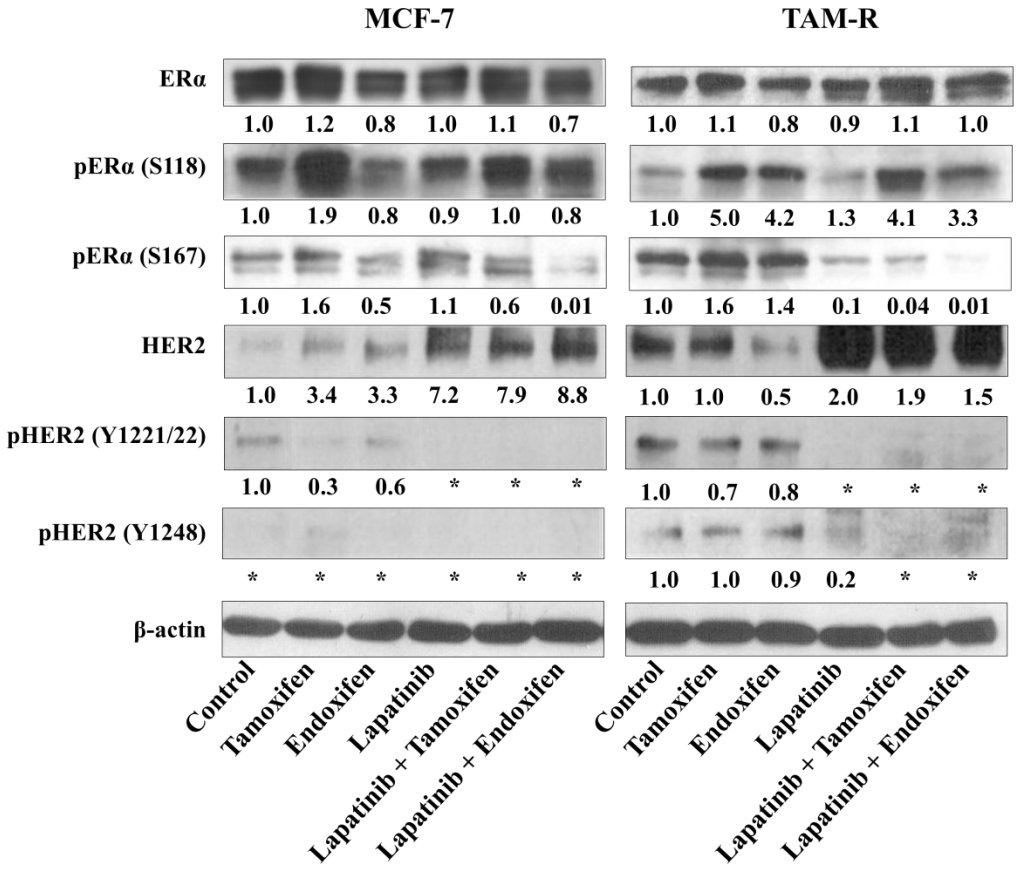

Figure 4-8 Effects of acquired tamoxifen resistance on the expression and phosphorylation of ERα and HER2 in MCF-7 and TAM-R cells after individual or combinatorial tamoxifen, endoxifen and lapatinib treatment. For comparative purposes, the densitometric analysis was normalized against values obtained in the untreated control of each cell line. *Not quantifiable

As illustrated in Figure 4-8, ERα expression was enhanced and reduced by tamoxifen and endoxifen monotherapy respectively in both cell lines. This phenomenon was recapitulated in the phosphorylation of ERα (pERα) at Ser-118 and Ser-167 in MCF-7 cells. Conversely, both anti-estrogenic monotherapy treatments led to an increase in ERα phosphorylation in TAM-R cells, where the increase relative to the control was greater at pERα Ser-118 as compared to pERα Ser-167. In this study, pERα Ser-104/106 was not observable in MCF-7 cells, and detected as a very faint band in TAM-R cells (results not shown). This could be attributed to the inherently low extent of phosphorylation at these sites (*332*).

Lapatinib had no significant impact on the expression and phosphorylation of ERα in MCF-7 cells, but yielded differential effects in TAM-R cells (Figure 4-8). Lapatinib monotherapy reduced pERα Ser-118 in TAM-R cells, but this reduction was masked when tamoxifen and endoxifen was introduced. In contrast, lapatinib appeared to reduce pERα Ser-167 significantly after monotherapy, which persisted even in combination with tamoxifen and endoxifen. Interestingly, when used in combination with lapatinib, treatment with endoxifen consistently resulted in lower expression and phosphorylation of ERα in both cell lines compared with tamoxifen. Separately, treatment with lapatinib up-regulated the expression of HER2, but completely attenuated its phosphorylation in both MCF-7 and TAM-R.

4.4.4 Pharmacokinetic Interaction between Lapatinib and Endoxifen in MDCKII-MDR1 Cells

4.4.4.1 Substrate Assay

Efflux ratios for lapatinib and endoxifen increased sharply as the concentration of both compounds increased, and peaked at approximately 1 μM before decreasing gradually and reaching a plateau (Figure 4-9). As the efflux ratios were generally above 1, our findings suggested susceptibility of both compounds to P-gp mediated efflux.

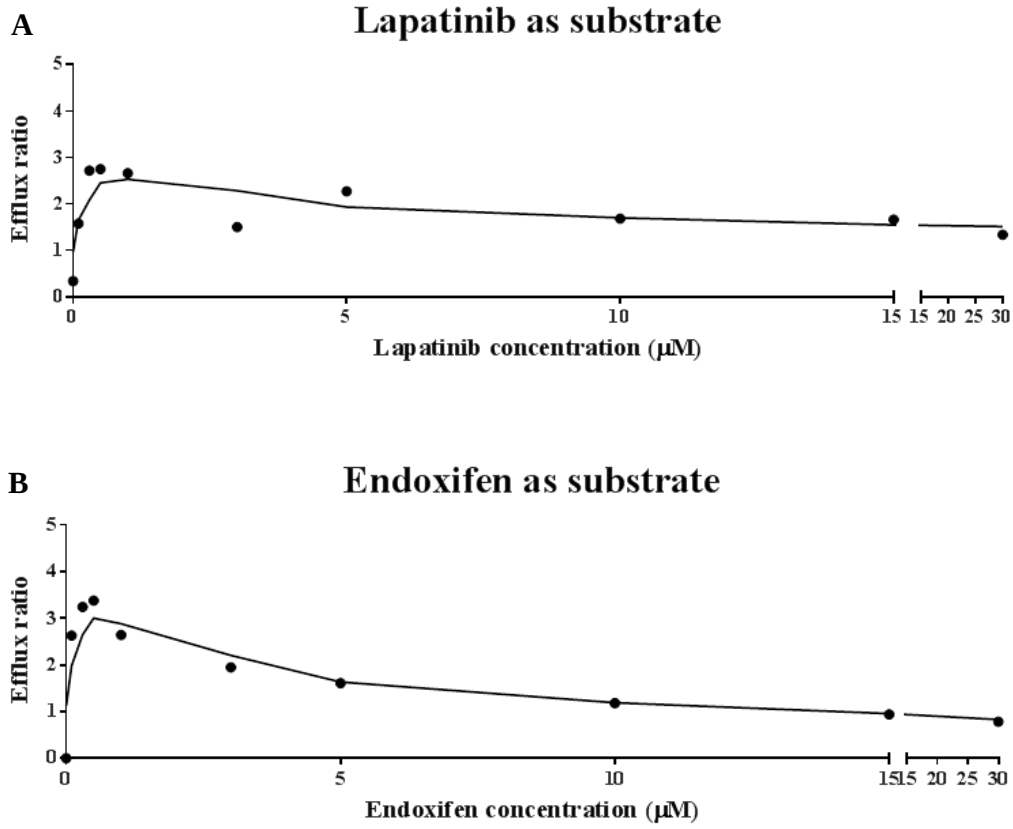

Figure 4-9 Efflux ratio of (A) lapatinib (0 – 30 μM) and (B) endoxifen (0 – 30 μM) across the MDCKII-MDR1 monolayer as a mean of duplicate determinations.

4.4.4.2 Inhibitor Assay

As shown in Figure 4-10, the efflux ratio of the P-gp probe substrate amprenavir decreased in a concentration-dependent manner as the concentration of lapatinib and endoxifen increased, suggesting that lapatinib and endoxifen inhibited P-gp mediated efflux of the probe substrate, amprenavir. The average IC_{50} values of lapatinib and endoxifen in inhibition of amprenavir efflux were 6.80 ± 4.20 μM and 7.16 ± 2.63 μM respectively.

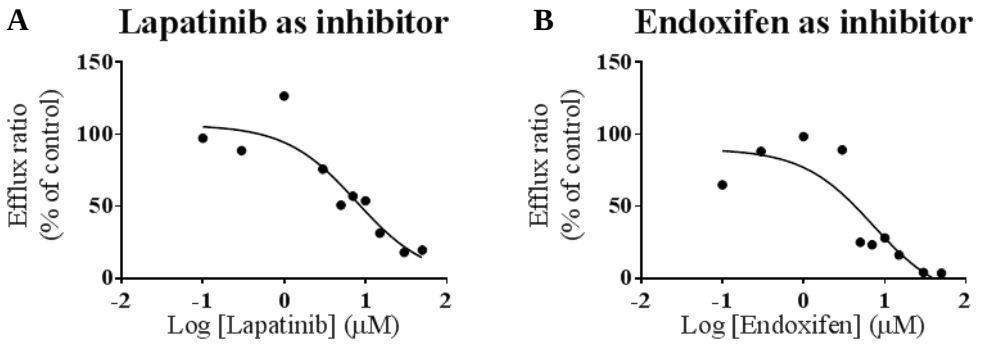

Figure 4-10 Efflux ratio of 10 μM amprenavir across the MDCKII-MDR1 monolayer, in the presence of (A) lapatinib (0 – 50 μM) and (B) endoxifen (0 – 50 μM) as a mean of duplicate determinations.

4.4.4.3 Pairwise Combinatorial Treatment

The efflux ratio of endoxifen decreased in a concentration-dependent manner as the concentration of lapatinib increased (Figure 4-11A). At increasing concentrations of endoxifen from 0 to 50 μM, the efflux ratios of lapatinib decreased in a concentration-dependent manner, suggesting that lapatinib inhibited P-gp mediated efflux of endoxifen. The average IC_{50} value of lapatinib in inhibiting endoxifen efflux was 0.45 ± 0.110 μM. Similarly, the efflux ratio of lapatinib decreased in a concentration-dependent manner as the concentration of endoxifen increased (Figure 4-11B). At increasing concentrations of endoxifen from 0 to 50 μM, the efflux ratios of lapatinib decreased in a concentration-dependent manner, suggesting that endoxifen inhibited P-gp mediated efflux of lapatinib. The average IC_{50} value of endoxifen in inhibiting lapatinib efflux was 4.16 ± 3.54 μM.

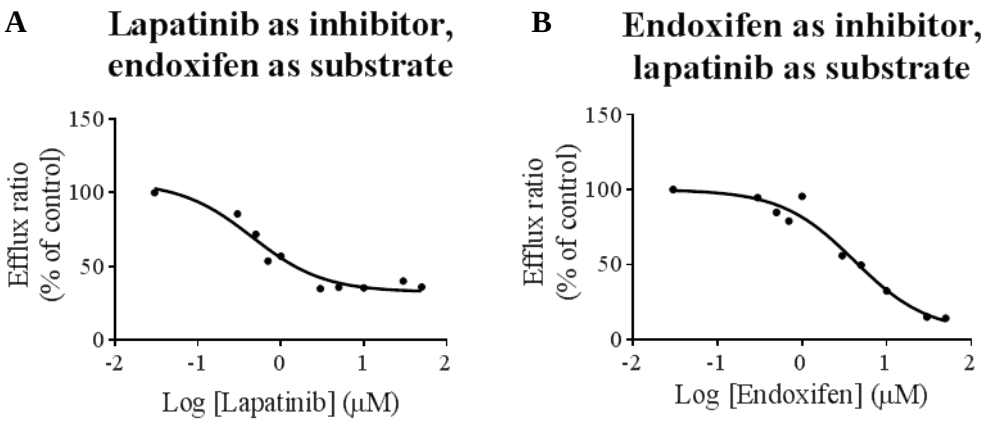

Figure 4-11 Efflux ratio of (A) endoxifen (1 μM) in the presence of lapatinib (0 – 50 μM) and (B) lapatinib (1 μM) in the presence of endoxifen (0 – 50 μM) across the MDCK-MDR1 monolayer, as a mean of duplicate determinations.

4.5 Discussion

4.5.1 Lapatinib Impairs CYP3A4/5-Dependent Bioactivation of Tamoxifen

While tamoxifen has been used successfully in treating ERα+ breast cancer, approximately 50% of ERα+ expressing tumours do not respond to tamoxifen (*de novo* resistance) (*333*), while for those that respond, another 30% become tamoxifen-resistant and the cancer relapses over a 15-year period (acquired resistance) (*302*), leading to tumour progression and death. Importantly, the development of resistance is not attributable to a loss in expression or mutation of ERα (*334*). One mechanism identified to promote tamoxifen resistance, whether *de novo* or acquired is the cross-talk between ER and HER2, where tamoxifen-resistant cells either overexpress or upregulate HER2 expression as an alternative pathway driving proliferation. Of note, HER2 overexpression is the only mechanism of anti-estrogen resistance with supportive clinical data (*335*).

These findings encouraged clinical explorations of combinatorial lapatinib and tamoxifen to circumvent the crosstalk and restore sensitivity to tamoxifen. However these trials were initiated before it was discovered that lapatinib is a potent and irreversible mechanism-based inactivator of CYP3A4/5 (*244*, *246*), which is a crucial enzyme mediating the biotransformation of tamoxifen to its primary active metabolite, endoxifen (Figure 4-1). The two-step incubation design was adapted from classical assays of mechanism-based inactivators to evaluate the effect of lapatinib on tamoxifen metabolism. This design permits mechanism-based covalent inactivation of CYP3A4/5 in the primary incubation, while a 10-fold dilution step in the secondary incubation where tamoxifen or NDMT was introduced is necessary to minimize potential competitive enzyme inhibition, thus allowing evaluation of the effects of mechanism-based inactivation of CYP3A4/5 by lapatinib. Through this approach, permanent and irreversible inactivation of

CYP3A4/5 is achieved while maintaining exposure to a conservative, clinically relevant concentration level of lapatinib of 1 µM. This concentration level of lapatinib falls within the plasma concentration levels of lapatinib in the recently published phase I trial of combinatorial lapatinib and tamoxifen (LAPATAM) (*336*). Our results demonstrate that lapatinib can indeed compromise the CYP3A4/5-mediated metabolism of tamoxifen *in vitro*, suggesting that the efficacy of tamoxifen when co-administered with lapatinib may be negated *in vivo* due to the inability to bioactivate tamoxifen. The LAPATAM study reported that the steady state concentration levels of tamoxifen were not affected by lapatinib (*336*). However, the systemic levels of tamoxifen metabolites such as NDMT, 4-OHT and endoxifen were not monitored in the study. Therefore, it is not possible to conclude whether antagonistic pharmacokinetic interactions existed between lapatinib and tamoxifen *in vivo*. The unchanged steady state concentration levels of tamoxifen can be attributed to the plurality of pathways for tamoxifen metabolism, i.e. inhibition of CYP3A4/5 by lapatinib may not result in an increase in tamoxifen plasma levels due to shunting of tamoxifen to alternative phase I and phase II elimination pathways (*337*). It is important to note that the extent of inhibition quantified in this study is conservative, because the dilution step employed in the experimental design nullifies the effects of competitive inhibition. In its FDA regulatory submission (Application Number 22-059), lapatinib was noted to be a mixed competitive and non-competitive inhibitor of CYP3A4/5, with a K_i of 4 µM as measured using testosterone as a probe substrate. As such, when administered *in vivo* lapatinib is likely to cause both reversible and irreversible inhibition of CYP3A4/5 simultaneously, and at concentrations more than two-fold higher than investigated here, as demonstrated by the mean steady state C_{max} achieved in the LAPATAM trial (*336*).

4.5.2 Lapatinib Exhibits Pharmacodynamic Synergism with Endoxifen in De Novo *Tamoxifen Resistant Luminal B BT474 Cells*

The finding that lapatinib could indeed impair the bioactivation of tamoxifen led to investigations of efficacy between lapatinib and other pharmacologically active tamoxifen metabolites such as 4-OHT, endoxifen and norendoxifen. In this pilot study, two breast cancer cell lines with different molecular profiles, namely MCF-7 and BT474 were used to investigate potential pharmacodynamic synergism in overcoming ERα/HER2 crosstalk, where MCF-7 represented the luminal A subtype, while BT474 represented the luminal B subtype. Consistent with literature reports, 4-OHT and endoxifen were equipotent in MCF-7 cells (*338*). In our study, these two drugs were also equipotent in BT474 cells. In agreement with reported data, lapatinib was significantly more cytotoxic in BT474 cells as expression of HER2 is up to 100-fold greater in these cells than MCF-7 cells (*304*). Norendoxifen was recently identified to be another active metabolite of tamoxifen which inhibits recombinant aromatase, ERα and ERβ with nanomolar potencies (*297*); however its cytotoxicity against breast cancer cells has not been reported thus far. In this study, the cytotoxicity of norendoxifen was generally comparable to 4-OHT or endoxifen in both cell lines.

Combinatorial treatment of breast cancer using lapatinib with tamoxifen or each of its active metabolites resulted in synergistic killing of the low HER2-expressing MCF-7 and, importantly, in high HER2-expressing BT474. Potent synergism between lapatinib and endoxifen as well as norendoxifen was demonstrated in both cell lines. In particular, the combination of lapatinib and endoxifen demonstrated the greatest dose reduction and synergism in BT474 and was chosen for further study in the acquired tamoxifen-resistant phenotype. The unexpected synergism observed for the combinatorial therapies in low HER2-

expressing MCF-7 suggests that there may be other crosstalk pathways responsible for cell proliferation and survival besides the crosstalk between ERα and HER2.

The luminal B subtype is reported to exhibit *de novo* resistance to tamoxifen where it is inherently less responsive to ER antagonism and has poorer tumour grade and poorer survival rates (*303-305*). However, the monotherapy IC_{50} values obtained for BT474 when treated with tamoxifen were lower than that of MCF-7. The reason for this observation is unclear; however similar trends have been reported in literature. For example, Sharma *et al.* reported the IC_{50} of tamoxifen as 10 µM in MCF-7 (*339*), while Ropero *et al.* found that the IC_{50} of tamoxifen in BT474 was 6.95 µM (*340*). In contrast, in combination therapy the DRI_{50} values of tamoxifen was clearly higher in BT474 versus MCF-7 cells. Using BT474 as a model for the luminal B phenotype, this suggests that the combination of lapatinib and endoxifen exhibits strong pharmacodynamic synergism in *de novo* tamoxifen resistance.

4.5.3 *Lapatinib Exhibits Pharmacodynamic Synergism with Endoxifen in Luminal A Subtypes with Acquired Tamoxifen Resistance*

4.5.3.1 Monotherapy and Combination Therapy

In agreement with literature and results presented in section 4.4.2.1, endoxifen consistently demonstrated greater cytotoxicity than tamoxifen in tamoxifen-sensitive MCF-7, and for the first time, in tamoxifen-resistant TAM-R and MCF-7/HER cells as well. Evidence of tamoxifen resistance is also apparent in the increased mean IC_{50} values of tamoxifen and endoxifen, although only endoxifen demonstrated statistical significance. Separately, lapatinib demonstrated equivalent potency in the isogenic MCF-7 and TAM-R pair, despite the 8-fold

higher HER2 expression in TAM-R (Figure 4-7). In contrast, sub-micromolar potencies were achieved in MCF-7/HER2, similar to that seen in BT474. Although HER2 levels were not determined in the MCF-7/HER2 and BT474 cell lines used in this study, it has been reported that MCF-7/HER2-18, a HER2 cDNA-transfected MCF-7 cell line, has a 45-fold higher HER2 expression than MCF-7 (*303*, *341*), while BT474 have 100-fold higher HER2-expression compared to MCF-7 (*304*). The significantly higher HER2 expression may account for the greater potency of lapatinib in these cells. On the other hand, HER2 levels, although elevated in TAM-R, appear to be insufficient for single therapy lapatinib to exhibit greater cytotoxicity than in MCF-7. This may be due in part to the ERα offering an escape pathway to maintain cellular proliferation when HER2 is inhibited. This is evidenced by the IC_{50} values of tamoxifen and its metabolites in all 5 cell lines investigated in this study, which fell within the same order of magnitude. In other words, despite the increased expression of HER2, cellular proliferation did not completely shift to HER2 (i.e. ERα independent), which would be characterized by significantly elevated IC_{50} values for tamoxifen and its metabolites in TAM-R and MCF-7/HER2 cells. This observation supports the existence of the crosstalk between ERα and HER2, and indicates that singular inhibition of either pathway alone is insufficient.

In parallel with the observations for *de novo* tamoxifen resistance, combinatorial therapy resulted in synergistic effects in the isogenic MCF-7 and TAM-R pair, as well as MCF-7/HER2 cells. The antagonism observed at low concentrations of lapatinib and tamoxifen or endoxifen (corresponding to $f_a < 0.3$ for TAM-R and $f_a < 0.2$ for MCF-7/HER2), which is absent in the tamoxifen-sensitive MCF-7 isogenic counterpart reflects the tamoxifen-resistant phenotype of both cell lines. This trend is less clear in the DRI_{50} values; however, the lower concentration of

endoxifen needed to effect 50% cytotoxicity compared with tamoxifen in TAM-R and MCF-7/HER2 clearly indicates that the combination of lapatinib with endoxifen is superior in achieving pharmacodynamic synergism in the luminal A subtype with acquired tamoxifen resistance.

4.5.3.2 Acquired Tamoxifen Resistance Alters ERα and HER2 Expression Patterns

As expected, TAM-R cells showed an increase expression and phosphorylation of HER2 as compared to MCF-7 cells, in agreement with the development of the ERα/HER2 crosstalk that is associated with tamoxifen resistance (Figure 4-7). TAM-R cells also showed a reduced expression of ERα relative to MCF-7. It has been reported that HER2 signaling members such as p44/42 MAPK and Akt can reduce ER expression at the mRNA and protein level, and may account for decreased ERα levels in HER2-expressing TAM-R cells (*296, 310*).

ERα phosphorylation is thought to permit ligand-independent activation of ERα and thus stimulate transcription of estrogen-responsive genes. Increased pERα Ser-167 has been demonstrated in tamoxifen-resistant MCF-7 cells, and associated with the acquisition of tamoxifen resistance (*342, 343*). In agreement with literature, our findings suggest that TAM-R cells are less sensitive to ER antagonism, mediated in part by pERα Ser-167. pERα Ser-118 has been well-studied and shown to decrease ERα affinity for tamoxifen (*344*), and is elevated with tamoxifen resistance *in vitro*. However we observed that basal levels of pERα Ser-118 was lower in TAM-R than MCF-7. Phosphorylation of ERα at Ser-118 is estrogen-dependent (*345*). In our study, parental MCF-7 cells were cultured in normal FBS that contains small amounts of estradiol, while TAM-R cells were cultured in charcoal-stripped FBS where growth factors including estradiol have

been removed. Thus the differential basal expression of pERα Ser-118 between MCF-7 and TAM-R might be a result of the different culture conditions.

4.5.3.3 Tamoxifen and Endoxifen Show Differential Effects on ERα Expression and Phosphorylation in MCF-7 and TAM-R Cells

The differential effects of tamoxifen and endoxifen on total ERα expression in MCF-7 are in line with literature, which reported the binding of tamoxifen to ERα increased its stability (*346*), while endoxifen caused the degradation of the receptor (*298*). Similarly, endoxifen decreased the levels of both pERα Ser-118 and pERα Ser-167 (Figure 4-8) and this may account for the greater potency of endoxifen in MCF-7 cells. Notably, the decrease in ERα, pERα Ser-118 and pERα Ser-167 by endoxifen was also sustained when combined with lapatinib. Interestingly, pERα Ser-118 is associated with a reduction in proteasomal degradation of ERα in MCF-7 cells (*347*). The mechanism of endoxifen-induced degradation of ERα is currently unknown, and this may in part explain the unique ability of endoxifen to reduce ERα levels (*298*). In contrast, when TAM-R was treated with tamoxifen and endoxifen, increases in pERα Ser-118 and pERα Ser-167 were observed, suggesting that the acquisition of tamoxifen resistance results in insensitivity to both tamoxifen and endoxifen mediated by phosphorylation of ERα, a finding that is supported by the higher IC_{50} values of both these compounds in TAM-R cells. Densitometric analysis suggests that ERα levels are lower in TAM-R cells when treated with endoxifen; however the expected decrease in pERα Ser-118 was not observed. The multi-factorial regulation of ERα turnover is a function of transcription, translation and degradation and may involve other pathways in the resistant phenotype. For example, as discussed earlier, HER2 can reduce ERα expression at the mRNA and protein level (*296, 342*).

4.5.3.4 Lapatinib Reverses Tamoxifen Resistance by Overcoming ERα/HER2 Crosstalk

Lapatinib exerts its pharmacological effect by binding to the intracellular domain of EGFR and HER2, blocking the auto-phosphorylation and consequently activation of downstream kinases. As expected, lapatinib completely abolished the phosphorylation and activation of HER2, both in monotherapy and combinatorial therapies against both cell lines. The increase in HER2 levels is in agreement with literature where lapatinib is reported to prevent the ubiquitination and degradation of HER2, leading to accumulation of inactive HER2 at the cell membrane (*348*).

In tamoxifen-sensitive MCF-7 cells, lapatinib alone had minimal effect on the expression and phosphorylation of ERα, due to the absence of direct pharmacological action on ERα and the minimal HER2 expression in these cells. In combination with tamoxifen and endoxifen, the total levels of ERα were similar as compared to either anti-estrogen alone. While decreased levels of pERα Ser-118 and pERα Ser-167 were observed in combination with endoxifen, this effect is attributed to the presence of endoxifen, and overall lapatinib did not affect pERα levels. Collectively these findings are in agreement with literature that ERα/HER2 crosstalk is not prominent in MCF-7 cells (*330*). Additionally, it suggests that lapatinib and endoxifen may interact through alternative pathways to account for the synergism observed in luminal A subtype. For example, lapatinib was recently reported to exert off-target pharmacological activity independently of EGFR/HER2 antagonism that promotes synergism even in non-EGFR/HER2 expressing, triple-negative breast cancer cells (*349-351*). However, the relevance of these off-target activities to the synergism observed in MCF-7 cells remains unknown and requires further investigation.

In tamoxifen-resistant TAM-R cells, lapatinib had minimal effect on ERα expression, while it exerted a greater effect on the decreased phosphorylation of ERα Ser-118, and ERα Ser-167, both in monotherapy and combination therapy. Phosphorylation of ERα Ser-118 is driven by a number of kinases including p44/42 MAPK, GSK-3β IKKα, CDK7, and mTOR/p70S6K, while ERα Ser-167 is phosphorylated by Akt, p90RSK and mTOR/p70S6K (*352*). Ligand-bound HER2 activates p44/42 MAPK and Akt, which in turn phosphorylates ERα, activating ERα in a ligand-independent manner and accounting for the crosstalk between ERα and HER2 (*343, 353*). By antagonizing HER2, lapatinib reduces phosphorylation of ERα Ser-118 and ERα Ser-167 and diminishes ERα/HER2 crosstalk. This effect is more prominent for the combination of lapatinib and endoxifen. This in in line with the general observation made previously that the combination of lapatinib and endoxifen consistently resulted in lower expression and phosphorylation of ERα in both cell lines compared with the combination of lapatinib and tamoxifen. Collectively, these results suggest that a greater benefit will be derived from combining lapatinib with endoxifen, instead of tamoxifen.

The overarching theme drawn from the results presented in sections 4.4.2 and 4.4.3 is that the combination of lapatinib with endoxifen is superior to that with tamoxifen in eliciting pharmacodynamic synergism to overcome tamoxifen resistance, supported by both cytotoxicity and molecular biology studies.

4.5.4 Lapatinib and Endoxifen Exhibit Mutual Pharmacokinetic Synergism via P-gp Inhibition

To study the interactions between lapatinib and endoxifen with P-gp, the MDCKII-MDR1 model, a kidney cell line that overexpresses P-gp transporters was used. Unlike Caco-2, an intestinal cell line that expresses many other uptake

and efflux transporters (*354*), the MDCKII-MDR1 presents a clean system, with three times more P-gp transporters than its un-transfected parental cell line (*355*). This model therefore facilitated our study of the effect of P-gp transport without the confounding effects of other transporters. While there are other similar P-gp specific transporter cell models such as the Lilly laboratories porcine kidney cells transfected with multi drug resistance protein 1 (LLCPK-MDR1), the MDCKII-MDR1 is an established cell model (*356*) recommended by the US Food and Drug Administration, and adopted by the pharmaceutical industry. The cell-free, 'inside-out' vesicle system is another alternative model system, where compounds which are P-gp substrates accumulate within the vesicles (*357*). However, the vesicle system is relatively new and it is also found to be unsuitable for testing lipophilic drugs that are highly permeable (*357*) which include lapatinib and endoxifen, as they would freely diffuse out and not be retained within the vesicles.

To understand the combined pharmacokinetic interaction between lapatinib and endoxifen, we first determined the individual P-gp interactions of both compounds. Although there are existing reports that lapatinib is both a P-gp substrate and inhibitor, while endoxifen is a P-gp substrate, these were performed using a single concentration of each compound as a substrate or inhibitor. We performed comprehensive dose-response investigations to ascertain the nature and magnitude of P-gp-mediated efflux for each compound, with an upper limit of 50 μM as the experimental data suggests that the monolayer integrity is compromised beyond 50 μM (results not shown), presumably due to non-specific cytotoxicity at higher drug concentration levels.

In agreement with the reports by Polli *et al.* (*311*) and Teft *et al. (313)*, both lapatinib and endoxifen were found to be P-gp substrates. Instead of displaying Michaelis–Menten kinetics as expected of a typical P-gp substrate, the efflux ratios of both compounds decreased at concentration levels beyond 1 μM. This observation was important as it suggested that apart from being P-gp substrates, lapatinib and endoxifen could exhibit P-gp inhibition as well where the decrease in efflux ratios could be a consequence of auto-inhibition of P-gp at higher concentration levels. Importantly, from these experiments, 1 μM of lapatinib or endoxifen was determined to be the optimal substrate concentration in the subsequent combinatorial treatment assays to ensure maximal efflux transport and mitigate potential auto-inhibition effects, demonstrating the value of dose-response investigations in contrast to typical single concentration investigations commonly reported in literature and performed during drug discovery.

Our observation of potential auto-inhibition of P-gp transport prompted further investigation of the inhibitory potential of both compounds. Amprenavir is a commonly used P-gp probe substrate that permits the assessment of P-gp inhibition (*358*). Consistent with the report by Polli *et al.*, we found that lapatinib was a P-gp inhibitor when tested against amprenavir using MDCKII-MDR1 (*311*). While endoxifen was reported by Teft *et al.* (*313*) and Iusuf *et al.* (*312*) to be a P-gp substrate, no reports about its possible role as a P-gp inhibitor are available. Our findings demonstrated for the first time that endoxifen is a P-gp inhibitor.

As lapatinib and endoxifen are both substrates and inhibitors of P-gp transporters, combinatorial experiments were carried out to elucidate the mutual inhibitory effects between these two compounds with regards to P-gp efflux transport. For

the first time, endoxifen was found to inhibit the efflux transport of lapatinib in a concentration-dependent manner. Similarly, lapatinib inhibited the efflux transport of endoxifen in a concentration-dependent manner. Notably, the inhibition of endoxifen efflux by lapatinib is more than 10-fold greater than the converse. Collectively, these novel findings suggested that when used in combination, lapatinib and endoxifen may potentially exhibit mutually beneficial pharmacokinetic interactions mediated via P-gp transport. This effect could potentially result in an overall increase in intra-tumoral accumulation of both drugs, thus allowing a lower dose and consequently a potential decrease in dose-dependent side effects. Since lapatinib appears to be the stronger P-gp inhibitor, the extent of intra-tumoral accumulation for endoxifen may be greater.

A number of studies have reported that increased P-gp expression in breast cancer may be associated with drug resistance, poor drug response, aggressive metastatic breast tumour, poor prognosis and lowered intra-tumoral drug accumulation (*317-320*). P-gp efflux also affects drug uptake and penetration in the gut and BBB respectively. The latter is intriguing because brain metastasis is a common clinical sequelae of breast cancer (*326*); however P-gp efflux in the BBB may not have a significant impact on brain penetration of lapatinib and endoxifen as the integrity of the BBB itself is known to be compromised in cancer. For example, increase lapatinib uptake into the brain was observed in patients with cranial metastasis, but not so in patients without cranial metastasis (*359*). Separately, increased systemic exposure may also be expected due to inhibition of intestinal efflux and biliary and urinary excretion. This effect could minimize dose-limiting toxicities such as lapatinib-induced diarrhea, which is a common reason for dose reduction or discontinuation of lapatinib (*360*). Collectively, the ability of lapatinib and endoxifen to mutually modulate P-gp efflux undoubtedly confers an additional

advantage to complement the pharmacodynamic synergism identified in breast cancer cells.

4.5.5 Lapatinib and Endoxifen: the Superior Combination

In BT474, TAM-R and MCF-7/HER cells associated with tamoxifen resistance, significantly lower concentration levels of endoxifen (393-722 nM) was required to achieve 50% cytotoxicity in combination with lapatinib than observed using tamoxifen (722-4537 nM). It is noteworthy that when used combinatorially with endoxifen, anti-proliferative activity was achieved in all three cell lines using concentration levels of lapatinib that are 3- to 685-fold lower than that observed clinically in the plasma (3.12-4.25 µM) (*361, 362*). Similarly, in MDCKII-MDR1 cells, the IC_{50} inhibition of endoxifen efflux by lapatinib falls within these concentrations levels as well, while the IC_{50} of endoxifen inhibition of lapatinib efflux is approximately 4.2 µM. The plasma concentration range of endoxifen is reported to be 10.2-83.7 nM after 20 mg daily tamoxifen administration, with levels near the upper limits achieved by CYP2D6 extensive metabolizers (*363*). Separately, Ahmad *et al.* reported plasma concentration levels of 40.4 nM after a single oral dose of 4 mg endoxifen, with a predicted steady state concentration level of 147.5 nM (*364*), while Goetz *et al*. reported that steady state plasma concentration levels after 28 days of endoxifen administration were 390 nM for a dose of 20 mg/day, 2480 nM for a dose of 100 mg/day, and 5200 nM for a dose of 160 mg/day which were well-tolerated (*365, 366*). The latter two doses provide sufficient endoxifen levels to reach the *in vitro* DRI_{50} in all cell lines evaluated combinatorially. The Mayo Clinic is further evaluating doses of 20 mg/day and 100 mg/day in subsequent studies (*365*). It is also important to note that tamoxifen and its metabolites are known to exhibit extensive tissue binding (*367*). 4-OHT levels in breast tumours were reported to be up to 3 times higher than

serum levels (*368*), while endoxifen levels in primary and metastatic breast tumours were reported to be markedly higher than serum levels when the standard dose of tamoxifen was administered (*367*). Collectively, these evidences suggest that the observed pharmacodynamic and pharmacokinetic synergistic concentration levels of endoxifen could possibly fall within target tissue concentration levels, particularly when endoxifen doses are adjusted to achieve maximally tolerated plasma concentration levels with adequate safety profiles. It should also be noted that in this study, breast cancer cells were only treated for 5 days, while *in vivo* malignant cells are exposed to these agents on the scale of months to years. Thus these short term cytotoxic concentration levels may not adequately reflect the potency of longer term treatments. Therefore, further *in vivo* studies on lapatinib and endoxifen combinatorial treatment is warranted.

Combinatorial lapatinib and endoxifen improves upon existing tamoxifen regimens on several fronts. Firstly, it circumvents the possible pharmacokinetic antagonism between lapatinib and tamoxifen since lapatinib inhibits the bioactivation of tamoxifen to its active metabolites via potent irreversible CYP3A4/5 inactivation (*244, 246*). Secondly, it bypasses the considerable confounding effects of CYP2D6 and CYP3A5 polymorphisms on tamoxifen response, whereby patients of certain CYP450 genotypes may experience insufficient systemic exposure of endoxifen. Thirdly, combinatorial therapy may mitigate the ERα/HER2 crosstalk, as suggested by the results of this study. And finally, it negates the effect of P-gp efflux which may result in improved oral absorption, intratumoral or brain penetration.

The attractiveness of endoxifen for clinical use is due in part to the vast history of clinical experience with tamoxifen from both an efficacy and safety perspective.

The clinical development of endoxifen is underway, where endoxifen was found to be safe even at the highest dose of 160 mg per day (*369*). Furthermore, preliminary evidence of efficacy following administration of endoxifen was observed in patients who failed standard hormonal therapies including tamoxifen, fulvestrant and aromatase inhibitors (*369*). Apart from inhibiting ERα, endoxifen is also reported to have a unique mechanism of action by targeting ERα for degradation. Interestingly, endoxifen exhibits similar positive effects as tamoxifen in protecting against bone loss (*370*). Separately, although norendoxifen shows similar synergism as endoxifen, the administration of norendoxifen in humans is not being studied currently, and its contribution to the anti-proliferative effect of tamoxifen is not expected to be significant as *in vivo* levels of norendoxifen are 6-fold lower than endoxifen (*371*). Additionally, while efforts have been made to investigate combinations of aromatase inhibitors such as letrozole with lapatinib (*241*), a drawback with such combinations is that aromatase inhibitors are not recommended in pre-menopausal women, and this may limit the population of patients who might benefit from such combinatorial therapy. Although endoxifen has been reported to inhibit aromatase (*294*), it is a weak inhibitor with an IC_{50} value more than 500 times greater than letrozole (*372*) and thus would not be contraindicated in pre-menopausal women. All these underscore the importance of establishing the efficacy of combinatorial lapatinib and endoxifen against breast cancer.

Another potential benefit of combination treatment is that the adverse drug reactions may be reduced since lower dosage and systemic exposure of each drug may be required. However, the specific adverse effects of administering tamoxifen metabolites in humans are currently not known and are being studied in clinical trials (NCT01327781, NCT01273168). For example, it has been reported

that endoxifen exhibits similar uterotrophic effects as tamoxifen in rats; however, given the superior anti-tumour activity of endoxifen, the authors suggested that the risk/benefit profile of endoxifen may be superior to that of tamoxifen (*373*). Given that the plasma concentration levels of endoxifen described in that study are much higher than the synergistic concentrations reported here, it is plausible that the uterotrophic effects of endoxifen may be less prominent in a combinatorial scenario; however care must be taken when comparing *in vitro* versus *in vivo* data and inter-species data. Some toxicities associated with tamoxifen, such as endometrial cancer are hypothesized to be associated with upstream metabolites of tamoxifen (*374*). The genotoxic α-hydroxylated metabolite of tamoxifen is believed to cause formation of DNA adducts which have been detected in the endometrial lining. Although it is not known if α-hydroxylation occurs with endoxifen, one may anticipate endoxifen to exhibit a better safety profile since it is a downstream metabolite of the genotoxic entity.

4.6 Chapter Conclusion

In conclusion, here we observed a deleterious effect of covalent and coordinate binding by lapatinib, which results in inhibition of CYP3A4/5 activity. When used in combination with tamoxifen, the detrimental effect elicited by covalent and coordinate binding was found to impair the crucial bioactivation of tamoxifen to its active metabolite, endoxifen. This can abrogate the expected pharmacodynamic synergism from this drug combination by compromising the inhibition of ERα/HER2 crosstalk. Despite this apparent liability, we postulated that co-administration of lapatinib with the active tamoxifen metabolite, endoxifen, could circumvent the inhibition of tamoxifen bioactivation by lapatinib. This new combination was investigated from both pharmacodynamic and pharmacokinetic angles, and was found to exhibit complementary synergism in both aspects. Importantly, these synergistic effects occurred at drug concentration levels achievable with current dose regimens, with the potential for dose reductions in a combinatorial setting. By leveraging covalent drug binding, we uncovered a novel drug combination that shows potential to enhance therapeutic efficacy in breast cancer at the pharmacodynamic and pharmacokinetic levels, thereby converting a liability into an opportunity. This novel and exciting drug combination is ripe for further preclinical investigations with the ultimate aim of improving efficacy in breast cancer pharmacotherapy.

Chapter 5 Conclusions and Future Perspectives

Unintended covalent drug binding is a prevalent phenomenon in pharmacotherapy, and has been implicated in ADRs, which is associated with a high economic and morbidity burden. Separately, covalent binding is also increasingly pursued as a pharmacological mechanism of action due to several advantages including a sustained duration of action and uncoupling of pharmacodynamic and pharmacokinetic parameters. While medicinal chemistry efforts attempt to tune the reactivity of the electrophile conferring the covalent interaction with the target protein, off-target effects are possible which could lead to unexpected toxicity. Despite decades of research, the mechanism by which covalent drug binding causes toxicity remains unclear. The consequences of covalent binding can be severe and unpredictable, which makes it challenging to anticipate and prevent or mitigate such deleterious effects.

Covalent binding can be classified as exerting overt or covert effects in biological systems. While a significant amount of research has been devoted to elucidating the overt consequences of covalent binding, the covert effects are far less understood. In Chapter 2, we explored the covert effects of covalent binding caused by APAP, which results in drug-induced protein glutathionylation. We present the possible mechanisms by which APAP causes protein glutathionylation, which can occur secondary to covalent binding. The perturbation of basal protein glutathionylation, which is a PTM regulating a variety of cellular processes, results in derangement of key biological processes such as energy metabolism, protein turnover, defense against cellular stress, calcium dynamics and MPTP opening. These processes can be correlated to the toxicity manifestations known to occur with APAP. Importantly, proteo-

metabonomic mapping provided further confidence in the importance of APAP-induced protein glutathionylation by associating the functional protein deficits caused by glutathionylation with metabolic derangements caused by APAP. Notably, aberrant glutathionylation also provides mechanistic insights which illuminate the mode of action of N-acetylcysteine, S-adenosyl methionine and fibrates which protect against or reverse APAP hepatotoxicity. This illustrates how a deep mechanistic understanding the covert effects of covalent binding may guide the development of therapeutic strategies to prevent or ameliorate instances of toxicity. Furthermore, longitudinal analysis suggested the classification of glutathionylated proteins into two groups: those that cause toxicity as a result of overt covalent binding, and those that are a consequence of toxicity as a result of increased oxidative stress, providing a deeper mechanistic definition of aberrant protein glutathionylation. The role of overt covalent binding in APAP-induced protein glutathionylation was strengthened by our observation that this phenomenon is dose- and bioactivation-dependent. We further demonstrated that AMAP and APAP unexpectedly exhibited broad overlaps in glutathionylated proteins, agreeing with recent findings that both agents were toxic in human liver. Collectively, in this chapter we establish drug-induced protein glutathionylation as a previously unrecognized covert mechanism of drug-induced liver injury, which is secondary to overt covalent binding.

We next revisited overt covalent binding in Chapter 3, in the form of covalent and coordinate inactivation of CYP3A4/5 by lapatinib. Based on our prior investigations into the mechanisms of irreversible inactivation of CYP3A4/5 by lapatinib, we identified two potential strategies to mitigate the deleterious effects of covalent binding caused by lapatinib. In the first, we attempt to ameliorate the bioactivation of lapatinib to its reactive metabolites by judicious deuteration at

positions critical to its bioactivation. Secondly, we also determined the dose-response relationship between CYP3A5 genotype and the susceptibility to inactivation by lapatinib. While strategic deuteration at the benzylic carbon could reduce the bioactivation potential of lapatinib, it did not result in a reduction in inactivation of CYP3A4/5. Separately, we observed that CYP3A5 *1/*1 carriers were most susceptible to inactivation and loss of CYP3A4/5 activity, which was accompanied by an increase in reactive metabolite formation. The role of prospective stratification of patients undergoing lapatinib pharmacotherapy using the CYP3A5 genotype will require further assessment using physiologically-based pharmacokinetic (PBPK) modeling, and may prove to be a viable strategy to mitigate DDIs, and potentially ADRs with lapatinib.

In **Error! Reference source not found.**, we identified a potential DDI as a result of covalent and coordinate binding of lapatinib to CYP3A4/5, between lapatinib and tamoxifen that could have major clinical implications. We leveraged the potential liability of this phenomenon to propose a combinatorial drug treatment using lapatinib and the active tamoxifen metabolite, endoxifen for the treatment of tamoxifen-resistant breast cancer. We determined that as expected, lapatinib could indeed reduce tamoxifen bioactivation to endoxifen, which may nullify the expected synergism between lapatinib and tamoxifen. We further investigated the characteristics of the lapatinib-endoxifen combination from a pharmacodynamic and pharmacokinetic perspective. We uncovered strong pharmacodynamic synergism between these two agents in *in vitro* models of *de novo* and acquired tamoxifen resistance and established that simultaneous administration of lapatinib and endoxifen disrupted the ERα/HER2 crosstalk responsible for tamoxifen resistance. From a pharmacokinetic angle, this combination demonstrated mutual inhibition of P-gp-mediated drug efflux, an effect that could complement the

pharmacodynamic synergism by potentially increasing systemic exposure, intratumoral drug accumulation and CNS penetration of these agents. We further determined that these synergistic effects occurred at concentration levels achievable with current clinical regimens. Lapatinib-endoxifen combinatorial therapy is poised for further translational studies using patient-derived xenograft models and PBPK modeling to quantify the extent of pharmacodynamic and pharmacokinetic synergism *in vivo*. We thus demonstrate how covalent binding, which is often regarded as a therapeutic liability can be circumvented strategically to inspire advancements in therapeutic efficacy.

In conclusion, this thesis provides a mechanistic exploration of the overt and covert effects of covalent binding using a variety of approaches. With a sound understanding of the mechanisms underlying the deleterious consequences of covalent binding, strategies can be developed not only to mitigate the undesirable outcomes of covalent binding, but to deliver advances in pharmacotherapy, thus improving safety and efficacy. The paradigms and approaches utilized in this thesis are not unique to APAP and lapatinib, hence we are convinced that this work provides an impetus for future mechanistic studies on other drugs that cause covalent protein binding to deliver innovation and improvement in clinical outcomes.

References

1. International drug monitoring: the role of national centres. Report of a WHO meeting. *World Health Organ Tech Rep Ser* **498**, 1 (1972).
2. M. Pirmohamed *et al.*, Adverse drug reactions as cause of admission to hospital: prospective analysis of 18 820 patients. *BMJ* **329**, 15 (Jul 3, 2004).
3. E. C. Davies *et al.*, Adverse drug reactions in hospital in-patients: a prospective analysis of 3695 patient-episodes. *PLoS One* **4**, e4439 (2009).
4. J. Sultana, P. Cutroneo, G. Trifiro, Clinical and economic burden of adverse drug reactions. *J Pharmacol Pharmacother* **4**, S73 (Dec, 2013).
5. P. Impicciatore *et al.*, Incidence of adverse drug reactions in paediatric in/out-patients: a systematic review and meta-analysis of prospective studies. *Br J Clin Pharmacol* **52**, 77 (Jul, 2001).
6. I. Kola, J. Landis, Can the pharmaceutical industry reduce attrition rates? *Nat Rev Drug Discov* **3**, 711 (Aug, 2004).
7. T. Hartung, Look back in anger - what clinical studies tell us about preclinical work. *ALTEX* **30**, 275 (2013).
8. K. E. Lasser *et al.*, Timing of new black box warnings and withdrawals for prescription medications. *JAMA* **287**, 2215 (May 1, 2002).
9. D. A. Smith, R. S. Obach, Metabolites in safety testing (MIST): considerations of mechanisms of toxicity with dose, abundance, and duration of treatment. *Chem Res Toxicol* **22**, 267 (Feb, 2009).
10. I. R. Edwards, J. K. Aronson, Adverse drug reactions: definitions, diagnosis, and management. *Lancet* **356**, 1255 (Oct 7, 2000).
11. A. S. Kalgutkar, M. T. Didiuk, Structural alerts, reactive metabolites, and protein covalent binding: how reliable are these attributes as predictors of drug toxicity? *Chem Biodivers* **6**, 2115 (Nov, 2009).
12. A. D. McNaught, A. Wilkinson, *IUPAC. Compendium of Chemical Terminology, 2nd ed. (the "Gold Book")*. (WileyBlackwell; 2nd Revised edition edition).
13. A. S. Kalgutkar, R. S. Obach, T. S. Maurer, Mechanism-based inactivation of cytochrome P450 enzymes: chemical mechanisms, structure-activity relationships and relationship to clinical drug-drug interactions and idiosyncratic adverse drug reactions. *Current drug metabolism* **8**, 407 (Jun, 2007).
14. E. C. Miller, J. A. Miller, The Presence and Significance of Bound Aminoazo Dyes in the Livers of Rats Fed p-Dimethylaminoazobenzene. *Cancer research* **7**, 468 (July 1, 1947, 1947).
15. D. J. Jollow *et al.*, Acetaminophen-induced hepatic necrosis. II. Role of covalent binding in vivo. *J Pharmacol Exp Ther* **187**, 195 (Oct, 1973).
16. D. C. Liebler, Protein damage by reactive electrophiles: targets and consequences. *Chem Res Toxicol* **21**, 117 (Jan, 2008).
17. S. T. Orr *et al.*, Mechanism-based inactivation (MBI) of cytochrome P450 enzymes: structure-activity relationships and discovery strategies to mitigate drug-drug interaction risks. *Journal of medicinal chemistry* **55**, 4896 (Jun 14, 2012).
18. M. E. Mullins *et al.*, Life-threatening interaction of mibefradil and beta-blockers with dihydropyridine calcium channel blockers. *JAMA* **280**, 157 (Jul 8, 1998).
19. J. Uetrecht, D. J. Naisbitt, Idiosyncratic adverse drug reactions: current concepts. *Pharmacological reviews* **65**, 779 (Apr, 2013).

20. A. Melet *et al.*, Substrate selectivity of human cytochrome P450 2C9: importance of residues 476, 365, and 114 in recognition of diclofenac and sulfaphenazole and in mechanism-based inactivation by tienilic acid. *Arch Biochem Biophys* **409**, 80 (Jan 1, 2003).
21. J. C. Homberg, C. Andre, N. Abuaf, A new anti-liver-kidney microsome antibody (anti-LKM2) in tienilic acid-induced hepatitis. *Clin Exp Immunol* **55**, 561 (Mar, 1984).
22. Y. Masubuchi, T. Horie, Toxicological significance of mechanism-based inactivation of cytochrome p450 enzymes by drugs. *Crit Rev Toxicol* **37**, 389 (Jun, 2007).
23. P. R. Oritz de Montellano, M. A. Correia, Suicidal destruction of cytochrome P-450 during oxidative drug metabolism. *Annual review of pharmacology and toxicology* **23**, 481 (1983).
24. S. Thunell, E. Pomp, A. Brun, Guide to drug porphyrogenicity prediction and drug prescription in the acute porphyrias. *Br J Clin Pharmacol* **64**, 668 (Nov, 2007).
25. T. Maurer, H. L. Fung, Comparison of methods for analyzing kinetic data from mechanism-based enzyme inactivation: application to nitric oxide synthase. *AAPS PharmSci* **2**, E8 (2000).
26. S. S. Ghosh, O. Said-Nejad, J. Roestamadji, S. Mobashery, The first mechanism-based inactivators for angiotensin-converting enzyme. *J Med Chem* **35**, 4175 (Oct 30, 1992).
27. A. K. Daly *et al.*, HLA-B*5701 genotype is a major determinant of drug-induced liver injury due to flucloxacillin. *Nat Genet* **41**, 816 (Jul, 2009).
28. M. Bharadwaj *et al.*, Drug hypersensitivity and human leukocyte antigens of the major histocompatibility complex. *Annual review of pharmacology and toxicology* **52**, 401 (2012).
29. M. M. Monshi *et al.*, Human leukocyte antigen (HLA)-B*57:01-restricted activation of drug-specific T cells provides the immunological basis for flucloxacillin-induced liver injury. *Hepatology* **57**, 727 (Feb, 2013).
30. A. R. Temple, Pediatric dosing of acetaminophen. *Pediatr Pharmacol (New York)* **3**, 321 (1983).
31. T. M. Alvarez-Diez, J. Zheng, Detection of glutathione conjugates derived from 4-ipomeanol metabolism in bile of rats by liquid chromatography-tandem mass spectrometry. *Drug Metab Dispos* **32**, 1345 (Dec, 2004).
32. M. R. Boyd, L. T. Burka, In vivo studies on the relationship between target organ alkylation and the pulmonary toxicity of a chemically reactive metabolite of 4-ipomeanol. *J Pharmacol Exp Ther* **207**, 687 (Dec, 1978).
33. J. R. Mitchell, S. S. Thorgeirsson, W. Z. Potter, D. J. Jollow, H. Keiser, Acetaminophen-induced hepatic injury: protective role of glutathione in man and rationale for therapy. *Clinical pharmacology and therapeutics* **16**, 676 (Oct, 1974).
34. W. Z. Potter, S. S. Thorgeirsson, D. J. Jollow, J. R. Mitchell, Acetaminophen-induced hepatic necrosis. V. Correlation of hepatic necrosis, covalent binding and glutathione depletion in hamsters. *Pharmacology* **12**, 129 (1974).
35. E. Verdin, M. Ott, 50 years of protein acetylation: from gene regulation to epigenetics, metabolism and beyond. *Nat Rev Mol Cell Biol* **16**, 258 (Apr, 2015).
36. K. A. Anderson, M. D. Hirschey, Mitochondrial protein acetylation regulates metabolism. *Essays Biochem* **52**, 23 (2012).
37. M. Cuperlovic-Culf, A. Culf, Protein acetylation as an integral part of metabolism in cancer development and progression. *American Journal of Cancer Review* **2**, 6 (2014).

38. L. F. Alfonso, K. S. Srivenugopal, G. J. Bhat, Does aspirin acetylate multiple cellular proteins? (Review). *Mol Med Rep* **2**, 533 (Jul-Aug, 2009).
39. E. H. Awtry, J. Loscalzo, Aspirin. *Circulation* **101**, 1206 (Mar 14, 2000).
40. J. Wang *et al.*, Mapping sites of aspirin-induced acetylations in live cells by quantitative acid-cleavable activity-based protein profiling (QA-ABPP). *Sci Rep* **5**, 7896 (2015).
41. M. S. Rashed, T. G. Myers, S. D. Nelson, Hepatic protein arylation, glutathione depletion, and metabolite profiles of acetaminophen and a non-hepatotoxic regioisomer, 3'-hydroxyacetanilide, in the mouse. *Drug Metab Dispos* **18**, 765 (Sep-Oct, 1990).
42. Y. Qiu, L. Z. Benet, A. L. Burlingame, Identification of hepatic protein targets of the reactive metabolites of the non-hepatotoxic regioisomer of acetaminophen, 3'-hydroxyacetanilide, in the mouse in vivo using two-dimensional gel electrophoresis and mass spectrometry. *Adv Exp Med Biol* **500**, 663 (2001).
43. Y. Qiu, L. Z. Benet, A. L. Burlingame, Identification of the hepatic protein targets of reactive metabolites of acetaminophen in vivo in mice using two-dimensional gel electrophoresis and mass spectrometry. *J Biol Chem* **273**, 17940 (Jul 10, 1998).
44. H. Jaeschke, M. L. Bajt, Intracellular signaling mechanisms of acetaminophen-induced liver cell death. *Toxicol Sci* **89**, 31 (Jan, 2006).
45. H. Takakusa *et al.*, Covalent binding and tissue distribution/retention assessment of drugs associated with idiosyncratic drug toxicity. *Drug Metab Dispos* **36**, 1770 (Sep, 2008).
46. A. P. Li, Accurate prediction of human drug toxicity: a major challenge in drug development. *Chem Biol Interact* **150**, 3 (Nov 1, 2004).
47. A. S. Kalgutkar, D. Dalvie, Predicting toxicities of reactive metabolite-positive drug candidates. *Annu Rev Pharmacol Toxicol* **55**, 35 (2015).
48. J. Singh, R. C. Petter, T. A. Baillie, A. Whitty, The resurgence of covalent drugs. *Nat Rev Drug Discov* **10**, 307 (Apr, 2011).
49. A. S. Kalgutkar, D. K. Dalvie, Drug discovery for a new generation of covalent drugs. *Expert Opin Drug Discov* **7**, 561 (Jul, 2012).
50. R. Mah, J. R. Thomas, C. M. Shafer, Drug discovery considerations in the development of covalent inhibitors. *Bioorg Med Chem Lett* **24**, 33 (Jan 1, 2014).
51. E. Weerapana *et al.*, Quantitative reactivity profiling predicts functional cysteines in proteomes. *Nature* **468**, 790 (Dec 9, 2010).
52. L. Lin, C. Xie, Z. Gao, X. Chen, D. Zhong, Metabolism and pharmacokinetics of allitinib in cancer patients: the roles of cytochrome P450s and epoxide hydrolase in its biotransformation. *Drug Metab Dispos* **42**, 872 (May, 2014).
53. Finishing the euchromatic sequence of the human genome. *Nature* **431**, 931 (Oct 21, 2004).
54. O. N. Jensen, Modification-specific proteomics: characterization of post-translational modifications by mass spectrometry. *Current opinion in chemical biology* **8**, 33 (Feb, 2004).
55. Y. L. Deribe, T. Pawson, I. Dikic, Post-translational modifications in signal integration. *Nature structural & molecular biology* **17**, 666 (Jun, 2010).
56. The Universal Protein Resource (UniProt) in 2010. *Nucleic acids research* **38**, D142 (Jan, 2010).
57. I. Pe'er *et al.*, Proteomic signatures: amino acid and oligopeptide compositions differentiate among phyla. *Proteins* **54**, 20 (Jan 1, 2004).

58. S. M. Marino, V. N. Gladyshev, Cysteine function governs its conservation and degeneration and restricts its utilization on protein surfaces. *Journal of molecular biology* **404**, 902 (Dec 17, 2010).
59. H. Wu, B. G. Ma, J. T. Zhao, H. Y. Zhang, How similar are amino acid mutations in human genetic diseases and evolution. *Biochemical and biophysical research communications* **362**, 233 (Oct 19, 2007).
60. C. L. Grek, J. Zhang, Y. Manevich, D. M. Townsend, K. D. Tew, Causes and consequences of cysteine S-glutathionylation. *The Journal of biological chemistry* **288**, 26497 (Sep 13, 2013).
61. H. S. Chung, S. B. Wang, V. Venkatraman, C. I. Murray, J. E. Van Eyk, Cysteine oxidative posttranslational modifications: emerging regulation in the cardiovascular system. *Circulation research* **112**, 382 (Jan 18, 2013).
62. J. R. Casey, S. Grinstein, J. Orlowski, Sensors and regulators of intracellular pH. *Nature reviews. Molecular cell biology* **11**, 50 (Jan, 2010).
63. P. Ghezzi, Protein glutathionylation in health and disease. *Biochimica et biophysica acta* **1830**, 3165 (May, 2013).
64. J. J. Mieyal, M. M. Gallogly, S. Qanungo, E. A. Sabens, M. D. Shelton, Molecular mechanisms and clinical implications of reversible protein S-glutathionylation. *Antioxidants & redox signaling* **10**, 1941 (Nov, 2008).
65. Y. Xiong, J. D. Uys, K. D. Tew, D. M. Townsend, S-glutathionylation: from molecular mechanisms to health outcomes. *Antioxidants & redox signaling* **15**, 233 (Jul 1, 2011).
66. E. Cabiscol, R. L. Levine, The phosphatase activity of carbonic anhydrase III is reversibly regulated by glutathiolation. *Proceedings of the National Academy of Sciences of the United States of America* **93**, 4170 (Apr 30, 1996).
67. P. Klatt, E. P. Molina, S. Lamas, Nitric oxide inhibits c-Jun DNA binding by specifically targeted S-glutathionylation. *The Journal of biological chemistry* **274**, 15857 (May 28, 1999).
68. E. Pineda-Molina *et al.*, Glutathionylation of the p50 subunit of NF-kappaB: a mechanism for redox-induced inhibition of DNA binding. *Biochemistry* **40**, 14134 (Nov 27, 2001).
69. D. A. Davis *et al.*, Thioltransferase (glutaredoxin) is detected within HIV-1 and can regulate the activity of glutathionylated HIV-1 protease in vitro. *The Journal of biological chemistry* **272**, 25935 (Oct 10, 1997).
70. J. N. Liang, M. R. Pelletier, Destabilization of lens protein conformation by glutathione mixed disulfide. *Experimental eye research* **47**, 17 (Jul, 1988).
71. N. Brandes, S. Schmitt, U. Jakob, Thiol-based redox switches in eukaryotic proteins. *Antioxidants & redox signaling* **11**, 997 (May, 2009).
72. A. Pastore, F. Piemonte, S-Glutathionylation signaling in cell biology: progress and prospects. *European journal of pharmaceutical sciences : official journal of the European Federation for Pharmaceutical Sciences* **46**, 279 (Aug 15, 2012).
73. I. Dalle-Donne, R. Rossi, D. Giustarini, R. Colombo, A. Milzani, S-glutathionylation in protein redox regulation. *Free radical biology & medicine* **43**, 883 (Sep 15, 2007).
74. S. E. Leonard, K. S. Carroll, Chemical 'omics' approaches for understanding protein cysteine oxidation in biology. *Current opinion in chemical biology* **15**, 88 (Feb, 2011).
75. J. A. Hinson, D. W. Roberts, L. P. James, Mechanisms of acetaminophen-induced liver necrosis. *Handbook of experimental pharmacology*, 369 (2010).
76. C. Saito, J. J. Lemasters, H. Jaeschke, c-Jun N-terminal kinase modulates oxidant stress and peroxynitrite formation independent of inducible nitric

oxide synthase in acetaminophen hepatotoxicity. *Toxicology and applied pharmacology* **246**, 8 (Jul, 2010).
77. H. Jaeschke, M. R. McGill, A. Ramachandran, Oxidant stress, mitochondria, and cell death mechanisms in drug-induced liver injury: lessons learned from acetaminophen hepatotoxicity. *Drug metabolism reviews* **44**, 88 (Feb, 2012).
78. A. B. Reid, R. C. Kurten, S. S. McCullough, R. W. Brock, J. A. Hinson, Mechanisms of acetaminophen-induced hepatotoxicity: role of oxidative stress and mitochondrial permeability transition in freshly isolated mouse hepatocytes. *The Journal of pharmacology and experimental therapeutics* **312**, 509 (Feb, 2005).
79. S. D. Cohen *et al.*, Selective protein covalent binding and target organ toxicity. *Toxicology and applied pharmacology* **143**, 1 (Mar, 1997).
80. M. A. Tirmenstein, S. D. Nelson, Acetaminophen-induced oxidation of protein thiols. Contribution of impaired thiol-metabolizing enzymes and the breakdown of adenine nucleotides. *The Journal of biological chemistry* **265**, 3059 (Feb 25, 1990).
81. T. R. Knight, Y. S. Ho, A. Farhood, H. Jaeschke, Peroxynitrite is a critical mediator of acetaminophen hepatotoxicity in murine livers: protection by glutathione. *The Journal of pharmacology and experimental therapeutics* **303**, 468 (Nov, 2002).
82. S. D. Nelson, S. A. Bruschi, in *Drug-Induced Liver Disease*. pp. 353-388.
83. M. Moore *et al.*, The toxicity of acetaminophen and N-acetyl-p-benzoquinone imine in isolated hepatocytes is associated with thiol depletion and increased cytosolic Ca2+. *The Journal of biological chemistry* **260**, 13035 (Oct 25, 1985).
84. E. Albano, M. Rundgren, P. J. Harvison, S. D. Nelson, P. Moldeus, Mechanisms of N-acetyl-p-benzoquinone imine cytotoxicity. *Molecular pharmacology* **28**, 306 (Sep, 1985).
85. W. Chen *et al.*, Protein and nonprotein cysteinyl thiol modification by N-acetyl-p-benzoquinone imine via a novel ipso adduct. *Biochemistry* **38**, 8159 (Jun 22, 1999).
86. X. Yang *et al.*, Changes in mouse liver protein glutathionylation after acetaminophen exposure. *The Journal of pharmacology and experimental therapeutics* **340**, 360 (Feb, 2012).
87. E. T. Chouchani, A. M. James, I. M. Fearnley, K. S. Lilley, M. P. Murphy, Proteomic approaches to the characterization of protein thiol modification. *Current opinion in chemical biology* **15**, 120 (Feb, 2011).
88. T. Rabilloud, M. Chevallet, S. Luche, C. Lelong, Two-dimensional gel electrophoresis in proteomics: Past, present and future. *Journal of proteomics* **73**, 2064 (Oct 10, 2010).
89. M. Zaffagnini *et al.*, The thioredoxin-independent isoform of chloroplastic glyceraldehyde-3-phosphate dehydrogenase is selectively regulated by glutathionylation. *The FEBS journal* **274**, 212 (Jan, 2007).
90. J. M. Souza, R. Radi, Glyceraldehyde-3-phosphate dehydrogenase inactivation by peroxynitrite. *Archives of biochemistry and biophysics* **360**, 187 (Dec 15, 1998).
91. M. M. Gallogly, D. W. Starke, A. K. Leonberg, S. M. Ospina, J. J. Mieyal, Kinetic and mechanistic characterization and versatile catalytic properties of mammalian glutaredoxin 2: implications for intracellular roles. *Biochemistry* **47**, 11144 (Oct 21, 2008).
92. S. A. Gravina, J. J. Mieyal, Thioltransferase is a specific glutathionyl mixed disulfide oxidoreductase. *Biochemistry* **32**, 3368 (Apr 6, 1993).

93. L. I. Leichert *et al.*, Quantifying changes in the thiol redox proteome upon oxidative stress in vivo. *Proceedings of the National Academy of Sciences of the United States of America* **105**, 8197 (Jun 17, 2008).
94. K. M. Robinson *et al.*, Selective fluorescent imaging of superoxide in vivo using ethidium-based probes. *Proc. Natl. Acad. Sci. U. S. A.* **103**, 15038 (Oct 10, 2006).
95. M. Milacic *et al.*, Annotating cancer variants and anti-cancer therapeutics in reactome. *Cancers* **4**, 1180 (2012).
96. M. Coen *et al.*, An integrated metabonomic investigation of acetaminophen toxicity in the mouse using NMR spectroscopy. *Chemical research in toxicology* **16**, 295 (Mar, 2003).
97. K. Fukuhara, A. Ohno, Y. Ando, T. Yamoto, H. Okuda, A 1H NMR-based metabolomics approach for mechanistic insight into acetaminophen-induced hepatotoxicity. *Drug metabolism and pharmacokinetics* **26**, 399 (2011).
98. J. W. Kim *et al.*, Pattern recognition analysis for hepatotoxicity induced by acetaminophen using plasma and urinary 1H NMR-based metabolomics in humans. *Analytical chemistry* **85**, 11326 (Dec 3, 2013).
99. R. D. Fannin *et al.*, Acetaminophen dosing of humans results in blood transcriptome and metabolome changes consistent with impaired oxidative phosphorylation. *Hepatology (Baltimore, Md.)* **51**, 227 (Jan, 2010).
100. J. Sun *et al.*, Metabonomics evaluation of urine from rats given acute and chronic doses of acetaminophen using NMR and UPLC/MS. *Journal of chromatography. B, Analytical technologies in the biomedical and life sciences* **871**, 328 (Aug 15, 2008).
101. T. Soga *et al.*, Differential metabolomics reveals ophthalmic acid as an oxidative stress biomarker indicating hepatic glutathione consumption. *The Journal of biological chemistry* **281**, 16768 (Jun 16, 2006).
102. S. Bhattacharyya *et al.*, Acylcarnitine profiles in acetaminophen toxicity in the mouse: comparison to toxicity, metabolism and hepatocyte regeneration. *Metabolites* **3**, 606 (2013).
103. C. Chen, K. W. Krausz, Y. M. Shah, J. R. Idle, F. J. Gonzalez, Serum metabolomics reveals irreversible inhibition of fatty acid beta-oxidation through the suppression of PPARalpha activation as a contributing mechanism of acetaminophen-induced hepatotoxicity. *Chemical research in toxicology* **22**, 699 (Apr, 2009).
104. M. R. McGill *et al.*, Circulating acylcarnitines as biomarkers of mitochondrial dysfunction after acetaminophen overdose in mice and humans. *Archives of toxicology* **88**, 391 (Feb, 2014).
105. J. Yu *et al.*, Targeted metabolomic study indicating glycyrrhizin's protection against acetaminophen-induced liver damage through reversing fatty acid metabolism. *Phytotherapy research : PTR* **28**, 933 (Jun, 2014).
106. H. Bi *et al.*, Targeted Metabolomics of Serum Acylcarnitines Evaluates Hepatoprotective Effect of Wuzhi Tablet (Schisandra sphenanthera Extract) against Acute Acetaminophen Toxicity. *Evidence-based complementary and alternative medicine : eCAM* **2013**, 985257 (2013).
107. A. D. Patterson, Y. M. Shah, T. Matsubara, K. W. Krausz, F. J. Gonzalez, Peroxisome proliferator-activated receptor alpha induction of uncoupling protein 2 protects against acetaminophen-induced liver toxicity. *Hepatology (Baltimore, Md.)* **56**, 281 (Jul, 2012).
108. S. Bhattacharyya *et al.*, Targeted liquid chromatography-mass spectrometry analysis of serum acylcarnitines in acetaminophen toxicity in children. *Biomarkers in medicine* **8**, 147 (2014).

109. Y. H. Xiong, Y. Xu, L. Yang, Z. T. Wang, Gas chromatography-mass spectrometry-based profiling of serum fatty acids in acetaminophen-induced liver injured rats. *Journal of applied toxicology : JAT* **34**, 149 (Feb, 2014).
110. J. A. Hinson, J. B. Mays, A. M. Cameron, Acetaminophen-induced hepatic glycogen depletion and hyperglycemia in mice. *Biochemical pharmacology* **32**, 1979 (Jul 1, 1983).
111. P. N. Newsome *et al.*, Development of an invasively monitored porcine model of acetaminophen-induced acute liver failure. *BMC gastroenterology* **10**, 34 (2010).
112. F. Y. Ghauri, A. E. McLean, D. Beales, I. D. Wilson, J. K. Nicholson, Induction of 5-oxoprolinuria in the rat following chronic feeding with N-acetyl 4-aminophenol (paracetamol). *Biochemical pharmacology* **46**, 953 (Sep 1, 1993).
113. M. Yamazaki *et al.*, Perturbation of bile acid homeostasis is an early pathogenesis event of drug induced liver injury in rats. *Toxicology and applied pharmacology* **268**, 79 (Apr 1, 2013).
114. B. L. Woolbright *et al.*, Glycodeoxycholic acid levels as prognostic biomarker in acetaminophen-induced acute liver failure patients. *Toxicological sciences : an official journal of the Society of Toxicology* **142**, 436 (Dec, 2014).
115. I. Dalle-Donne *et al.*, Molecular mechanisms and potential clinical significance of S-glutathionylation. *Antioxidants & redox signaling* **10**, 445 (Mar, 2008).
116. M. J. Peltoniemi, A. R. Karala, J. K. Jurvansuu, V. L. Kinnula, L. W. Ruddock, Insights into deglutathionylation reactions. Different intermediates in the glutaredoxin and protein disulfide isomerase catalyzed reactions are defined by the gamma-linkage present in glutathione. *The Journal of biological chemistry* **281**, 33107 (Nov 3, 2006).
117. J. R. Wisniewski, A. Zougman, N. Nagaraj, M. Mann, Universal sample preparation method for proteome analysis. *Nature methods* **6**, 359 (May, 2009).
118. J. R. Wisniewski, D. F. Zielinska, M. Mann, Comparison of ultrafiltration units for proteomic and N-glycoproteomic analysis by the filter-aided sample preparation method. *Analytical biochemistry* **410**, 307 (Mar 15, 2011).
119. Y. Hamnell-Pamment, C. Lind, C. Palmberg, T. Bergman, I. A. Cotgreave, Determination of site-specificity of S-glutathionylated cellular proteins. *Biochemical and biophysical research communications* **332**, 362 (Jul 1, 2005).
120. E. C. Yi, D. R. Goodlett, Quantitative protein profile comparisons using the isotope-coded affinity tag method. *Current protocols in protein science / editorial board, John E. Coligan ... [et al.]* **Chapter 23**, Unit 23 2 (Feb, 2004).
121. R. E. Hansen, J. R. Winther, An introduction to methods for analyzing thiols and disulfides: Reactions, reagents, and practical considerations. *Analytical biochemistry* **394**, 147 (Nov 15, 2009).
122. Y. M. Go, J. R. Roede, M. Orr, Y. Liang, D. P. Jones, Integrated redox proteomics and metabolomics of mitochondria to identify mechanisms of cd toxicity. *Toxicological sciences : an official journal of the Society of Toxicology* **139**, 59 (May, 2014).
123. X. Zhang, B. Huang, X. Zhou, C. Chen, Quantitative proteomic analysis of S-nitrosated proteins in diabetic mouse liver with ICAT switch method. *Protein & cell* **1**, 675 (Jul, 2010).

124. D. Su *et al.*, Proteomic identification and quantification of S-glutathionylation in mouse macrophages using resin-assisted enrichment and isobaric labeling. *Free radical biology & medicine* **67**, 460 (Feb, 2014).
125. S. Garcia-Santamarina *et al.*, The oxidized thiol proteome in fission yeast--optimization of an ICAT-based method to identify H2O2-oxidized proteins. *Journal of proteomics* **74**, 2476 (Oct 19, 2011).
126. D. J. McGarry *et al.*, Proteome-wide identification and quantification of S-glutathionylation targets in mouse liver. *The Biochemical journal*, (Apr 20, 2015).
127. V. Kumar, T. Kleffmann, M. B. Hampton, M. B. Cannell, C. C. Winterbourn, Redox proteomics of thiol proteins in mouse heart during ischemia/reperfusion using ICAT reagents and mass spectrometry. *Free radical biology & medicine* **58**, 109 (May, 2013).
128. Z. Qu *et al.*, Proteomic quantification and site-mapping of S-nitrosylated proteins using isobaric iodoTMT reagents. *Journal of proteome research* **13**, 3200 (Jul 3, 2014).
129. C. Abdallah, E. Dumas-Gaudot, J. Renaut, K. Sergeant, Gel-based and gel-free quantitative proteomics approaches at a glance. *International journal of plant genomics* **2012**, 494572 (2012).
130. C. Aninat *et al.*, Expression of cytochromes P450, conjugating enzymes and nuclear receptors in human hepatoma HepaRG cells. *Drug metabolism and disposition: the biological fate of chemicals* **34**, 75 (Jan, 2006).
131. S. Antherieu, C. Chesne, R. Li, C. Guguen-Guillouzo, A. Guillouzo, Optimization of the HepaRG cell model for drug metabolism and toxicity studies. *Toxicology in vitro : an international journal published in association with BIBRA* **26**, 1278 (Dec, 2012).
132. T. B. Andersson, K. P. Kanebratt, J. G. Kenna, The HepaRG cell line: a unique in vitro tool for understanding drug metabolism and toxicology in human. *Expert opinion on drug metabolism & toxicology* **8**, 909 (Jul, 2012).
133. M. R. McGill *et al.*, HepaRG cells: a human model to study mechanisms of acetaminophen hepatotoxicity. *Hepatology (Baltimore, Md.)* **53**, 974 (Mar, 2011).
134. C. Kampf *et al.*, The human liver-specific proteome defined by transcriptomics and antibody-based profiling. *FASEB journal : official publication of the Federation of American Societies for Experimental Biology* **28**, 2901 (Jul, 2014).
135. S. Mohr, H. Hallak, A. de Boitte, E. G. Lapetina, B. Brune, Nitric oxide-induced S-glutathionylation and inactivation of glyceraldehyde-3-phosphate dehydrogenase. *The Journal of biological chemistry* **274**, 9427 (Apr 2, 1999).
136. D. Han *et al.*, Sites and mechanisms of aconitase inactivation by peroxynitrite: modulation by citrate and glutathione. *Biochemistry* **44**, 11986 (Sep 13, 2005).
137. S. W. Shin, C. J. Oh, I. S. Kil, J. W. Park, Glutathionylation regulates cytosolic NADP+-dependent isocitrate dehydrogenase activity. *Free radical research* **43**, 409 (Apr, 2009).
138. E. S. Yang *et al.*, Inactivation of NADP(+)-dependent isocitrate dehydrogenase by nitric oxide. *Free radical biology & medicine* **33**, 927 (Oct 1, 2002).
139. S. Moncada, J. D. Erusalimsky, Does nitric oxide modulate mitochondrial energy generation and apoptosis? *Nature reviews. Molecular cell biology* **3**, 214 (Mar, 2002).
140. A. H. Chang *et al.*, Respiratory Substrates Regulate S-Nitrosylation of Mitochondrial Proteins through a Thiol-Dependent Pathway. *Chemical research in toxicology* **27**, 794 (May 19, 2014).

141. M. Halloran, S. Parakh, J. D. Atkin, The role of s-nitrosylation and s-glutathionylation of protein disulphide isomerase in protein misfolding and neurodegeneration. *International journal of cell biology* **2013**, 797914 (2013).
142. P. Aracena, W. Tang, S. L. Hamilton, C. Hidalgo, Effects of S-glutathionylation and S-nitrosylation on calmodulin binding to triads and FKBP12 binding to type 1 calcium release channels. *Antioxidants & redox signaling* **7**, 870 (Jul-Aug, 2005).
143. L. Michelet *et al.*, Redox regulation of the Calvin-Benson cycle: something old, something new. *Frontiers in plant science* **4**, 470 (2013).
144. A. Martinez-Ruiz, S. Lamas, Signalling by NO-induced protein S-nitrosylation and S-glutathionylation: convergences and divergences. *Cardiovascular research* **75**, 220 (Jul 15, 2007).
145. S. Casagrande *et al.*, Glutathionylation of human thioredoxin: a possible crosstalk between the glutathione and thioredoxin systems. *Proceedings of the National Academy of Sciences of the United States of America* **99**, 9745 (Jul 23, 2002).
146. P. C. Burcham, A. W. Harman, Acetaminophen toxicity results in site-specific mitochondrial damage in isolated mouse hepatocytes. *The Journal of biological chemistry* **266**, 5049 (Mar 15, 1991).
147. K. D. Tew *et al.*, The role of glutathione S-transferase P in signaling pathways and S-glutathionylation in cancer. *Free radical biology & medicine* **51**, 299 (Jul 15, 2011).
148. S. Kehr *et al.*, Protein S-glutathionylation in malaria parasites. *Antioxidants & redox signaling* **15**, 2855 (Dec 1, 2011).
149. L. R. Gray, S. C. Tompkins, E. B. Taylor, Regulation of pyruvate metabolism and human disease. *Cellular and molecular life sciences : CMLS* **71**, 2577 (Jul, 2014).
150. N. Giangregorio, F. Palmieri, C. Indiveri, Glutathione controls the redox state of the mitochondrial carnitine/acylcarnitine carrier Cys residues by glutathionylation. *Biochimica et biophysica acta* **1830**, 5299 (Nov, 2013).
151. K. H. Moon *et al.*, Inactivation of oxidized and S-nitrosylated mitochondrial proteins in alcoholic fatty liver of rats. *Hepatology (Baltimore, Md.)* **44**, 1218 (Nov, 2006).
152. J. E. Manautou *et al.*, Clofibrate pretreatment diminishes acetaminophen's selective covalent binding and hepatotoxicity. *Toxicology and applied pharmacology* **129**, 252 (Dec, 1994).
153. J. E. Manautou, S. G. Emeigh Hart, E. A. Khairallah, S. D. Cohen, Protection against acetaminophen hepatotoxicity by a single dose of clofibrate: effects on selective protein arylation and glutathione depletion. *Fundamental and applied toxicology : official journal of the Society of Toxicology* **29**, 229 (Feb, 1996).
154. F. A. Nicholls-Grzemski, I. C. Calder, B. G. Priestly, P. C. Burcham, Clofibrate-induced in vitro hepatoprotection against acetaminophen is not due to altered glutathione homeostasis. *Toxicological sciences : an official journal of the Society of Toxicology* **56**, 220 (Jul, 2000).
155. C. Chen, G. E. Hennig, H. E. Whiteley, J. C. Corton, J. E. Manautou, Peroxisome proliferator-activated receptor alpha-null mice lack resistance to acetaminophen hepatotoxicity following clofibrate exposure. *Toxicological sciences : an official journal of the Society of Toxicology* **57**, 338 (Oct, 2000).
156. L. Burri, G. H. Thoresen, R. K. Berge, The Role of PPARalpha Activation in Liver and Muscle. *PPAR research* **2010**, (2010).
157. A. L. McLain, P. J. Cormier, M. Kinter, L. I. Szweda, Glutathionylation of alpha-ketoglutarate dehydrogenase: the chemical nature and relative

susceptibility of the cofactor lipoic acid to modification. *Free radical biology & medicine* **61**, 161 (Aug, 2013).
158. I. S. Kil, J. W. Park, Regulation of mitochondrial NADP+-dependent isocitrate dehydrogenase activity by glutathionylation. *The Journal of biological chemistry* **280**, 10846 (Mar 18, 2005).
159. Y. R. Chen, C. L. Chen, D. R. Pfeiffer, J. L. Zweier, Mitochondrial complex II in the post-ischemic heart: oxidative injury and the role of protein S-glutathionylation. *The Journal of biological chemistry* **282**, 32640 (Nov 9, 2007).
160. C. Saito, C. Zwingmann, H. Jaeschke, Novel mechanisms of protection against acetaminophen hepatotoxicity in mice by glutathione and N-acetylcysteine. *Hepatology (Baltimore, Md.)* **51**, 246 (Jan, 2010).
161. L. L. Meyers, W. P. Beierschmitt, E. A. Khairallah, S. D. Cohen, Acetaminophen-induced inhibition of hepatic mitochondrial respiration in mice. *Toxicology and applied pharmacology* **93**, 378 (May, 1988).
162. P. J. Donnelly, R. M. Walker, W. J. Racz, Inhibition of mitochondrial respiration in vivo is an early event in acetaminophen-induced hepatotoxicity. *Archives of toxicology* **68**, 110 (1994).
163. R. R. Ramsay, M. S. Rashed, S. D. Nelson, In vitro effects of acetaminophen metabolites and analogs on the respiration of mouse liver mitochondria. *Archives of biochemistry and biophysics* **273**, 449 (Sep, 1989).
164. D. V. Parmar, G. Ahmed, M. A. Khandkar, S. S. Katyare, Mitochondrial ATPase: a target for paracetamol-induced hepatotoxicity. *European journal of pharmacology* **293**, 225 (Oct 6, 1995).
165. R. J. Mailloux *et al.*, Glutaredoxin-2 is required to control oxidative phosphorylation in cardiac muscle by mediating deglutathionylation reactions. *The Journal of biological chemistry* **289**, 14812 (May 23, 2014).
166. S. B. Wang *et al.*, Redox regulation of mitochondrial ATP synthase: implications for cardiac resynchronization therapy. *Circulation research* **109**, 750 (Sep 16, 2011).
167. M. J. Kohr *et al.*, Simultaneous measurement of protein oxidation and S-nitrosylation during preconditioning and ischemia/reperfusion injury with resin-assisted capture. *Circulation research* **108**, 418 (Feb 18, 2011).
168. H. Jaeschke, Glutathione disulfide formation and oxidant stress during acetaminophen-induced hepatotoxicity in mice in vivo: the protective effect of allopurinol. *The Journal of pharmacology and experimental therapeutics* **255**, 935 (Dec, 1990).
169. E. R. Taylor *et al.*, Reversible glutathionylation of complex I increases mitochondrial superoxide formation. *The Journal of biological chemistry* **278**, 19603 (May 30, 2003).
170. R. Radi, G. Peluffo, M. N. Alvarez, M. Naviliat, A. Cayota, Unraveling peroxynitrite formation in biological systems. *Free radical biology & medicine* **30**, 463 (Mar 1, 2001).
171. C. Cover *et al.*, Peroxynitrite-induced mitochondrial and endonuclease-mediated nuclear DNA damage in acetaminophen hepatotoxicity. *The Journal of pharmacology and experimental therapeutics* **315**, 879 (Nov, 2005).
172. T. R. Knight, A. Kurtz, M. L. Bajt, J. A. Hinson, H. Jaeschke, Vascular and hepatocellular peroxynitrite formation during acetaminophen toxicity: role of mitochondrial oxidant stress. *Toxicological sciences : an official journal of the Society of Toxicology* **62**, 212 (Aug, 2001).
173. A. W. Harman, L. J. Fischer, Hamster hepatocytes in culture as a model for acetaminophen toxicity studies with inhibitors of drug metabolism. *Toxicology and applied pharmacology* **71**, 330 (Dec, 1983).

174. B. H. Lauterburg, J. R. Mitchell, Toxic doses of acetaminophen suppress hepatic glutathione synthesis in rats. *Hepatology (Baltimore, Md.)* **2**, 8 (Jan-Feb, 1982).
175. S. C. Lu, Glutathione synthesis. *Biochimica et biophysica acta* **1830**, 3143 (May, 2013).
176. I. Perez-Mato, C. Castro, F. A. Ruiz, F. J. Corrales, J. M. Mato, Methionine adenosyltransferase S-nitrosylation is regulated by the basic and acidic amino acids surrounding the target thiol. *The Journal of biological chemistry* **274**, 17075 (Jun 11, 1999).
177. M. V. Terneus, K. K. Kiningham, A. B. Carpenter, S. B. Sullivan, M. A. Valentovic, Comparison of S-Adenosyl-L-methionine and N-acetylcysteine protective effects on acetaminophen hepatic toxicity. *The Journal of pharmacology and experimental therapeutics* **320**, 99 (Jan, 2007).
178. W. N. Niu, P. K. Yadav, J. Adamec, R. Banerjee, S-glutathionylation enhances human cystathionine beta-synthase activity under oxidative stress conditions. *Antioxidants & redox signaling* **22**, 350 (Feb 10, 2015).
179. J. Gwynn, J. R. Fry, J. W. Bridges, The effects of paracetamol and other foreign compounds on protein synthesis in isolated adult rat hepatocytes [proceedings]. *Biochemical Society transactions* **7**, 117 (Feb, 1979).
180. D. Beales, D. P. Hue, A. E. McLean, Lipid peroxidation, protein synthesis, and protection by calcium EDTA in paracetamol injury to isolated hepatocytes. *Biochemical pharmacology* **34**, 19 (Jan 1, 1985).
181. S. S. Thorgeirsson, H. A. Sasame, J. R. Mitchell, D. J. Jollow, W. Z. Potter, Biochemical changes after hepatic injury from toxic doses of acetaminophen or furosemide. *Pharmacology* **14**, 205 (1976).
182. O. O. Assaf Katz, in *Cell-Free Protein Synthesis* P. M. Biyani, Ed. (2012).
183. J. Ling, D. Soll, Severe oxidative stress induces protein mistranslation through impairment of an aminoacyl-tRNA synthetase editing site. *Proceedings of the National Academy of Sciences of the United States of America* **107**, 4028 (Mar 2, 2010).
184. T. J. Hohn, T. Grune, The proteasome and the degradation of oxidized proteins: part III-Redox regulation of the proteasomal system. *Redox biology* **2**, 388 (2014).
185. R. Agarwal *et al.*, Acetaminophen-induced hepatotoxicity in mice occurs with inhibition of activity and nitration of mitochondrial manganese superoxide dismutase. *The Journal of pharmacology and experimental therapeutics* **337**, 110 (Apr, 2011).
186. G. C. Kuriakose, M. G. Kurup, Antioxidant and hepatoprotective activity of Aphanizomenon flos-aquae Linn against paracetamol intoxication in rats. *Indian journal of experimental biology* **48**, 1123 (Nov, 2010).
187. X. G. Lei, J. H. Zhu, J. P. McClung, M. Aregullin, C. A. Roneker, Mice deficient in Cu,Zn-superoxide dismutase are resistant to acetaminophen toxicity. *The Biochemical journal* **399**, 455 (Nov 1, 2006).
188. K. C. Wilcox *et al.*, Modifications of superoxide dismutase (SOD1) in human erythrocytes: a possible role in amyotrophic lateral sclerosis. *The Journal of biological chemistry* **284**, 13940 (May 15, 2009).
189. D. Candas, J. J. Li, MnSOD in oxidative stress response-potential regulation via mitochondrial protein influx. *Antioxidants & redox signaling* **20**, 1599 (Apr 1, 2014).
190. A. L. Dafre, H. Sies, T. Akerboom, Protein S-thiolation and regulation of microsomal glutathione transferase activity by the glutathione redox couple. *Archives of biochemistry and biophysics* **332**, 288 (Aug 15, 1996).
191. H. Z. Chae, H. Oubrahim, J. W. Park, S. G. Rhee, P. B. Chock, Protein glutathionylation in the regulation of peroxiredoxins: a family of thiol-

specific peroxidases that function as antioxidants, molecular chaperones, and signal modulators. *Antioxidants & redox signaling* **16**, 506 (Mar 15, 2012).
192. N. Fedoroff, Redox regulatory mechanisms in cellular stress responses. *Annals of botany* **98**, 289 (Aug, 2006).
193. M. J. Berridge, P. Lipp, M. D. Bootman, The versatility and universality of calcium signalling. *Nature reviews. Molecular cell biology* **1**, 11 (Oct, 2000).
194. J. R. Williamson, R. H. Cooper, J. B. Hoek, Role of calcium in the hormonal regulation of liver metabolism. *Biochimica et biophysica acta* **639**, 243 (Dec 30, 1981).
195. D. E. Clapham, Calcium signaling. *Cell* **131**, 1047 (Dec 14, 2007).
196. R. Rizzuto, D. De Stefani, A. Raffaello, C. Mammucari, Mitochondria as sensors and regulators of calcium signalling. *Nature reviews. Molecular cell biology* **13**, 566 (Sep, 2012).
197. B. H. Lauterburg, Early disturbance of calcium translocation across the plasma membrane in toxic liver injury. *Hepatology (Baltimore, Md.)* **7**, 1179 (Nov-Dec, 1987).
198. J. O. Tsokos-Kuhn, E. L. Todd, J. B. McMillin-Wood, J. R. Mitchell, ATP-dependent calcium uptake by rat liver plasma membrane vesicles. Effect of alkylating hepatotoxins in vivo. *Molecular pharmacology* **28**, 56 (Jul, 1985).
199. S. A. Bruschi, B. G. Priestly, Implication of alterations in intracellular calcium ion homoeostasis in the advent of paracetamol-induced cytotoxicity in primary mouse hepatocyte monolayer cultures. *Toxicology in vitro : an international journal published in association with BIBRA* **4**, 743 (1990).
200. J. O. Tsokos-Kuhn, Evidence in vivo for elevation of intracellular free Ca2+ in the liver after diquat, acetaminophen, and CCl4. *Biochemical pharmacology* **38**, 3061 (Sep 15, 1989).
201. M. A. Tirmenstein, S. D. Nelson, Subcellular binding and effects on calcium homeostasis produced by acetaminophen and a nonhepatotoxic regioisomer, 3'-hydroxyacetanilide, in mouse liver. *The Journal of biological chemistry* **264**, 9814 (Jun 15, 1989).
202. P. Nicotera *et al.*, On the role of Ca2+ in the toxicity of alkylating and oxidizing quinone imines in isolated hepatocytes. *Chemical research in toxicology* **2**, 46 (Jan-Feb, 1989).
203. A. R. Boobis, C. E. Seddon, P. Nasseri-Sina, D. S. Davies, Evidence for a direct role of intracellular calcium in paracetamol toxicity. *Biochemical pharmacology* **39**, 1277 (Apr 15, 1990).
204. N. Thibault, G. Peytavin, J. R. Claude, Calcium channel blocking agents protect against acetaminophen-induced cytotoxicity in rat hepatocytes. *Journal of biochemical toxicology* **6**, 237 (Fall, 1991).
205. S. Ellouk-Achard *et al.*, Protective effect of nifedipine against cytotoxicity and intracellular calcium alterations induced by acetaminophen in rat hepatocyte cultures. *Drug and chemical toxicology* **18**, 105 (May-Aug, 1995).
206. T. Okamoto *et al.*, Expression of the alpha1D subunit of the L-type voltage gated calcium channel in human liver. *International journal of molecular medicine* **8**, 413 (Oct, 2001).
207. J. T. Lock, W. G. Sinkins, W. P. Schilling, Effect of protein S-glutathionylation on Ca2+ homeostasis in cultured aortic endothelial cells. *American journal of physiology. Heart and circulatory physiology* **300**, H493 (Feb, 2011).
208. S. Lancel *et al.*, Nitroxyl activates SERCA in cardiac myocytes via glutathiolation of cysteine 674. *Circulation research* **104**, 720 (Mar 27, 2009).

209. P. C. Burcham, A. W. Harman, Effect of acetaminophen hepatotoxicity on hepatic mitochondrial and microsomal calcium contents in mice. *Toxicology letters* **44**, 91 (Nov, 1988).
210. L. Missiaen, C. W. Taylor, M. J. Berridge, Spontaneous calcium release from inositol trisphosphate-sensitive calcium stores. *Nature* **352**, 241 (Jul 18, 1991).
211. L. Missiaen, C. W. Taylor, M. J. Berridge, Luminal Ca2+ promoting spontaneous Ca2+ release from inositol trisphosphate-sensitive stores in rat hepatocytes. *The Journal of physiology* **455**, 623 (Sep, 1992).
212. M. Periasamy, A. Kalyanasundaram, SERCA pump isoforms: their role in calcium transport and disease. *Muscle & nerve* **35**, 430 (Apr, 2007).
213. J. L. Greene, The structural proteomics of S-nitrosylation: From global identification to elucidating protein function through structural bioinformatics. **Ph.D.**, 187 (2011, 2011).
214. E. Kheradpezhouh, L. Ma, A. Morphett, G. J. Barritt, G. Y. Rychkov, TRPM2 channels mediate acetaminophen-induced liver damage. *Proceedings of the National Academy of Sciences of the United States of America* **111**, 3176 (Feb 25, 2014).
215. F. Di Lisa, R. Menabo, M. Canton, M. Barile, P. Bernardi, Opening of the mitochondrial permeability transition pore causes depletion of mitochondrial and cytosolic NAD+ and is a causative event in the death of myocytes in postischemic reperfusion of the heart. *The Journal of biological chemistry* **276**, 2571 (Jan 26, 2001).
216. B. Buelow, Y. Song, A. M. Scharenberg, The Poly(ADP-ribose) polymerase PARP-1 is required for oxidative stress-induced TRPM2 activation in lymphocytes. *The Journal of biological chemistry* **283**, 24571 (Sep 5, 2008).
217. M. Donmez *et al.*, PARP inhibition prevents acetaminophen-induced liver injury and increases survival rate in rats. *Turkish journal of medical sciences* **45**, 18 (2015).
218. M. Weis, G. E. Kass, S. Orrenius, P. Moldeus, N-acetyl-p-benzoquinone imine induces Ca2+ release from mitochondria by stimulating pyridine nucleotide hydrolysis. *The Journal of biological chemistry* **267**, 804 (Jan 15, 1992).
219. K. Inamura *et al.*, Response to ADP-ribose by activation of TRPM2 in the CRI-G1 insulinoma cell line. *The Journal of membrane biology* **191**, 201 (Feb 1, 2003).
220. K. Togashi, H. Inada, M. Tominaga, Inhibition of the transient receptor potential cation channel TRPM2 by 2-aminoethoxydiphenyl borate (2-APB). *British journal of pharmacology* **153**, 1324 (Mar, 2008).
221. S. Brnjic, M. H. Olofsson, A. M. Havelka, S. Linder, Chemical biology suggests a role for calcium signaling in mediating sustained JNK activation during apoptosis. *Molecular bioSystems* **6**, 767 (May, 2010).
222. R. Wong, C. Steenbergen, E. Murphy, Mitochondrial permeability transition pore and calcium handling. *Methods Mol Biol* **810**, 235 (2012).
223. U. Saeed *et al.*, Knockdown of cytosolic glutaredoxin 1 leads to loss of mitochondrial membrane potential: implication in neurodegenerative diseases. *PloS one* **3**, e2459 (2008).
224. V. Petronilli *et al.*, The voltage sensor of the mitochondrial permeability transition pore is tuned by the oxidation-reduction state of vicinal thiols. Increase of the gating potential by oxidants and its reversal by reducing agents. *The Journal of biological chemistry* **269**, 16638 (Jun 17, 1994).
225. C. S. Queiroga *et al.*, Glutathionylation of adenine nucleotide translocase induced by carbon monoxide prevents mitochondrial membrane

permeabilization and apoptosis. *The Journal of biological chemistry* **285**, 17077 (May 28, 2010).
226. A. P. Halestrap, K. Y. Woodfield, C. P. Connern, Oxidative stress, thiol reagents, and membrane potential modulate the mitochondrial permeability transition by affecting nucleotide binding to the adenine nucleotide translocase. *The Journal of biological chemistry* **272**, 3346 (Feb 7, 1997).
227. F. Di Lisa, A. Carpi, V. Giorgio, P. Bernardi, The mitochondrial permeability transition pore and cyclophilin D in cardioprotection. *Biochimica et biophysica acta* **1813**, 1316 (Jul, 2011).
228. M. Pratt-Hyatt, H. L. Lin, P. F. Hollenberg, Mechanism-based inactivation of human CYP2E1 by diethyldithocarbamate. *Drug metabolism and disposition: the biological fate of chemicals* **38**, 2286 (Dec, 2010).
229. M. Younes, C. Sause, C. P. Siegers, R. Lemoine, Effect of deferrioxamine and diethyldithiocarbamate on paracetamol-induced hepato- and nephrotoxicity. The role of lipid peroxidation. *Journal of applied toxicology : JAT* **8**, 261 (Aug, 1988).
230. V. V. Lauriault, P. J. O'Brien, Molecular mechanism for prevention of N-acetyl-p-benzoquinoneimine cytotoxicity by the permeable thiol drugs diethyldithiocarbamate and dithiothreitol. *Molecular pharmacology* **40**, 125 (Jul, 1991).
231. H. Ishiyama, K. Ogino, Y. Shimomura, T. Kanbe, T. Hobara, Hepatotoxicity of diethyldithiocarbamate in rats. *Pharmacology & toxicology* **67**, 426 (Nov, 1990).
232. H. Ishiyama, K. Ogino, T. Hobara, Role of Kupffer cells in rat liver injury induced by diethyldithiocarbamate. *European journal of pharmacology* **292**, 135 (Jan 13, 1995).
233. C. J. Patten *et al.*, Cytochrome P450 enzymes involved in acetaminophen activation by rat and human liver microsomes and their kinetics. *Chemical research in toxicology* **6**, 511 (Jul-Aug, 1993).
234. P. T. Manyike, E. D. Kharasch, T. F. Kalhorn, J. T. Slattery, Contribution of CYP2E1 and CYP3A to acetaminophen reactive metabolite formation. *Clinical pharmacology and therapeutics* **67**, 275 (Mar, 2000).
235. J. E. Laine, S. Auriola, M. Pasanen, R. O. Juvonen, Acetaminophen bioactivation by human cytochrome P450 enzymes and animal microsomes. *Xenobiotica; the fate of foreign compounds in biological systems* **39**, 11 (Jan, 2009).
236. T. G. Myers *et al.*, A comparative study of mouse liver proteins arylated by reactive metabolites of acetaminophen and its nonhepatotoxic regioisomer, 3'-hydroxyacetanilide. *Chemical research in toxicology* **8**, 403 (Apr-May, 1995).
237. M. Hadi *et al.*, AMAP, the alleged non-toxic isomer of acetaminophen, is toxic in rat and human liver. *Archives of toxicology* **87**, 155 (Jan, 2013).
238. D. W. Rusnak *et al.*, The effects of the novel, reversible epidermal growth factor receptor/ErbB-2 tyrosine kinase inhibitor, GW2016, on the growth of human normal and tumor-derived cell lines in vitro and in vivo. *Molecular cancer therapeutics* **1**, 85 (Dec, 2001).
239. W. Xia *et al.*, Anti-tumor activity of GW572016: a dual tyrosine kinase inhibitor blocks EGF activation of EGFR/erbB2 and downstream Erk1/2 and AKT pathways. *Oncogene* **21**, 6255 (Sep 12, 2002).
240. C. E. Geyer *et al.*, Lapatinib plus capecitabine for HER2-positive advanced breast cancer. *The New England journal of medicine* **355**, 2733 (Dec 28, 2006).
241. S. Johnston *et al.*, Lapatinib combined with letrozole versus letrozole and placebo as first-line therapy for postmenopausal hormone receptor-positive

metastatic breast cancer. *Journal of clinical oncology : official journal of the American Society of Clinical Oncology* **27**, 5538 (Nov 20, 2009).
242. B. Sherrill *et al.*, Quality of life in hormone receptor-positive HER-2+ metastatic breast cancer patients during treatment with letrozole alone or in combination with lapatinib. *The oncologist* **15**, 944 (2010).
243. W. C. Teng *et al.*, Mechanism-based inactivation of cytochrome P450 3A4 by lapatinib. *Molecular pharmacology* **78**, 693 (Oct, 2010).
244. H. Takakusa *et al.*, Metabolic intermediate complex formation of human cytochrome P450 3A4 by lapatinib. *Drug metabolism and disposition: the biological fate of chemicals* **39**, 1022 (Jun, 2011).
245. J. E. Barbara, F. Kazmi, A. Parkinson, D. B. Buckley, Metabolism-dependent inhibition of CYP3A4 by lapatinib: evidence for formation of a metabolic intermediate complex with a nitroso/oxime metabolite formed via a nitrone intermediate. *Drug metabolism and disposition: the biological fate of chemicals* **41**, 1012 (May, 2013).
246. E. C. Chan *et al.*, Interaction of lapatinib with cytochrome P450 3A5. *Drug metabolism and disposition: the biological fate of chemicals* **40**, 1414 (Jul, 2012).
247. M. J. Rieder, J. Uetrecht, N. H. Shear, S. P. Spielberg, Synthesis and in vitro toxicity of hydroxylamine metabolites of sulfonamides. *The Journal of pharmacology and experimental therapeutics* **244**, 724 (Feb, 1988).
248. S. Castellino *et al.*, Human metabolism of lapatinib, a dual kinase inhibitor: implications for hepatotoxicity. *Drug metabolism and disposition: the biological fate of chemicals* **40**, 139 (Jan, 2012).
249. A. K. Bence *et al.*, Phase I pharmacokinetic studies evaluating single and multiple doses of oral GW572016, a dual EGFR-ErbB2 inhibitor, in healthy subjects. *Investigational new drugs* **23**, 39 (Jan, 2005).
250. H. A. Burris, 3rd *et al.*, Phase I safety, pharmacokinetics, and clinical activity study of lapatinib (GW572016), a reversible dual inhibitor of epidermal growth factor receptor tyrosine kinases, in heavily pretreated patients with metastatic carcinomas. *Journal of clinical oncology : official journal of the American Society of Clinical Oncology* **23**, 5305 (Aug 10, 2005).
251. H. L. Gomez *et al.*, Efficacy and safety of lapatinib as first-line therapy for ErbB2-amplified locally advanced or metastatic breast cancer. *Journal of clinical oncology : official journal of the American Society of Clinical Oncology* **26**, 2999 (Jun 20, 2008).
252. C. F. Spraggs *et al.*, HLA-DQA1*02:01 is a major risk factor for lapatinib-induced hepatotoxicity in women with advanced breast cancer. *Journal of clinical oncology : official journal of the American Society of Clinical Oncology* **29**, 667 (Feb 20, 2011).
253. D. S. CF Spraggs, LR Parham, SK McDonnell, LP Briley, KS King, E Rappold, and PE Goss, HLA-DQA1*02:01/DRB1*07:01 as a biomarker for lapatinib-induced hepatotoxicity: prospective confirmation in a large randomised clinical trial (TEACH, EGF105485) *Cancer research* **72**, (2012).
254. D. J. Schaid *et al.*, Prospective validation of HLA-DRB1*07:01 allele carriage as a predictive risk factor for lapatinib-induced liver injury. *Journal of clinical oncology : official journal of the American Society of Clinical Oncology* **32**, 2296 (Aug 1, 2014).
255. L. R. Parham *et al.*, Comprehensive genome-wide evaluation of lapatinib-induced liver injury yields a single genetic signal centered on known risk allele HLA-DRB1*07:01. *The pharmacogenomics journal*, (May 19, 2015).

256. P. M. O'Neill *et al.*, The effect of fluorine substitution on the metabolism and antimalarial activity of amodiaquine. *Journal of medicinal chemistry* **37**, 1362 (Apr 29, 1994).
257. N. E. Tayar, H. van de Waterbeemd, M. Gryllaki, B. Testa, W. F. Trager, The lipophilicity of deuterium atoms. A comparison of shake-flask and HPLC methods. *International Journal of Pharmaceutics* **19**, 271 (5//, 1984).
258. M. Turowski *et al.*, Deuterium isotope effects on hydrophobic interactions: the importance of dispersion interactions in the hydrophobic phase. *Journal of the American Chemical Society* **125**, 13836 (Nov 12, 2003).
259. C. L. Perrin, Y. Dong, Secondary deuterium isotope effects on the acidity of carboxylic acids and phenols. *Journal of the American Chemical Society* **129**, 4490 (Apr 11, 2007).
260. C. L. Perrin, B. K. Ohta, J. Kuperman, J. Liberman, M. Erdelyi, Stereochemistry of beta-deuterium isotope effects on amine basicity. *Journal of the American Chemical Society* **127**, 9641 (Jul 6, 2005).
261. G. T. Miwa, A. Y. Lu, Kinetic isotope effects and 'metabolic switching' in cytochrome P450-catalyzed reactions. *BioEssays : news and reviews in molecular, cellular and developmental biology* **7**, 215 (Nov, 1987).
262. A. Morales, in *46th Annual Meeting*. (Idsa, 2008).
263. A. E. Mutlib *et al.*, The species-dependent metabolism of efavirenz produces a nephrotoxic glutathione conjugate in rats. *Toxicology and applied pharmacology* **169**, 102 (Nov 15, 2000).
264. D. B. Northrop, Steady-state analysis of kinetic isotope effects in enzymic reactions. *Biochemistry* **14**, 2644 (Jun 17, 1975).
265. J. A. Krauser, F. P. Guengerich, Cytochrome P450 3A4-catalyzed testosterone 6beta-hydroxylation stereochemistry, kinetic deuterium isotope effects, and rate-limiting steps. *The Journal of biological chemistry* **280**, 19496 (May 20, 2005).
266. L. Shao, C. Abolin, M. C. Hewitt, P. Koch, M. Varney, Derivatives of tramadol for increased duration of effect. *Bioorganic & medicinal chemistry letters* **16**, 691 (Feb, 2006).
267. Y. L. Teo *et al.*, Effect of CYP3A4 inducer dexamethasone on hepatotoxicity of lapatinib: clinical and in vitro evidence. *Breast cancer research and treatment* **133**, 703 (Jun, 2012).
268. K. D. Hardy *et al.*, Studies on the role of metabolic activation in tyrosine kinase inhibitor-dependent hepatotoxicity: induction of CYP3A4 enhances the cytotoxicity of lapatinib in HepaRG cells. *Drug metabolism and disposition: the biological fate of chemicals* **42**, 162 (Jan, 2014).
269. D. A. Smith *et al.*, Effects of ketoconazole and carbamazepine on lapatinib pharmacokinetics in healthy subjects. *British journal of clinical pharmacology* **67**, 421 (Apr, 2009).
270. M. Ingelman-Sundberg, Genetic polymorphisms of cytochrome P450 2D6 (CYP2D6): clinical consequences, evolutionary aspects and functional diversity. *The pharmacogenomics journal* **5**, 6 (2005).
271. P. Kuehl *et al.*, Sequence diversity in CYP3A promoters and characterization of the genetic basis of polymorphic CYP3A5 expression. *Nature genetics* **27**, 383 (Apr, 2001).
272. D. Kniepeiss *et al.*, The role of CYP3A5 genotypes in dose requirements of tacrolimus and everolimus after heart transplantation. *Clinical transplantation* **25**, 146 (Jan-Feb, 2011).
273. H. de Jonge, L. Elens, H. de Loor, R. H. van Schaik, D. R. Kuypers, The CYP3A4*22 C>T single nucleotide polymorphism is associated with reduced midazolam and tacrolimus clearance in stable renal allograft recipients. *The pharmacogenomics journal* **15**, 144 (Apr, 2015).

274. L. C. Phua *et al.*, Investigation of the drug-drug interaction between alpha-lipoic acid and valproate via mitochondrial beta-oxidation. *Pharmaceutical research* **25**, 2639 (Nov, 2008).
275. R. Yuan, S. Madani, X. X. Wei, K. Reynolds, S. M. Huang, Evaluation of cytochrome P450 probe substrates commonly used by the pharmaceutical industry to study in vitro drug interactions. *Drug metabolism and disposition: the biological fate of chemicals* **30**, 1311 (Dec, 2002).
276. J. R. Kenny *et al.*, Drug-drug interaction potential of marketed oncology drugs: in vitro assessment of time-dependent cytochrome P450 inhibition, reactive metabolite formation and drug-drug interaction prediction. *Pharmaceutical research* **29**, 1960 (Jul, 2012).
277. E. Tseng *et al.*, Relative contributions of cytochrome CYP3A4 versus CYP3A5 for CYP3A-cleared drugs assessed in vitro using a CYP3A4-selective inactivator (CYP3cide). *Drug metabolism and disposition: the biological fate of chemicals* **42**, 1163 (Jul, 2014).
278. V. Uttamsingh *et al.*, Altering Metabolic Profiles of Drugs by Precision Deuteration: Reducing Mechanism-Based Inhibition of CYP2D6 by Paroxetine. *The Journal of pharmacology and experimental therapeutics* **354**, 43 (Jul, 2015).
279. M. D. Wahlin, University of Washington (2014).
280. A. J. Morgan, B. A. Pandya, C. E. Masse, S. L. Harbeson, Old Drugs Yield New Discoveries: Examples from the Prodrug, Chiral Switch, and Site-Selective Deuteration Strategies (Book Chapter). *Drug Repositioning*, 291 (2012).
281. G. E. Konecny *et al.*, Activity of the dual kinase inhibitor lapatinib (GW572016) against HER-2-overexpressing and trastuzumab-treated breast cancer cells. *Cancer research* **66**, 1630 (Feb 1, 2006).
282. P. W. Manley, F. Blasco, J. Mestan, R. Aichholz, The kinetic deuterium isotope effect as applied to metabolic deactivation of imatinib to the des-methyl metabolite, CGP74588. *Bioorganic & medicinal chemistry* **21**, 3231 (Jun 1, 2013).
283. G. K. Darland *et al.*, Oxidative and defluorinative metabolism of fludalanine, 2-2H-3-fluoro-D-alanine. *Drug metabolism and disposition: the biological fate of chemicals* **14**, 668 (Nov-Dec, 1986).
284. Y. Shirasaka *et al.*, Effect of CYP3A5 expression on the inhibition of CYP3A-catalyzed drug metabolism: impact on modeling CYP3A-mediated drug-drug interactions. *Drug metabolism and disposition: the biological fate of chemicals* **41**, 1566 (Aug, 2013).
285. Y. H. Wang, D. R. Jones, S. D. Hall, Differential mechanism-based inhibition of CYP3A4 and CYP3A5 by verapamil. *Drug metabolism and disposition: the biological fate of chemicals* **33**, 664 (May, 2005).
286. N. Hanioka *et al.*, Functional characterization of three human cytochrome p450 2E1 variants with amino acid substitutions. *Xenobiotica; the fate of foreign compounds in biological systems* **33**, 575 (Jun, 2003).
287. N. Hanioka, M. Yamamoto, T. Tanaka-Kagawa, H. Jinno, S. Narimatsu, Functional characterization of human cytochrome P4502E1 allelic variants: in vitro metabolism of benzene and toluene by recombinant enzymes expressed in yeast cells. *Archives of toxicology* **84**, 363 (May, 2010).
288. H. Kawai, H. Li, S. Avraham, S. Jiang, H. K. Avraham, Overexpression of histone deacetylase HDAC1 modulates breast cancer progression by negative regulation of estrogen receptor alpha. *International journal of cancer. Journal international du cancer* **107**, 353 (Nov 10, 2003).
289. L. C. Dorssers *et al.*, Tamoxifen resistance in breast cancer: elucidating mechanisms. *Drugs* **61**, 1721 (2001).

290. A. J. Wood, C. K. Osborne, Tamoxifen in the treatment of breast cancer. *New England Journal of Medicine* **339**, 1609 (1998).
291. B. Fisher *et al.*, Tamoxifen for the prevention of breast cancer: current status of the National Surgical Adjuvant Breast and Bowel Project P-1 study. *J Natl Cancer Inst* **97**, 1652 (2005).
292. Early Breast Cancer Trialists' Collaborative Group. Effects of chemotherapy and hormonal therapy for early breast cancer on recurrence and 15-year survival: an overview of the randomised trials. *Lancet* **365**, 1687 (May 14-20, 2005).
293. S. Borges *et al.*, Quantitative effect of CYP2D6 genotype and inhibitors on tamoxifen metabolism: implication for optimization of breast cancer treatment. *Clinical pharmacology and therapeutics* **80**, 61 (Jul, 2006).
294. W. J. Lu *et al.*, The tamoxifen metabolite norendoxifen is a potent and selective inhibitor of aromatase (CYP19) and a potential lead compound for novel therapeutic agents. *Breast cancer research and treatment* **133**, 99 (May, 2012).
295. M. D. Johnson *et al.*, Pharmacological characterization of 4-hydroxy-N-desmethyl tamoxifen, a novel active metabolite of tamoxifen. *Breast cancer research and treatment* **85**, 151 (May, 2004).
296. M. Giuliano, M. V. Trivedi, R. Schiff, Bidirectional Crosstalk between the Estrogen Receptor and Human Epidermal Growth Factor Receptor 2 Signaling Pathways in Breast Cancer: Molecular Basis and Clinical Implications. *Breast care (Basel, Switzerland)* **8**, 256 (Aug, 2013).
297. W. Lv, J. Liu, D. Lu, D. A. Flockhart, M. Cushman, Synthesis of mixed (E,Z)-, (E)-, and (Z)-norendoxifen with dual aromatase inhibitory and estrogen receptor modulatory activities. *J Med Chem* **56**, 4611 (Jun 13, 2013).
298. X. Wu *et al.*, The tamoxifen metabolite, endoxifen, is a potent antiestrogen that targets estrogen receptor alpha for degradation in breast cancer cells. *Cancer research* **69**, 1722 (Mar 1, 2009).
299. N. Fleeman *et al.*, The clinical effectiveness and cost-effectiveness of genotyping for CYP2D6 for the management of women with breast cancer treated with tamoxifen: a systematic review. *Health Technology Assessment* **15**, (2011).
300. D. L. Holliday, V. Speirs, Choosing the right cell line for breast cancer research. *Breast cancer research : BCR* **13**, 215 (2011).
301. P. Eroles, A. Bosch, J. A. Perez-Fidalgo, A. Lluch, Molecular biology in breast cancer: intrinsic subtypes and signaling pathways. *Cancer treatment reviews* **38**, 698 (Oct, 2012).
302. Effects of chemotherapy and hormonal therapy for early breast cancer on recurrence and 15-year survival: an overview of the randomised trials. *Lancet* **365**, 1687 (May 14-20, 2005).
303. A. Ring, M. Dowsett, Mechanisms of tamoxifen resistance. *Endocrine-related cancer* **11**, 643 (2004).
304. A. F. Leary *et al.*, Lapatinib restores hormone sensitivity with differential effects on estrogen receptor signaling in cell models of human epidermal growth factor receptor 2-negative breast cancer with acquired endocrine resistance. *Clinical cancer research : an official journal of the American Association for Cancer Research* **16**, 1486 (Mar 1, 2010).
305. J. Shou *et al.*, Mechanisms of tamoxifen resistance: increased estrogen receptor-HER2/neu cross-talk in ER/HER2-positive breast cancer. *Journal of the National Cancer Institute* **96**, 926 (Jun 16, 2004).
306. I. Chu, K. Blackwell, S. Chen, J. Slingerland, The dual ErbB1/ErbB2 inhibitor, lapatinib (GW572016), cooperates with tamoxifen to inhibit both

cell proliferation- and estrogen-dependent gene expression in antiestrogen-resistant breast cancer. *Cancer research* **65**, 18 (Jan 1, 2005).
307. S. Kato *et al.*, Activation of the estrogen receptor through phosphorylation by mitogen-activated protein kinase. *Science* **270**, 1491 (Dec 1, 1995).
308. A. S. Clark, K. West, S. Streicher, P. A. Dennis, Constitutive and inducible Akt activity promotes resistance to chemotherapy, trastuzumab, or tamoxifen in breast cancer cells. *Molecular cancer therapeutics* **1**, 707 (Jul, 2002).
309. C. J. Creighton *et al.*, Activation of mitogen-activated protein kinase in estrogen receptor alpha-positive breast cancer cells in vitro induces an in vivo molecular phenotype of estrogen receptor alpha-negative human breast tumors. *Cancer research* **66**, 3903 (Apr 1, 2006).
310. S. Guo, G. E. Sonenshein, Forkhead box transcription factor FOXO3a regulates estrogen receptor alpha expression and is repressed by the Her-2/neu/phosphatidylinositol 3-kinase/Akt signaling pathway. *Molecular and cellular biology* **24**, 8681 (Oct, 2004).
311. J. W. Polli *et al.*, The role of efflux and uptake transporters in [N-{3-chloro-4-[(3-fluorobenzyl)oxy]phenyl}-6-[5-({[2-(methylsulfonyl)ethyl]amino }methyl)-2-furyl]-4-quinazolinamine (GW572016, lapatinib) disposition and drug interactions. *Drug metabolism and disposition: the biological fate of chemicals* **36**, 695 (Apr, 2008).
312. D. Iusuf *et al.*, P-glycoprotein (ABCB1) transports the primary active tamoxifen metabolites endoxifen and 4-hydroxytamoxifen and restricts their brain penetration. *The Journal of pharmacology and experimental therapeutics* **337**, 710 (Jun, 2011).
313. W. A. Teft, S. E. Mansell, R. B. Kim, Endoxifen, the active metabolite of tamoxifen, is a substrate of the efflux transporter P-glycoprotein (multidrug resistance 1). *Drug metabolism and disposition: the biological fate of chemicals* **39**, 558 (Mar, 2011).
314. M. M. Gottesman, I. Pastan, Biochemistry of multidrug resistance mediated by the multidrug transporter. *Annual review of biochemistry* **62**, 385 (1993).
315. U. L. Larsen *et al.*, Human intestinal P-glycoprotein activity estimated by the model substrate digoxin. *Scandinavian journal of clinical and laboratory investigation* **67**, 123 (2007).
316. D. Hochhauser, A. L. Harris, Drug resistance. *British medical bulletin* **47**, 178 (Jan, 1991).
317. E. Mechetner *et al.*, Levels of multidrug resistance (MDR1) P-glycoprotein expression by human breast cancer correlate with in vitro resistance to taxol and doxorubicin. *Clinical cancer research : an official journal of the American Association for Cancer Research* **4**, 389 (Feb, 1998).
318. B. J. Trock, F. Leonessa, R. Clarke, Multidrug resistance in breast cancer: a meta-analysis of MDR1/gp170 expression and its possible functional significance. *Journal of the National Cancer Institute* **89**, 917 (Jul 2, 1997).
319. J. Schneider *et al.*, P-glycoprotein, HER-2/neu, and mutant p53 expression in human gynecologic tumors. *Journal of the National Cancer Institute* **86**, 850 (Jun 1, 1994).
320. S. C. Linn *et al.*, Prognostic relevance of P-glycoprotein expression in breast cancer. *Annals of oncology : official journal of the European Society for Medical Oncology / ESMO* **6**, 679 (Sep, 1995).
321. S. R. Johnston *et al.*, Acquired tamoxifen resistance in human breast cancer and reduced intra-tumoral drug concentration. *Lancet* **342**, 1521 (Dec 18-25, 1993).
322. V. Ling, Multidrug resistance: molecular mechanisms and clinical relevance. *Cancer chemotherapy and pharmacology* **40 Suppl**, S3 (1997).

323. J. R. Molina *et al.*, Evaluation of lapatinib and topotecan combination therapy: tissue culture, murine xenograft, and phase I clinical trial data. *Clinical cancer research : an official journal of the American Association for Cancer Research* **14**, 7900 (Dec 1, 2008).
324. S. Y. Chun, Y. S. Kwon, K. S. Nam, S. Kim, Lapatinib enhances the cytotoxic effects of doxorubicin in MCF-7 tumorspheres by inhibiting the drug efflux function of ABC transporters. *Biomedicine & pharmacotherapy = Biomedecine & pharmacotherapie* **72**, 37 (May, 2015).
325. M. F. Fromm, Importance of P-glycoprotein at blood-tissue barriers. *Trends in pharmacological sciences* **25**, 423 (Aug, 2004).
326. B. C. Pestalozzi, Brain metastases and subtypes of breast cancer. *Annals of oncology : official journal of the European Society for Medical Oncology / ESMO* **20**, 803 (May, 2009).
327. P. S. Ong, X. Q. Wang, H. S. Lin, S. Y. Chan, P. C. Ho, Synergistic effects of suberoylanilide hydroxamic acid combined with cisplatin causing cell cycle arrest independent apoptosis in platinum-resistant ovarian cancer cells. *International journal of oncology* **40**, 1705 (May, 2012).
328. T. C. Chou, P. Talalay, Quantitative analysis of dose-effect relationships: the combined effects of multiple drugs or enzyme inhibitors. *Advances in enzyme regulation* **22**, 27 (1984).
329. T. C. Chou, Theoretical basis, experimental design, and computerized simulation of synergism and antagonism in drug combination studies. *Pharmacological reviews* **58**, 621 (Sep, 2006).
330. J. M. Knowlden *et al.*, Elevated levels of epidermal growth factor receptor/c-erbB2 heterodimers mediate an autocrine growth regulatory pathway in tamoxifen-resistant MCF-7 cells. *Endocrinology* **144**, 1032 (Mar, 2003).
331. C. Warburton *et al.*, Treatment of HER-2/neu overexpressing breast cancer xenograft models with trastuzumab (Herceptin) and gefitinib (ZD1839): drug combination effects on tumor growth, HER-2/neu and epidermal growth factor receptor expression, and viable hypoxic cell fraction. *Clinical cancer research : an official journal of the American Association for Cancer Research* **10**, 2512 (Apr 1, 2004).
332. D. A. Lannigan, Estrogen receptor phosphorylation. *Steroids* **68**, 1 (Jan, 2003).
333. R. Schiff, S. Massarweh, J. Shou, C. K. Osborne, Breast cancer endocrine resistance: how growth factor signaling and estrogen receptor coregulators modulate response. *Clinical cancer research : an official journal of the American Association for Cancer Research* **9**, 447S (Jan, 2003).
334. R. Garcia-Becerra, N. Santos, L. Diaz, J. Camacho, Mechanisms of Resistance to Endocrine Therapy in Breast Cancer: Focus on Signaling Pathways, miRNAs and Genetically Based Resistance. *International journal of molecular sciences* **14**, 108 (2012).
335. B. Kaufman *et al.*, Trastuzumab plus anastrozole versus anastrozole alone for the treatment of postmenopausal women with human epidermal growth factor receptor 2-positive, hormone receptor-positive metastatic breast cancer: results from the randomized phase III TAnDEM study. *Journal of clinical oncology : official journal of the American Society of Clinical Oncology* **27**, 5529 (Nov 20, 2009).
336. P. Fumoleau *et al.*, A phase I pharmacokinetics study of lapatinib and tamoxifen in metastatic breast cancer (EORTC 10053 Lapatam study). *Breast* **23**, 663 (Oct, 2014).
337. D. J. Klein *et al.*, PharmGKB summary: tamoxifen pathway, pharmacokinetics. *Pharmacogenetics and genomics* **23**, 643 (Nov, 2013).

338. V. Stearns *et al.*, Active tamoxifen metabolite plasma concentrations after coadministration of tamoxifen and the selective serotonin reuptake inhibitor paroxetine. *J Natl Cancer Inst* **95**, 1758 (2003).
339. R. I. Sharma, A. E. Welch, L. Schweiger, S. Craib, T. A. Smith, [F]fluoro-2-deoxy-d-glucose incorporation by mcf-7 breast tumour cells in vitro is modulated by treatment with tamoxifen, Doxorubicin, and docetaxel: relationship to chemotherapy-induced changes in ATP content, hexokinase activity, and glucose transport. *International journal of molecular imaging* **2011**, 874585 (2011).
340. S. Ropero *et al.*, Trastuzumab plus tamoxifen: anti-proliferative and molecular interactions in breast carcinoma. *Breast cancer research and treatment* **86**, 125 (Jul, 2004).
341. C. C. Benz *et al.*, Estrogen-dependent, tamoxifen-resistant tumorigenic growth of MCF-7 cells transfected with HER2/neu. *Breast cancer research and treatment* **24**, 85 (1992).
342. J. P. Guo *et al.*, IKKepsilon phosphorylation of estrogen receptor alpha Ser-167 and contribution to tamoxifen resistance in breast cancer. *The Journal of biological chemistry* **285**, 3676 (Feb 5, 2010).
343. S. Pancholi *et al.*, ERBB2 influences the subcellular localization of the estrogen receptor in tamoxifen-resistant MCF-7 cells leading to the activation of AKT and RPS6KA2. *Endocrine-related cancer* **15**, 985 (Dec, 2008).
344. V. S. Likhite, F. Stossi, K. Kim, B. S. Katzenellenbogen, J. A. Katzenellenbogen, Kinase-specific phosphorylation of the estrogen receptor changes receptor interactions with ligand, deoxyribonucleic acid, and coregulators associated with alterations in estrogen and tamoxifen activity. *Molecular endocrinology (Baltimore, Md.)* **20**, 3120 (Dec, 2006).
345. P. B. Joel, A. M. Traish, D. A. Lannigan, Estradiol-induced phosphorylation of serine 118 in the estrogen receptor is independent of p42/p44 mitogen-activated protein kinase. *The Journal of biological chemistry* **273**, 13317 (May 22, 1998).
346. A. L. Wijayaratne, D. P. McDonnell, The human estrogen receptor-alpha is a ubiquitinated protein whose stability is affected differentially by agonists, antagonists, and selective estrogen receptor modulators. *The Journal of biological chemistry* **276**, 35684 (Sep 21, 2001).
347. J. Grisouard, S. Medunjanin, A. Hermani, A. Shukla, D. Mayer, Glycogen synthase kinase-3 protects estrogen receptor alpha from proteasomal degradation and is required for full transcriptional activity of the receptor. *Molecular endocrinology (Baltimore, Md.)* **21**, 2427 (Oct, 2007).
348. M. Scaltriti *et al.*, Lapatinib, a HER2 tyrosine kinase inhibitor, induces stabilization and accumulation of HER2 and potentiates trastuzumab-dependent cell cytotoxicity. *Oncogene* **28**, 803 (Feb 12, 2009).
349. W. C. Huang, Y. J. Chen, M. C. Yu, Y. L. Wei, M. H. Yeh, P02.07OFF-TARGET ACTIVITY OF LAPATINIB SENSITIZES TRIPLE-NEGATIVE BREAST CANCER CELLS TO PROTEASOME INHIBITORS THROUGH ACTIVATION OF NF-κB IN A SFK-DEPENDENT MANNER. *Annals of Oncology* **24**, i22 (March 1, 2013, 2013).
350. B. Lim, N. G. Dolloff, J. E. Allen, D. T. Dicker, W. S. El-Deiry, Abstract 2943: Lapatinib restores TRAIL-mediated apoptosis in TRAIL-resistant Triple Negative Breast Cancer (TNBC) through an off-target strategy that appears to be independent of increased death receptor expression. *Cancer research* **73**, 2943 (April 15, 2013, 2013).
351. Y. J. Chen *et al.*, Lapatinib-induced NF-kappaB activation sensitizes triple-negative breast cancer cells to proteasome inhibitors. *Breast cancer research : BCR* **15**, R108 (2013).

352. R. de Leeuw, J. Neefjes, R. Michalides, A role for estrogen receptor phosphorylation in the resistance to tamoxifen. *International journal of breast cancer* **2011**, 232435 (2011).
353. T. T. Duplessis, C. C. Williams, S. M. Hill, B. G. Rowan, Phosphorylation of Estrogen Receptor alpha at serine 118 directs recruitment of promoter complexes and gene-specific transcription. *Endocrinology* **152**, 2517 (Jun, 2011).
354. Y. Sambuy *et al.*, The Caco-2 cell line as a model of the intestinal barrier: influence of cell and culture-related factors on Caco-2 cell functional characteristics. *Cell biology and toxicology* **21**, 1 (Jan, 2005).
355. K. Kuteykin-Teplyakov, C. Luna-Tortos, K. Ambroziak, W. Loscher, Differences in the expression of endogenous efflux transporters in MDR1-transfected versus wildtype cell lines affect P-glycoprotein mediated drug transport. *British journal of pharmacology* **160**, 1453 (Jul, 2010).
356. D. Gartzke, G. Fricker, Establishment of optimized MDCK cell lines for reliable efflux transport studies. *Journal of pharmaceutical sciences* **103**, 1298 (Apr, 2014).
357. H. Glavinas *et al.*, Utilization of membrane vesicle preparations to study drug-ABC transporter interactions. *Expert opinion on drug metabolism & toxicology* **4**, 721 (Jun, 2008).
358. J. Rautio *et al.*, In vitro p-glycoprotein inhibition assays for assessment of clinical drug interaction potential of new drug candidates: a recommendation for probe substrates. *Drug metabolism and disposition: the biological fate of chemicals* **34**, 786 (May, 2006).
359. A. Saleem *et al.*, Lapatinib access into normal brain and brain metastases in patients with Her-2 overexpressing breast cancer. *EJNMMI research* **5**, 30 (2015).
360. C. Frankel, F. M. Palmieri, Lapatinib side-effect management. *Clinical journal of oncology nursing* **14**, 223 (Apr, 2010).
361. A. M. Storniolo *et al.*, Phase I dose escalation and pharmacokinetic study of lapatinib in combination with trastuzumab in patients with advanced ErbB2-positive breast cancer. *Journal of clinical oncology : official journal of the American Society of Clinical Oncology* **26**, 3317 (Jul 10, 2008).
362. Q. S. Chu *et al.*, A phase I and pharmacokinetic study of lapatinib in combination with letrozole in patients with advanced cancer. *Clinical cancer research : an official journal of the American Association for Cancer Research* **14**, 4484 (Jul 15, 2008).
363. W. J. Irvin, Jr. *et al.*, Genotype-guided tamoxifen dosing increases active metabolite exposure in women with reduced CYP2D6 metabolism: a multicenter study. *Journal of clinical oncology : official journal of the American Society of Clinical Oncology* **29**, 3232 (Aug 20, 2011).
364. A. Ahmad *et al.*, Endoxifen, a new cornerstone of breast cancer therapy: demonstration of safety, tolerability, and systemic bioavailability in healthy human subjects. *Clinical pharmacology and therapeutics* **88**, 814 (Dec, 2010).
365. J. M. Reid *et al.*, Abstract 4631: Pharmacokinetics and in vivo metabolism of Z-endoxifen: Results from two phase I studies in women with ER+ breast cancer, gynecologic malignancies and desmoids. *Cancer research* **74**, 4631 (October 1, 2014, 2014).
366. M. Goetz *et al.*, Abstract PD3-4: A first-in-human phase I study of the tamoxifen (TAM) metabolite, Z-endoxifen hydrochloride (Z-Endx) in women with aromatase inhibitor (AI) refractory metastatic breast cancer (MBC) (NCT01327781). *Cancer research* **73**, PD3 (December 15, 2013, 2013).

367. E. A. Lien, E. Solheim, P. M. Ueland, Distribution of tamoxifen and its metabolites in rat and human tissues during steady-state treatment. *Cancer research* **51**, 4837 (Sep 15, 1991).
368. J. MacCallum, J. Cummings, J. M. Dixon, W. R. Miller, Concentrations of tamoxifen and its major metabolites in hormone responsive and resistant breast tumours. *British journal of cancer* **82**, 1629 (May, 2000).
369. Endoxifen Shows Promise in Breast Cancer. *Cancer Discovery*, (January 9, 2014, 2014).
370. A. Gingery *et al.*, The effects of a novel hormonal breast cancer therapy, endoxifen, on the mouse skeleton. *PloS one* **9**, e98219 (2014).
371. W. Lu *et al.*, in *American Association of Pharmaceutical Scientists Annual Meeting and Exposition*. (2012).
372. E. R. Trosken, K. Fischer, W. Volkel, W. K. Lutz, Inhibition of human CYP19 by azoles used as antifungal agents and aromatase inhibitors, using a new LC-MS/MS method for the analysis of estradiol product formation. *Toxicology* **219**, 33 (Feb 15, 2006).
373. K. M. Schweikart *et al.*, Comparative Uterotrophic Effects of Endoxifen and Tamoxifen in Ovariectomized Sprague-Dawley Rats. *Toxicologic pathology*, (Mar 26, 2014).
374. S. Y. Kim, N. Suzuki, Y. R. Laxmi, S. Shibutani, Genotoxic mechanism of tamoxifen in developing endometrial cancer. *Drug metabolism reviews* **36**, 199 (May, 2004).

Appendices

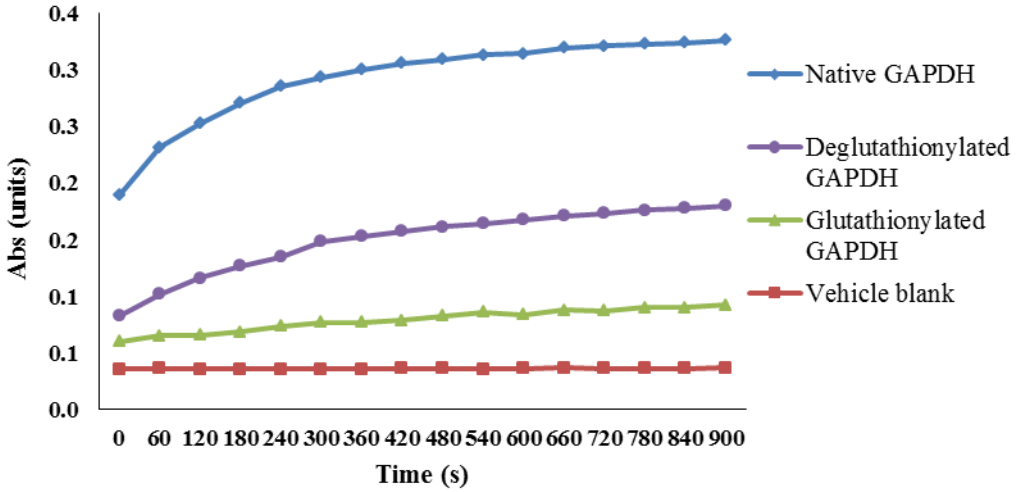

Figure S1 Indirect monitoring of GAPDH glutathionylation and deglutathionylation using DTT as a chemical reductant based on GADPH activity.

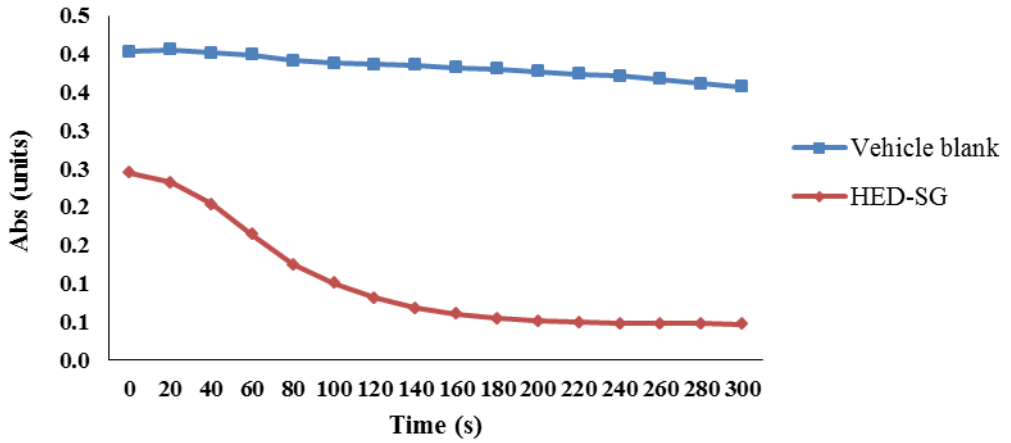

Figure S2 Direct monitoring of HED-SG deglutathionylation based on NADPH consumption.

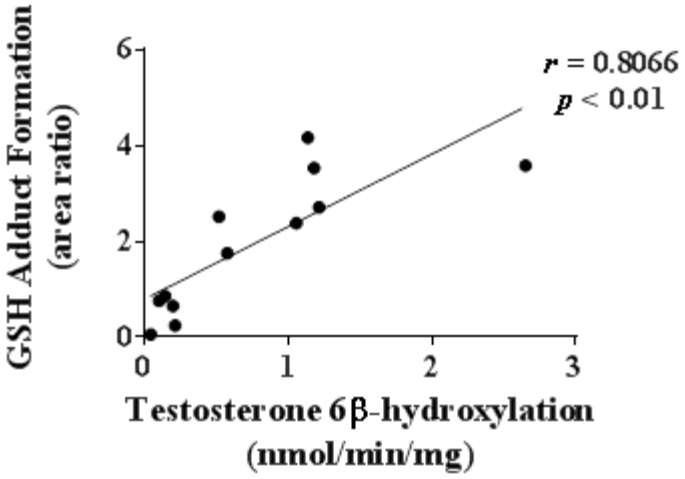

Figure S3 Correlation between GSH adduct formation and baseline CYP3A4/5 activity where the outlier (donor H0331) is included.

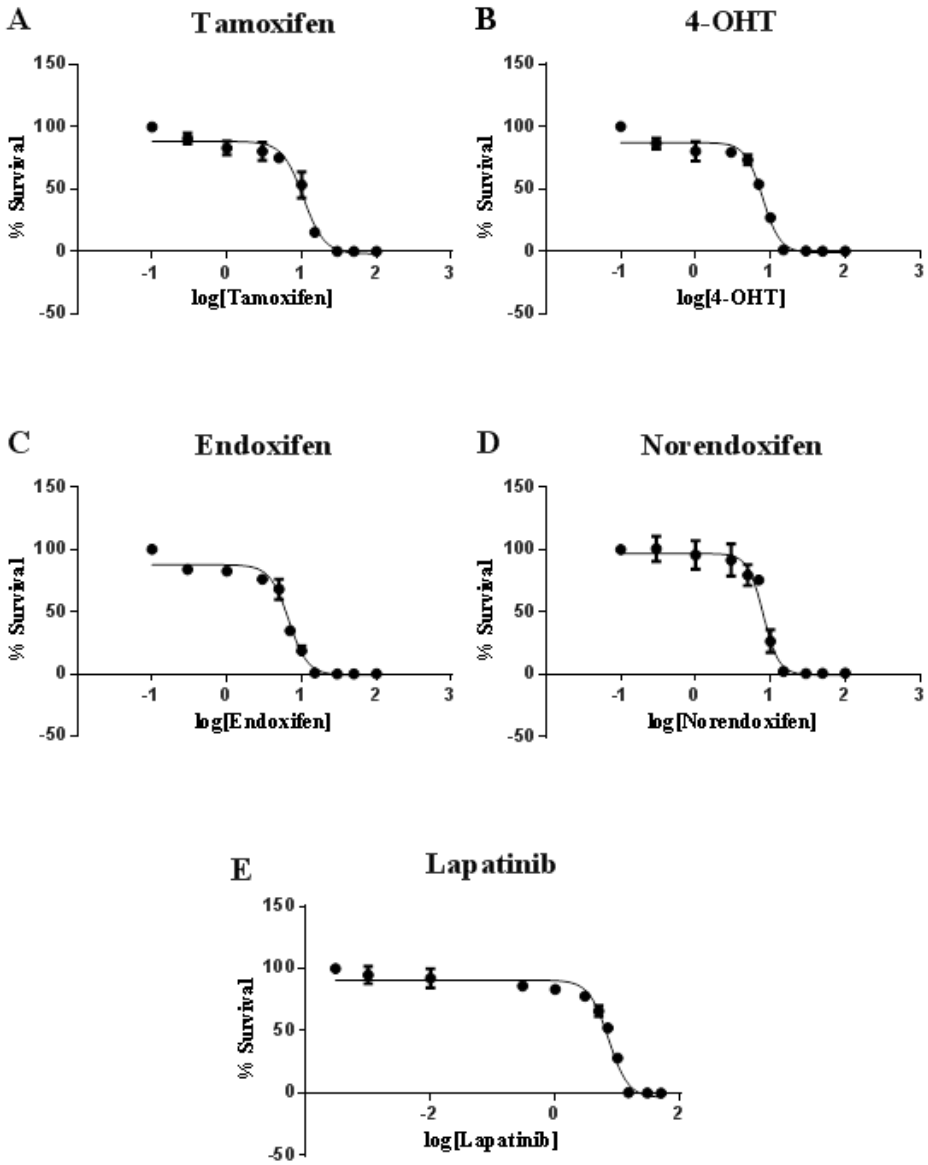

Figure S4 The cytotoxicity effect of (A) tamoxifen, (B) 4-OHT, (C) endoxifen, (D) norendoxifen, and (E) lapatinib against MCF-7 cells. Each data point is the average of at least 2 independent experiments with at least 5 replicates each.

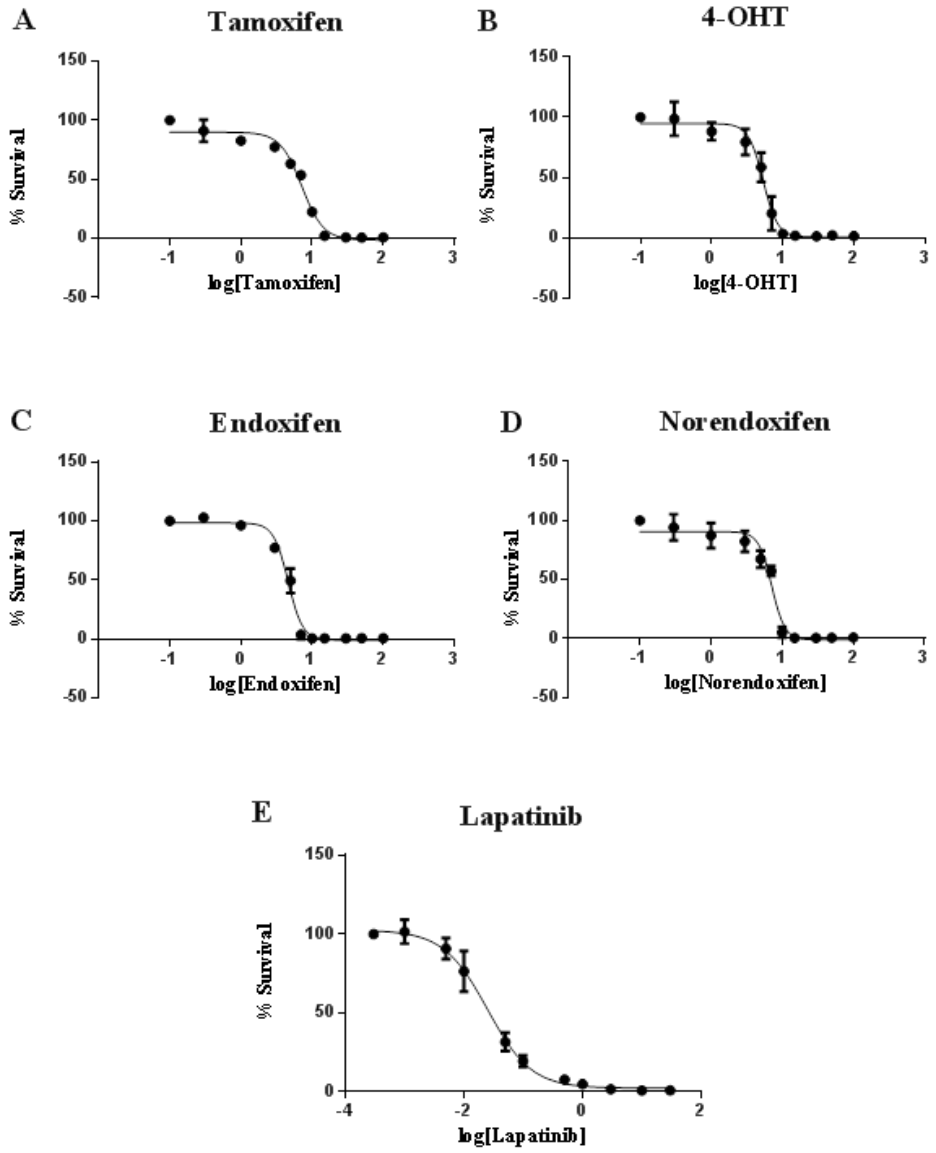

Figure S5 The cytotoxicity effect of (A) tamoxifen, (B) 4-OHT, (C) endoxifen, (D) norendoxifen, and (E) lapatinib against BT474 cells. Each data point is the average of at least 2 independent experiments with at least 5 replicates each.

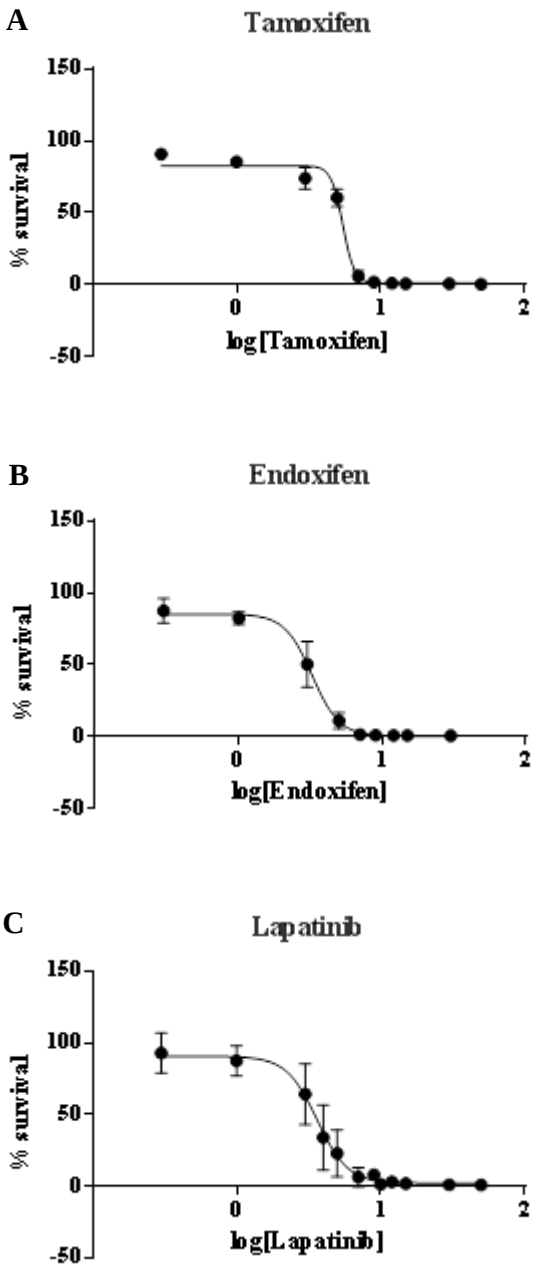

Figure S6 The cytotoxicity effect of (A) tamoxifen, (B) endoxifen and (C) lapatinib against MCF-7 cells. Each data point is the average of at least 2 independent experiments with at least 5 replicates each.

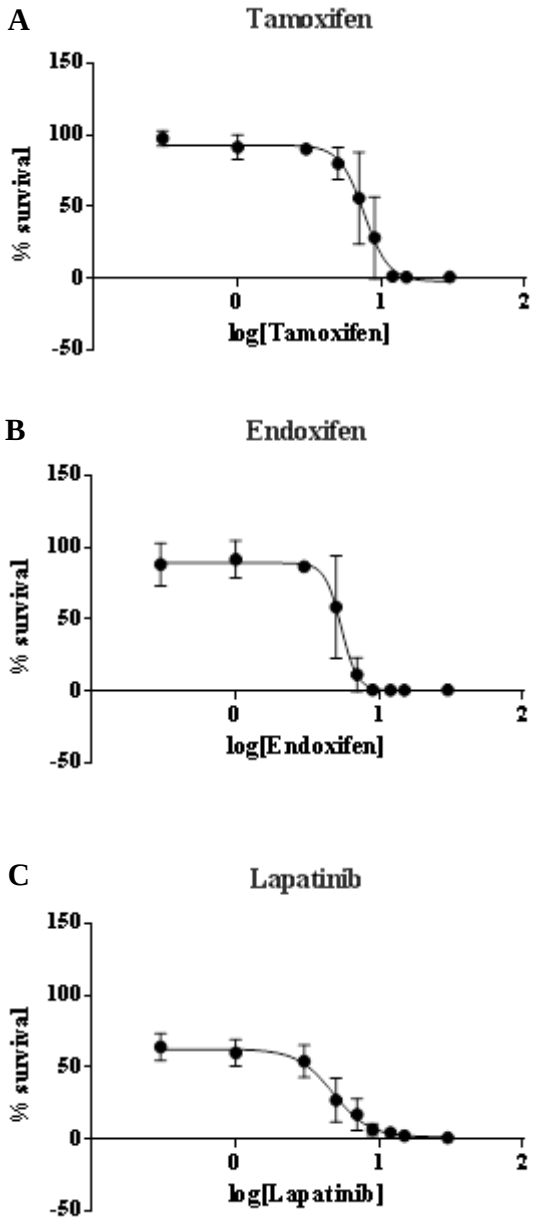

Figure S7 The cytotoxicity effect of (A) tamoxifen, (B) endoxifen and (C) lapatinib against TAM-R cells. Each data point is the average of at least 2 independent experiments with at least 5 replicates each.

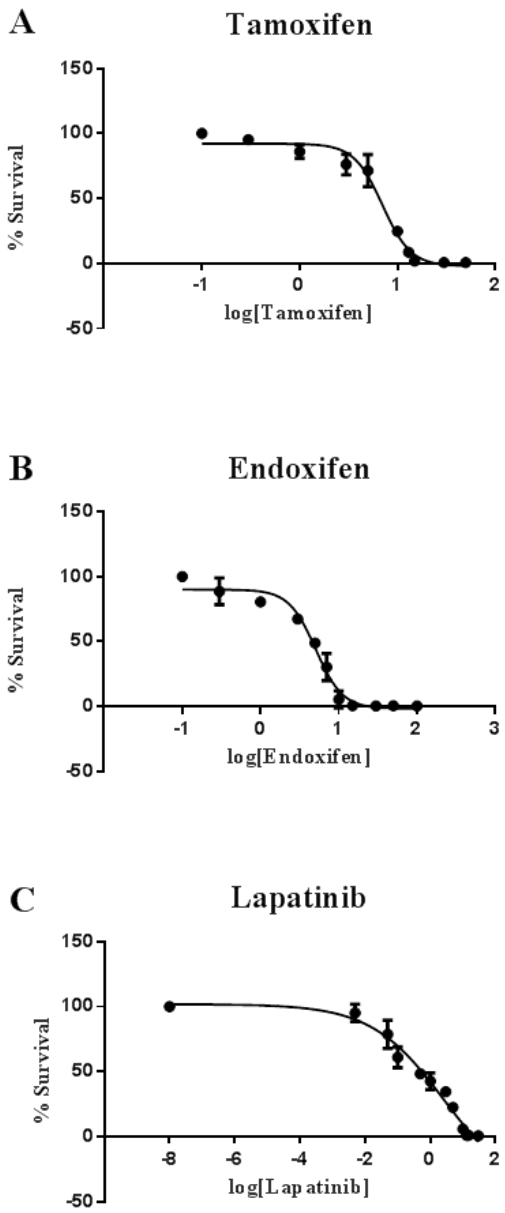

Figure S8 The cytotoxicity effect of (A) tamoxifen, (B) endoxifen and (C) lapatinib against MCF-7/HER2 cells. Each data point is the average of at least 2 independent experiments with at least 5 replicates each.

Table S1 List of proteins found to be glutathionylated by APAP in at least 1 time-point as determined by H:L fold-change threshold greater than 1.5.

Accession	Description	Gene symbol	Peptide
Q04446	1,4-alpha-glucan-branching enzyme	GLGB	CADGGLYCK CIAYAESHDQALVGDK HFTCNVLPR
Q15029	116 kDa U5 small nuclear ribonucleoprotein component	U5S1	VEESGEHVILGTGELYLDCVMHDLR
P31946	14-3-3 protein beta/alpha	1433B	IEAELQDICNDVLELLDK
Q04917	14-3-3 protein eta	1433F	NCNDFQYESK
P27348	14-3-3 protein theta	1433T	SICTTVLELLDK YLAEVACGDDR
P15428	15-hydroxyprostaglandin dehydrogenase [NAD(+)]	PGDH	TLFIQCDVADQQQLR
O14756	17-beta-hydroxysteroid dehydrogenase type 6	H17B6	VLAACLTEK
P09543	2',3'-cyclic-nucleotide 3'-phosphodiesterase	CN37	LDEDLAAYCR
Q16698	2,4-dienoyl-CoA reductase, mitochondrial	DECR	VHAIQCDVRDPDMVQNTVSELIK
P62333	26S protease regulatory subunit 10B	PRS10	AVASQLDCNFLK
P62191	26S protease regulatory subunit 4	PRS4	AICTEAGLMALR
Q99460	26S proteasome non-ATPase regulatory subunit 1	PSMD1	QCVENADLPEGEK MEEADALIESLCR
O00232	26S proteasome non-ATPase regulatory subunit 12	PSD12	AIYDTPCIQAESEK
Q9UNM6	26S proteasome non-ATPase regulatory subunit 13	PSD13	FLGCVDIK
Q16401	26S proteasome non-ATPase regulatory subunit 5	PSMD5	FFGNLAVMDSPQQICER TTLCVSILER
Q15008	26S proteasome non-ATPase regulatory subunit 6	PSMD6	VYQGLYCVAIR
Q9Y2R5	28S ribosomal protein S17, mitochondrial	RT17	TYFAHDALQQCTVGDIVLLR
Q96EL2	28S ribosomal protein S24, mitochondrial	RT24	GNQLEICAVVLR
P82933	28S ribosomal protein S9, mitochondrial	RT09	LLTSQCGAAEEEFVQR
Q02218	2-oxoglutarate dehydrogenase, mitochondrial	ODO1	DVVVDLVCYR CSTPGNFFHVLR
Q9ULD0	2-oxoglutarate dehydrogenase-like, mitochondrial	OGDHL	DVVVDLVCYR
P12694	2-oxoisovalerate dehydrogenase subunit alpha, mitochondrial	ODBA	DYPLELFMAQCYGNISDLGK
P21953	2-oxoisovalerate dehydrogenase subunit beta, mitochondrial	ODBB	GLLLSCIEDK TIIPWDVDTICK
P31937	3-hydroxyisobutyrate dehydrogenase, mitochondrial	3HIDH	HGYPLIIYDVFPDACK
P25398	40S ribosomal protein S12	RS12	LVEALCAEHQINLIK QAHLCVLASNCDEPMYVK
P15880	40S ribosomal protein S2	RS2	AGIDDCYTSAR
P63220	40S ribosomal protein S21	RS21	TYAICGAIR
P23396	40S ribosomal protein S3	RS3	GLCAIAQAESLR GCEVVVSGK ACYGVLR
P61247	40S ribosomal protein S3a	RS3A	LFCVGFTK
P62701	40S ribosomal protein S4, X isoform	RS4X	ECLPLIIFLR ECLPLIIF
P62753	40S ribosomal protein S6	RS6	LNISFPATGCQK
P62241	40S ribosomal protein S8	RS8	LDVGNFSWGSECCTR NCIVLIDSTPYR
P80404	4-aminobutyrate aminotransferase, mitochondrial	GABT	CLEEVEDLIVK
P49189	4-trimethylaminobutyraldehyde dehydrogenase	AL9A1	SPLIIFSDCDMNNAVK TVCVEMGDVESAF
P10809	60 kDa heat shock protein, mitochondrial	CH60	CEFQDAYVLLSEK AAVEEGIVLGGGCALLR
P10155	60 kDa SS-A/Ro ribonucleoprotein	RO60	GMLDMCGFDTGALDVIR
P05388	60S acidic ribosomal protein P0	RLA0	AGAIAPCEVTVPAQNTGLGPEK NVASVCLQIGYPTVASVPH CFIVGADNVGSK
P27635	60S ribosomal protein L10	RL10	MLSCAGADR
P62906	60S ribosomal protein L10a	RL10A	VLCLAVAVGH VLCLAVAVGHVK
P30050	60S ribosomal protein L12	RL12	CTGGEVGATSALAPK

Accession	Description	Gene symbol	Peptide
P50914	60S ribosomal protein L14	RL14	ALVDGPCTQVR
P62829	60S ribosomal protein L23	RL23	ISLGLPVGAVINCADNTGAK
P39023	60S ribosomal protein L3	RL3	VACIGAWHPAR TVFAEHISDECK YCQVIR
P62910	60S ribosomal protein L32	RL32	ELEVLLMCNK
Q969Q0	60S ribosomal protein L36a-like	RL36L	LECVEPNCR
P36578	60S ribosomal protein L4	RL4	SGQGAFGNMCR GPCIIYNEDNGIIK
P46777	60S ribosomal protein L5	RL5	IEGDMIVCAAYAHELPK VGLTNYAAAYCTGLLLAR AAAYCTGLLLAR DIICQIAY
P62424	60S ribosomal protein L7a	RL7A	TCTTVAFTQVNSEDK
P62917	60S ribosomal protein L8	RL8	AQLNIGNVLPVGTMPEGTIVCCLEE KPGDR
P52209	6-phosphogluconate dehydrogenase, decarboxylating	6PGD	SAVENCQDSWR MVHNGIEYGDMQLICEAYHLMK
Q9BWD1	Acetyl-CoA acetyltransferase, cytosolic	THIC	IGEMPLTDSILCDGLTDAFHNCHM GITAENVAK
Q9NR19	Acetyl-coenzyme A synthetase, cytoplasmic	ACSA	GATTNICYNVLDR
Q99798	Aconitate hydratase, mitochondrial	ACON	CTTDHISAAGPWLK
P60709	Actin, cytoplasmic 1	ACTB	DDDIAALVVDNGSGMCK
P63261	Actin, cytoplasmic 2	ACTG	EEEIAALVIDNGSGMCK
O96019	Actin-like protein 6A	ACL6A	SPLAGDFITMQCR AGYAGEDCPK
P59998	Actin-related protein 42065 complex subunit 4	ARPC4	ATLQAALCLENFSSQVVER
P61158	Actin-related protein 3	ARP3	TLTGTVIDSGDGVTHVIPVAEGYVI GSCIK
O95433	Activator of 90 kDa heat shock protein ATPase homolog 1	AHSA1	NGETELCMEGR
Q96CM8	Acyl-CoA synthetase family member 2, mitochondrial	ACSF2	TVGQCLETTAQR
Q08AH3	Acyl-coenzyme A synthetase ACSM2A, mitochondrial	ACS2A	ELSENSQQAANVLSGACGLQR
Q53FZ2	Acyl-coenzyme A synthetase ACSM3, mitochondrial	ACSM3	ANCIITNDVLAPAVDAVASK
O95372	Acyl-protein thioesterase 2	LYPA2	DLAILQCHGELDPMVPVR
P07741	Adenine phosphoribosyltransferase	APT	LQAEVLECVSLVELTSLK
P23526	Adenosylhomocysteinase	SAHH	QAQYLGMSCDGPFKPDHYR
P54819	Adenylate kinase 2, mitochondrial	KAD2	LAENFCVCHLATGDMLR
Q01518	Adenylyl cyclase-associated protein 1	CAP1	CVNTTLQIK INSITVDNCK
P12235	ADP/ATP translocase 1	ADT1	QYKGIIDCVVR
P05141	ADP/ATP translocase 2	ADT2	QYKGIIDCVVR
O43488	Aflatoxin B1 aldehyde reductase member 2	ARK72	LQCPQVDLFYLHAPDHGTPVEETL HACQR
P07327	Alcohol dehydrogenase 1A	ADH1A	NPESNYCLK
P00325	Alcohol dehydrogenase 1B	ADH1B	MVAVGICR NPESNYCLK
P00326	Alcohol dehydrogenase 1C	ADH1G	NPESNYCLK
P08319	Alcohol dehydrogenase 4	ADH4	ALGATDCLNPR
Q06278	Aldehyde oxidase	AOXA	IPAICDMPTELHIALLPPSQNSNTLY SSK NLIQCWR TAEHLSDVNSFCFFTEAEK
Q04828	Aldo-keto reductase family 1 member C1	AK1C1	SPVLLEDPVLCAL
P52895	Aldo-keto reductase family 1 member C2	AK1C2	ILFDTVDLCATWEAMEK KLLDFCK SPVLLEDPVLCAL
P42330	Aldo-keto reductase family 1 member C3	AK1C3	KLLDFCK YKPVCNQVECHPYFNR
P12814	Alpha-actinin-1	ACTN1	CQLEINFNTLQTK DGLGFCALIHR

Accession	Description	Gene symbol	Peptide
			EGLLLWCQR
O43707	Alpha-actinin-4	ACTN4	CQLEINFNTLQTK
			EGLLLWCQR
Q9UDR5	Alpha-aminoadipic semialdehyde synthase, mitochondrial	AASS	AGGILQEDISEACLILGVK
			QLLCDLVGISPSSEHDVLK
P06733	Alpha-enolase	ENOA	QIGSVTESLQACK
P21397	Amine oxidase [flavin-containing] A	AOFA	ICELYAK
			KICELYAK
P27338	Amine oxidase [flavin-containing] B	AOFB	LCELYAK
			CIVYYK
			KLCELYAK
Q9H4A4	Aminopeptidase B	AMPB	AFFPCFDTPAVK
Q9P2R3	Ankyrin repeat and FYVE domain-containing protein 1	ANFY1	NQLPLVVDAICTR
P04083	Annexin A1	ANXA1	CLTAIVK
P07355	Annexin A2	ANXA2	GDLENAFLNLVQCIQNK
			GLGTDEDSLIEIICSR
			SLIEIICSR
			STVHEILCK
P09525	Annexin A4	ANXA4	FLTVLCSR
P08133	Annexin A6	ANXA6	ALLALCGGED
			FMTILCTR
P20073	Annexin A7	ANXA7	VLIEILCTR
Q10567	AP-1 complex subunit beta-1	AP1B1	YESVIATLCENLDSLDEPEAR
O95782	AP-2 complex subunit alpha-1	AP2A1	AADLLYAMCDR
			ACNQLGQFLQHR
			LVECLETVLNK
			QSAALCLLR
Q96CW1	AP-2 complex subunit mu	AP2M1	MCDVMAAYFGK
O14617	AP-3 complex subunit delta-1	AP3D1	YISQCIDEIK
			DLILQCLDDKDESIR
P02649	Apolipoprotein E	APOE	LGADMEDVCGR
O95831	Apoptosis-inducing factor 1, mitochondrial	AIFM1	SITIIGGGFLGSELACALGR
			SNIWVAGDAACFYDIK
P54136	Arginine--tRNA ligase, cytoplasmic	SYRC	AYQCVVLLQGK
			IVFVPGCSIPLTIVK
			MDVLVSECSAR
			MLLCEAVAAVMAK
P04424	Argininosuccinate lyase	ARLY	MAEDLILYCTK
			CAGLLMTLK
P00966	Argininosuccinate synthase	ASSY	SGGLDTSCILVWLK
O43776	Asparagine--tRNA ligase, cytoplasmic	SYNC	HLAEYTHVEAECPFLTFDDLLNR
			LEDLVCDVVDR
P00505	Aspartate aminotransferase, mitochondrial	AATM	TCGFDFTGAVEDISK
			VGAFTMVCK
P14868	Aspartate--tRNA ligase, cytoplasmic	SYDC	LEYCEALAMLR
Q9ULA0	Aspartyl aminopeptidase	DNPEP	NDTPCGTTIGPILASR
P24539	ATP synthase F(0) complex subunit B1, mitochondrial	AT5F1	CIADLK
Q8NBU5	ATPase family AAA domain-containing protein 1	ATAD1	DAALLCVR
Q9NP58	ATP-binding cassette sub-family B member 6, mitochondrial	ABCB6	FYDISSGCIR
Q8NE71	ATP-binding cassette sub-family F member 1	ABCF1	TLLIVSHDQGFLDDVCTDIIHLDAQ R
P53396	ATP-citrate synthase	ACLY	FICTTSAIQNR
			AVQGMLDFDYVCSR
P17858	ATP-dependent 6-phosphofructokinase, liver type	PFKAL	LPLMECVQMTK
Q08211	ATP-dependent RNA helicase A	DHX9	NFLYAWCGK
			LQISHEAAACITGLR
			SSVNCPFSSQDMK
O00148	ATP-dependent RNA helicase DDX39A	DX39A	CMALAQLLVEQNFPAIAIHR
			HFVLDECDK
O15523	ATP-dependent RNA helicase DDX3Y	DDX3Y	KGADSLEDFLYHEGYACTSIHGDR

Accession	Description	Gene symbol	Peptide
			VRPCVVYGGADIGQQIR
O95816	BAG family molecular chaperone regulator 2	BAG2	FQSIVIGCALEDQK
P35613	Basigin	BASI	SSEHINEGETAMLVCK
Q9BXK5	Bcl-2-like protein 13	B2L13	HTSPVFSPANPESSMEDCLAHLGE K
Q3LXA3	Bifunctional ATP-dependent dihydroxyacetone kinase/FAD-AMP lyase (cyclizing)	DHAK	VCSTLLGLEEHLNALDR
P07814	Bifunctional glutamate/proline--tRNA ligase	SYEP	INEAVECLLSLK HEELMLGDPCLK EAPCVLIYIPDGHTK
O60502	Bifunctional protein NCOAT	NCOAT	SMMACLLSSLK
P31939	Bifunctional purine biosynthesis protein PURH	PUR9	MSSFGDFVALSDVCDVPTAK VCMVYDLYK
Q06520	Bile salt sulfotransferase	ST2A1	ICQFLGK
P53004	Biliverdin reductase A	BIEA	ILHCLGLAEEIQK
O15382	Branched-chain-amino-acid aminotransferase, mitochondrial	BCAT2	LELLECIR EVFGSGTACQVCPVHR LCLPSFDK
P04632	Calpain small subunit 1	CPNS1	YSDESGNMDFDNFISCLVR
P07384	Calpain-1 catalytic subunit	CAN1	LEICNLTPDALK
Q15417	Calponin-3	CNN3	DGIILCELINK
P13861	cAMP-dependent protein kinase type II-alpha regulatory subunit	KAP2	LLGPCMDIMK
P31327	Carbamoyl-phosphate synthase [ammonia], mitochondrial	CPSM	SAYALGGLGSGICPNR SVDYPCLLR
P16152	Carbonyl reductase [NADPH] 1	CBR1	DVCTELLPLIK
Q96DG6	Carboxymethylenebutenolidase homolog	CMBL	ANEAYPCPCDIGHR
P50416	Carnitine O-palmitoyltransferase 1, liver isoform	CPT1A	SCTTESCDFVR FCLTYEASMTR
P29466	Caspase-1	CASP1	CFYLFPGH
P04040	Catalase	CATA	LCENIAGHLK
P35221	Catenin alpha-1	CTNA1	IVAECNAVR
P35222	Catenin beta-1	CTNB1	MMVCQVGGIEALVR
O60716	Catenin delta-1	CTND1	TPAILEASAGAIQNLCAGR
P07858	Cathepsin B	CATB	ICEPGYSPTYK
P07339	Cathepsin D	CATD	AIGAVPLIQGEYMIPCEK EGCEAIVDTGTSLMVGPVDEVR IQGEYMIPCEK LLDIACWIH TVVFDTGSSNLWVPSIHCK
P07711	Cathepsin L1	CATL1	NHCGIASAASYPTV
A5YKK6	CCR4-NOT transcription complex subunit 1	CNOT1	CPVVLAPLLYPEK
P48509	CD151 antigen	CD151	TVVALCGQR
Q13740	CD166 antigen	CD166	QIGDALPVSCTISASR SAYGDTIIIPCR TCSVTYYGPSGQK
Q8N163	Cell cycle and apoptosis regulator protein 2	CCAR2	GEASEDLCEMALDPELLLLR TVDSPICDFLELQR
Q7Z7K6	Centromere protein V	CENPV	CGVQSFYTPR
P00450	Ceruloplasmin	CERU	DIASGLIGPLIICK
O00299	Chloride intracellular channel protein 1	CLIC1	LHIVQVVCK
Q9Y696	Chloride intracellular channel protein 4	CLIC4	AGSDGESIGNCPFSQR IEEFLEEVLCPPK
O75390	Citrate synthase, mitochondrial	CISY	LPCVAAK
Q00610	Clathrin heavy chain 1	CLH1	LECSEELGDLVK LPVVIGGLLDVDCSEDVIK CNEPAVWSQLAK VIQCFAETGQVQK AHIAQLCEK EDKLECSEELGDLVK GQCDLELINVCNENSLFK IHEGCEEPATHNALAK QNLQICVQVASK

Accession	Description	Gene symbol	Peptide
P09497	Clathrin light chain B	CLCB	VAQLCDFNPK
Q16630	Cleavage and polyadenylation specificity factor subunit 6	CPSF6	VLISSLQDCLHGIESK
O75153	Clustered mitochondria protein homolog	CLU	CLTQQAVALQR DAAAFLLSCQIPGLVK
P53621	Coatomer subunit alpha	COPA	FPVFNMSYNPAENAVLLCTR GNNVYCLDR HAIVICNR QEIAEAQQLITICR
P53618	Coatomer subunit beta	COPB	AAAQCYIDLIIK
P35606	Coatomer subunit beta'	COPB2	VDACLELLIR TFEVCDLPVR
O14579	Coatomer subunit epsilon	COPE	NAFYIGSYQQCINEAQR
Q9Y678	Coatomer subunit gamma-1	COPG1	ELAPAVSVLQLFCSSPK CVMDDDNEVR HEMVVYEAASAIVNLPGCSAK
Q9UBF2	Coatomer subunit gamma-2	COPG2	ELAPAVSVLQLFCSSPK
P23528	Cofilin-1	COF1	AVLFCLSEDK HELQANCYEEVKDR
O75534	Cold shock domain-containing protein E1	CSDE1	QRPGQQVATCVR
P0C0L5	Complement C4-B	CO4B	VDVQAGACEGK
Q13098	COP9 signalosome complex subunit 1	CSN1	CAAGLAELAAR
Q9UNS2	COP9 signalosome complex subunit 3	CSN3	CIELDER
Q9BT78	COP9 signalosome complex subunit 4	CSN4	CQQLAAYGILEK
Q7L5N1	COP9 signalosome complex subunit 6	CSN6	QVCEIIESPLFLK
O75131	Copine-3	CPNE3	ISLNSLCYGDMDK
O75367	Core histone macro-H2A.1	H2AY	NCLALADDKK
Q9BR76	Coronin-1B	COR1B	NDQCYEDIR
P28845	Corticosteroid 11-beta-dehydrogenase isozyme 1	DHI1	VVSHCLELGAASAH
P17812	CTP synthase 1	PYRG1	GLGLSPDLVVCR
Q86VP6	Cullin-associated NEDD8-dissociated protein 1	CAND1	FCNVDDDELR TVIGELPPASSGSALAANVCK TYIQCIAAISR CLDAVVSTR
O43927	C-X-C motif chemokine 13	CXL13	CVQESSVFIPR
P35520	Cystathionine beta-synthase	CBS	CIIVMPEK
P21291	Cysteine and glycine-rich protein 1	CSRP1	TVYFAEEVQCEGNSFHK
P31930	Cytochrome b-c1 complex subunit 1, mitochondrial	QCR1	NALVSHLDGTTPVCEDIGR SICYAETGLLGAHFVCDR
P22695	Cytochrome b-c1 complex subunit 2, mitochondrial	QCR2	ENMAYTVECLR NALANPLYCPDYR
P08574	Cytochrome c1, heme protein, mitochondrial	CY1	HLVGVCYTEDEAK
P10632	Cytochrome P450 2C8	CP2C8	DFIDCFLIK
P05181	Cytochrome P450 20	CP2E1	DLTDCLLVEMEK
Q9HBI6	Cytochrome P450 4F11	CP4FB	LQCFPQPPK
Q14204	Cytoplasmic dynein 1 heavy chain 1	DYHC1	SSLQSQCLNEVLK MLSAVSQQVQCIQEALR
Q7L576	Cytoplasmic FMR1-interacting protein 1	CYFP1	NFVGPPHFQVICR
Q96KP4	Cytosolic non-specific dipeptidase	CNDP2	FCLEGMEESGSEGLDELIFAR
Q15392	Delta(24)-sterol reductase	DHC24	GLEAICAK
P30038	Delta-1-pyrroline-5-carboxylate dehydrogenase, mitochondrial	AL4A1	CDDSVGYFVEPCIVESK
P13716	Delta-aminolevulinic acid dehydratase	HEM2	CVLIFGVPSR
P15924	Desmoplakin	DESP	YCYLQNEVFGLFQK
P60981	Destrin	DEST	LGGSLIVAFEGCPV ASGVQVADEVCR HECQANGPEDLNR
P09622	Dihydrolipoyl dehydrogenase, mitochondrial	DLDH	ILGPGAGEMVNEAALALEYGASCE DIAR
P10515	Dihydrolipoyllysine-residue acetyltransferase component of pyruvate dehydrogenase complex, mitochondrial	ODP2	ASALACLK
P09417	Dihydropteridine reductase	DHPR	GAVHQLCQSLAGK

Accession	Description	Gene symbol	Peptide
P49326	Dimethylaniline monooxygenase [N-oxide-forming] 5	FMO5	ICGQSLANK
Q9NY33	Dipeptidyl peptidase 3	DPP3	FSTIASSYEECR ADTQYILPNDIGVSSLDCR
P27487	Dipeptidyl peptidase 4	DPP4	CSGPGLPLYTLH
Q16531	DNA damage-binding protein 1	DDB1	IGRPSETGIIGIIDPECR
P49736	DNA replication licensing factor MCM2	MCM2	FDILCVVR
P25205	DNA replication licensing factor MCM3	MCM3	GVVCIDEFDK AILCLLLGGVER
P33992	DNA replication licensing factor MCM5	MCM5	CPLDPYFIMPDK GVVCIDEFDK
P33993	DNA replication licensing factor MCM7	MCM7	CSILAAANPAYGR
P11387	DNA topoisomerase 1	TOP1	CDFTQMSQYFK
P27695	DNA-(apurinic or apyrimidinic site) lyase	APEX1	EEAPDILCLQETK ICSWNVDGLR
P78527	DNA-dependent protein kinase catalytic subunit	PRKDC	INLVEFCR INQVFHGSCITEGNELTK DILPCLDGYLK ELLNPVVEFVSHPSTTCR FNNYVDCMK GLSSLLCNFTK LAAVVSACK CFGTGAAGNR CGAALAGHQLIR GYGLFAGPCK LACDVDQVTR LLELMTEVLCR LPVLAGCLK NCISTVVHQGLIR SLGTIQQCCDAIDHLCR
O60884	DnaJ homolog subfamily A member 2	DNJA2	NVLCSACSGQGGK
P04843	Dolichyl-diphosphooligosaccharide--protein glycosyltransferase subunit 1	RPN1	TEGSDLCDR
Q14203	Dynactin subunit 1	DCTN1	DLETSCSDIR
P50570	Dynamin-2	DYN2	CVDLVIQELINTVR
P49792	E3 SUMO-protein ligase RanBP2	RBP2	IAELLCK
Q14258	E3 ubiquitin/ISG15 ligase TRIM25	TRI25	NTVLCNVVEQFLQADLAR
Q7Z6Z7	E3 ubiquitin-protein ligase HUWE1	HUWE1	VLGPAACR
Q63HN8	E3 ubiquitin-protein ligase RNF213	RN213	STDFLPVDCPVR
Q9HC35	Echinoderm microtubule-associated protein-like 4	EMAL4	VIAVADDFCK
P13804	Electron transfer flavoprotein subunit alpha, mitochondrial	ETFA	TIYAGNALCTVK LGGEVSCLVAGTK
P38117	Electron transfer flavoprotein subunit beta	ETFB	HSMNPFCEIAVEEAVR
Q16134	Electron transfer flavoprotein-ubiquinone oxidoreductase, mitochondrial	ETFD	FCPAGVYEFVPVEQGDGFR
P68104	Elongation factor 1-alpha 1	EF1A1	KDGNASGTTLLEALDCILPPTRPTDKPLR NMITGTSQADCAVLIVAAGVGEFEAGISK DGNASGTTLLEALDCILPPTRPTDK SGDAAIVDMVPGKPMCVESFSDYPPLGR DGNASGTTLLEALDCILPPTR DGNASGTTLLEALDCILPPTRPTDKPLR CLYASVLTAQPR
P13639	Elongation factor 2	EF2	STLTDSLVCK YVEPIEDVPCGNIVGLVGVDQFLVK
P43897	Elongation factor Ts, mitochondrial	EFTS	ALETCGGDLK
P49411	Elongation factor Tu, mitochondrial	EFTU	NMITGTAPLDGCILVVAANDGPMPQTR
Q9NZ08	Endoplasmic reticulum aminopeptidase 1	ERAP1	MAFPCFDEPAFK
Q9BS26	Endoplasmic reticulum resident protein 44	ERP44	TPADCPVIAIDSFR

Accession	Description	Gene symbol	Peptide
P14625	Endoplasmin	ENPL	LTESPCALVASQYGWSGNMER
P42126	Enoyl-CoA delta isomerase 1, mitochondrial	ECI1	SAGLDLTEMCGR
O75521	Enoyl-CoA delta isomerase 2, mitochondrial	ECI2	EFVGCFIDFPK EFVGCFIDFPKPL
Q96DC8	Enoyl-CoA hydratase domain-containing protein 3, mitochondrial	ECHD3	DYHAEVFQTCSK
P30084	Enoyl-CoA hydratase, mitochondrial	ECHM	ALNALCDGLIDELNQALK
P61916	Epididymal secretory protein E1	NPC2	AVVHGILMGVPVPFPIPEPDGCK DCGSVDGVIK SGINCPIQK
O94905	Erlin-2	ERLN2	ADAECYTAMK
Q96HE7	ERO1-like protein alpha	ERO1A	YSEEANNLIEECEQAER
P30042	ES1 protein homolog, mitochondrial	ES1	VVTTPAFMCETALHYIHDGIGAMV R
Q9H0W9	Ester hydrolase C11orf54	CK054	APLVCLPVFVSR
Q8NBQ5	Estradiol 17-beta-dehydrogenase 11	DHB11	VHTFVVDCSNR
Q53GQ0	Estradiol 17-beta-dehydrogenase 12	DHB12	MININILSVCK
P60842	Eukaryotic initiation factor 4A-I	IF4A1	VVMALGDYMGASCHACIGGTNVR
P15170	Eukaryotic peptide chain release factor GTP-binding subunit ERF3A	ERF3A	QDQVCIAR
P62495	Eukaryotic peptide chain release factor subunit 1	ERF1	CGTIVTEEGK
P47813	Eukaryotic translation initiation factor 1A, X-chromosomal	IF1AX	LEAMCFDGVK
P41091	Eukaryotic translation initiation factor 2 subunit 3	IF2G	YNIEVVCEYIVK
P55884	Eukaryotic translation initiation factor 3 subunit B	EIF3B	NLFNVVDCK YWLEEAECR
Q99613	Eukaryotic translation initiation factor 3 subunit C	EIF3C	CLEEFELLGK
O15371	Eukaryotic translation initiation factor 3 subunit D	EIF3D	TQGNVFATDAILATLMSCTR
P60228	Eukaryotic translation initiation factor 3 subunit E	EIF3E	FQYECGNYSGAAEYLYFFR LFIFETFCR IHQCISIN
O75822	Eukaryotic translation initiation factor 3 subunit J	EIF3J	ITNSLTVLCSEK
Q9UBQ5	Eukaryotic translation initiation factor 3 subunit K	EIF3K	FICHVVGITYQHIDR
Q15056	Eukaryotic translation initiation factor 4H	IF4H	GFCYVEFDEVDSLK
O60841	Eukaryotic translation initiation factor 5B	IF2P	APIICVLGHVDTGK
Q9Y2L1	Exosome complex exonuclease RRP44	RRP44	LACLSEEGNEIESGK
O14980	Exportin-1	XPO1	DLLGLCEQK
P55060	Exportin-2	XPO2	NLFEDQNTLTSICEK
P49327	Fatty acid synthase	FAS	AAPLDSIHSLAAYYIDCIR TGGAYGEDLGADYNLSQVCDGK AALQEELQLCK ACLDTAVENMPSLK DGLLENQTPEFFQDVCK LTPGCEAEAETEAICFFVQQFTDME HNR MASCLEVLDLFLNQPH AINCATSGVVGLVNCLR CTVFHGAQVEDAFR LSIPTYGLQCTR SFYGSTLFLCR SGVVGLVNCLR
P51648	Fatty aldehyde dehydrogenase	AL3A2	EKDILTAIAADLCK DILTAIAADLCK
P02792	Ferritin light chain	FRIL	TDPHLCDFLETHFLDEEVK
P02675	Fibrinogen beta chain	FIBB	LESDVSAQMEYCR TPCTVSCNIPVVSGK ECEEIIR NYCGLPGEYWLGNDK
P02679	Fibrinogen gamma chain	FIBG	CHAGHLNGVYYQGGTYSK VAQLEAQCQEPCKDTVQIHDITGK
Q53EP0	Fibronectin type III domain-containing protein 3B	FND3B	LECAAAGPQSLK
P21333	Filamin-A	FLNA	VHSPSGALEECYVTEIDQDK
O75369	Filamin-B	FLNB	SPFVVQVGEACNPNACR
P30043	Flavin reductase (NADPH)	BLVRB	CLTTDEYDGHSTYPSHQYQ

Accession	Description	Gene symbol	Peptide
P04075	Fructose-bisphosphate aldolase A	ALDOA	ALANSLACQGK
P07954	Fumarate hydratase, mitochondrial	FUMH	FEALAAHDALVELSGAMNTTACSL MK
P51570	Galactokinase	GALK1	MTGGGFGGCTVTLLEASAAPH
O75223	Gamma-glutamylcyclotransferase	GGCT	NPSAAFFCVAR
P36269	Gamma-glutamyltransferase 5	GGT5	FLNVVQAVSQEGACVYAVSDLR HQAPCGPQAF
P57764	Gasdermin-D	GSDMD	ELCQLLLEGLEGVLR
Q9NQX3	Gephyrin	GEPH	VGVLTVSDSCFR
P11413	Glucose-6-phosphate 1-dehydrogenase	G6PD	LILDVFCGSQMH DNIACVILTFK DVMQNHLLQMLCL DVMQNHLLQMLCLVAMEK LILDVFCGSQM LILDVFCGSQMHF
P14314	Glucosidase 2 subunit beta	GLU2B	YEQGTGCWQGPNR
P00367	Glutamate dehydrogenase 1, mitochondrial	DHE3	CAVVDVPFGGAK
P48506	Glutamate--cysteine ligase catalytic subunit	GSH1	GYVSDIDCR
Q06210	Glutamine--fructose-6-phosphate aminotransferase [isomerizing] 1	GFPT1	ETDCGVHINAGPEIGVASTK CQNALQQVVAR
P47897	Glutamine--tRNA ligase	SYQ	VGVTVAQTTMEPHLLEACVR
P35754	Glutaredoxin-1	GLRX1	AQEFVNCK
Q9Y2Q3	Glutathione S-transferase kappa 1	GSTK1	SWLGFEILCR
P48637	Glutathione synthetase	GSHB	IEPEPFENCLLR
P21695	Glycerol-3-phosphate dehydrogenase [NAD(+)], cytoplasmic	GPDA	VCYEGQPVGEFIHCLQNHPEHM
P43304	Glycerol-3-phosphate dehydrogenase, mitochondrial	GPDM	NYLSCDVEVR
P35573	Glycogen debranching enzyme	GDE	HLSLGSVQLCGVGK
P11216	Glycogen phosphorylase, brain form	PYGB	MSVIEEGDCK
Q9UBQ7	Glyoxylate reductase/hydroxypyruvate reductase	GRHPR	GVAGAHGLLCLLSDHVDK NCVILPH
P49915	GMP synthase [glutamine-hydrolyzing]	GUAA	NFLYDIAGCSGTFTVQNR
Q12849	G-rich sequence factor 1	GRSF1	YIELFLNSCPK
Q14353	Guanidinoacetate N-methyltransferase	GAMT	TEVMALVPPADCR
P63244	Guanine nucleotide-binding protein subunit beta-2-like 1	GBLP	HLYTLDGGDIINALCFSPNR FSPNSSNPIIVSCGWDK YTVQDESHSEWVSCVR
O60832	H/ACA ribonucleoprotein complex subunit 4	DKC1	DSAVNAICYGAK
P00738	Haptoglobin	HPT	SCAVAEYGVYVK
P08107	Heat shock 70 kDa protein 1A/1B	HSP71	FEELCSDLFR CQEVISWLDANTLAEKDEFEHK
P34932	Heat shock 70 kDa protein 4	HSP74	FLEMCNDLLAR
O95757	Heat shock 70 kDa protein 4L	HS74L	AQFEQLCASLLAR
P11142	Heat shock cognate 71 kDa protein	HSP7C	CNEIINWLDK
P07900	Heat shock protein HSP 90-alpha	HS90A	CLELFTELAEDK FENLCK
P08238	Heat shock protein HSP 90-beta	HS90B	VFIMDSCDELIPEYLNFIR AKFENLCK FENLCK
Q15477	Helicase SKI2W	SKIV2	GLDPTGTVILLCK
Q13151	Heterogeneous nuclear ribonucleoprotein A0	ROA0	MENSQLCK
P09651	Heterogeneous nuclear ribonucleoprotein A1	ROA1	SHFEQWGTLTDCVVMR LTDCVVMR
P51991	Heterogeneous nuclear ribonucleoprotein A3	ROA3	LTDCVVMR
P52597	Heterogeneous nuclear ribonucleoprotein F	HNRPF	GLPFGCTK
P31943	Heterogeneous nuclear ribonucleoprotein H	HNRH1	GLPWSCSADEVQR
P61978	Heterogeneous nuclear ribonucleoprotein K	HNRPK	IIPTLEEGLQLPSPTATSQLPLESDA VECLNYQHYK
P14866	Heterogeneous nuclear ribonucleoprotein L	HNRPL	QPAIMPGQSYGLEDGSCSYK
P52272	Heterogeneous nuclear ribonucleoprotein M	HNRPM	ACQIFVR
O60506	Heterogeneous nuclear ribonucleoprotein Q	HNRPQ	HIGVCISVANNR SAFLCGVMK
O43390	Heterogeneous nuclear ribonucleoprotein R	HNRPR	GYAFITFCGK

Accession	Description	Gene symbol	Peptide
			HLGVCISVANNR
			SAFLCGVMK
Q00839	Heterogeneous nuclear ribonucleoprotein U	HNRPU	GNFTLPEVAECFDEITYVELQK
			TCNCETEDYGEK
			CAVEFNFGQK
			VLCHNCAVEFNFGQK
Q9BUJ2	Heterogeneous nuclear ribonucleoprotein U-like protein 1	HNRL1	NCAVEFNFGQR
			WDVLIQQATQCLNR
P37235	Hippocalcin-like protein 1	HPCL1	LLQCDPSSASQF
P84243	Histone H3.3	H33	FQSAAIGALQEASEAYLVGLFEDT
			NLCAIHAK
P30481	HLA class I histocompatibility antigen, B-44 alpha chain	1B44	AYLEGLCVESLR
Q9NYQ3	Hydroxyacid oxidase 2	HAOX2	ALVITLDTPVCGNR
P35914	Hydroxymethylglutaryl-CoA lyase, mitochondrial	HMGCL	LLEAGNFICQALNR
Q01581	Hydroxymethylglutaryl-CoA synthase, cytoplasmic	HMCS1	NNLSYDCIGR
P54868	Hydroxymethylglutaryl-CoA synthase, mitochondrial	HMCS2	CVSPEEFTEIMNQR
Q9Y4L1	Hypoxia up-regulated protein 1	HYOU1	VEFEELCADLFER
O00629	Importin subunit alpha-3	IMA3	SGILPILVHCLER
P52294	Importin subunit alpha-5	IMA5	IQAVIDAGVCR
O60684	Importin subunit alpha-7	IMA7	IQAVIDSGVCR
Q14974	Importin subunit beta-1	IMB1	HFIMQVVCEATQCPDTR
Q8TEX9	Importin-4	IPO4	APAALPALCDLLASAADPQIR
			ACYALENFVENLGPK
			DNICGALAR
O00410	Importin-5	IPO5	TIECISLIGLAVGK
O95373	Importin-7	IPO7	CLIDDR
Q96P70	Importin-9	IPO9	VSSVALCK
Q68E01	Integrator complex subunit 3	INT3	EHPEALSCLLLQLR
P26006	Integrin alpha-3	ITA3	SETVLTCATGR
Q12906	Interleukin enhancer-binding factor 3	ILF3	CLAALASLR
			GDLDLELVLLCK
			SCVIVIR
Q27J81	Inverted formin-2	INF2	CSNEEVAAMIR
P50213	Isocitrate dehydrogenase [NAD] subunit alpha, mitochondrial	IDH3A	CSDFTEEICR
			TFDLYANVRPCVSIEGYK
P51553	Isocitrate dehydrogenase [NAD] subunit gamma, mitochondrial	IDH3G	HACVPVDFEEVHVSSNADEEDIR
			LGDGLFLQCCR
O75874	Isocitrate dehydrogenase [NADP] cytoplasmic	IDHC	CATITPDEK
P48735	Isocitrate dehydrogenase [NADP], mitochondrial	IDHP	DLAGCIHGLSNVK
P41252	Isoleucine--tRNA ligase, cytoplasmic	SYIC	MGITEYNNQCR
Q9NSE4	Isoleucine--tRNA ligase, mitochondrial	SYIM	CGFSELYSWQR
P13645	Keratin, type I cytoskeletal 10	K1C10	AETECQNTEYQQLLDIK
Q86UP2	Kinectin	KTN1	TMMFSEDEALCVVDLLK
P33176	Kinesin-1 heavy chain	KINH	VFQSSTSQEQVYNDCAK
Q04760	Lactoylglutathione lyase	LGUL	GFGHIGIAVPDVYSACK
P42167	Lamina-associated polypeptide 2, isoforms beta/gamma	LAP2B	EMFPYEASTPTGISASCR
P20700	Lamin-B1	LMNB1	CQSLTEDLEFR
O43813	LanC-like protein 1	LANC1	IPQSHIQQICETILTSGENLAR
Q16850	Lanosterol 14-alpha demethylase	CP51A	CIGENFAYVQIK
Q6PKG0	La-related protein 1	LARP1	YGLECLFR
P42704	Leucine-rich PPR motif-containing protein, mitochondrial	LPPRC	LEDVALQILLACPVSK
			LIASYCNVGDIEGASK
Q96AG4	Leucine-rich repeat-containing protein 59	LRC59	VAGDCLDEK
Q9P2J5	Leucine--tRNA ligase, cytoplasmic	SYLC	NFEATLGWLQEHACSR
P23141	Liver carboxylesterase 1	EST1	LSEDCLYLNIYTPADLTK
			GDVKPLAEQIAITAGCK
			KGDVKPLAEQIAITAGCK
			SYPLVCIAK
			TTTSAVMVHCLR
			CLYLNIYTPADLTK
			PLAEQIAITAGCK

Accession	Description	Gene symbol	Peptide
P36776	Lon protease homolog, mitochondrial	LONM	VLFICTANVTDTIPEPLR
P28330	Long-chain specific acyl-CoA dehydrogenase, mitochondrial	ACADL	AFVDNCLQLHEAK
P33121	Long-chain-fatty-acid--CoA ligase 1	ACSL1	LIAIVVPDVETLCSWAQK CGVEVTSMK GFEGSFEELCR GIQVSNNGPCLGSR AAEGEGEVCVK
O95573	Long-chain-fatty-acid--CoA ligase 3	ACSL3	NTPLCDSFVFR
O60488	Long-chain-fatty-acid--CoA ligase 4	ACSL4	GDCTVLKPTLMAAVPEIMDR TALLDISCVK
Q9ULC5	Long-chain-fatty-acid--CoA ligase 5	ACSL5	GLAVSDNGPCLGYR IVQAVVYSCGAR
Q7Z4W1	L-xylulose reductase	DCXR	GVPGAIVNVSSQCSQR
Q14108	Lysosome membrane protein 2	SCRB2	DEVLYVFPSDFCR
Q96C86	m7GpppX diphosphatase	DCPS	WNQQQLDDLYLIAICHR
P14174	Macrophage migration inhibitory factor	MIF	LLCGLLAER
Q14764	Major vault protein	MVP	LFSVPDFVGDACK
P40925	Malate dehydrogenase, cytoplasmic	MDHC	MGVLDGVLMELQDCALPLLK
P40926	Malate dehydrogenase, mitochondrial	MDHM	GCDVVVIPAGVPR
Q96IJ6	Mannose-1-phosphate guanyltransferase alpha	GMPPA	LLPAITILGCR
Q9Y5P6	Mannose-1-phosphate guanyltransferase beta	GMPPB	YGVVVCEADTGR
Q658P3	Metalloreductase STEAP3	STEA3	ESNAEYLASLFPTCTVVK QVPICGDQPEAK
P56192	Methionine--tRNA ligase, cytoplasmic	SYMC	VPVLQLDSGNYLFSTSAICR
Q96PE7	Methylmalonyl-CoA epimerase, mitochondrial	MCEE	DCGGVLVELEQA
Q9BQA1	Methylosome protein 50	MEP50	AHAAQVTCVAASPHK
Q5TGZ0	MICOS complex subunit MIC10	MIC10	CLADAVVK
P10620	Microsomal glutathione S-transferase 1	MGST1	VFANPEDCVAFGK
P27816	Microtubule-associated protein 4	MAP4	CSLPAEEDSVLEK
Q15691	Microtubule-associated protein RP/EB family member 1	MARE1	NIELICQENEGENDPVLQR
O43772	Mitochondrial carnitine/acylcarnitine carrier protein	MCAT	CLLQIQASSGESK
Q9Y6C9	Mitochondrial carrier homolog 2	MTCH2	LCSGVLGTVVHGK QVCQLPGLFSY
Q9Y276	Mitochondrial chaperone BCS1	BCS1	GYLLYGPPGCGK
Q9H1K4	Mitochondrial glutamate carrier 2	GHC2	LINGGVAGLVGVTCVFPIDLAK
O94826	Mitochondrial import receptor subunit TOM70	TOM70	ILLDQVEEAVADFDECIR CAEGYALYAQALTDQQQFGK
Q15070	Mitochondrial inner membrane protein OXA1L	OXA1L	CLIFPLIVTGQR
Q7L0Y3	Mitochondrial ribonuclease P protein 1	MRRP1	LNLATECLPLDK
Q10713	Mitochondrial-processing peptidase subunit alpha	MPPA	MVLAGVGVEHEHLVDCAR
P26038	Moesin	MOES	ILALCMGNHELYMR
P08183	Multidrug resistance protein 1	MDR1	TCIVIAHR
P22234	Multifunctional protein ADE2	PUR6	ITSCIFQLLQEAGIK ACGNFGIPCELR
Q9NUJ1	Mycophenolic acid acyl-glucuronide esterase, mitochondrial	ABHDA	ALAIEEFCK
P35580	Myosin-10	MYH10	VEDMAELTCLNEASVLHNLK CNGVLEGIR EDQSILCTGESGAGK
Q7Z406	Myosin-14	MYH14	CNGVLEGIR
P35579	Myosin-9	MYH9	VEDMAELTCLNEASVLHNLK CNGVLEGIR KQELEEICHDLEAR EDQSILCTGESGAGK
O95299	NADH dehydrogenase [ubiquinone] 1 alpha subcomplex subunit 10, mitochondrial	NDUAA	CEVLQYSAR
P49821	NADH dehydrogenase [ubiquinone] flavoprotein 1, mitochondrial	NDUV1	GAGAYICGEETALIESIEGK
P28331	NADH-ubiquinone oxidoreductase 75 kDa subunit, mitochondrial	NDUS1	DCFIIYQGHHGDVGAPIADVILPGA AYTEK VVAACAMPVMK

Accession	Description	Gene symbol	Peptide
Q16798	NADP-dependent malic enzyme, mitochondrial	MAON	FGINCLIQFEDFANANAFR
Q9BXJ9	N-alpha-acetyltransferase 15, NatA auxiliary subunit	NAA15	GELLLQLCR
Q8TBC4	NEDD8-activating enzyme E1 catalytic subunit	UBA3	VLVIGAGGLGCELLK
Q09666	Neuroblast differentiation-associated protein AHNAK	AHNK	EVFSSCSSEVVLSGDDEEYQR
Q9BYT8	Neurolysin, mitochondrial	NEUL	MSELCIDFNK
Q14697	Neutral alpha-glucosidase AB	GANAB	TCEESSFCK
Q15758	Neutral amino acid transporter B(0)	AAAT	CVEENNGVAK
P40261	Nicotinamide N-methyltransferase	NNMT	IFCLDGVK
P43490	Nicotinamide phosphoribosyltransferase	NAMPT	DLLNCSFK
Q86X76	Nitrilase homolog 1	NIT1	LGACLAFLPEAFDFIAR
P22307	Non-specific lipid-transfer protein	NLTP	KADCTITMADSDFLALMTGK SAVDQACVGYVFGDSTCGQR QLIQGGVAECVLALGFEK
Q09161	Nuclear cap-binding protein subunit 1	NCBP1	LDTMNTTCVDR
Q8N1F7	Nuclear pore complex protein Nup93	NUP93	CGDLLAASQVVNR
Q9BZE4	Nucleolar GTP-binding protein 1	NOG1	TLLLCGYPNVGK
P78316	Nucleolar protein 14	NOP14	CPILSLQDVVK
O00567	Nucleolar protein 56	NOP56	LVAFCPF
P22392	Nucleoside diphosphate kinase B	NDKB	GDFCIQVGR
O00151	PDZ and LIM domain protein 1	PDLI1	CGTGIVGVFVK GCTDNLTLTVAR
Q96HC4	PDZ and LIM domain protein 5	PDLI5	FFAPECGR
P62937	Peptidyl-prolyl cis-trans isomerase A	PPIA	ANAGPNTNGSQFFICTAK GSQFFICTAK TNGSQFFICTAK
P30405	Peptidyl-prolyl cis-trans isomerase F, mitochondrial	PPIF	VIPSFMCQAGDFTNHNGTGGK
Q13451	Peptidyl-prolyl cis-trans isomerase FKBP5	FKBP5	EEQCILYLGPR
Q06830	Peroxiredoxin-1	PRDX1	LNCQVIGASVDSHFCH
P30044	Peroxiredoxin-5, mitochondrial	PRDX5	GVLFGVPGAFTPGCSK
Q9NUI1	Peroxisomal 2,4-dienoyl-CoA reductase	DECR2	CLPLSMDVR
Q08426	Peroxisomal bifunctional enzyme	ECHP	LCNKPIQSLPNMDSIFSEALLK GGGLELALGCHYR
O96011	Peroxisomal membrane protein 11B	PX11B	NACDLFIPLDK
P51659	Peroxisomal multifunctional enzyme type 2	DHB4	CEAVVADVLDK
Q9NSD9	Phenylalanine--tRNA ligase beta subunit	SYFB	YDLLCLEGLVR
P30086	Phosphatidylethanolamine-binding protein 1	PEBP1	APVAGTCYQAEWDDYVPK CDEPILSNR
Q16822	Phosphoenolpyruvate carboxykinase [GTP], mitochondrial	PCKGM	YVAAAFPSACGK FPGCMQGR
P36871	Phosphoglucomutase-1	PGM1	LSLCGEESFGTGSDHIR
P00558	Phosphoglycerate kinase 1	PGK1	ACANPAAGSVILLENLR
P20020	Plasma membrane calcium-transporting ATPase 1	AT2B1	TICLAFR
P13797	Plastin-3	PLST	IIQENLNLALNSASAIGCHVVNIGA EDLR LENCNYAVELGK
Q15149	Plectin	PLEC	EYGSCSHHYQQLLQSLEQGAQEES R CVEDPETGLCLLPLTDK CVEDPETGLR LPLLAVCDYK
Q15365	Poly(rC)-binding protein 1	PCBP1	LVVPATQCGSLIGK QICLVMLETLSQSPQGR
O95758	Polypyrimidine tract-binding protein 3	PTBP3	NLFIEAGCSVK
Q6P2Q9	Pre-mRNA-processing-splicing factor 8	PRP8	FICISDLR
Q9UHG3	Prenylcysteine oxidase 1	PCYOX	CPSIILHDR
Q5JRX3	Presequence protease, mitochondrial	PREP	THFLMPFPVNYVGECIR EFQITCGPDSFATDPSK LGCGLLDYR
Q96HY7	Probable 2-oxoglutarate dehydrogenase E1 component DHKTD1, mitochondrial	DHTK1	DVIIDLLCYR
Q92841	Probable ATP-dependent RNA helicase DDX17	DDX17	STCIYGGAPK

Accession	Description	Gene symbol	Peptide
P17844	Probable ATP-dependent RNA helicase DDX5	DDX5	LIDFLECGK STCIYGGAPK
P26196	Probable ATP-dependent RNA helicase DDX6	DDX6	GNEFEDYCLK
Q8NBJ5	Procollagen galactosyltransferase 1	GT251	ALQAQEIECR
P07737	Profilin-1	PROF1	CYEMASHLR IDNLMADGTCQDAAIVGYK
Q8WUM4	Programmed cell death 6-interacting protein	PDC6I	FIQQTYPSGGEEQAQYCR
P35232	Prohibitin	PHB	GVQDIVVGEGTHFLIPWVQKPIIFD CR PIIFDCR
Q9UQ80	Proliferation-associated protein 2G4	PA2G4	AAHLCAEAALR VAHSFNCTPIEGMLSHQLK
P48147	Prolyl endopeptidase	PPCE	QNCFDDFQCAAEYLIK
P05165	Propionyl-CoA carboxylase alpha chain, mitochondrial	PCCA	MADEAVCVGPAPTSK
P05166	Propionyl-CoA carboxylase beta chain, mitochondrial	PCCB	AFENDVDALCNLR CADFGMAADK
Q15185	Prostaglandin E synthase 3	TEBP	LTFSCLGGSDNFK
Q14914	Prostaglandin reductase 1	PTGR1	IAICGAISTYNR FGLLEICGVK ASPDGYDCYFDNVGGEFSNTVIGQ MK
P60900	Proteasome subunit alpha type-6	PSA6	YGYEIPVDMLCK
Q5VYK3	Proteasome-associated protein ECM29 homolog	ECM29	DIALVQQLFEALCK IVAISCAADILK TIAALLPCLLDK
O14744	Protein arginine N-methyltransferase 5	ANM5	QGFDFLCMPVFHPR
P35659	Protein DEK	DEK	SICEVLDLER
O60610	Protein diaphanous homolog 1	DIAP1	AGCAVTSLLASELTK
O60879	Protein diaphanous homolog 2	DIAP2	HECTLSSQEYVHELR
P30101	Protein disulfide-isomerase A3	PDIA3	VDCTANTNTCNK
Q99497	Protein DJ-1	PARK7	GLIAAICAGPTALLAHEIGFGSK
P49257	Protein ERGIC-53	LMAN1	NDYEFCAK
Q52LJ0	Protein FAM98B	FA98B	SLCNLEESITSAGR
P49354	Protein farnesyltransferase/geranylgeranyltransferase type-1 subunit alpha	FNTA	ALELCEILAK
Q15435	Protein phosphatase 1 regulatory subunit 7	PP1R7	CIENLEELQSLR
P29590	Protein PML	PML	LQDLSSCITQGK
Q14690	Protein RRP5 homolog	RRP5	CVVSSLGITDR VVVLNCEPSK
P31949	Protein S100-A11	S10AB	CIESLIAVFQK
P05109	Protein S100-A8	S10A8	LLETECPQYIR
Q15436	Protein transport protein Sec23A	SC23A	ISGAIGPCVSLNSK
P53992	Protein transport protein Sec24C	SC24C	NCASPSSAGQLILPECMK
O94855	Protein transport protein Sec24D	SC24D	SCETDALINFFAK
O94979	Protein transport protein Sec31A	SC31A	CLSSATDPQTK EIVESCDLK LVACWTK
P21980	Protein-glutamine gamma-glutamyltransferase 2	TGM2	CLGIPTR DCLTESNLIK SVPLCILYEK
Q2TB90	Putative hexokinase HKDC1	HKDC1	CDVTFMLSEDGSGK ATDCEGEDVVDMLR LPLGLTFSFPCR
Q9Y383	Putative RNA-binding protein Luc7-like 2	LC7L2	VCEVCSAYLGLHDNDR DQDLASCDR SHLLNCCPHDVLSGTR
P11498	Pyruvate carboxylase, mitochondrial	PYC	GLYAAFDCTATMK DMAGLLKPTACTMLVSSLR
P08559	Pyruvate dehydrogenase E1 component subunit alpha, somatic form, mitochondrial	ODPA	VDGMDILCVR
P14618	Pyruvate kinase PKM	KPYM	AAMADTFLEHMCR

Accession	Description	Gene symbol	Peptide
			GIFPVLCK
			NTGIICTIGPASR
Q08257	Quinone oxidoreductase	QOR	AGESVLVHGASGGVGLAACQIAR
Q53FA7	Quinone oxidoreductase PIG3	QORX	NVNCLALDGR
			GAGVNLILDCIGGSYWEK
P50395	Rab GDP dissociation inhibitor beta	GDIB	TDDYLDQPCYETINR
			QLICDPSYVK
			VICILSHPIK
P35241	Radixin	RADI	ILALCMGNHELYMR
O60518	Ran-binding protein 6	RNBP6	LCDIFAVLAR
P46940	Ras GTPase-activating-like protein IQGAP1	IQGA1	QLSSSVTGLTNIEEENCQR
Q13576	Ras GTPase-activating-like protein IQGAP2	IQGA2	EACNVPEPEEK
P63000	Ras-related C3 botulinum toxin substrate 1	RAC1	AVLCPPPVK
Q9UL25	Ras-related protein Rab-21	RAB21	GIEELFLDLCK
Q8WUD1	Ras-related protein Rab-2B	RAB2B	SCLLLQFTDK
P18754	Regulator of chromosome condensation	RCC1	SGQVYSFGCNDEGALGR
Q9NQC3	Reticulon-4	RTN4	YSNSALGHVNCTIK
P00352	Retinal dehydrogenase 1	AL1A1	FPVFNPATEEELCQVEEGDKEDVD K
			LECGGGPWGNK
			AYLNDLAGCIK
			LNDLAGCIK
			YCAGWADK
O75452	Retinol dehydrogenase 16	RDH16	VLAACLTEK
P08134	Rho-related GTP-binding protein RhoC	RHOC	LVIVGDGACGK
			HFCPNVPIILVGNK
P13489	Ribonuclease inhibitor	RINI	LGDVGMAELCPGLLHPSSR
P52758	Ribonuclease UK114	UK114	AAGCDFTNVVK
P23921	Ribonucleoside-diphosphate reductase large subunit	RIR1	SAGGIGVAVSCIR
Q8TDN6	Ribosome biogenesis protein BRX1 homolog	BRX1	LFVINEVCEMK
Q9Y3A5	Ribosome maturation protein SBDS	SBDS	KEDLISAFGTDDQTEICK
Q9P2E9	Ribosome-binding protein 1	RRBP1	LTAEFEEAQTSACR
A0AV96	RNA-binding protein 47	RBM47	SFGQFNPGCVER
P22087	rRNA 2'-O-methyltransferase fibrillarin	FBRL	ANCIDSTASAEAVFASEVK
Q5JTH9	RRP12-like protein	RRP12	FCIQEIEK
			VTVCQALR
P16615	Sarcoplasmic/endoplasmic reticulum calcium ATPase 2	AT2A2	ANACNSVIK
			GTAVAICR
Q13228	Selenium-binding protein 1	SBP1	CELAFLHTSHCLASGEVMISSLGDV K
Q9UHD8	Septin-9	Sep-09	WGTIEVENTTHCEFAYLR
P34896	Serine hydroxymethyltransferase, cytosolic	GLYC	LIIAGTSCYSR
P34897	Serine hydroxymethyltransferase, mitochondrial	GLYM	YYGGAEVVDEIELLCQR
			GLELIASENFCSR
Q92743	Serine protease HTRA1	HTRA1	GACGQGQEDPNSLR
Q8TDX7	Serine/threonine-protein kinase Nek7	NEK7	AACLLDGVPVALK
Q14738	Serine/threonine-protein phosphatase 2A 56 kDa regulatory subunit delta isoform	2A5D	CVSSPHFQVAER
P30153	Serine/threonine-protein phosphatase 2A 65 kDa regulatory subunit A alpha isoform	2AAA	EFCENLSADCR
			LNIISNLDCVNEVIGIR
Q9BRF8	Serine/threonine-protein phosphatase CPPED1	CPPED	FFVLCGDLIH
P62140	Serine/threonine-protein phosphatase PP1-beta catalytic subunit	PP1B	IFCCHGGLSPDLQSMEQIR
			QSLETICLLLAYK
			HDLDLICR
			IYGFYDECK
P21549	Serine--pyruvate aminotransferase	SPYA	FLTHGESSTGVLQPLDGFGELCHR
P10768	S-formylglutathione hydrolase	ESTD	VFEHDSVELNCK
P42224	Signal transducer and activator of transcription 1-alpha/beta	STAT1	NLSFFLTPPCAR
P62316	Small nuclear ribonucleoprotein Sm D2	SMD2	NNTQVLINCR
O75691	Small subunit processome component 20 homolog	UTP20	VLYLLELYCEDK

Accession	Description	Gene symbol	Peptide
P05023	Sodium/potassium-transporting ATPase subunit alpha-1	AT1A1	CSSILLHGK LIIVEGCQR
P05026	Sodium/potassium-transporting ATPase subunit beta-1	AT1B1	YNPNVLPVQCTGK
Q13813	Spectrin alpha chain, non-erythrocytic 1	SPTN1	CTELNQAWSSLGK EQADYCVSH
Q01082	Spectrin beta chain, non-erythrocytic 1	SPTB2	AELFTQSCADLDK NDSFTTCIELGK DALLLWCQMK SWHNVYCVINNQEMGFYK
P19623	Spermidine synthase	SPEE	QFCQSLFPVVAY
P52788	Spermine synthase	SPSY	LYCPVEFSK
Q13838	Spliceosome RNA helicase DDX39B	DX39B	CIALAQLLVEQNFPAIAIHR HFILDECDK
O75533	Splicing factor 3B subunit 1	SF3B1	VQENCIDLVGR
Q15393	Splicing factor 3B subunit 3	SF3B3	FGNICVVR
Q9GZT3	SRA stem-loop-interacting RNA-binding protein, mitochondrial	SLIRP	CILPFDK
Q7KZF4	Staphylococcal nuclease domain-containing protein 1	SND1	DIQNTQCLLNVEHLSAGCPHVTLQ FADSK ETCLITFLLAGIECPR MVLSGCAIIVR TCATVTIGGINIAEALVSK
Q15738	Sterol-4-alpha-carboxylate 3-dehydrogenase, decarboxylating	NSDHL	FFLGDLCSR
Q9HCN8	Stromal cell-derived factor 2-like protein 1	SDF2L	TGAELVTCGSVLK
Q14683	Structural maintenance of chromosomes protein 1A	SMC1A	ALVCDNVEDAR EQSTCNFQAIVISLK
P31040	Succinate dehydrogenase [ubiquinone] flavoprotein subunit, mitochondrial	SDHA	GLSEAGFNTACVTK TYFSCTSAH GVIALCIEDGSIHR
P21912	Succinate dehydrogenase [ubiquinone] iron-sulfur subunit, mitochondrial	SDHB	CGPMVLDALIK
Q99643	Succinate dehydrogenase cytochrome b560 subunit, mitochondrial	C560	SLCLGPALIHTAK
P51649	Succinate-semialdehyde dehydrogenase, mitochondrial	SSDH	WLPAAATFPVQDPASGAALGMVA DCGVR AAYEAFCR
P53597	Succinyl-CoA ligase [ADP/GDP-forming] subunit alpha, mitochondrial	SUCA	IICQGFTGK LIGPNCPGVINPGECK
P00441	Superoxide dismutase [Cu-Zn]	SODC	HVGDLGNVTADKDGVADVSIEDS VISLSGDHCIIGR
P04179	Superoxide dismutase [Mn], mitochondrial	SODM	GHLQIAACPNQDPLQGTTGLIPLLG ID
O15260	Surfeit locus protein 4	SURF4	LCLISTFLEDGIR
Q12846	Syntaxin-4	STX4	CNSMQSEYR
Q9Y490	Talin-1	TLN1	NCGQMSEIEAK TMQFEPSTMVYDACR TVTDMLMTICAR VQELGHGCAALVTK
O15533	Tapasin	TPSN	WASGLTPAQNCPR
Q13148	TAR DNA-binding protein 43	TADBP	AFAFVTFADDQIAQSLCGEDLIIK
P17987	T-complex protein 1 subunit alpha	TCPA	GANDFMCDEMER IACLDFSLQK ALNCVVGSQGMPK ICDDELILIK
P50991	T-complex protein 1 subunit delta	TCPD	SIHDALCVIR IGLIQFCLSAPK
P48643	T-complex protein 1 subunit epsilon	TCPE	SLHDALCVIR VVYGGGAAEISCALAVSQEADKCP TLEQYAMR
P49368	T-complex protein 1 subunit gamma	TCPG	NLQDAMQVCR
P50990	T-complex protein 1 subunit theta	TCPQ	IGLSVSEVIEGYEIACR

Accession	Description	Gene symbol	Peptide
P51580	Thiopurine S-methyltransferase	TPMT	SWGIDCLFEK
Q8NBS9	Thioredoxin domain-containing protein 5	TXND5	IAEVDCTAER VDCTAHSDVCSAQGVR
P30048	Thioredoxin-dependent peroxide reductase, mitochondrial	PRDX3	ANEFHDVNCEVVAVSVDSHFSHLA WINTPR
Q16762	Thiosulfate sulfurtransferase	THTR	VDLSQPLIATCR KVDLSQPLIATCR
P26639	Threonine--tRNA ligase, cytoplasmic	SYTC	CGPLIDLCR
Q9BV79	Trans-2-enoyl-CoA reductase, mitochondrial	MECR	ELILTLCDLIR
P37837	Transaldolase	TALDO	ALAGCDFLTISPK
Q9Y4P3	Transducin beta-like protein 2	TBL2	YLATCADDR
P61586	Transforming protein RhoA	RHOA	LVIVGDGACGK HFCPNVPIILVGNK
P55072	Transitional endoplasmic reticulum ATPase	TERA	LADDVDLEQVANETHGHVGADLA ALCSEAALQAIR EAVCIVLSDDTCSDEK
P29401	Transketolase	TKT	AIIVDGHSVEELCK CSTFAAFFTR
Q92616	Translational activator GCN1	GCN1L	CLQNPSSDIR LVEVQCLLLLEVLGGSHK VLQEALCVISGVPGLK YLLDSCAPLLR
Q99805	Transmembrane 9 superfamily member 2	TM9S2	DACVISSDFHER FYLPGLAPVNFCDEEK HTHIDKPDCSGPPMDISNK
Q9BVK6	Transmembrane emp24 domain-containing protein 9	TMED9	CFIEEIPDETMVIGNYR
Q6NUQ4	Transmembrane protein 214	TM214	SSGFLPASQQACAK
Q92973	Transportin-1	TNPO1	CVNLVQK SHAVACVNQF
P53007	Tricarboxylate transport protein, mitochondrial	TXTP	GIGDCVR
P55084	Trifunctional enzyme subunit beta, mitochondrial	ECHB	FNNWGGSLSLGHPFGATGCR
P22102	Trifunctional purine biosynthetic protein adenosine-3	PUR2	QVLVAPGNAGTACSEK
P60174	Triosephosphate isomerase	TPIS	IAVAAQNCYK IIYGGSVTGATCK
P23381	Tryptophan--tRNA ligase, cytoplasmic	SYWC	GIFGFTDSDCIGK DIIACGFDINK
P68363	Tubulin alpha-1B chain	TBA1B	MVDNEAIYDICR YMACCLLYR AYHEQLSVAEITNACFEPANQMVK LADQCTGLQGF
Q9BQE3	Tubulin alpha-1C chain	TBA1C	MVDNEAIYDICR YMACCLLYR AVCMLSNTTAVAEAWAR LADQCTGLQGFLVFHSF TTLEHSDCAFMVDNEAIYDICR
P68366	Tubulin alpha-4A chain	TBA4A	MVDNEAIYDICR YMACCLLYR AYHEQLSVAEITNACFEPANQMVK SIQFVDWCPTGF TTLEHSDCAFMVDNEAIYDICR
P07437	Tubulin beta chain	TBB5	TAVCDIPPR EIVHIQAGQCGN EIVHIQAGQCGNQIGAK NMMAACDPR
Q9BVA1	Tubulin beta-2B chain	TBB2B	LTTPTYGDLNHLVSATMSGVTTCL R
P54577	Tyrosine--tRNA ligase, cytoplasmic	SYYC	ISEECIAQWK
O75643	U5 small nuclear ribonucleoprotein 200 kDa helicase	U520	AALETDENLLLCAPTGAGK LTAIDILTTCAADIQR CTLLASAQSEAEK
O75208	Ubiquinone biosynthesis protein COQ9, mitochondrial	COQ9	DGSELILHFVTQCNTR

Accession	Description	Gene symbol	Peptide
Q92890	Ubiquitin fusion degradation protein 1 homolog	UFD1	CFSVSMLAGPNDR
P61086	Ubiquitin-conjugating enzyme E2 K	UBE2K	ISSVTGAICLDILK
O60701	UDP-glucose 6-dehydrogenase	UGDH	DVLNLVYLCEALNLPEVAR DPYEACDGAH
O60656	UDP-glucuronosyltransferase 42248	UD19	NHIMHLEEHLLCHR
O43795	Unconventional myosin-Ib	MYO1B	AAHIFNEALVCHQIR LNQVCATHQHFESR
Q5T6V5	UPF0553 protein C9orf64	CI064	DCLLELIEQK FGGSFLNCVR
P06132	Uroporphyrinogen decarboxylase	DCUP	AAQDFFSTCR
P26640	Valine--tRNA ligase	SYVC	GIEDNPMVVPLCNR ICLQPPPTSR
P50552	Vasodilator-stimulated phosphoprotein	VASP	MQPDQQVVINCAIVR
P49748	Very long-chain specific acyl-CoA dehydrogenase, mitochondrial	ACADV	CLTEPSSGSDAASIR GLQVPSELGGVGLCNTQYAR VTDECIQIMGGMGFMK
Q12907	Vesicular integral-membrane protein VIP36	LMAN2	WTELAGCTADFR NCIDITGVR
Q00341	Vigilin	VIGLN	CDIIIISGR
P18206	Vinculin	VINC	IAELCDDPK TNLLQVCER
Q9BQB6	Vitamin K epoxide reductase complex subunit 1	VKOR1	ALCDVGTAISCSR
P04004	Vitronectin	VTNC	GQYCYELDEK
P21796	Voltage-dependent anion-selective channel protein 1	VDAC1	YQIDPDACFSAK
P45880	Voltage-dependent anion-selective channel protein 2	VDAC2	WCEYGLTFTEK
Q9Y277	Voltage-dependent anion-selective channel protein 3	VDAC3	SCSGVEFSTSGHAYTDTGK VCNYGLTFTQK SCSGVEFSTSGH
P21281	V-type proton ATPase subunit B, brain isoform	VATB2	IPIFSAAGLPHNEIAAQICR
Q8IWB7	WD repeat and FYVE domain-containing protein 1	WDFY1	GLMVTCGTDR
O75083	WD repeat-containing protein 1	WDR1	MTVDESGQLISCSMDDTVR
P13010	X-ray repair cross-complementing protein 5	XRCC5	CFSVLGFCK CFSVLGF
Q15043	Zinc transporter ZIP14	S39AE	IGSSELQEFCPTILQQLDSR
Q15942	Zyxin	ZYX	QNVAVNELCGR

Table S2 H:L fold-change values of MAT1 and MAT2 as observed in a pilot study, and in the triplicates of the 3 h time-point for the longitudinal study. Values in red represent H:L fold-change values that exceed the 1.5-fold threshold.

Accession	Description	Gene symbol	H:L fold-change value			
			Pilot study	3 h (1)	3 h (2)	3 h (3)
Q00266	S-adenosylmethionine synthase isoform type-1	MAT1	39.2	3.12	0.73	0.92
P31153	S-adenosylmethionine synthase isoform type-2	MAT2	1.5	1.09	-	0.71

Table S3 Characteristics of the CYP3A5-genotyped HLM donors. Testosterone 6β-hydroxylation was determined in-house, while all other data were obtained from the respective vendors.

Donor	Vendor	Genotype	Western Blot		% CYP3A5 Content	Testosterone 6β-Hydroxylation
			CYP3A5	CYP3A4		
			pmol/mg			*nmol/min/mg*
HH785	BDGentest	*1/*1	13	170	7.10	1.06
HH860	BDGentest		35	320	9.86	1.14
HH867	BDGentest		17	110	13.39	0.58
H0331	XenoTech		NA	NA	NA	2.65
Mean ± S.D.					**10.12 ± 3.15**	**1.36 ± 0.90**
HH757	BDGentest	*1/*3	9	19	32.14	0.21
HH868	BDGentest		13	23	36.11	0.10
H0239	XenoTech		NA	NA	NA	0.52
H0280	XenoTech		NA	NA	NA	1.22
Mean ± S.D.					**34.13 ± 2.81**	**0.51 ± 0.50**
HH507	BDGentest	*3/*3	ND	15	0.07	0.04
H0307	XenoTech		NA	NA	NA	1.18
H0204	XenoTech		NA	NA	NA	0.14
H0182	XenoTech		NA	NA	NA	0.20
Mean ± S.D.						**0.39 ± 0.53**

ND, not detected; NA, not available.